

# Heat and mass transfer in frozen porous media

Wilko van Loon

CENTRALE LANDBOUWCATALOGUS



0000 0454 6517

**Promotor: Dr. ir. J. Schenk,  
emeritus hoogleraar technische natuurkunde**

**Co-promotor: Dr. I. A. van Haneghem,  
universitair hoofddocent algemene natuurkunde**

1432  
11082011

Wilko van Loon

# Heat and mass transfer in frozen porous media

## Proefschrift

ter verkrijging van de graad van doctor  
in de landbouw- en milieuwetenschappen,  
op gezag van de rector magnificus,  
dr. H. C. van der Plas,  
in het openbaar te verdedigen  
op dinsdag 25 juni 1991  
des namiddags te vier uur in de aula  
van de Landbouwuniversiteit te Wageningen.

18n 540 660

BIBLIOTHEEK  
LANDBOUWUNIVERSITEIT  
WAGENINGEN

## STELLINGEN

1. Er zijn meer overeenkomsten dan verschillen tussen de twee belangrijkste concepten voor de vorming van ijslenzen (te weten het 'star-ijs'-concept [Miller, 1972] en het scheidingspotentiaalconcept [Konrad, 1980]).

*Dit proefschrift, 3.1.*

2. Het imaginaire deel van de diëlektrische constante zoals is voorgesteld door Yanuka et al. [1988], dient slechts als een soort ijkconstante voor de metingen van de bulk elektrische geleidbaarheid met behulp van tijddomein-reflektometrie en heeft verder geen fysische betekenis.

*Dit proefschrift, 3.2.*

3. Bij metingen van de diëlektrische constante van vloeibaar water dient men er rekening mee te houden, dat deze in de onmiddellijke nabijheid van ijs lager is dan in water op grotere afstand.

*Dit proefschrift, 3.3.*

4. Het concept van 'thermodynamisch evenwicht' in bevriezende poreuze media is een contradictio in terminis.
5. Uit de experimenten van Vignes-Adler mag niet geconcludeerd worden dat de temperatuurgradiënt over de 'frozen fringe' geen invloed heeft op de vorstheffing.

*M. Vignes-Adler, 1976, Étude fondamentale de la congélation des milieux dispersés à l'échelle du pore, C.N.R.S. thèse, Paris, France.*

6. Anergie is een in de thermodynamika ten onrechte verwaarloosd begrip.
7. Voor goed inzicht in de ventilatie van tuinbouwkassen kan niet worden volstaan met alleen schaal- of computermodellen.

*T. de Jong, 1990, Natural ventilation of large multi-span greenhouses, proefschrift Landbouwuniversiteit Wageningen.*

8. Het opdrogen van dauw is sterk afhankelijk van de gezondheidstoestand van de bladeren van de betrokken plant.

*M.Y. Leclerc, G.W. Thurtell and T.J. Gillespie, 1985, Laboratory simulation of evaporation of water droplets on artificial soybeans, Agric. Meteorol. 36, pp 105-111.*

9. Indien lage concentraties ethyleen foto-akoestisch on-line worden gemeten, bijvoorbeeld als hormoon van verwelkende bloemen, is het aan te bevelen poly-ethyleen aan- en afvoerslangen af te schermen tegen (UV)- licht.

*D.D. Bicanic, A. Sólyom, G. Angeli, H. Wegh, M. Posthumus and H. Jalink, 1991, J. Applied Spectroscopy (submitted).*

10. Het is mogelijk om met behulp van de inverse foto-pyro-elektrische methode de relatieve waarde van de thermische effusiviteit van een monster in gecondenseerde fase te bepalen.

*D.D. Bicanic, M. Chirtoc, D. Dadarlat, W.K.P. van Loon and I. Chirtoc, 1991, J. of Food Analysis and Composition (submitted).*

11. Indien compost als een poreus medium wordt opgevat, dient het "Reference Elementary Volume" (REV, referentie volume-element) in de orde van 1 dm<sup>3</sup> te zijn.

*J. Bear, 1987, Mathematical modeling of transport in porous media, VKI lecture series 1988-01, Von Karman Institute, Brussel België.*

12. 'Beta-mensen' hebben te veel en te weinig invloed.
13. Houtjes-touwtjes technologie kan nog altijd een wezenlijke bijdrage leveren aan actueel technisch-wetenschappelijk onderzoek.
14. Wetenschap bedrijven is soms niets meer dan het bevestigen van boerenwijseden.
15. Een oorlog benaderen als een strijd van goed tegen kwaad, is als een één-bits digitale benadering van een analoog proces.

*Bij voorbeeld: Samir al-Khalil, Iraks laatste kans. In: Intermediair 15, 12 april 1991.*

Stellingen behorende bij het proefschrift 'Heat and mass transfer in frozen porous media', geschreven door Wilko van Loon.

Wageningen, 25 juni 1991.

## ABSTRACT

Loon, W.K.P. van, 1991. Heat and mass transfer in frozen porous media Ph.D. Thesis, Agricultural University Wageningen, the Netherlands.

200 pp., 203 eqs., 49 figs., 23 tables, 119 refs, English and Dutch summary.

In this thesis processes and parameters associated with heat and mass transfer in frozen porous media both on a theoretical and empirical basis are studied. To obtain the required measurements some existing measuring methods needed to be improved.

Firstly, an improved model has been developed for the measurement of thermal conductivity with use of the nonsteady-state probe method. The measurements of thermal conductivity indicate four separate effects caused by the freezing process.

The second improved measuring method is the measurement of bulk electrical conductivity with use of time-domain reflectometry.

And the third improvement is the use of the dispersion theory in the description of relations between water content and bulk electrical conductivity or dielectric constant.

This thesis shows that time-domain reflectometry can be used to measure the unfrozen water content and bulk electrical conductivity simultaneously under frozen conditions and that from the latter parameter solute redistribution can be monitored.

From the measured heat flows a time delay in the forming of pore ice can be concluded. From the measured moisture transport (resulting in frost heave) a relation with some soil properties could be established. For some of the materials studied a minimum temperature gradient has been observed at which heave starts. From this and other results an effort was made to come to a synthesis of the rigid ice concept and the segregation potential concept.

The thesis finishes with some recommendations in connection with the improvement of soil structure by freezing, frost heave and artificial ground freezing.

Key words: bulk electrical conductivity, dielectric constant of water, frost heave, ice lenses, in situ measurements, mixing rules, nonsteady-state probe method, pore ice, segregation potential, solute redistribution, thermal conductivity, time-domain reflectometry, unfrozen water content.

## i TABLE OF CONTENTS

	page
PREFACE	
1 INTRODUCTION	1
1.1 Fields of interest	1
1.2 Macroscopic freezing test	2
1.3 Microscopic model	2
1.4 Aim of the thesis	5
1.5 Overview of the thesis	7
2 THEORY	9
2.0 Introduction to the chapter	9
2.1 Theory of different soil analyses	10
2.1.1 Particle size distribution	11
2.1.2 Specific surface area	13
2.1.3 Cation exchange capacity	14
2.1.4 Zeta potential	14
2.1.5 Water retention	15
2.1.6 Hydraulic conductivity	16
2.1.7 Thermal conductivity	17
2.2 Determination of soil water content by time-domain reflectometry	19
2.2.1 Transmission line theory	19
2.2.2 Water content	23
2.2.3 Bulk electrical conductivity	25
2.3 Transfer of heat and mass	28
2.3.1 Moisture transport	29
2.3.2 Heat transport	35
2.3.3 Solute transport	39
3 NEW MODELS AND METHODS	42
3.0 Introduction to the chapter	42

	page
3.1 A new model for the nonsteady-state probe method to measure thermal properties of porous media	43
3.1.0 Abstract	43
3.1.1 Introduction	44
3.1.2 Present approach	45
3.1.3 Experimental set-up	46
3.1.4 The perfect line source model	47
3.1.5 The modified Jaeger model	48
3.1.6 Gauss-Newton iteration	54
3.1.7 Calibration measurements	57
3.1.8 Conclusions	61
3.2 A new method to measure bulk electrical conductivity in soil using time-domain reflectometry	62
3.2.0 Abstract	62
3.2.1 Introduction	62
3.2.2 Measurement theory	63
3.2.3 Materials and methods	68
3.2.4 Results and discussion	69
3.2.5 Conclusions	72
3.3 Application of dispersion theory to time-domain reflectometry in soils	74
3.3.0 Abstract	74
3.3.1 Introduction	74
3.3.2 Dielectric constant as a function of water content	75
3.3.2.1 Soil as a two phase dielectric medium	75
3.3.2.2 Unfrozen soils	76
3.3.2.3 Frozen soils	80
3.3.3 Bulk electrical conductivity as a function of water content	83
3.3.4 Materials and methods	84

	page
3.3.5 Results and discussion	85
3.3.5.1 Validation of the model for bulk electrical conductivity	85
3.3.5.2 Comparison with other models	89
3.3.6 Conclusions	91
3.3.7 Appendix	92
3.4 Description of the experiments to measure heat and mass transfer in freezing porous media	94
3.4.1 Experimental set-up	94
3.4.2 Used materials	97
3.4.3 Relations between soil physical and electrochemical properties	100
<b>4 RESULTS AND DISCUSSION</b>	<b>103</b>
4.0 Introduction to the chapter	103
4.1 Thermal conductivity of unsaturated frozen sands	104
4.1.0 Abstract	104
4.1.1 Introduction	104
4.1.2 Experimental set-up	105
4.1.3 Theoretical approach	107
4.1.4 Properties of the used sands	109
4.1.5 Measured heat flows	111
4.1.6 Measured thermal conductivities	115
4.1.7 Discussion	116
4.2 Heat transfer	118
4.2.1 Heat capacity	118
4.2.2 Thermal conductivity	123
4.2.2.1 Influence of the temperature dependence of the pore ice versus unfrozen water content	124
4.2.2.2 Contribution of the apparent thermal conductivity	127

	page
4.2.2.3 Segregated ice content	128
4.2.2.4 Presence of the freezing front close to the measuring probe	130
4.2.3 Latent heat of in situ freezing	132
4.2.4 Heat balances	135
4.2.5 Temperature fields	138
4.2.6 Dynamics of heat flows in frozen porous materials	141
4.3 Moisture transfer	146
4.3.1 Segregation potential	146
4.3.2 Influence of soil physical and electrochemical properties	150
4.4 Application of time-domain reflectometry to measure solute concentration during soil freezing	156
4.4.0 Abstract	156
4.4.1 Introduction	156
4.4.2 Materials and methods	158
4.4.3 Results and discussion	160
4.4.3.1 Influence of temperature	161
4.4.3.2 Influence of liquid water content	163
4.4.3.3 Redistribution of solutes	165
4.4.4 Conclusions	167
4.5 Influence of added solutes on moisture transfer	168
5 CONCLUSIONS AND FINAL DISCUSSION	171
5.1 General discussion	171
5.2 Recommandations in connection with frost in porous media	179
6 SUMMARY	181
7 SAMENVATTING	186
8 REFERENCES	192
9 LIST OF SYMBOLS	201
10 CURRICULUM VITAE	204

## PREFACE

The writing of this part means that the thesis work has been completed and that it is time to look back to the last few years. It is a good feeling to recall all the (small) steps that formed together the exploration through the field of frozen porous media. The exploration has been carried out in cooperation with many people.

In the first place I am greatly indebted to the people who selected me for the job and coached me during the last few years.

With Hennie Boshoven, who assisted in designing and performing the experiments, I shared most time during the research. He showed me around in the department and the rest of the university. I am grateful for his technical coaching.

As co-promotor, Ies van Haneghem took care of the general line and evaluation of the research. I enjoyed the scientific discussions with him. I am grateful for his general and scientific coaching.

With my promotor, Jaap Schenk I discussed each page of this book at least four times. He, and also Ies, made a far better product of my drafts. I am grateful for his scientific coaching.

As a real 'Wageningen' scientist, Bert Wartena took care of the possible application of the research on the field of soil science and civil engineering. I am grateful for his practical coaching.

The experiments could not have been realised without the men with the 'golden hands' from the Duivendaal-location. I owe a lot to the skills and good ideas of Anton Jansen, Teun Jansen, Willy Hillen, Dimitri van den Akker, Ate Brink, Peter Jansen and Kees van Asselt. The latter also taught me a lot about measuring electronics.

In fact the work could not have been realised without the friendly and enthusiastic atmosphere of the former department of Physics and Meteorology, and later the two departments: Meteorology, and Agricultural Engineering and Physics.

One of the stimulating circumstances was the cooperation with (former) students, that spent a few months in our project: Wilfred Otten, Ger Cruts and Erik Boons from Wageningen; Tim Allen and Al Bertrand from Guelph, Canada; and Wido Westbroek from Waterloo, Canada.

The cooperation was not limited to the own department(s). I appreciated the discussions with Arie de Keizer in the field of physical chemistry. With Chris Dirksen I enjoyed discussing soil physics and the different models for frost heave. I am greatly indebted to him for the permission to use his cable tester to perform the time-domain reflectometry measurements. Without this cable tester a large part of the experiments could not have been performed.

I am grateful to all the people that performed part of the analysis: Willy Ackerman (water retention and hydraulic conductivity), Twan Jongmans (geological determination of the soils), Anton Korteweg (specific surface area), Ab van der Linde (zeta potential) and Tini van Mensvoort (cation exchange capacity).

The research has not only been carried out in Wageningen. With great pleasure I remember the time I spent in Guelph, Canada. In that respect I feel greatly indebted to Bev Kay, who invited me to stay half a year at the department of Land Resource Sciene at the University of Guelph, Ontario, Canada. He gave me the opportunity to work in an internationally respected group and to learn a lot about ground freezing.

One of the people who made this period so motivating was Pieter Groenevelt. I appreciated not only the vivid scientific discussions with him, but also the social events he organised.

But my stay in Canada has become extraordinary fruitful by the interaction with Ed Perfect. His conscientiousness, his feeling for language and his profound knowledge of scientific literature made it a big pleasure to write articles with him. And of course the friendship, that he and his wife Barbara Burton offered, made the stay in Canada very pleasant.

Also in the Netherlands I appreciated the opportunity to work with people from institutes outside Wageningen. The Northern Road Testing Laboratorium in Groningen gave me some insight in the practical testing methods used in road construction.

Hans Bakker introduced me in some of these methods and in other details how business is done in the road construction world.

With Jaap Zeilmaker, then working at the Road and Hydraulic Engineering Division, Public Works Department in Delft, I often discussed frost heave measurements. Furthermore we traveled together beyond the Polar Circle to attend a conference on frost in geotechnical engineering.

With his successor at the Public Works Department, Wouter van Schelt, the cooperation has been continued. This will soon result in a movie about frost heave in porous media. With respect to the technical realisation of the movie I am also indebted to Wim van Hof from our university.

After the thesis had been (type-)written and drafts of the figures had been made, the work needed to be transformed into a book. In that respect I owe a lot to Hedy D'hondt-de Jong, who restyled the thesis, worked out the equations and tables, and made the layout consistent.

The large amount of figures in this book were skillfully drawn by Paul van Espelo. I am also largely indebted to him for the design of the cover.

I am convinced that doing a Ph.D.-research does not imply that you have to work day and night, but there should be time for other things as well.

Therefore I would like to finish this section with a 'thank you' to Anita van Hoof. The start of the thesis research was also the start of forming one household with her. It was and still is a source of joy and inspiration. This has even become stronger after the birth of our son Kors.

So 'thanks' Anita and Kors for keeping me in touch with life.

## 1 INTRODUCTION

### 1.1 Fields of interest

Frost phenomena in porous media are important before all in agricultural engineering. The major field of interest is probably ground freezing. Since ages farmers know that seasonal ground freezing might cause an improvement of the soil structure. Perfect et al. [1990b] proved that freezing increases the wet aggregate stability, while the dispersible clay content decreases. This suggests flocculation and/or cementation by precipitates formed at low unfrozen water contents. Artificial ground freezing is important in technical engineering: it is applied in constructing shafts and tunnels. Recent state of art articles on this subject have been written by Klein [1988] and Harris [1988]. Artificial ground freezing can also be used in paralysing serious soil contamination, because pollutants are to a high degree impeded to move in frozen soils (or through a barrier of frozen soil) [Sullivan and Stefanov, 1990].

Frost phenomena in porous media are also important in civil engineering: they might cause severe damages to road constructions and buildings. Even in the Netherlands the cost due to frost damage to roads is about Dfl 100 million (\$ 50 million) per annum [Werkgroep E4, 1986]. Special attention needs to be paid to the foundations of roads.

Because in our country a shortage of workable sands exists, new materials are investigated on their suitability. A group of possible substitutes are the waste materials. Over six million tonnes of construction waste is produced each year in the Netherlands [Van Loon and Zeilmaker, 1989a]. This material consists of more than 80% of stone materials. An attendant advantage to recycle these materials is the less rapid growth of refuse dumps, which form a serious problem in our densely populated country.

Other applications of frost in non-homogeneous media are conservation techniques by freezing (for instance food, sperm or human organs) and freeze-drying processes.

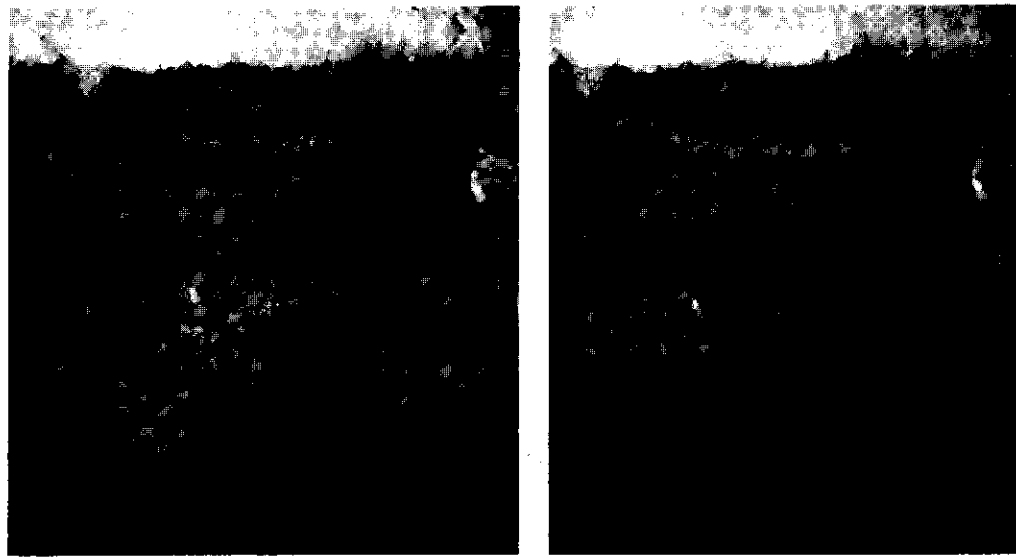
## 1.2 Macroscopic freezing test

The present research will be concentrated on seasonal ground freezing. Let us first describe a sample experiment that shows the major process: heave caused by a temperature gradient in one dimension. This restriction to one dimension agrees well with reality, because in natural soils the transport phenomena caused by freezing occur mainly in the vertical direction. If temperatures are measured and pictures are taken, it is possible to monitor all parameters involved: temperature, position and heave.

In Fig. 1.2.1 it can be seen, that a crack is forming and widening, which means that it is filled with pure ice. This is called an ice lens. The growing ice lens actually heaves the soil. With thermocouples the temperature can be measured. The position of the 0°C isotherm can then be determined by interpolation. It appears to be about 15 mm below the warm side of the ice lens. That means that there has to be a zone between the 0°C isotherm and the warmest ice lens, where water transport takes place. Miller [1972] called this zone the frozen fringe. In the frozen fringe pore ice coexists with unfrozen water layers around the soil particles (see Fig. 1.2.2). These unfrozen water layers are thinner at lower temperatures because the thermodynamic equilibrium between ice and unfrozen water shifts to ice at lower temperatures. The mobility of the unfrozen water is expressed in the hydraulic conductivity  $k_{ff}$  inside the frozen fringe. Analogue to unsaturated soils the hydraulic conductivity in frozen soils is very (liquid) water dependent.

## 1.3 Microscopic model

The heaving process is not to understand from a macroscopic point of view, because on this scale water transport at temperatures below 0°C is impossible. To understand the existence of the frozen fringe and the transport of liquid water through this zone, it is necessary to study the frozen fringe on a microscopic scale. Water can remain unfrozen at temperatures below 0°C due to the interaction between the dipole of the water molecules and the surface charge (related with the crystallographic properties) of the soil particles [Miller, 1972].



A. at 170 hours after start of test;

B. at 226 hours

Fig. 1.2.1 Pictures of growing ice lenses in a freezing loamy sand during freezing test, with at  $z=50$  cm the top of the soil column, at  $z>50$  cm the cooling plate, at  $z=49$  cm the ice lens with developing drying crack to  $z=45\frac{1}{2}$  cm and at  $z=49$  and 44 cm measuring probes (e.g. thermocouples).

The unfrozen water content at a certain temperature is increasing with an increasing specific surface area according to Horiguchi [1986], in which the specific surface area  $S$  is the sum of particle surfaces per unit of soil mass. The relation between specific surface area and frost heave was shown by Rieke et al. [1983] and Horiguchi [1985]. Another parameter which relates closely to  $S$  is the amount of small particles  $\Phi$  (Analogue parameters of  $\Phi$  are the silt and clay fractions of the granular materials). All soil physical and electro-chemical properties will be defined in section 2.1.

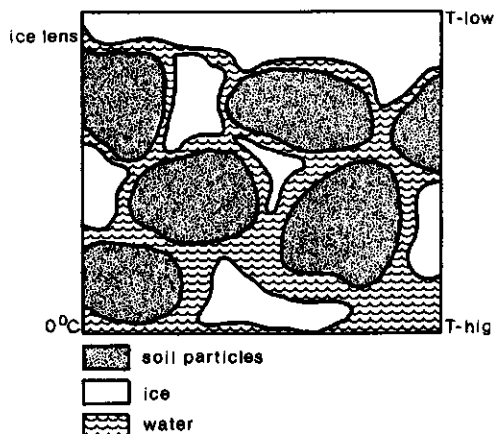


Fig. 1.2.2 Schematic cross section of the frozen fringe (with lower temperatures at the top). Note that the thickness of the unfrozen layers is increasing at increasing temperature.

Apart from  $S$ , the thickness  $d_u$  of the unfrozen water layers is an other important parameter that determines  $k_{ff}$ ;  $d_u$  is not only a function of the temperature, but also a function of the surface charge. The surface charge density can be expressed with the zeta-potential ( $\zeta$ , see section 2.1). Powder materials with a large surface charge are more frost susceptible than powders with small surface charges, even if the surface area per unit volume is the same [Horiguchi, 1985]. The surface charge creates an electrical field which acts in two different ways. Firstly, it binds ions in an electrical double layer, so the unfrozen water content increases. Secondly, it binds the closest water layers more tightly: water molecules close to a clay surface are less mobile than water molecules close to a sand surface. A parameter which is closely related to the total surface charge is the Cation Exchange Capacity (CEC, see section 2.1).

The phenomenon is even more complicated, as the surface charge on its turn is influenced by the acid rate pH, because most of the soil particles (and the concrete) consists of oxydes [Gregg and Sing, 1982]. It may be clear that we need some simplification in order to come to a practical model for  $d_u$ . Because the measurements for CEC and  $\zeta$  are relatively easy to obtain, we assume that those two parameters together define well enough the complex interactions between the electrical charges to obtain a relation for  $d_u$  (the influence of pH is built in these two parameters). So we state:

$$d_u = f(CEC, \zeta) \quad (1.3.1)$$

From the above paragraphs we can conclude that the hydraulic conductivity in the frozen fringe is a function of the following parameters:

$$k_{ff} = f(\Phi, S, CEC, \zeta) \quad (1.3.2)$$

From relation (1.3.2) it can be concluded, that the determination of soil physical and soil chemical parameters is required to give a better understanding of the soil freezing process.

#### 1.4 Aim of the thesis

To investigate the transport phenomena that occur during soil freezing it is necessary to describe the physical processes involved, both on microscopic and macroscopic scale. Next, those processes have to be pictured into models and from these models mathematical equations can be developed. The models and equations can only be developed on the basis of empirical results. Thus, the purpose of the thesis is to investigate processes and parameters associated with heat and mass transfer in frozen porous media on an empirical basis. In this, the transport processes are limited to the simultaneous fluxes of heat, water and solutes (relative to the soil matrix) in response to gradients of temperature, hydrostatic pressure and solute concentration.

Transfer of any component can occur as a result of a direct process or as a result of coupled processes [Perfect et al., 1991]. However, the driving force for most freezing processes is the temperature gradient [Konrad and Morgenstern,

1980]. Thus, the major field of interest in this research is the behaviour of the three earlier mentioned fluxes as a result of the temperature gradient. Because the coupling processes are so important, it would be usefull to estimate in situ all the parameter involved:

temperature, water content, solute concentration, thermal conductivity, hydraulic conductivity and diffusion coefficient.

Of those parameters, temperature is the only one which can be measured easily in situ (by means of thermocouples, thermistors or electronic devices like AD-590).

A comprehensive review of different methods to measure unfrozen water contents was presented by Anderson and Morgenstern [1973]. Significant improvements have been achieved since that time. Patterson and Smith [1984] introduced the use of time domain reflectometry (TDR), which gave a fast and easy method to determine the unfrozen water content.

The in situ measurement of solute concentration in frozen soil is very complicated. The only direct method used is the extraction of very small quantities of solution. However, the unfrozen water content is small and hard to extract. Probably the most convenient in situ method is measuring soil electrical conductivity. This is also possible using TDR [Dalton et al. 1984]. Some improvement of this method is developed (see section 3.2) and also better relations are derived between measured soil electrical conductivity and solute concentration (section 3.3).

A comprehensive review of different measuring methods of thermal properties of soils is given by Farouki [1986]. One of the major in situ methods is thermal conductivity measurement with the nonsteady state probe method [Bruijn et al., 1983]. Our laboratory has a large experience in performing these measurements [De Vries, 1952, Van Haneghem, 1981 and Van Haneghem and Leij, 1985]. Some improvements of this method are yet introduced (see chapter 3.1). The results of the thermal conductivity measurements are given in section 4.1 and incorporated in the heat balance equation in section 4.2.

The direct measurement of liquid and ice pressure in frozen soils needs to be developed further [Kay and Perfect, 1988]. Therefore it is hard to give esti-

mates of the in situ hydraulic conductivity. Konrad and Morgenstern [1980, 1981] showed that another parameter is representing the influence of the soil on the water transport in freezing soils: the segregation potential (SP). This parameter relates the water flux to the temperature gradient. The segregation potential will be discussed in section 4.3.

The most important mechanism for solute redistribution in frozen porous media appears to be the reverse osmosis: the transport of solutes that occurs in conjunction with the unfrozen water [Perfect et al. 1991]. Therefore the self diffusion coefficient (expressing the coupling between solute transport and concentration gradients) has not been investigated. The solute redistribution by unfrozen water flow is investigated in section 4.4.

### 1.5 Overview of the thesis

In this thesis the following chapters will come along. In chapter 2 all relevant models, equations and definitions are reviewed, consisting of (2.1) definitions of all soil physical and electrochemical properties, (2.2) theory of time domain reflectometry and (2.3) the equations of heat and mass transfer in frozen soils. In chapter 3 the (improved) measuring procedures and relations are presented including (3.1) the thermal conductivity, (3.2) the bulk electrical conductivity, (3.3) the relation between bulk electrical conductivity and solute concentration and (3.4) the general experimental set up. Knowing the procedures to measure the different parameters in chapter 4 first the thermal conductivity measurements below 0°C are discussed (4.1), then the fluxes of heat, water and solutes are presented (in 4.2, 4.3 and 4.4, respectively) and in (4.5) the influence of solutes on heave is discussed. In chapter 5 the results and conclusions of the different chapters are related to one another and compared with recent literature.

During the past four years parts of the research have been published as independent articles in several journals and conference proceedings. Most of these articles have been incorporated in the thesis with some minor corrections. However, the first article published (4.1) needed to be revised to a greater extend, due to a growing understanding of the complicated influence of the

freezing proces on the thermal conductivity. The articles can be found in the following sections:

- 3.1 Loon W.K.P. van, Haneghem I.A. and Schenk J., 1989b. A new model for the nonsteady state probe method to measure thermal properties of porous materials, *Int. J. Heat Mass Transfer* 32, pp 1473-1481.
- 3.2 Loon W.K.P. van, Perfect E., Groeneveld P.H. and Kay B.D., 1990b. A new method to measure bulk electrical conductivity in soils with time-domain reflectometry, *Can. J. Soil Sci.* 70, pp 403-410.
- 3.3 Loon W.K.P. van, Perfect E., Groeneveld P.H. and Kay B.D., 1991. Application of dispersion theory to time-domain reflectometry, *J. Porous Media* (in press).
- 4.1 Loon W.K.P. van, Haneghem I.A. van and Boshoven H.P.A., 1988. Thermal and hydraulic conductivity of unsaturated frozen sands, *Proc. Fifth Int. Sym. Ground Freezing*, Vol 1, Balkema, Rotterdam NL, pp 81-90.
- 4.4 Loon W.K.P. van, Perfect E., Groeneveld P.H. and Kay B.D., 1990a. Application of time-domain reflectometry to measure solute redistribution during soil freezing. *Proc. Int. Frozen Soil Symp.*, CRREL report 90-1, Hannover NH, USA, pp 186-194.

## 2 THEORY

### 2.0 Introduction to the chapter

The essence of transport processes is that a gradient of an external property (e.g. temperature, pressure or concentration) causes a flux. For most practical applications a linear relationship is adopted. So the flux is proportional to the gradient of the given external property and with a certain characteristic of the medium. In section 2.1 all soil characteristics are described that might influence the transport processes in freezing soil. Here not only the direct coupling parameters are described, but also properties that largely influence the coupling parameters. Some soil properties are largely influenced by the water content. The measurement of water content is described in section 2.2. The measuring methods for these properties (that are mainly standard methods) have been indicated in principle. Only for those properties where the measuring method has been part of the present research a more detailed treatment is given. The chapter finishes with the description of the transport processes in frozen porous materials in section 2.3.

## 2.1 Theory of different soil analyses

*Particle size analysis* is the measurement of the size distribution of individual particles in a soil sample [Koorevaar et al, 1983] and is important to classify the soil. Particle size distribution curves are used extensively by geologists to evaluate sedimentation and alluvial processes. By civil engineers it is used to evaluate materials for (road) foundations and other constructions. It is also used as a selection criterion in the frost susceptibility of roads [Roe and Webster, 1984, Jessberger and Jagow, 1989].

Many physical and chemical properties of the soil are largely determined by the *surface area of the soil particles*. For instance physical adsorption of molecules and heat loss or gain resulting from that adsorption are closely related to surface area. Also the transport of water in the frozen fringe, that is supposed to take place close to the surface of the soil particles is related to the surface area [Ratkje et al., 1982]. Cation exchange capacity and water retention are closely related to the specific surface area [Klute, 1986]. Usually this property is defined as the surface area per unit of mass soil (in  $\text{m}^2/\text{g}$ ). Different soils may vary widely in their surface area because of differences in mineralogical and organic composition and in particle size distribution. Clay-size particles contribute much more to the inorganic surface area of soils than e.g. sand-size particles.

Due to the charged surface of the soil particles, water molecules are more or less ordered in the resulting electrostatic field. Because of this ordering the water molecules do not fit in the crystal structure of ice and the water remains unfrozen at temperatures just below  $0^\circ\text{C}$  (the water will freeze at lower temperatures). The electrostatic force is inversely proportional with distance, so at a certain distance from the soil particle surface the water freezes. The thickness of the unfrozen water layer depends on the surface charge density. A measure for the surface charge density is the *cation exchange capacity*, which is defined as the sum of the exchangeable cations neutralizing the negative charge in a soil.

Another measure for the surface charge density is the *zeta potential*: the electrostatic potential due to the surface charge determined at the kinetic surface [Hunter, 1981]. This kinetic surface is the nearest surface around the soil particle at which water molecules can move with respect to that soil particle (water molecules more close to the soil particle, in the so called Stern layer, are unable to move).

The soil properties that determine the behaviour of soil water flow are the *hydraulic conductivity* and the *water retention* characteristics. In saturated conditions the hydraulic conductivity is the most important parameter, it is the direct coupling coefficient between water flow and water pressure gradient. In seasonal ground freezing low air temperatures cause the soil to freeze, so frost penetration takes place starting from the soil surface. In general, the soil close to the surface is not saturated with water. In dealing with the problems of water flow in unsaturated conditions, the water retention is the most important parameter. It is the ability of the soil matrix to retain water at negative water pressures (the relationship between the volume fraction of water and an appropriate component of the matric head [Koorevaar et al., 1983]).

When soil freezes, a phase transition of the soil water takes place in which the latent heat is released. In general the energy transport takes place by conduction to the soil surface. The soil property that governs the heat conduction is the *thermal conductivity*, which is an effective property of the soil- water- ice- air mixture. The thermal conductivity of a given soil is dependent on temperature and water content [Van Genughem and Leij, 1985].

### 2.1.1 *Particle size distribution*

Particle size distribution is determined on the primary soil particles, which are mineral particles. In soils these particles can be cemented to larger units: soil aggregates or secondary particles. To obtain the individual (or primary) soil particles, the soil cementing agents need to be removed. In general, first the organic matter is removed by using oxidants (e.g.  $H_2O_2$ ) in an aqueous solution. Next iron oxydes and different types of carbonates are to be removed. Then, the exchange complex (of the soil particles) is saturated with sodium in order to obtain inter particle repulsion. And finally, mechanical dispersion

(stirring or shaking) is applied on the suspension to separate the individual primary particles.

The sand fraction is obtained by pouring the suspension through a 50  $\mu\text{m}$  sieve, while the sand is washed thoroughly on the sieve. The fraction with a diameter  $d > 50 \mu\text{m}$  is called the sand fraction. This fraction is oven dried and then passed through a nest of sieves with different meshes. The nest of sieves is shaked during several minutes and each sieve fraction is weighed.

The mass fractions  $\Phi$  with  $d < 50 \mu\text{m}$  are separated by sedimentation. This analysis is based on the relationship between the settling velocity  $v$  and the particle diameter. As early as 1851 Stokes derived a form of the relation for the terminal settling velocity [Klute, 1986]. when sedimentation takes place by gravitational forces only, the Stokes's law for  $v$  can be written as:

$$v = g (\rho_s - \rho_w)d^2/(18\eta) \quad (2.1.1)$$

with  $g$  the gravitational acceleration,  $\rho_s$  and  $\rho_w$  the density of the soil particle and water, respectively and  $\eta$  the dynamic viscosity ( $\text{kg m}^{-1}\text{s}^{-1}$ ).

Four assumptions are made in applying Stokes' law to sedimenting soil suspensions:

1. Terminal velocity is reached as soon as the settling begins.
2. Settling and resistance are entirely due to the viscosity of the fluid.
3. Particles are smooth and spherical. Since soil particles are not smooth and spherical  $d$  must be considered as an effective diameter.
4. There is no interaction between the individual particles in suspension. Because the settling of the particles causes a counterflow of water, the settling velocity is dependent on the amount of displaced water. According to Richardson and Zaki (as quoted in Beek and Muttzal [1975] the settling velocity is changed less than 5% if the particle concentration is less than  $0.01 \text{ m}^3/\text{m}^3$  (laminar flow conditions).

The settling velocity is determined by measuring the settling distance and time. Next the equivalent diameter is calculated with use of (2.1.1). When at different settling times samples are taken from the suspension, the concentration

of particles can be determined for different values of the equivalent diameter. By choosing the appropriate series of settling velocities the desired particle size distribution can now be obtained.

### 2.1.2 Specific surface area

The specific surface area ( $S$ ) can be measured with the adsorption of gas molecules on the surface of soil particles. The volume of the added gas is measured as a function of the pressure under isothermal conditions. In physical chemistry this relation is known as an adsorption isotherm. Gas molecules close to the solid surface are attracted by forces arising from the solid phase surface atoms. The quantity of the gas adsorbed can provide a measure of surface area. Brunauer, Ermitt and Teller derived a relation from multimolecular adsorption theory, that provides the calculation of the number of molecules in a monomolecular layer. This relation is called the BET equation.

In the BET equation three assumptions are made: firstly, the heat of adsorption of the first monolayer  $E_1$  is higher than the energy of liquification  $E_2$ , secondly, the heat of adsorption of all molecular layers after the first one equals  $E_2$  and thirdly, at equilibrium, the condensation rate on the surface is equal to the evaporation rate from the molecular layers.

The BET equation reads [e.g. Gregg and Sing, 1982]:

$$\frac{p}{V(p_0-p)} = \frac{1}{V_m C} - \frac{(C-1)p}{V_m C p_0} \quad (2.1.2)$$

With  $V$  the gas volume adsorbed at pressure  $p$ ,  $V_m$  is the volume of the gas required for the monolayer.  $p_0$  the gas pressure required for saturation at the temperature  $T$  of the experiment and  $C$  the BET constant, with  $C = \exp(E_1 - E_2)/RT$  and  $R$  the gas constant. The quantity  $V_m$  is determined from (2.1.2). The surface area can then be calculated by multiplying  $V_m$  with the cross sectional area of the adsorbed molecule and by dividing by the molar volume, in which the density of the adsorbed monolayer is assumed to be that of the liquified gas. Generally the surface area depends on the gas used as adsorbate: the smaller the gas molecules, the larger the measured surface area.

In this research the experimental set up of the department of Physical and Colloid Chemistry of the Wageningen Agricultural University was used. Here nitrogen gas ( $N_2$ ) was used as adsorbate.

### 2.1.3 Cation exchange capacity

Cation exchange capacity (CEC) is defined as the sum of exchangeable cations (usually expressed in mmol/kg) neutralizing negative charge in a soil [Rhoades, 1982]. To determine the CEC the exchange complex is saturated with an index cation which is originally not present in the soil. In the department of Soil Science and Geology at the Wageningen Agricultural University, where the CEC determination took place,  $\text{Li}^+$  of  $\text{Na}^+$  ions are used. To enhance the coupling of the exchanged cation to the solution anion, the latter has to possess about the same chemical properties as the soil exchange complex. In our case EDTA (EDTA = ethylene diamine tetra acetic acid) has been used.

The concentration of the saturating cation and anion are then determined in the resulting extract, and their difference is taken as the CEC of the soil. Also the cations that are washed out can be determined using spectroscopy. In the spectroscope (Perkin Elmer 560), used at the department of Soil Genesis and Geology of the Wageningen Agricultural University, two different methods are used: atomic absorption spectroscopy for Ca and Mg and flame emission spectroscopy for Na, K and Li. The principle of this kind of spectroscopy is that ions can be excited to a higher energy state by absorbing discrete units of energy (energy quanta). In the first method the energy spectra of the flame before and after it has been transmitted through the sample are measured. In the second method the energy spectrum caused by returning of the excited ions to a lower energy state is determined. Both energy spectra consist of characteristic wave lengths. (The wave length is coupled to an energy quantum by Planck's law). Thus the different ions can be recognised by their specific energy spectra and the amount of ions in the excited state is proportional with the concentration.

### 2.1.4 Zeta potential

The electrical double layer around charged particles in water exists of the Stern layer and the diffuse double layer. In the diffuse double layer water molecules are still able to move, where the Stern layer consists of some molecule layers of water, which are fixed to the surface of the solid particle. So the kinetic surface of a moving particle is different from the soil-water

(interfacial) surface. This surface is also called the shear plane [Hunter, 1981]. The zeta potential is the electrical potential at this shear plane.

The zeta potential can be measured with an electro-kinetic method. One of the methods is micro-electrophoresis. With this method an external electrical field causes charged particles to move. It is assumed that the electrical force is in equilibrium with the friction forces and that the gravitational forces can be neglected (allowed if the particles are small enough). The resulting electroforetic velocity  $v$  is proportional to the zeta potential  $\zeta$  [Hunter, 1981]:

$$v = (\epsilon \times E / \eta) \zeta \quad (2.1.3)$$

with  $E$  the electrical field force,  $\epsilon$  and  $\eta$  the dielectric constant and the kinematic viscosity of water, respectively.

The electroforetic mobility ( $v/E$ ) is determined with a Malvern Zetasizer II, at the department of Physical and Colloid chemistry of the Wageningen Agricultural University. Because  $\epsilon$  and  $\eta$  are known,  $\zeta$  can now be calculated from eq (2.1.3).

### 2.1.5 Water retention

Water retention is the ability of the soil to hold water at a certain pressure. The water retention function is determined by establishing a series of equilibria between the soil water and a body of water at fixed known negative pressure [Klute, 1986]. When this water pressure is expressed in an equivalent height of water column it is called head (of water). In the unsaturated soil the soil water has been partly replaced by air, which is at atmospheric pressure  $p_a$ . The Laplace surface tension equation couples the soil water pressure  $p_w$  to the air pressure:

$$p_a - p_w = 2 \times \gamma_{aw} / r_{aw} \quad (2.1.4)$$

with  $\gamma_{aw}$  the surface tension of the air water interface and  $r_{aw}$  the mean radius of curvature of the interfacial surface.

Thus the lower the water content, the smaller the mean radius of the pores which are filled with water and the higher the pressure difference between air and water and the higher the water retention. To obtain a large pressure difference (which is more convenient to measure) it is possible to increase the air pressure by placing the soil sample in a pressure chamber.

The soil water system is in hydraulic contact with the body of water via a water-wetted porous plate or membrane. At each equilibrium, the volumetric water content  $\theta_w$  of the soil is determined and paired with the value of the matric head  $h_m$ . (The matric head is the negative water pressure caused by the soil matrix, expressed in meters water.) The retention function shows hysteresis: the water content at a given pressure head for a wetting soil is less than that for a draining soil. In our experiments values were obtained for drying soils. In soils that contain a wide range of grain sizes, a release of water occurs at several decades of the pressure head  $h_m$ . In such cases it is convenient to use a logarithmic scale. The most used is the pF value:

$$pF = 10 \log(-h_m/h_0) \quad (2.1.5)$$

with  $h_0 = 1 \text{ cm}$ .

### 2.1.6 Hydraulic conductivity

The hydraulic conductivity  $k$  of a soil is a measure of its ability to transmit water [Klute, 1986]. It is dependent on the volumetric water content  $\theta_w$ , on the geometry of the pores and on the viscosity of the soil water. The hydraulic conductivity is defined by Darcy's law, which for one-dimensional vertical flow can be written as:

$$v = -k \frac{\partial (h_m + z)}{\partial z} \quad (2.1.6)$$

with  $v$  the volume flux density or apparent velocity (in m/s),  $h_m$  the matric head (see section 2.1.5) and  $z$  the gravitational head.

Measurement of the saturated hydraulic conductivity is based on the direct application of Darcy's law:

$$k = V_t l / (\Delta H) \quad (2.1.7)$$

with  $V_t$  the volume flux of water through the sample, with lenght  $l$  and cross-sectional area  $A$ , caused by a hydraulic head difference  $\Delta H = \Delta(h_m + z)$ .

### 2.1.7 Thermal conductivity

The thermal conductivity of a soil is a measure to its ability to transmit heat by conduction and is defined by Fourier's law:

$$Q = -\lambda \times \text{grad}(T) \quad (2.1.8)$$

with  $Q$  the heat flux density [ $\text{W m}^{-2}$ ],  $\text{grad}(T)$  the temperature gradient and  $\lambda$  the thermal conductivity.

It can be measured for instance with the nonsteady state probe method, which is well suited for measurements in moist porous media. The principle of this method is the measurement of the temperature response on an energy dissipation in the medium. To describe the temperature response mathematically Van Haneghem [1981] developed the modified Jaeger model. In this model three thermal properties are to be distinguished: the thermal conductivity  $\lambda$  and the heat capacity  $C$  of the porous medium (e.g. soil) and the contact resistance  $\Gamma$  between the measuring probe and the porous medium.

For the solution of  $\lambda$ ,  $C$  and  $\Gamma$  two situations are to be considered: the situation in which  $C$  is previously known and the one in which  $C$  is previously unknown. In the first situation accurate values for  $\lambda$  and  $\Gamma$  are obtained. If  $C$  is previously unknown,  $\lambda$  and  $\Gamma$  are determined to a lower degree of accuracy and an estimate of  $C$  is obtained. Bruijn et al. [1983] tried to cope with the problem by introducing their four regions-models. This gives an independent calculation to check the Jaeger model. However, the four regions model, though it is physically more attractive, results into only one equation with three unknowns. An iteration process, in which the modified Jaeger model and the four regions model

were used successively did not result into a stable solution. For measurements in frozen soils the accuracy of the simultaneous determination of  $\lambda$ , C and  $\Gamma$  is too low, because the latent heat effects both  $\lambda$  and C, while  $\Gamma$  is influenced by the changing structure of the medium. Therefore, an improved model for the nonsteady state probe method to measure thermal properties of porous media has to be developed. The result is presented in section 3.1. In that section also more details are presented about the measuring method itself.

## 2.2 Determination of soil water content by time-domain reflectometry

Soil water content is a very important property in many applications of soil science. It is relevant in road construction and in cleaning contaminated soil, as well as in research into the growth and vitality of plants. Until ten years ago, in general two methods had been used:

1. Gravimetric method: soil samples are (destructively) taken, weighed, dried in the oven and weighed again.
2. Neutron probe method: a neutron source is inserted into the soil, neutrons are scattered by H-nuclei (protons) of the water molecules and the scattered neutrons are registered. A large disadvantage of this method is the use of radioactive material, which requires very careful handling and extensive safety measures.

A promising *in situ* method to measure water content is Time-Domain Reflectometry (TDR). Topp et al. [1980] first introduced the method to measure the effective dielectric constant of the soil. This dielectric constant is a unique function of liquid water content for most soils, so that with TDR the liquid soil water content can be measured indirectly.

Time-domain reflectometry is based upon the velocity of propagation and reflection of an electromagnetic pulse along transmission lines. To understand the mechanism, the behaviour of an electromagnetic wave in transmission lines has to be discussed first. Secondly the signal needs to be analysed in such a way that its velocity of propagation in the soil can be measured and from this the dielectric constant of the soil can be determined. Thirdly, by extension, Dalton et al. [1984] have developed a method to obtain simultaneously the bulk electrical conductivity from analysing the amplitude of the reflected pulse.

### 2.2.1 Transmission line theory

In time-domain reflectometry high frequency waves are used, with frequencies up to the GHz range. These waves can travel along transmission lines. A long transmission line can be approximated as a system with different distributed electrical properties. It has a resistance  $R$  and a self inductance  $L$ . With respect to a reference potential, the transmission line has a capacitance  $C$  and a leak

resistance. To distinguish the leak resistance from internal resistance  $R$ , the former often is expressed as a conductance  $G$  [Dalton and Van Genuchten, 1986]. These electrical properties are all taken per unit of length. The electrical scheme of a parallel transmission line is shown in Fig. 2.2.1.

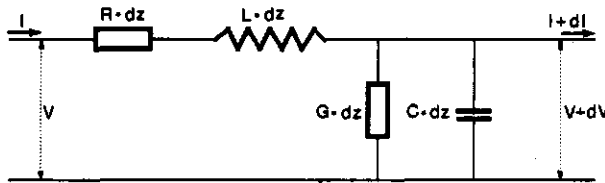


Fig. 2.2.1 Section  $dz$  of a long transmission line, with electrical current  $I$ , potential  $V$  and distributed electrical properties: self inductance  $L$ , capacitance  $C$ , resistance  $R$  and conductance  $G$ .

Both current  $I$  and potential  $V$  are a function of time  $t$  and distance  $z$ , as measured along the transmission line. The potential gradient in the transmission line over the distributed  $R$  and  $L$  can be written as (see Fig. 2.2.1):

$$\frac{\partial V}{\partial z} = -(I \times R + L \times \frac{\partial I}{\partial t}) \quad (2.2.1)$$

The interaction of the current with the reference potential is twofold: the current decreases due to the charging of capacitance  $C$ , and due to the leak through conductance  $G$ . This causes a gradient in current that can be written as:

$$\frac{\partial I}{\partial z} = -(C \times \frac{\partial V}{\partial t} + G \times V) \quad (2.2.2)$$

Equations (2.2.1) and (2.2.2) have only two independent parameters:  $I$  and  $V$ . To eliminate  $I$  (2.2.1) is differentiated with respect to  $z$  and (2.2.2) to  $t$ . Substitution then results in:

$$\frac{\partial^2 V}{\partial z^2} = L \times C \frac{\partial^2 V}{\partial t^2} + (R \times C + L \times G) \frac{\partial V}{\partial t} + R \times G \times V \quad (2.2.3)$$

Equation (2.2.3) can be seen as a wave equation. An analytical solution can be obtained when at position  $z=0$  a periodical, sinusoidal potential is applied. Then the potential along the transmission line can be written as:

$$V = V(z) \times \exp(i\omega t) \quad (2.2.4)$$

with  $V(z)$  the location dependent part of the solution,  $i=\sqrt{-1}$  and  $\omega$  the angular frequency.

For the location dependent part of the potential a new wave equation can be obtained by substituting (2.2.4) into (2.2.3) and dividing by  $\exp(it)$ :

$$d^2V(z)/dz^2 = [R(i\omega C + G) - \omega^2 L(C - iG/\omega)] \times V(z) \quad (2.2.5)$$

In order to solve  $V(z)$  (2.2.5) needs to be reworked. First, the total loss current between the two lines (sum of loss current through  $G$  and charging current through  $C$ ) can be seen as a complex variable consisting of real and imaginary components. Dalton and Van Genuchten [1986] introduced a complex relative dielectric constant to express the total loss current as a function of the potential:

$$\epsilon = \epsilon' - i\epsilon'' = C/C_0 - iG/(\omega C_0) \quad (2.2.6)$$

with  $C_0$  the capacitance in air,  $\epsilon'$  the real part of the dielectric constant (which is the conventional definition) and  $\epsilon''$  the imaginary part. Introducing  $\epsilon$  together with (2.2.4) into (2.2.2) a new expression for the gradient in electrical current can be obtained:

$$\partial I / \partial z = -i\omega \times \epsilon C_0 \times V(z) \times \exp(i\omega t) \quad (2.2.7)$$

Because the solution of (2.2.3) will include also higher harmonic functions (i.e  $V=V(z) \times \exp(i\omega nt)$ , with  $n$  an integer), the measured  $\epsilon''$  is larger than  $G/(\omega C_0)$ . The higher harmonic functions also contribute to the energy loss<sup>1</sup>).

<sup>1</sup>) To stress the importance of the energy consuming processes, Yanuka et al. [1988] introduced a definition for their imaginary part of the dielectric constant solely to account for these processes:  $\epsilon_Y'' = \epsilon'' - G/\omega C_0$

To obtain a solution of wave equation (2.2.3), the assumption is made that for high frequency waves the resistance  $R$  in the transmission line is considered to be negligible. In that case  $R \ll \omega L$  and, with use of the complex relative dielectric constant (2.2.6), wave equation (2.2.5) can be rewritten as:

$$\frac{d^2V(z)/dz^2}{ } = -\omega^2 L \times \epsilon_0 V(z) \quad (2.2.8)$$

The transmission line is now called a 'low loss line'. For this line (2.2.1) can be rewritten as:

$$(dV(z)/dz) \times \exp(i\omega t) = -i\omega L \times I(z) \times \exp(i\omega t) \quad (2.2.9)$$

with the assumption that  $I$  can be represented as  $I(z) \times \exp(i\omega t)$ .

The solution of (2.2.8) is the combination of waves traveling in positive and negative  $z$ -direction:

$$V(z) = V_+ \times \exp(-ikz) + V_- \times \exp(+ikz) \quad (2.2.10)$$

with  $V_+$  and  $V_-$  the amplitudes of the waves traveling in positive and negative directions, respectively, and with  $k$  the complex wave number:

$$k = \omega \sqrt{(LC_0 \epsilon)} \quad (2.2.11)$$

A wave travelling in the positive direction can now be expressed as:

$$V = V_+ \times \exp(i\omega t - ikz) \quad (2.2.12)$$

The velocity of this wave can be obtained from the condition  $i\omega t - ikz$  is constant. Differentiating this condition results in:

$$v = dz/dt = \omega/k \quad (2.2.13)$$

For non-magnetic materials, where the relative magnetic permeability equals one,  $LC_0 = 1/c^2$ , with  $c$  the speed of an electromagnetic wave in vacuum. Thus, with

use of (2.2.11) the absolute value  $|v|$  of the velocity of propagation in a medium with complex dielectric constant yields:

$$|v| = c/\sqrt{|\epsilon|} \quad (2.2.14)$$

## 2.2.2 Water content

For TDR applications in soils it is often reasonable to assume that  $\epsilon' \gg \epsilon''$  [Topp et al., 1980]. In such cases (2.2.14) reduces to  $v=c/\gamma\epsilon'$ . The authors quoted determined  $v$  using TDR by measuring the travel time of a signal in a known length of the transmission line. From the simplified eq (2.2.14) they calculated  $\epsilon'$ . They demonstrated empirically that  $\epsilon'$  was essentially a unique function of water content for a large variety of soils. A unique function can be expected because the dielectric constant of water is very different from that of the individual components of the soil: for air  $\epsilon_a=1$ , for the solid mineral particles  $\epsilon_s=4$  and for water  $\epsilon_w=81$  [Weast, 1978]. The measured dielectric constant is an effective value that depends on the volume fractions of the different components. Because  $\epsilon_s/\epsilon_a \ll \epsilon_w/\epsilon_a$  the effective dielectric constant is highly dependent on the volume fraction of water  $\theta_w$ . This is confirmed by the empirical relation of Topp et al. [1980]:

$$\epsilon = 3.03 + 9.3\theta_w + 146\theta_w^2 - 76.7\theta_w^3 \quad (2.2.15)$$

In order to obtain the dielectric constant, the velocity of propagation,  $v$ , has to be determined. This velocity is the length of the transmission line divided by the travel time. The way of determining the travel time is by analysing the influences of changing impedances on the signal and measuring on which point in the time-domain these changes occur. For non magnetic soils the characteristic impedance  $Z$  of the line can be obtained by dividing (2.2.9) by (2.2.7):

$$Z = \sqrt{\frac{\partial^2 V}{\partial I^2}} = \sqrt{\frac{i\omega L}{i\omega C_0}} = \frac{Z_0}{\gamma\epsilon} \quad (2.2.16)$$

with  $Z_0$  the impedance of the line in air or vacuum (where  $\epsilon=1$ ).

When a sudden change in impedance occurs in a transmission line, part of the wave is reflected back to the source, and the other part is transmitted. A change in impedance might be caused by a short in the transmission line, a junction between two succeeding lines or a change of the electrical properties of the transmission line itself. This impedance change (or discontinuity) can be approximated with a load impedance  $Z_L$  (see Fig. 2.2.2).

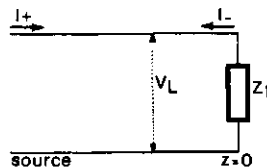


Fig. 2.2.2 Reflection in a transmission line caused by a load impedance  $Z_L$  at position  $z=0$ .

The impedance of the soil can also be expressed with use of a load impedance. Assuming a discontinuity at  $z=0$ , then with use of Kirchhoff's laws the following relations can be obtained for the potential  $V_L$ , the current  $I_L$  and the impedance  $Z_L$ :

$$V_L = V_+ + V_- \quad (2.2.17)$$

$$I_L = I_+ - I_- \quad (2.2.18)$$

$$Z_L = V_L / I_L \quad (2.2.19)$$

The impedance of the original transmission line itself is:

$$Z = V_+ / I_+ = V_- / I_- \quad (2.2.20)$$

The reflection coefficient  $V'$  can now be obtained by combining eq's (2.2.17) through (2.2.20) into its definition:

$$V' \equiv V_- / V_+ = (Z_L - Z) / (Z_L + Z) \quad (2.2.21)$$

In time-domain reflectometry this reflection coefficient is measured as a function of time. In Fig. 2.2.3 is shown where the impedance mismatches occur, when a transmission line is inserted in the soil. With use of (2.2.16) and (2.2.21) the TDR signal can be explained. For an impedance mismatch at distance  $x$ , the wave has to travel back and forth to this position and the reflection is registered at time  $t=2x/v$ . In soils the effective dielectric constant varies between 4 (dry soil) and 30 (saturated soil), which is always higher than in air ( $\epsilon=1$ ). With use of eq (2.2.16) it can be seen that even in non-conducting soils the impedance of the transmission line is smaller, than the impedance in air. Thus, at the position where an electromagnetic wave enters the soil, the reflection coefficient will decrease sharply (see eq (2.2.21)). At the open end of the transmission line (which results in a very high load impedance) the reflection coefficient will increase sharply.

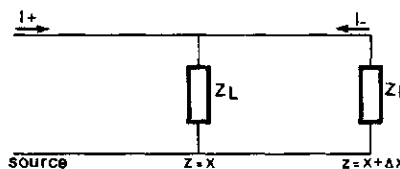


Fig. 2.2.3 Changes in Load impedance  $Z_L$  for a parallel transmission line partly inserted in soil, with at  $z=x$  transmission line enters soil and  $z=x+\Delta x$  open end of transmission line.

The travel time to both positions can be measured with a cable tester, and so the velocity of propagation in the soil can be calculated. Then with use of eq (2.2.14) the in situ dielectric constant of the soil can be obtained. The experimental procedure of TDR will be described in section 3.2.

### 2.2.3 Bulk electrical conductivity

The voltage  $V$  of the TDR signal in soils is weaker at higher bulk soil electrical conductivities [Dalton and Van Genuchten, 1986]. In other words the signal

is attenuated when travelling through a conductive medium. The attenuation of a wave travelling a distance  $dz$  in positive direction along the transmission lines can be written with use of 2.2.10 as:

$$\frac{V(z+\Delta z)}{V(z)} = \text{Re}[\exp(-ik\Delta z)] \quad (2.2.22)$$

Thus, the attenuation coefficient is defined as  $\alpha \equiv \text{Re}(ik)$  or with use of eq (2.2.11):

$$\alpha = (\omega/c) \text{Im}\{\sqrt{\epsilon}\} \quad (2.2.23)$$

Assuming that important conduction losses take place in the parallel transmission lines in soil, where the wave is reflected at the end of the transmission line (thus  $\Delta z = 2 \times 1$ ) the attenuated signal  $V_\alpha$  can be written as follows:

$$V_\alpha = V_0 \times \exp(-2\alpha l) \quad (2.2.24)$$

with  $V_0$  the potential amplitude when no attenuation takes place.

An approximate relation for  $\alpha$  applicable to steady-state sinusoidal input conditions and low loss lines is given by [Ramo and Whinnery, 1959]:

$$\alpha = (RC + GL)/(2\sqrt{LC}) \quad (2.2.25)$$

Expressions for  $L$ ,  $C$  and  $G$  for parallel transmission lines are, respectively [Dalton and Van Genuchten, 1986]:

$$L = (\mu_0 u / \pi) \times \cosh^{-1}(s/d) \quad (2.2.26)$$

$$C = (\pi \times \epsilon_0 \epsilon) / \cosh^{-1}(s/d) \quad (2.2.27)$$

and

$$G = (\pi \times \sigma) / \cosh^{-1}(s/d) \quad (2.2.28)$$

with  $\mu_0$  the magnetic permeability in a vacuum ( $\mu_0 = 4\pi \times 10^7 \text{ H/m}$ ),  $\mu$  the relative magnetic permeability of the soil,  $\epsilon_0$  the dielectric constant in a vacuum ( $\epsilon_0 = 10^9 / 36\pi \text{ F/m}$ ),  $\sigma$  the bulk electrical conductivity of the soil (in  $\text{S/m}$ ),  $s$  the spacing between the two lines and  $d$  the diameter of one line. For most soils  $\mu=1$ . Substituting (2.2.26), (2.2.27) and (2.2.28) into (2.2.25) and assuming  $\text{RC} \ll \text{GL}$  the following expression of the attenuation coefficient is obtained:

$$\alpha = (\sigma/2) \times \sqrt{\eta_0/\epsilon} \quad (2.2.29)$$

$$\text{with } \sqrt{\eta_0} = \sqrt{\mu_0/\epsilon_0} = 120 \pi \Omega$$

However, the procedure to measure as proposed by Dalton and Van Genuchten [1986] is not very accurate. Recently Topp et al. [1988] proposed the 'thin sample' approach, which gives more accurate results. A disadvantage is the rather extensive measuring procedure. A simplified method which is as accurate as the 'thin sample' approach is presented in section 3.2.

### 2.3 Transfer of heat and mass

During freezing, the heat and mass transfer and the variation of stresses and temperatures are all interrelated. Thus, analyses must deal with the coupling of all these effects. The mathematical model needs several systems of equations to express the interrelations.

To keep the mathematical model as simple as possible, only variations in the vertical direction ( $z$ ) are considered, so that a one dimensional model can be built. This is allowed because in real soils most of the transport phenomena caused by freezing occur in the vertical direction. Furthermore, the temperature and pressure gradients are much more important in the vertical direction than in the horizontal. And in general, even the soil structure has its largest variation perpendicularly to the soil surface.

In Fig. 2.3.1 the most important physical parameters for the freezing process can be seen as a function of position: temperature  $T$ , hydraulic conductivity  $k$  and water pressure  $p_w$ . Consider a constant heat flux leaving the soil at the (upper) soil surface, which causes the soil to freeze. The two major processes during soil freezing are: the penetration of the  $0^\circ\text{C}$  isotherm and the growth of ice lenses. The formation of pure ice at the upper soil surface is called primary heave, while the formation of ice lenses inside the soil (at a certain overburden pressure) is called secondary heave. During the penetration of the  $0^\circ\text{C}$  isotherm (at  $z=X$ ) free pore water freezes. In this process latent heat is released, which is transported by conduction towards the cold upper surface of the soil column. Therefore, the temperature gradient becomes larger at the cold side of  $X$ . During the growth of an ice lens (at  $z=S$ ) water freezes at temperature  $T_s < 0^\circ\text{C}$ . Again latent heat is released, which has to be transported by conduction. Thus, at  $z>S$  the temperature gradient is larger than at  $z < S$  (see Fig. 2.3.1). The freezing soil can now be divided in three zones: The unfrozen zone at  $z < X$  and  $T > 0^\circ\text{C}$ , the frozen fringe at  $X > z > S$  and the frozen zone at  $z > S$  and  $T < T_s$ . In the latter zone absence of transport of liquid water is assumed.

If a ground water table with external water supply is situated not far from the frost front, the unfrozen zone in the soil is saturated with water. Therefore the hydraulic conductivity  $k$  can be considered constant at  $T > 0^\circ\text{C}$ . At  $T = 0^\circ\text{C}$   $k$

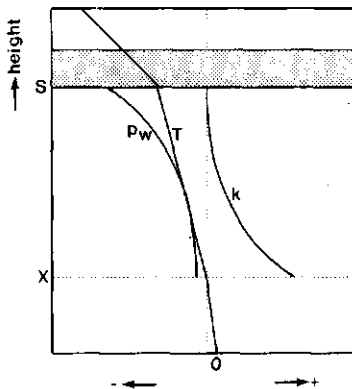


Fig. 2.3.1 Changes of temperature  $T$ , hydraulic conductivity  $k$  and pressure  $p_w$  in the frozen fringe as function of position  $z$  during an advancing freezing front. With  $S$  the position of the warm side of the lens and  $X$  the position of the freezing front.

decreases stepwise some orders of magnitude. At  $T < 0^\circ\text{C}$  the hydraulic conductivity decreases exponentially with temperature [Nixon, 1988]. Because the water flux density is continuous, the product of  $k$  and pressure gradient  $\text{grad}(p_w)$  has to be constant (Darcy's law). This results in a maximum value of  $\text{grad}(p_w)$  at the minimum value of  $k$ . Also a an opposite curvature of  $p$ -curve (with respect to  $k$ -curve) is caused by this continuity demand (see Fig. 2.3.1).

### 2.3.1 Moisture transport

For the moisture transfer, only liquid water flow driven by a gradient in unfrozen water pressure is considered. Vapor transport is neglected, because the absolute vapor pressure is very low. The moisture transport equation can be written as follows [Sheppard et al., 1978]:

$$\frac{\partial}{\partial t} \left( \theta_w + \frac{\rho_i}{\rho_w} \theta_i \right) = - \frac{\partial v}{\partial z} \quad (2.3.1)$$

with  $\rho_i$  the density of ice,  $\theta_i$  the volumetric ice content and  $v$  the apparent or superficial velocity of the soil water, or water flux density (volume flow of

water per area of soil). When the gravitational potential is also neglected, (2.3.1) can be rewritten with use of Darcy's law (2.1.6) as:

$$\frac{\partial}{\partial t} (\theta_w + \frac{p_i}{p_w} \theta_i) = \frac{\partial}{\partial z} (k \times \frac{\partial h_m}{\partial z}) \quad (2.3.2)$$

with  $k$  the hydraulic conductivity and  $h_m$  the pressure head of water.

Miller [1972] suggested that the driving force for ice lens growth was the difference between ice and liquid water pressure caused by surface tension. This is the so-called capillary model. According to this model, when ice attempts to penetrate into small pores, capillary suction is developed due to the curvature of the ice-water interphase, and water is drawn towards the ice front (Fig. 2.3.2). At the ice-(liquid) water interface, local pressures in the ice  $p_i$  and in the unfrozen water  $p_w$  are linked according to the Laplace surface tension equation:

$$p_i - p_w = 2 \times \gamma_{iw} / r_{iw} \quad (2.3.3)$$

with  $\gamma_{iw}$  the surface tension of the ice-(liquid) water interface and  $r_{iw}$  the mean radius of curvature. This radius depends not only on the size of the soil particles and pore space, but also on temperature (Fig. 2.3.2). Miller [1972] called the test of eq (2.3.3) at isotherm conditions 'encouraging' in (soil) samples where the variation in particle size (and hence in  $r_{iw}$ ) was small. However, when the variation in  $r_{iw}$  is larger, a discrepancy was observed between pore sizes computed from desorption curves and the  $r_{iw}$  values of (2.3.3). The heaving forces developed by the growing ice lenses were large compared with the forces indicated with this equation.

Another origin for the observed heaving pressure needed to be found. Kay and Groenevelt [1974] used the thermodynamic treatment to determine water pressures that accompany freezing point depression. In this way they derived three independent Clapeyron equations in frozen soils for the equilibria between ice (i), liquid water (w) and vapor (v). When the vapor phase is assumed to remain at constant (e.g. at saturation pressure at 0°C), only the ice-water equilibrium has to be considered. This equilibrium is given with the identity in chemical potential (or free enthalpy) of the solid and liquid water phase. Using the

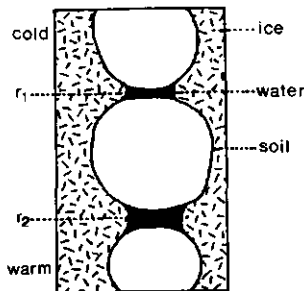


Fig. 2.3.2 Schematic cross section of frozen soil with a vertical temperature gradient, showing the capillary model [Miller, 1972]. The radius of curvature of the ice-water interface is smaller at lower temperatures:  $r_1 < r_2$ .

Gibbs-Duhem equation the identity can be given in differential form as [Kay and Groeneveld, 1974]:

$$\bar{V}_w \times (dp_w - d\pi) - \bar{V}_i \times dp_i = (\bar{\Sigma}_w - \bar{\Sigma}_i) dT \quad (2.3.4)$$

with  $\bar{V}$  the partial specific volume on a differential basis,  $\bar{\Sigma}$  the partial specific entropy,  $p$  the pressure ( $p_w = h_m/A$ ,  $A = 1*10^{-4}m^3/N$ ),  $\pi$  the osmotic pressure and  $T$  the temperature. The difference in specific entropy is due to the latent heat of fusion  $L$ :

$$(\bar{\Sigma}_w - \bar{\Sigma}_i) dT = L \times dT/T \quad (2.3.5)$$

If the partial specific volume is considered to be constant, the specific density can be used:  $\rho = 1/\bar{V}$ . Now (2.3.4) and (2.3.5) can be combined into a new differential equation:

$$d(p_w - \pi) - (\rho_w/\rho_i) dp_i = (\rho_w L/T) dT \quad (2.3.6)$$

In contrary with the equilibrium between free water and ice, it follows from (2.3.6) that for soils at  $dT = 0$  the ice pressure is not equal to the liquid

water pressure (this agrees with Miller [1972], see eq (2.3.3)). At  $dT = 0$   $d(p_w - \pi) = (\rho_w/\rho_i) \times dp_i$ . To integrate (2.3.6) the following assumptions need to be made:  $\rho_w$ ,  $\rho_i$  and  $L$  are constant. For  $L$  this assumption is only valid if the temperature interval considered is small ( $\Delta T \ll 10^\circ\text{C}$ ). Integrating (2.3.6) then results in the form in which the Clapeyron equation is often represented:

$$(p_w - \pi) = \rho_w L \times \ln(T/T_0) + (\rho_w/\rho_i) \times p_i + \text{Constant} \quad (2.3.7)$$

with  $T_0$  the freezing temperature of the bulk water ( $T_0 \approx 273\text{ K}$  if  $\pi=0$ ).

The integration constant can be obtained from the boundary conditions at  $T=T_0$  and  $T=T_s$ .  $T=T_0 (\approx 273\text{ K})$  can be considered as the reference state, with height  $z=X$ . When a constant water table is present at  $z=0$ , the reference pressure head equals  $h_m = -X$ , or  $p_w = -X/A$ . If it is assumed that no solutes are dissolved in the water ( $\pi=0$ ), the equilibrium ice pressure can now be calculated using (2.3.6):  $p_i = -(\rho_i/\rho_w)(X/A)$ . (Thus the ice pressure can be negative, which is in contrast with the often made assumption of zero ice pressure [e.g. Konrad and Morgenstern, 1980]). Using these boundary conditions into (2.3.7), it can be shown that the constant equals zero. Regarding the temperature domain we are interested in ( $T \approx T_0$ ),  $\ln(T/T_0)$  can be approximated by  $(T-T_0)/T_0 \ll 1$ , so (2.3.7) can be simplified into:

$$p_w = \rho_w L \times (T-T_0)/T_0 + (\rho_w/\rho_i) \times p_i \quad (2.3.8)$$

Among others, Konrad and Morgenstern [1981] have used this integrated form of the Clapeyron equation to derive the pressure gradient that causes heave. They introduced the following assumptions:

1. Water flow is continuous across the frozen fringe, and therefore accumulates at the base of the ice lens.
2. The frozen fringe can be characterised by an overall hydraulic conductivity  $k_{ff}$ , which is an effective value.
3. The temperature conditions at the interface between ice lens and the frozen fringe may be characterised by a particular segregation freezing temperature  $T_s$ , at the warm side of the ice lens (position S in Fig. 2.3.1).
4. There are no solutes dissolved in the water ( $\pi=0$ ).

Then it can be stated that at the moment heave occurs, the mechanical pressure or overburden needs to be equal to the equilibrium ice pressure at the warm side of the ice lens, so that:  $p_i(S) = p_{load}$  or, with use of (2.3.8):

$$p_w(S) = (\rho_w/\rho_i) p_{load} + \rho_w L (T_s - T_0) / T_0 \quad (2.3.9)$$

The equilibrium water pressure at freezing front X has been defined already as:

$$p_w(X) = -X/A \quad (2.3.10)$$

From (2.3.9) and (2.3.10) the pressure gradient over the frozen fringe can now be expressed as:

$$\frac{p_w(S) - p_w(X)}{\Delta z} = \frac{\rho_w \times p_{load}}{\rho_i \times \Delta z} + \frac{X}{A \times \Delta z} + \frac{\rho_w L}{T_0} \times \frac{\Delta T}{\Delta z} \quad (2.3.11)$$

with  $\Delta z$  the thickness of the frozen fringe ( $\Delta z = S - X$ ).

Because of the large value of L, in general the first two terms of the right hand side of the above equation are much smaller than the third term, so the pressure gradient over the frozen fringe is in some approximation proportional to the temperature gradient:

$$\frac{\partial p_w}{\partial z} = (\rho_w L / T_0) \times \partial T / \partial z \quad (2.3.12)$$

in which  $\rho_w L / T_0 = 1.22 \times 10^6 \text{ Pa/K}$  is a constant.

Konrad and Morgenstern [1981] used the proportionality in deriving the relationship between water intake flux  $v$  and temperature gradient. (Instead of the water intake flux, also the heave rate  $dh/dt$  can be used:  $dh/dt = (\rho_w/\rho_i) \times v$ ). This may be expressed as:

$$v = -SP \times \partial T / \partial z \quad (2.3.13)$$

with  $SP$  the segregation potential.

The effective hydraulic conductivity of the frozen fringe  $k_{ff}$  can now be obtained by combining Darcy's law with eq's (2.3.12) and (2.3.13):

$$k_{ff} = (g \times T_0 / L) \times SP \quad (2.3.14)$$

with  $g \times T_0 / L = 8.2 \times 10^{-3}$  K/m

Konrad and Morgenstern [1981] showed, that the difference between ice pressure  $p_i$  and water pressure  $p_w$  is linearly proportional to the subzero temperature (see also eq 2.3.8). Because the temperature gradient in the frozen fringe is considered constant,  $\Delta p = p_w - p_i$  will then vary linearly with position. Now the ice pressure as a function of position  $z$  can be calculated by a simple subtraction:  $p_i(z) = p_w(z) - \Delta p(z)$ .

The different pressures can be seen in Fig. 2.3.3. The ice pressure first increases with increasing height, reaches a maximum indicated with  $S'$ , and then decreases. When the maximum ice pressure is high enough to lift the overburden pressure of the soil layers above  $S'$  and also high enough to create at the same time a discontinuity in the soil structure, a new ice lens is created on  $S'$ . Using a stress partition function, Nixon [1988] comes to similar pressure functions as shown in Fig. 2.3.3. However, the mechanics of frozen soil, in which the complicated interaction of stresses and strains could be explained, is beyond the scope of this thesis.

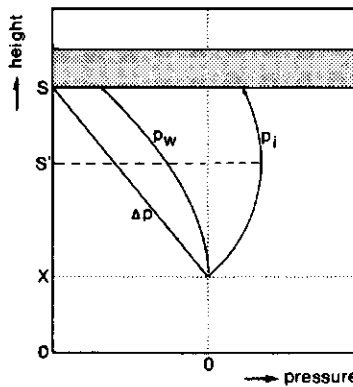


Fig. 2.3.3 Different pressures in the frozen fringe as a function of position  $z$ . With  $S$  and  $S'$  the position of the warm sides of the old lens and new lens, respectively,  $p_w$  liquid water pressure,  $\Delta p$  pressure difference determined by Clapeyron equation (2.3.8) and  $p_i$  ice pressure.

When the frost front is still advancing, the frozen fringe becomes thicker. This causes a decrease in the average hydraulic conductivity of the frozen fringe. At the same time the suction at the warm side of the ice lens hardly increases, so that the volume flux of water towards the ice lens decreases. This causes on its turn a reduction in the release of latent heat, thus the freezing front can penetrate even faster. At the same time the maximum ice pressure increases. This process continues until a new lens is created at  $S'$  (see Fig. 2.3.3). When a new ice lens is formed, the effective hydraulic conductivity of the frozen fringe increases sharply and this causes a large increase in water flux density.

In a real soil the growth of ice lenses does not have such a discontinuous behaviour as in our one dimensional model. Because of inhomogeneities ice lenses will start to grow at different temperatures. The orientation of the ice lenses will not be perfectly horizontal and also the isotherms will not be straight lines. Due to these inhomogeneities the heat flux and the heave rate will be more averaged. However, the one dimensional model is an important tool to understand the complex behaviour of freezing soils.

Resuming, it can be concluded that three major theories are used to explain the secondary heave. Firstly Miller [1972] demonstrated that ice lenses grow at temperatures below  $0^{\circ}\text{C}$  and he developed the concept of the frozen fringe. Secondly, Kay and Groenevelt [1974] provided with use of thermodynamics the theoretical background for suction of liquid water towards the ice lens. And thirdly, Konrad and Morgenstern [1980] used this theory in their segregation potential concept to link the heave rate to a macroscopic temperature gradient.

### 2.3.2 Heat transport

For the case in which convective heat transfer by vapor and ice transport is negligible and in which all liquid water that accumulates at any position  $z$  freezes, the heat balance equation in a frozen soil can be written as [Kay et al., 1981]:

$$C \frac{\partial T}{\partial t} + L \times \rho_w \frac{\partial \theta_w}{\partial t} = \frac{\partial}{\partial z} (\lambda \frac{\partial T}{\partial z} - L \times \rho_w \times v - C_w \times T \times v) \quad (2.3.15)$$

with  $C$  the effective volumetric heat capacity of the soil,  $T$  the temperature,  $t$  the time,  $L$  the latent heat of fusion of water,  $\rho_w$  the density of water,  $\theta_w$  the volume fraction of water,  $\lambda$  the effective thermal conductivity of the soil,  $v$  the apparent or superficial velocity of water and  $C_w$  the volumetric heat capacity of water.

The left hand side of equation (2.3.15) accounts for an increase in temperature of the medium and for the latent heat required to melt ice. The right hand side consists of the conduction term and the convection terms of latent heat and sensible heat, respectively. To obtain a solution of (2.3.15) values for  $\lambda$  and  $C$  are needed. The real values of these parameters can not be found by the usual measuring methods, due to melting of small quantities of ice during the measurement itself. Since the melting effect also plays a role during the process of heat transport (see eq (2.3.15)), Kay et al. [1981] introduced the use of an apparent heat capacity  $C'$  and an apparent thermal conductivity  $\lambda'$ , to explain the measured values of the thermal properties of frozen soils.

The apparent heat capacity can directly be measured with use of a calorimeter. A calorimeter is based on measurement of the temperature change in a sample due to a given heat input. When a sample is heated at an initial temperature just below  $0^\circ\text{C}$  a small amount of ice will melt in order to obtain a new thermodynamic equilibrium between water and ice in the soil. The temperature rise in the sample will be less than in a situation without melting ice. This results in an apparent heat capacity  $C'$ , which is higher than the real heat capacity  $C$ :

$$C' = C + \rho_w L (\partial \theta_w / \partial T) \quad (2.3.16)$$

The apparent thermal conductivity is also influenced by melting of small amounts of ice at temperatures close to  $0^\circ\text{C}$ . Then coupled transport of latent heat in soils occurs as a result of water migration. Horiguchi and Miller [1980] were the first to demonstrate experimentally this transport of heat due to a water flux. The significance of convective transport of latent heat due to liquid water flow during the measurements of thermal conductivity was proved by Kay et al. [1981]. These authors incorporated the coupled transport with use of the Clapeyron equation and Darcy's law into an apparent thermal conductivity. Like

the apparent heat capacity, the apparent thermal conductivity  $\lambda'$  is also higher than the real thermal conductivity:

$$\lambda' = \lambda + L^2 \rho_w^2 A \times k / T_0 \quad (2.3.17)$$

Van Haneghem and Leij [1985] measured this apparent thermal conductivity in glass beads. However, measurements in soils are scarce. In sections 4.1 and 4.2 our measurements of the apparent thermal conductivity in five different soils and in crushed concrete will be presented.

In general, convection of sensible heat can be neglected with respect to heat conduction. However, close to the freezing front the convection of latent heat may be important. The modified Fourier equation based on the apparent thermal parameters must then be written as:

$$C' \partial T / \partial t = \partial / \partial z (\lambda' \times \partial T / \partial z) \quad (2.3.18)$$

When temperature differences within the soil are not too large, the apparent thermal conductivity  $\lambda'$  can be considered constant (the approximation depends on the magnitude of  $\partial \lambda' / \partial T$ , which must be small). We call this situation the quasi steady state condition for  $\lambda'$ . Under (quasi) steady state conditions for the thermal properties, the modified Fourier equation can be integrated over  $z$ , and a constant heat flow  $Q$  is obtained. In frozen soils, apart from heat conduction, the local release of internal (latent) heat contributes substantially to the heat balance. As a first approximation it is sufficient to distinguish two different locations, where ice formation takes place and where the latent heat is released [Konrad and Morgenstern, 1980]. Firstly, where the ice lens is being formed, the release of latent heat  $Q_h$  is related to the heave rate:

$$Q_h = -\rho_i L (dh / dt) \quad (2.3.19)$$

Secondly, at the advancing freezing front (at penetration rate  $dX / dt$ ) pore ice is being formed. This causes a release of latent heat  $Q_L$ , which originates from the second term of the apparent heat capacity:

$$Q_L = -\rho_w \theta_w L (dX / dt) \quad (2.3.20)$$

In this equation it is assumed that all pore water freezes at once. However, this is not always the case. In general, it is better to deal with the formation of pore ice by considering the entire part of the soil, where the  $d\theta_w/dT$ -relation has a significant value. The total decrease of liquid water content  $\Delta\theta_w$  must then be calculated in this area. In this case  $Q_L$  can be approximated as:

$$Q_L = -\rho_w \Delta\theta_w L (dX/dt) \quad (2.3.21)$$

with  $\Delta\theta_w$  the decrease in unfrozen water content in a relevant time interval. It should be noted that  $\Delta\theta_w$  is a function of  $z$ .

Because  $Q_L$  is dissipated over a finite length of the soil column, the derivation of a heat balance equation with constant heat flows is quite complicated. The most simple approach is to compare the heat flow by conduction in the frozen part (subscript f) with the one in the unfrozen part (subscript u, see also Fig. 2.3.4). The equation 'jumps over' the frozen fringe, where the complicated freezing processes occur. In (deep) frozen soil  $d\theta_w/dT$  is negligible, because all pore water has been frozen already. Then, the heat balance for the frozen fringe can be written as:

$$-\lambda_f (\partial T / \partial z)_f + \lambda_u (\partial T / \partial z)_u = \rho_i L (dh/dt) - \rho_w \Delta\theta_w L (dX/dt) \quad (2.3.22)$$

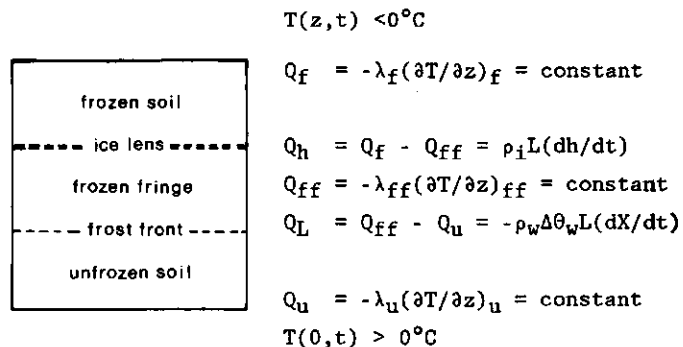


Fig. 2.3.4 Heat balance equations for the one dimensional frost heave model, in which  $X$  the time dependent position of the frost front and  $S$  the position of ice segregation. Because quasi steady state conditions are assumed no capacitive heat storage occurs.

In Fig. 2.3.4 all relevant heat balance equations are shown, together with the boundary conditions. This system of equations has to be solved together with the equations of mass transport, described in section 2.3.1. These coupled equations can only be solved analytically for some very special one dimensional cases. In general, the equations are solved numerically using a finite difference or a finite element method. These numerical solutions are beyond the scope of this thesis, but some recent literature is given as an overview of possibilities:

1. Lewis and Sze [1988] presented nonlinear flux equations to describe the moisture flux characteristics in the frozen fringe.
2. Pikul et al. [1989] evaluated field experiments of heat interaction between frozen soil and atmosphere in daily freeze-thaw cycles.
3. Duquennoi et al. [1989] evaluated the profit of insulation on the temperatures near the foundation of a house.
4. Shen and Ladanyi [1989] analysed numerically the temperature field in a thawing highway embankment.
5. Sheng et al. [1989] used finite difference methods to evaluate the insulation effect of a layer of expanded clayballs in a road in North Sweden.
6. Jessberger et al. [1988] predicted and followed with use of the finite element method temperature fields in an artificial frozen soil structure for the stabilisation of the soil on top of two parallel metro tunnels in Vienna.

### 2.3.3 Solute transport

In the transport of solutes two mechanisms are important: convective (advective) transport and diffusive transport [Klute, 1986]. Convective transport  $J_s$  refers to the coupled transport of solutes with the flowing soil water (also called reverse osmosis):

$$J_s = v \times SC \quad (2.3.23)$$

with SC the local volume averaged solute concentration in  $[kg/m^3]$ .

Diffusive transport ( $J_D$ ) is the process that results from the thermal motion of dissolved ions and water molecules. Diffusive transport in soils tends to decrease existing concentration gradients and can be described by:

$$J_D = -\theta_w \times D_m \times (\partial SC / \partial z) \quad (2.3.24)$$

with  $D_m$  the porous medium molecular diffusion coefficient.

Another transport mechanism that must be mentioned is dispersion. Dispersive transport ( $J_h$ ) results from the variations in local fluid velocities inside the pores. Every pore has a different shape and size, thus the velocity distribution will vary from pore to pore.

These variations cause the ions to be transported down-gradient at different rates, thus leading to a mixing process that is macroscopically similar to mixing caused by molecular diffusion. Dispersion is a passive process, that, unlike diffusion, only occurs during water movement [Klute, 1986]. Mixing caused by local velocity variation is often called mechanical dispersion. It is shown that dispersive transport can be described with an equation similar to (2.3.24):

$$J_h = -\theta_w D_h \times (\partial SC / \partial z) \quad (2.3.25)$$

Substituting eq's (2.3.23), (2.3.24) and (2.3.25) into the continuity equation, the following expression can be obtained:

$$\frac{\partial}{\partial t} (\theta_w SC + \rho_s \times SC_a) = \frac{\partial}{\partial z} (\theta_w \times D \frac{\partial SC}{\partial z} - v \times SC) \quad (2.3.26)$$

with  $D$  the dispersion or dispersion-diffusion coefficient:  $D=D_m+D_h$ ,  $SC_a$  the adsorbed concentration of ions and  $\rho_s$  the density of the soil mineral particles.

The osmotic potential  $\pi$  in dilute solutions is directly proportional to the solute concentration (Van 't Hoff's law):

$$\pi = SC \times R \times T / m^o \quad (2.3.27)$$

with  $R$  the gasconstant ( $R=8.31 \text{ J/mol K}$ ) and  $m^o$  the molar weight.

The solute concentration on a water basis  $SC$  can be changed by two reasons: the available volume fraction of liquid water is changing and the amount of ions may change on a bulk bases.

In unfrozen conditions  $SC = SC^0 / \theta_w$ , with  $SC^0$  the local concentration on a bulk basis. If we assume that the penetration of the frost front takes place at a much higher rate than the macroscopic solute redistribution process, it is allowed as a first approximation to consider  $SC^0$  constant at any place.

Microscopic redistribution takes place because inside the pores all solutes concentrate in the unfrozen water. In the frozen soil the solute concentration on unfrozen water basis  $SC_u$  will then be:  $SC_u = SC^0 / \theta_u$ . Because  $SC^0$  is considered constant, and salts dissolve much easier in liquid water than in ice, the solute concentration on liquid water basis will be very high in the volume element just behind the frost front (still no macroscopic redistribution is assumed):

$$SC_u = SC \times \theta_w / \theta_u \quad (2.3.28)$$

with  $\theta_w$  the liquid water content in the volume element concerned, before the soil was frozen.

Of course, this increase in  $SC_u$  causes a gradient in osmotic pressure, which will act as a driving force in the (macroscopic) redistribution of solutes.

### 3 NEW MODELS AND METHODS

#### 3.0 Introduction to the chapter

This chapter starts with three separate papers, in which new developments of different measuring techniques are described. Each paper has been restyled into the lay out of this thesis and some minor errors have been corrected. The papers can be found in the following sections:

- 3.1 Loon W.K.P. van, Haneghem I.A. van and Schenk J., 1989b. A new model for the nonsteady state probe method to measure thermal properties of porous materials, *Int. J. Heat Mass Transfer* 32, pp 1473-1481.
- 3.2 Loon W.K.P. van, Perfect E., Groenevelt P.H. and Kay B.D., 1990b. A new method to measure bulk electrical conductivity in soils with time-domain reflectometry, *Can. J. Soil Sci.* 70, pp 403-410.
- 3.3 Loon W.K.P. van, Perfect E., Groenevelt P.H. and Kay B.D., 1991. Application of dispersion theory to time-domain reflectometry, *J. Porous Media* (in press).

Section 3.4 has been written exclusively for the thesis. In this section the experimental set up and the materials, used for the majority of the experiments, are described.

### 3.1 A new model for the nonsteady-state probe method to measure thermal properties of porous media

#### 3.1.0 Abstract

The starting point is the modified Jaeger model. This cylindrical model takes into account the major properties of the probe, the thermal conductivity and the heat capacity of the medium and the contact resistance between the probe and the medium. Because the mathematical description results in nonlinear functions of these three thermal parameters, the Gauss-Newton iteration method has been used. To obtain a better description of the measurement for small time values, a second order time correction has been added. The experimental test results in an inaccuracy of 0.5 to 2% for the thermal conductivity, while the two other parameters were accurate to within 5 to 15%.

#### Nomenclature

symbol	description	unit
$a$	thermal diffusivity of the medium	$\text{m}^2\text{s}^{-1}$
$C$	volumetric heat capacity	$\text{J m}^{-3}\text{K}^{-1}$
$d$	iteration step in the Gauss-Newton method $d=(\Delta\lambda, \Delta C, \Delta T)$	-
$F$	mathematical description of the temperature response; a nonlinear function of the state vector $\underline{x}$	K
$Q$	heat production per unit length	$\text{W m}^{-1}$
$R$	effective distance between temperature sensor and heating wire	m
$s$	radius of the heating wire	m
$t$	time	s
$t_b$	time of the first measuring point for which the model is valid	s
$u$	inside radius of the tube	m
$v$	outside radius of the probe	m
$W$	internal heat resistance per unit length between the temperature sensor and the outer wall of the probe	$\text{K m W}^{-1}$
$\underline{x}$	state vector $\underline{x}=(\lambda, C, \Gamma)$	-

symbol	description	unit
$\Gamma$	(external) contact resistance per unit length	$\text{K m W}^{-1}$
$\Gamma_t$	total heat resistance per unit length	$\text{K m W}^{-1}$
$\theta$	measured temperature response	K
$\theta^0$	theoretical zeroth order temperature response	K
$\theta'$	theoretical first order temperature response	K
$\theta''$	theoretical second order temperature response	K
$\lambda$	thermal conductivity	$\text{W m}^{-1}\text{K}^{-1}$
$\tau$	dimensionless time, $\tau=4at/v^2$	-
$\tau'$	modified dimensionless time	-
$\tau''$	second modified dimensionless time	-
$\Phi$	sum of squares of the differences between model results and measuring points	$\text{K}^2$

#### subscripts

j	iteration step j	n	needle shaped probe
is	insulating material	tu	tube
hw	heating wire		

#### 3.1.1 *Introduction*

In the nonsteady state probe method a needle shaped probe is embedded in the material to be examined. The probe consists of a heating wire and a temperature sensor, which are fitted into a long, thin tube. To fix the position of the wires and to prevent electrical contact, the remaining space inside the tube is filled with an insulating material.

Characteristic for the nonsteady state probe method is the measurement of the temperature response of the probe on a suddenly changing energy dissipation in the probe. This response is a function of the dimensions and the thermal properties of the probe, the thermal properties of the medium and the thermal contact resistance between probe and medium.

Nonsteady state probe methods are widely employed for thermal conductivity measurements in dry or wet porous media. In technical science for instance it can be applied to measure the insulating properties as well as the heat storage properties of building materials. In geology a thorough knowledge of the thermal parameters of the various strata may be obtained by this method, which is useful for studies in earth history, for predicting earth quakes and for research on oil bearing layers. In agriculture, the thermal parameters of the soil must be determined for studies about the heat balance at the earth's surface, frost penetration and storage of agricultural products and foods.

Thermal conductivity measurements with the probe method have several advantages. The method can be used *in situ*, the measuring time is rather short and, compared with other kinds of thermal conductivity measurements, this method is in a high degree non-destructive to the material examined. Apart from these, the possibility to gain simultaneously values for the volumetric heat capacity can be mentioned. However, up to now the accuracy of the determination of this latter physical property remains poor. In this paper a more reliable simultaneous determination of heat capacity and thermal conductivity is presented.

### *3.1.2 Present approach*

Several mathematical models have been developed to calculate the thermal parameters of the medium. The simple, perfect line source analysis is still often used. However, for dry materials the accuracy is not so high: accurate results for the volumetric heat capacity are hard to obtain and the contact resistance does not occur in this model.

More accurate results can be obtained from the theoretical approach of Blackwell [1954], Jaeger [1956] and De Vries and Peck [1958].

They started all from a cylindrical model of the measuring probe, which allows to account for the different thermal properties of the probe and the surroundings. The dimensions of the probe and its components, as well as the contact resistance were introduced. The mathematical approach of the three models was very similar: they all resulted into a first order time model. There were only some differences in composition and in the introduction of the several thermal

properties of the probe. However, none of these models described a proper way to calculate the thermal conductivity and the heat capacity simultaneously from the temperature response.

Van Haneghem [1981] and Bruijn et al. [1983] developed a revised model for the probe, based on that of Jaeger and hence called the modified Jaeger model. Using that model, the thermal conductivity  $\lambda$ , the volumetric heat capacity  $C$  and the contact resistance  $\Gamma$  (per unit of length) could be determined. Two approaches were considered. If  $C$  was previously known,  $\lambda$  and  $\Gamma$  could be calculated accurately to within 1% and 5% respectively. If  $C$  was previously unknown, the method allowed simultaneous determination of  $\lambda$ ,  $C$  and  $\Gamma$  with accuracies of about 5%, 25% and 10% respectively. A disadvantage of the latter approach was the rather unstable iteration method in which the heat capacity  $C$  was determined: only very well performed measuring series could be evaluated in this way.

In this paper the temperature response according to the modified Jaeger model will be worked out in more detail. If the accuracy of the measurements is high enough also a second order time correction can be taken into account. Then using the Gauss-Newton iteration method it is possible to determine simultaneously the three thermal parameters  $\lambda$ ,  $C$  and  $\Gamma$  with higher accuracy.

### 3.1.3 *Experimental set-up*

The most important parts of the needle-shaped probe are a double fold constantan heating wire and a constantan-manganine thermocouple, both with a diameter of 0.1 mm and carefully fitted into a stainless steel envelope (see Fig. 3.1.1). The hot junction of the thermocouple is placed very close to the heating wire; the cold junction is situated at the end of the probe and is considered to stay at its original temperature. To fix the position of the wires in the cylindrical envelope and to prevent electrical contact, the remaining space is filled with a silicon rubber compound. The length of the probe is about 200 mm and its diameter varies from 1 to 2 mm for different probes.

In our case the temperature response of the probe on a suddenly starting constant energy dissipation inside the probe is measured. For that purpose on time  $t=0$  a constant electrical heating current is switched on and the temperature response is recorded once per second.

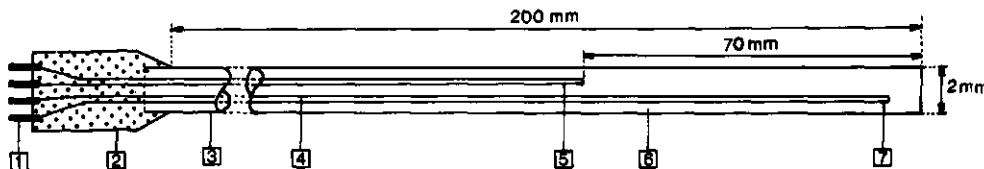


Fig. 3.1.1 Axial cross-section of the needle-shaped probe with:  
 1. contacting wires, 2. polyvinyl chlorid protector, 3. tube,  
 4. hot junction of thermocouple, 5. heating wire, 6. insulating  
 material, 7. cold junction of thermocouple.

### 3.1.4 The perfect line source model

To introduce our approach we have to resume the simple perfect line source model that is still used sometimes for the analysis of the temperature response ( $\theta$ - $t$  curve) [Fukuda, 1976]. In this model the probe is considered to be an infinitely long, infinitely thin heating wire, embedded in a homogeneous, isotropic medium. The exact solution of this one dimensional cylinder symmetrical problem is the exponential integral, which can be written in a series expansion of  $R^2/4at$ , with  $R$  the distance between the heating wire and the temperature sensor and  $a$  the thermal diffusivity ( $a=\lambda/C$ ). If we use the first two terms of the series the temperature response  $\theta^0(t)$  is given by:

$$\theta^0(t) = A \ln(t) + B \quad (t \gg R^2/4a) \quad (3.1.1)$$

where

$$A = Q/(4\pi\lambda) \quad (3.1.2)$$

and

$$B = \{Q/(4\pi\lambda)\} \{ \ln(4\lambda/CR^2) - C_E \} \quad (3.1.3)$$

in which  $C_E$  is Euler's constant ( $C_E = 0.5772\dots$ ).

A big advantage of this simple relation is that the coefficients A and B can be determined by linear regression (a least squares method) and hence  $\lambda$  and C can be calculated.

However, the accuracy is not so good. Especially the determination of C is unreliable. This is caused by the representation of the probe, which is too simple in this model. A real probe has finite dimensions and finite thermal parameters. Moreover the temperature rise is measured inside the probe and not directly in the medium. In addition, there will be in general a heat resistance between the temperature sensor and the medium. This parameter consists of two parts: the internal heat resistance  $W$ , which accounts for the temperature difference between the temperature sensor and the surface of the probe, and the contact resistance  $\Gamma$ , which accounts for the disturbance in the thermal conductivity of the granular material close to the probe. This disturbance is caused by the less close packing in the neighbourhood of the probe surface and will extend to about one grain diameter [Van Haneghem, 1981].

### 3.1.5 *The modified Jaeger model*

As mentioned before, the modified Jaeger model [Van Haneghem, 1981 and Bruijn et al., 1983] accounts for the dimensions and thermal parameters of the probe and for the thermal contact resistance between probe and medium. The modified Jaeger model was developed in two steps (see Fig. 3.1.2).

In the first step the real probe was represented by an idealised probe in which the double fold heating wire was replaced by a cylindrical core. Around that core the silicon rubber compound was placed as a coaxial cylinder, enveloped in turn by the outer steel cylinder. The hot junction of the thermocouple was assumed to be infinitely small and its position was defined by the effective radial distance  $R$  to the axis of the system.

In the second step this idealised probe was replaced by a perfectly conducting, massive cylinder with the same radius  $v$  as the original probe and with the following definitions:

- the volumetric heat capacity of this cylinder is equal to the sum of the heat capacities of the idealised probe:

$$C_n = \{s^2 C_{hw} + (u^2 - s^2) C_{is} + (v^2 - u^2) C_{tu}\}/v^2 \quad (3.1.4)$$

- the "heat resistance"  $\Gamma_t$  between this cylinder and the medium is equal to the real contact resistance  $\Gamma$  and the internal heat resistance  $W$  of the probe for  $r > R$ :

$$\Gamma_t = \Gamma + W \quad (3.1.5)$$

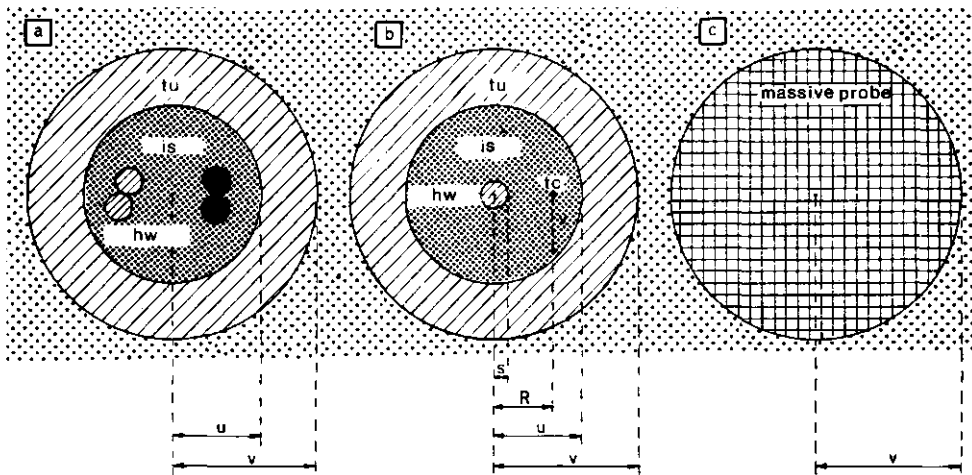


Fig. 3.1.2 From probe to modified Jaeger model, with: a. real probe, b. idealised probe, c. simplified, idealised probe; tu- tube, is- insulating material, hw- heating wire and tc- thermocouple.

Under quasi steady state conditions, using the well known equation for heat conduction in cylinders we obtain for the internal heat resistance:

$$W = \frac{\ln(u/R)}{2\pi\lambda_{is}} + \frac{\ln(v/u)}{2\pi\lambda_{tu}} \quad (3.1.6)$$

De Vries and Peck [1952] showed that the steady state profile is obtained with good approximation after about 5 s. This is sufficiently small compared with the usual measuring time of about 200 s.

For the modified Jaeger model the first order temperature response  $\theta'(t)$  can be given by (according to Bruijn et al. [1983]):

$$\theta'(t) = A \ln(t) + B + D/t + E \ln(t)/t \quad (3.1.7)$$

in which the coefficients A, B, D and E are nonlinear functions of heat conductivity  $\lambda$ , heat capacity C and thermal resistance  $\Gamma$ . They are also functions of the probe radius  $v$ , the dissipated heat Q, the heat capacity of the probe  $C_n$  and the internal heat resistance W. The four latter parameters ( $v$ , Q,  $C_n$  and W) are considered to be known constants. Of course they can differ from probe to probe and Q can differ from measurement to measurement. For the coefficients A, B, D and E it holds respectively [Bruijn et al., 1983; Van Loon, 1987]:

$$A = Q/4\pi\lambda \quad (3.1.8)$$

$$B = \{Q/4\pi\lambda\} \{ \ln(4a/v^2\epsilon) + 4\pi\lambda(\Gamma+W) \} \quad (3.1.9)$$

$$D = \{QCv^2/8\pi\lambda^2\} \{ (1-C_n/C) \ln(4a/v^2\epsilon) + 1 - (C_n/C)4\pi\lambda(\Gamma+W) \} \quad (3.1.10)$$

$$E = \{QCv^2/8\pi\lambda^2\} (1-C_n/C) \quad (3.1.11)$$

in which  $\epsilon = \exp(C_E)$

The modified Jaeger model is valid for time values at which the higher order terms of the series expansion are much smaller than the sum of the four terms of (3.1.7). As the first one of these higher order terms has the order of  $t^{-2}$ , we can formulate this condition as:

$$\text{Order}(1/t^2) \ll \theta'(t)$$

In working out this condition, we first have to obtain an expression for the second order time correction  $\text{Order}(1/t^2)$ . De Vries and Peck [1958] derived the second order time correction for their model if  $r > v$  (outside the probe). We will apply their conclusions about the correction on our model.

We follow their way of notation by introducing the dimensionless time  $\tau$ :

$$\tau = 4at/v^2 \quad (3.1.12)$$

With reference to (3.1.8) and (3.1.9) the first two terms of (3.1.7) can be described with  $\tau$ :

$$A \ln(t) + B = \{Q/4\pi\lambda\} \{\ln(\tau) - C_E + 4\pi\lambda(\Gamma+W)\} \quad (3.1.13)$$

(This could be considered as a zeroth order time model). With a modified dimensionless time  $\tau'$  (3.1.13) can be written more simply:

$$A \ln(t) + B = \{Q/4\pi\lambda\} \ln(\tau') \quad (3.1.14)$$

with

$$\tau' = \tau \exp\{4\pi\lambda(\Gamma+W) - C_E\} \quad (3.1.15)$$

The third and fourth term of equation (3.1.7) are similarly:

$$D/t + E \ln(t)/t = \{Q/2\pi\lambda\} \{\ln(\tau')/\tau\} (1-C_n/C) \quad (3.1.16)^1$$

With  $\tau''$ , which is a second modification of the dimensionless time, the modified Jaeger model has the form:

$$\theta'(t) = \{Q/4\pi\lambda\} \{\ln(\tau') + 2 \ln(\tau'')/\tau\} \quad (3.1.17)$$

in which

$$\begin{aligned} \tau'' &= \exp [\tau (D + E \ln(t))/2At] \\ &\approx \exp [\ln(\tau')/(1-C_n)] \end{aligned} \quad (3.1.18)$$

<sup>1</sup>) Equation (3.1.16) is not entirely correct: looking at (3.1.10) we see that in the definition of coefficient D the second term equals to 1 instead of  $4\pi\lambda(\Gamma+w)$ . This error is ignored because we are only interested in the order of magnitude of the second order time correction.

Both (3.1.17) and (3.1.7) represent the modified Jaeger model, a model with first order time correction. As remarked before there is no essential difference between the modified Jaeger model and, for instance, the model of De Vries and Peck [1958]. So the relations (3.1.7) and (3.1.17) are also valid for the model of De Vries and Peck; in relation (3.1.7) only the coefficients D and E differ slightly, in relation (3.1.17) a slightly different definition of  $\tau''$  is required.

The model of De Vries and Peck describes the temperature response both inside the probe ( $r \leq v$ ) and outside the probe ( $r > v$ ). In the latter area also a second order time correction  $\text{Order}(1/t^2)$  was derived:

$$\text{Order}(1/t^2) = \{-3Q/4\pi\lambda\} [(1-C_n/C)\ln(\tau')/\tau]^2 + \text{Order}(\ln(\tau'/\tau^2)) \quad (3.1.19)$$

Our modified Jaeger model gives the temperature rise inside the probe ( $r \leq v$ ) and just in this area we must find a second order time correction. As a consequence of the above called similarity between the two models and using the results of De Vries and Peck (3.1.19) for the second order time correction, it is possible to extend also the modified Jaeger model with a second order time correction. This correction provides only the order of magnitude, but that is the only thing we want to know: an expression for the time interval where the modified Jaeger model is valid. Using (3.1.18), the second order time correction can be written as:

$$\text{Order}(1/t^2) = \{-3Q/4\pi\lambda\} [\ln(\tau)/\tau]^2 \quad (3.1.20)$$

From these results the time interval for which the modified Jaeger model (3.1.17) is valid can be determined:

$$|-3\{Q/4\pi\lambda\}[\ln(\tau'')/\tau]^2| \ll \{Q/4\pi\lambda\}[\ln(\tau') + 2\ln(\tau'')/\tau] \quad (3.1.21)$$

Considering that  $\ln(\tau') \approx \ln(\tau'')$  and supposing that the left hand side of the inequality is a factor f smaller than the right hand side, we obtain an expression of the dimensionless starting time  $\tau_b'$  of the time interval:

$$\tau_b' = -1 + \sqrt{1 + 3f \ln(\tau_b')} \quad (3.1.22)$$

This expression can be solved by a numerical method; for instance by the successive substitution method [Dahlquist and Björck, 1986]. It is quite simple now to obtain the (normal) starting time of the time interval:  $t_b'' = \tau_b' v^2 / 4a$ .

The second order term (3.1.20) can be seen as an extension of the modified Jaeger model, but it must be stressed that it will be an approximation. The term is relatively small (if  $\tau > 1$ ) and decreases rapidly for increasing time. With this term the second order time model for the temperature response can now be written as:

$$\theta''(t) = \{Q/4\pi\lambda\}[\ln(\tau') + 2\ln(\tau'')/\tau - 3(\ln(\tau')/\tau)^2] \quad (3.1.23)$$

in which the model error is in the order of magnitude of  $\{3Q/4\pi\lambda\}[\ln(\tau'')/\tau^2]$ . The use of the extended model is only possible if:

$$\{Q/4\pi\lambda\}[\ln(\tau'')/\tau^2] \ll \{Q/4\pi\lambda\}[\ln(\tau') + 2\ln(\tau'')/\tau] \quad (3.1.24)$$

Considering again that  $\ln(\tau') \approx \ln(\tau'') > 0$  and that the right hand side of the inequality is at least a factor  $g$  bigger than the left hand side, it is possible to calculate the dimensionless starting time:

$$\tau_b'' = -1 + \sqrt{1 + 3g} \quad \text{with } g \approx f \quad (3.1.25)$$

whereas the starting time for the second order time model is:

$$t_b'' = \tau_b'' v^2 / 4a$$

The modified Jaeger model with second order time correction is to be preferred in the time interval  $[t_b'', t_b]$ , where the response is relatively steep. The temperature increase in the immediate surrounding of the hot junction of the thermocouple is relatively large (some centiKelvins per second). In this time interval a lot of heat is stored in the probe itself and in the medium close to it. So a good description of the temperature response in this interval is important if we want to determine the heat capacity of the medium. The more accurate we can describe this part, the better we will evaluate the heat capacity of the medium.

### 3.1.6 Gauss-Newton iteration

The modified Jaeger model with second order time correction describes the temperature response quite accurately. The other way around, the calculation of the parameters  $\lambda$ ,  $C$  and  $\Gamma$  from the temperature response, is complicated. As stated before the mathematical description of the model is a nonlinear function of the thermal parameters of the probe and the medium. The thermal parameters of the probe are known from calibration, whereas the two thermal parameters of the medium ( $\lambda$  and  $C$ ) and the contact resistance  $\Gamma$  are unknown. This set of three parameters is what we want to determine. We define the state vector  $\underline{x}$  as the set of these three thermal parameters:  $\underline{x} = (\lambda, C, \Gamma)$ . Rewriting the second order time model (3.1.23) as a function  $F$  of  $\underline{x}$  and  $t$  and eliminating at the same time  $\tau'$  with (3.1.15) and  $\tau''$  with (3.1.18), it follows:

$$F(\underline{x}, t) = A(\lambda) \ln(t) + B(\lambda, C, \Gamma) + [D(\lambda, C, \Gamma) + E(\lambda, C) \ln(t)]/t - 3[D(\lambda, C, \Gamma) + E(\lambda, C) \ln(t)]^2/[4A(\lambda)t^2] \quad (3.1.26)$$

if  $t > t_b''$  and where  $A(\lambda)$ ,  $B(\lambda, C, \Gamma)$ ,  $D(\lambda, C, \Gamma)$  and  $E(\lambda, C)$  are non-linear functions of the state vector  $\underline{x}$ . They are defined in the modified Jaeger model in eqs. (3.1.8) to (3.1.11).

The temperature response exists of  $t_b'' + n$  measuring points. For each of these measuring points we want to apply (3.1.26) (if  $t > t_b''$ ). This gives  $n$  equations of the kind  $\theta(t) = F(\underline{x}, t)$ ; a set of  $n$  equations with only three unknown parameters. This set has to be solved with a least squares method. For that aim we minimize the sum of squares  $\Phi$  as a function of the state vector  $\underline{x}$ , where is defined as:

$$\Phi(\underline{x}) = \sum_{t=t_b''}^{t_b''+n} (F(\underline{x}, t) - \theta(t))^2 \quad (3.1.27)$$

If we minimize  $\Phi$ , its derivatives must be zero, so:

$$d\Phi(\underline{x})/d\underline{x} = 0 \quad (3.1.28)$$

Equation (3.1.28) results in three sub-equations:

$$\partial\Phi(\underline{x})/\partial\lambda = 0; \quad \partial\Phi(\underline{x})/\partial C = 0 \quad \text{and} \quad \partial\Phi(\underline{x})/\partial\Gamma = 0 \quad (3.1.29)$$

This set of three equations contains the three unknown parameters  $\lambda$ ,  $C$  and  $\Gamma$ . They could be solved straightaway if they were linear. Dealing with nonlinearity with respect to the state vector, we need to take the first order approximation of the temperature response  $F(\underline{x},t)$ . Here we will use the well known Newton linearisation, which is allowed if none of the three derivatives  $dF(\underline{x})/d\underline{x}$  equals to zero in the neighbourhood of  $\underline{x}$ .

Starting with an already known state vector  $\underline{x}_0$  in the neighbourhood of the desired state vector  $\underline{x}$ , we can write in first approximation:

$$F(\underline{x}_0, t) = F(\underline{x}, t) - [dF(\underline{x}, t)/d\underline{x}, (\underline{x} - \underline{x}_0)] \quad (3.1.30)$$

where the second term of the right hand side is the inproduct of two vectors, which equals to:

$$\partial F(\underline{x})/\partial \lambda (\lambda - \lambda_0) + \partial F(\underline{x})/\partial C (C - C_0) + \partial F(\underline{x})/\partial \Gamma (\Gamma - \Gamma_0)$$

Because we chose  $\underline{x}_0$  in the neighbourhood of  $\underline{x}$ , it can be assumed that the derivatives of the model function  $F$  are almost equal in both points:

$$dF(\underline{x}, t)/d\underline{x} \approx dF(\underline{x}_0, t)/d\underline{x}_0$$

so

$$F(\underline{x}_0, t) = F(\underline{x}, t) - [dF(\underline{x}_0, t)/d\underline{x}_0, \underline{d}] \quad (3.1.31)$$

with

$$\underline{d} = \underline{x} - \underline{x}_0$$

Writing  $F(\underline{x}, t)$  in (3.1.31) explicitely, we see that it is a nonlinear function of the known state vector  $\underline{x}_0$  and at the same time it is a linear function of the difference state vector  $\underline{d} = (\lambda - \lambda_0, C - C_0, \Gamma - \Gamma_0)$ . The difference state vector  $\underline{d}$  can be solved from (3.1.31) and (3.1.27):

$$\Phi(\underline{x}) = \sum_{t=t_b}^{t_b+n} \{F(\underline{x}_0, t) + [dF(\underline{x}_0, t)/d\underline{x}_0, \underline{d}] - \theta(t)\}^2 \quad (3.1.32)$$

Now the sum  $\Phi(\underline{x})$  is linear with respect to the state vector. It has to be minimized according to (3.1.28). This can be done with the Householder transfor-

mation [Dahlquist and Björck, 1986], which is widely employed for multiple regression analysis.

Starting from  $\underline{x}_0$ , a better solution for the state vector  $\underline{x}$  is:

$$\underline{x}_1 = \underline{x}_0 + \underline{d} \quad (3.1.33)$$

where  $\underline{x}_1$  is the first iteration step.

The  $j$ -th iteration step is given by:

$$\underline{x}_j = \underline{x}_{j-1} + \underline{d}_j \quad (3.1.34)$$

The difference state vector  $\underline{d}_j$  must be calculated for each step  $j$  using (3.1.29) (with replacing  $\underline{x}_0$  by  $\underline{x}_{j-1}$ ) and the Householder transformation. The stop criterion of the iteration is determined by the sum of squares  $\Phi(\underline{x}_j)$ . When  $\Phi(\underline{x}_j)$  does not get smaller anymore the iteration must be finished. This iteration method is well-known as the Gauss-Newton method. A disadvantage of this method is that the first try for the state vector must be chosen near to the real value (the value to be calculated). The iteration method can only be used in a little area in the vector space, because outside this area the method looses its square convergence and only a very slow linear convergence remains. It is even possible that no global convergence will take place at all; then the method will reach a local minimum in  $\Phi(\underline{x})$  and a wrong  $\underline{x}$  will be calculated.

To enlarge the convergence area of the iteration method (in other words: to enlarge a possible choice of  $\underline{x}_0$ ), relation (3.1.34) can be extended:

$$\underline{x}_j = \underline{x}_{j-1} + f_j \underline{d}_j \quad (3.1.35)$$

in which  $f_j$  is a fitting constant.

This is called the Gauss-Newton method with line minimization [Dahlquist and Björck, 1986]. For each iteration step  $j$ ,  $f_j$  is determined to obtain the best  $\underline{x}_j$ . The best  $\underline{x}_j$  of course is the state vector in which  $\Phi(\underline{x}_j)$  reaches its minimum. (It must be noticed that still attention has to be paid to avoid local minima).

### 3.1.7 Calibration measurements

To evaluate the theory developed in the previous sections calibration measurements were performed for several temperatures. For that goal a measuring cylinder-filled with the calibration material and supplied with a probe along its axis- was placed into a thermostatic bath. The temperature of the bath was controlled with a stability of less than 0.01 K. Because the mathematical model requires very well defined measuring conditions, the calibration material has to be as homogeneous and isotropic as possible. For that reason a dilute agar gel of 0.4 mass percent was used, which has thermal parameters almost equal to those of pure water. The heat capacity of water is equal to  $4.19 \text{ MJ/m}^3\text{K}$  [Weast, 1975] and the thermal conductivity can be compared with Powell et al. [1966], in good approximation represented by  $\lambda = 0,560 + 19 \times 10^{-3} T$ , with  $T$  in  $^{\circ}\text{C}$ . As a consequence of the zero contact resistance  $\Gamma$  between the probe and the medium, the measured total heat resistance  $\Gamma_t$  now equals the internal heat resistance  $W$ . This heat resistance  $W$  is a probe property, which will be used in future measurements to determine the real contact resistance  $\Gamma$  in case of an arbitrary porous medium. The thermal parameters  $\lambda$ ,  $C$  and  $\Gamma_t$  are calculated using the method of the previous sections.

To avoid electromagnetical noise from the thermostat, we switched off the temperature control during the measurements themselves. However, temperature drift in the thermostatic bath can now be the consequence. Especially if the temperature difference between the measuring cylinder and the room increases, also this temperature drift increases. To investigate the influence of this drift two different measuring series were performed. First the series without drift correction was carried out with the probes numbered as 19, 25 and 26. Second the series with the (mathematically calculated) drift correction was carried out in which the probes numbered as 20 and 24 were used.

Fig. 3.1.3 shows that the measured thermal conductivities agree well with the above mentioned literature values: all lines are parallel to each other with relative distances up to 3%. Especially probe 26 ( $\Delta$ ) and probe 20 ( $\circ$ ) are very close to the measurements of Powell et al. [1966]. Apart from this all measurements have relative errors of about 0.3%. The results of Bruijn et al. [1983] are systematically about 3% higher than our values. As pointed out before the method of Bruijn et al. [1983] and our method are based on the modified Jaeger model. The differences between both methods are:

- the second order time correction which has been added to our model;
- another iteration method to calculate the thermal parameters.

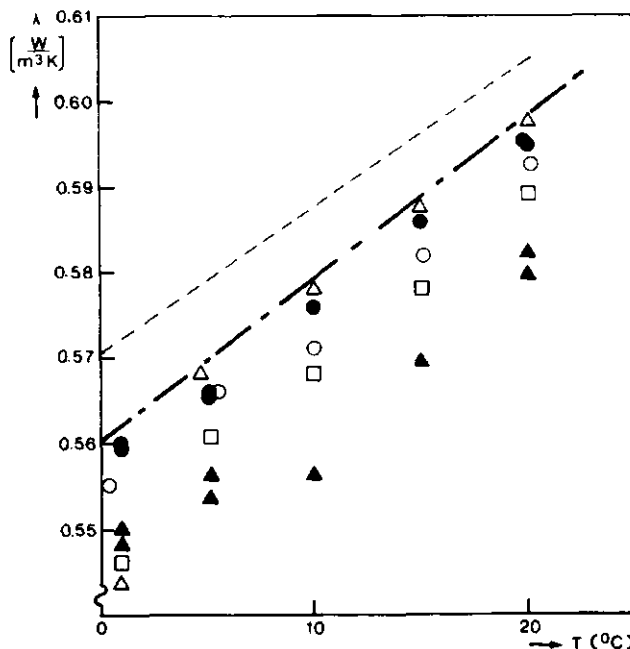


Fig. 3.1.3 Thermal conductivity as a function of the temperature  $T$  measured with different probes, with probe 19 ( $\circ$ ), probe 20 ( $\bullet$ ), probe 24 ( $\blacktriangle$ ), probe 25 ( $\square$ ), probe 26 ( $\Delta$ ), literature value [Powell et al., 1966] and literature value [Bruijn et al., 1983].

As can be seen the accuracy of the first series (outlined signs) is less at smaller temperatures; a consequence of the increasing temperature difference between the cylinder and the ambient room. In the second series the accuracy is

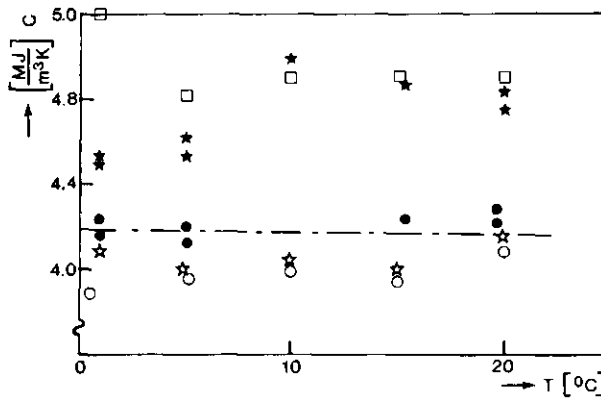


Fig. 3.1.4 Heat capacity  $C$  as a function of the temperature  $T$  measured with different probes: probe 19 ( $\circ$ ), probe 20 ( $\bullet$ ), probe 24 ( $\star$ ), probe 25 ( $\square$ ), probe 26 ( $\times$ ) and literature value [Weast, 1975].

constant over the total temperature range. In this series the temperature drift was determined immediately before a measurement was carried out. Afterwards for this drift (between 0.1 and 0.3 nV/s) a correction was applied.

For the measured heat capacities (Fig. 3.1.4) similar conclusions as for the thermal conductivities can be drawn. The errors in  $C$  however are high compared with the errors in  $\lambda$ ; the relative errors are about ten times bigger. This can be explained as follows: for the calculation of  $C$  we need at least the first order time correction of the temperature response:  $(D+E \ln(t))/t$ . This term is much smaller than the temperature response itself, hence the relative error in this term will strongly influence the value of  $C$ . When the second order time correction is added the sum of the first and second order time correction is bigger (mainly because we apply the interval for smaller time values), so the value of  $C$  will be more accurate. But still the accuracy is essential less than the accuracy in  $\lambda$ .

At last the total heat resistance  $\Gamma_t = \Gamma + W$  is discussed. In agar gel the contact resistance can be considered zero (perfect contact between the gel and the probe), so the total heat resistance equals to the internal resistance  $W$  (3.1.5). This way is used to calibrate  $W$ . For measurements in materials with a contact resistance  $\Gamma$  (for instance in porous materials) this calibrated value for  $W$  is subtracted from the calculated total heat resistance  $\Gamma_t$  to obtain a value for  $\Gamma$ .

It is clear that the internal heat resistance is a property of the probe itself. It changes from probe to probe (see Fig. 3.1.5). As can be seen the relative error is less than 3%. Again slight influence of the temperature drift can be observed (probe 25 and 26). From the internal heat resistance it is possible to calculate an effective radius  $R$  (see eq 3.1.6 and Fig. 3.1.2). This radius can be seen as the effective distance between the heating wire and the hot junction of the thermocouple inside the probe.

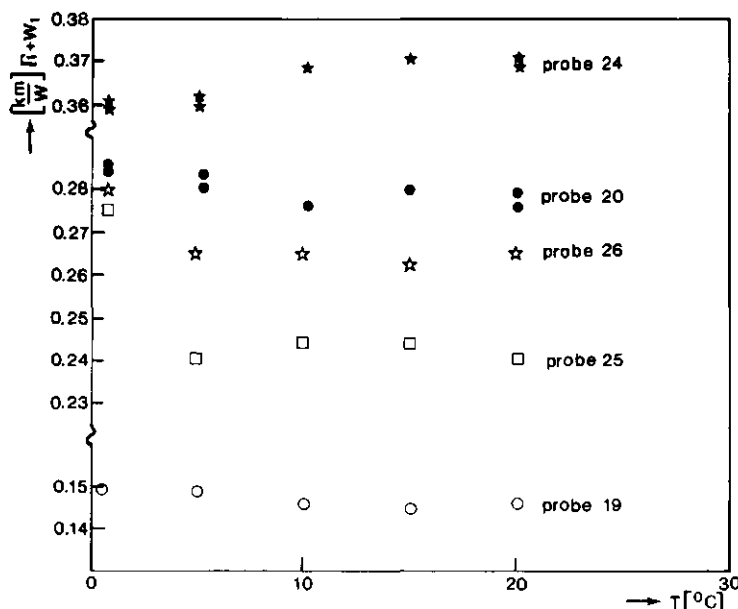


Fig. 3.1.5 Total heat resistance  $\Gamma_t$  as a function of the temperature  $T$  measured with different probes: probe 19 ( $\circ$ ), probe 20 ( $\bullet$ ), probe 24 ( $*$ ), probe 25 ( $\square$ ) and probe 26 ( $\times$ ).

### 3.1.8 Conclusions

The modified Jaeger model provides the physical basis to describe the temperature response of a needle shaped probe in a medium. If a second order time correction is added, also the steeper part of the temperature response is described accurately. This part is important for the calculation of the heat capacity of the medium.

To obtain the three desired thermal parameters (conductivity, heat capacity and contact resistance) a least squares method can be applied: the Householder transformation (for multiple regression analysis) in combination with the Gauss-Newton iteration (for dealing with non linearity).

The iteration method has been successfully applied in a numerical model called 'NAALD' [Van Loon, 1987]. Results of measurements in agar gel with randomly chosen probes show that the inaccuracy in the thermal conductivity  $\lambda$  is less than 3%, the estimation of the volumetric heat capacity  $C$  is accurate to within 5 to 25% and the total heat resistance  $\Gamma_t$  can be determined with a relative error of about 3%. Furthermore it can be remarked that not all probes give the same results. This probe dependence in the accuracy of  $\lambda$  and  $C$  is probably caused by small deviations in the construction. The very thin wires of the thermocouple as well as the heating wire always tordate and bend a bit when they are fitted into the stainless steel envelope. This phenomenon was shown by Van Haneghem [1981, page 64]. To obtain better results, especially for the heat capacity, the probes have to be constructed carefully, and they have to be selected on their physical cylinder symmetry (e.g. after inspecting X-ray photographs).

### 3.2 A new method to measure bulk electrical conductivity in soil using time-domain reflectometry

#### 3.2.0 *Abstract*

The bulk electrical conductivity of a porous medium can be determined by measuring the reflection of an electromagnetic pulse in transmission lines which are installed in this medium (the method is known as Time Domain Reflectometry, or TDR). The reflection is not only influenced by the medium, but also by the measuring system. A new method is described which corrects for influences of the measuring system by comparing a reflection measurement with a reference measurement performed in air. Calibration measurements were made in water and in water saturated sand and loam soils. Columns with different, well determined solute concentrations were prepared. Linear regression analyses were performed between the electrical conductivity determined with TDR and the electrical conductivity of the solutions. All slopes were close to one and the correlation coefficients were high: 0.993, 0.993 and 0.968 for water, sand and loam respectively. For the two soils significant intercepts were found. These might be related to the surface charge of the soil particles.

#### 3.2.1 *Introduction*

Time Domain Reflectometry (TDR) is based upon the velocity of propagation and reflection of an electromagnetic pulse along transmission lines. When transmission lines are placed inside a soil the dielectric constant and impedance of the medium can be measured. The dielectric constant can be related to the soil water content. Topp et al. [1980] presented an empirical equation that describes the non-linear relation between dielectric constant and water content. This relation is widely employed for unfrozen soils. Smith and Tice [1988] developed a similar relation between the unfrozen water content and the dielectric constant of partially frozen soils.

The impedance of the transmission lines inside the medium results in an attenuation of the signal, which can be related to the bulk electrical conductivity of the medium. Dalton et al. [1984] were the first to obtain the soil dielectric

constant and bulk electrical conductivity, simultaneously using TDR. Both parameters have a non-linear relation with the water content. The bulk conductivity is also dependent on the conductivity of the soil water itself. The present paper proposes a new method to calculate the bulk electrical conductivity from the attenuation of the pulse. The method is calibrated for different materials and solute concentrations. Finally the results are compared with some literature values [Dalton, 1987; Topp et al., 1988].

### 3.2.2 *Measurement theory*

A convenient way of measuring the dielectric constant of a soil is using the TDR method with a cable tester. This instrument has been designed to detect damage in cables and to determine at which distance this damage occurs. The output of the cable tester is the reflection coefficient of the cable as a function of the distance relative to this device. The reflection coefficient,  $V'$ , is the ratio of the voltage reflected back from the cable or circuit divided by the voltage applied by the cable tester [Tektronix, 1987]. In a cable with an open end nearly all electromagnetic energy will be reflected back and  $V' \approx 1$ . Conversely in a cable with a closed end nearly all the energy will come back through the 'ground' or return connector, thus  $V' \approx -1$ . The reflection coefficient is not exactly equal to one, due to energy losses caused by cable faults or impedance mismatches. Thus, the reflection coefficient will vary in between these two extreme cases.

The cable tester is designed to be used with  $50 \Omega$  coaxial cables [Tektronix, 1987]. This coaxial arrangement is not so convenient for *in situ* measurements in soil. In general, two parallel probes are used [Topp et al., 1982]. The electromagnetic pulse in the cable has to be transformed from the symmetric coaxial configuration into a parallel configuration. This can be done by means of an impedance matching transformer or 'balun'. For perfect impedance matching the parallel cable needs to have a specific impedance of  $200 \Omega$ . In addition the connecting probes themselves need to have a specific impedance of  $200 \Omega$ . For parallel lines the impedance,  $Z_0$ , for high frequency waves is given by [Ramo and Whinnery, 1959]:

$$Z_0 = \sqrt{\frac{\mu \times \mu_0}{\epsilon \times \epsilon_0}} \times \frac{\operatorname{arccosh}(s/d)}{\pi} \quad (3.2.1)$$

where  $\mu$  and  $\epsilon$  are the relative magnetic permeability and relative dielectric constant, respectively,  $\mu_0$  and  $\epsilon_0$  are the magnetic permeability and dielectric constant, respectively, in vacuum,  $s$  is the spacing between the probes and  $d$  the diameter of the probes.

Using eq (3.2.1) it is possible to match the impedance for different probe diameters by changing the spacing,  $s$ . For an impedance of  $200 \Omega$  we find in air ( $\mu=\epsilon=1$ )  $s/d = 2.6$ . When  $s/d > 2$ , eq. (3.2.1) can be simplified to:

$$Z_0 = (n_0/\pi) \times \ln(2s/d) \quad (3.2.2)$$

$$\text{with } n_0 = \sqrt{(\mu_0/\epsilon_0)} = 120 \times \pi \Omega.$$

However, many mismatches of the impedance still occur. Every junction between two different pieces of cable, the impedance matching transformer itself and the two parallel probes, when they are inserted in the soil ( $\epsilon$  is not equal to 1), result in impedance mismatches.

The travel time in soil is easy to obtain [Topp et al., 1980]. Because  $\epsilon > 1$  in soil, the impedance of the two parallel probes will be less than in air and  $V'$  will be negative [Ramo and Whinnery, 1959]. Thus, at the place where the electromagnetic wave enters the soil,  $V'$  drops sharply. At the end of the probes, the electromagnetic pulse will be reflected and  $V'$  will rise steeply. On the output of the cable tester this drop and rise can be recognised and the time interval,  $\Delta t$ , can be determined.

This method of measuring the time delay has been widely discussed [Dalton et al., 1984, Dasberg and Dalton, 1985 and Topp et al. 1982]. However, in the definition of  $\epsilon$  we find some ambiguity. The definition depends on the way in which the TDR instrument is calibrated, namely, one way or two way travel time. To prevent this ambiguity the  $\epsilon$  can be given as a result of measuring quantities, independently of travel time:

$$\epsilon = (\Delta x/L)^2 \quad (3.2.3)$$

with  $L$  the physical length of the probes in soil and  $\Delta x$  the apparent length as measured with the TDR device.

The attenuation of the signal in the parallel probes is very useful, because there is a relation between the attenuation coefficient,  $\alpha$  and the bulk (or effective) electrical conductivity,  $\sigma$ . For non magnetic soil the attenuation coefficient is [Yanuka et al., 1988]:

$$\alpha = \frac{\eta_0}{2\sqrt{\epsilon}} (\sigma + \omega\epsilon_0\epsilon_Y) \quad (3.2.4)$$

where  $\epsilon_Y$  is the imaginary part of the dielectric constant according to Yanuka et al. [1988] and  $\omega$  is the frequency of the wave. In order to estimate  $\alpha$ . Dalton and van Genuchten [1986] assumed perfect reflection at the end of the transmission line. They also assumed that  $\sigma \gg \omega\epsilon_0\epsilon_Y$ . For this method the reflection amplitude of both the reflected wave  $V_r$  and of the transmitted wave  $V_t$  have to be determined. The attenuation coefficient  $\alpha$  is then obtained from the following equation:

$$\alpha = (1/2L) \ln(V_t/V_r) \quad (3.2.5)$$

Topp et al. [1988] have shown that the non-uniform frequency dependence of the outstanding impedance mismatches (referred to previously) must be taken into account. They deal with this problem by attributing the difference in electrical conductivity to the contribution of the imaginary part of the dielectric constant of the soil.

We now describe a new method to estimate the attenuation coefficient which corrects for all impedance mismatches. Three assumptions are made in this method:

1. The attenuation due to the measuring system itself (including the balun, the junctions between two different cables, etc) is a constant at a certain point in the time domain. Thus it can be described as a function of time:  $A(t)$ .

2. The influence of the imaginary part of the dielectric constant  $\epsilon_y$  can be neglected with respect to dc conductivity of the soil system  $\omega \epsilon_y \ll \sigma$  (which is different from the approach of Topp et al. [1988] or Yanuka et al. [1988]).
3. By superposition, the attenuation of the signal due to conductivity losses, can be added to  $A(t)$ . The superposition principle is a widely accepted approach to correct for influences of measurement system itself.

Taken together the above assumptions result in the following expression for the measured reflection:

$$V(t) = A(t) \times \exp(-2\alpha L) \quad (3.2.6)$$

In order to determine  $A(t)$  a measurement  $V_0(t)$  is taken in vacuum or dry air. In these media  $\alpha = 0$ , thus:

$$V_0(t) = A(t) \quad (3.2.7)$$

To determine the electrical attenuation  $\alpha$  in a medium the following two steps are to be taken (see Fig. 3.2.1):

1. The reference signal  $V_0(x_c)$  is measured first. A convenient value on the x axis  $x_c$  is chosen in order to be on a smooth part of the  $V(x)$  curve;  $V(x_c)$  should be close to the maximum (to make the resolution as high as possible) and at  $V(x_c)$  no more significant (multiple) reflections should be added to the signal. We analysed the signal after ten reflections or  $x_{c0} = 10 \times \Delta x_0$ .
2. The 'normal'  $V(x_c)$  measurement in soil is then performed. From the cable-tester until the place where the probes enter the soil ( $x=0$ ) this signal is identical to the reference signal (see Fig. 3.2.1).

However, in soil the travel 'distance'  $\Delta x$  is longer than in air  $\Delta x_0$ :  $\Delta x = \Delta x_0 \times \sqrt{\epsilon}$ . Thus, the actual measurement in soil should be made at a different position on the x-axis, in order to correspond with the reference measurement. This position is given by:  $x_c = x_{c0} \times \sqrt{\epsilon}$ .

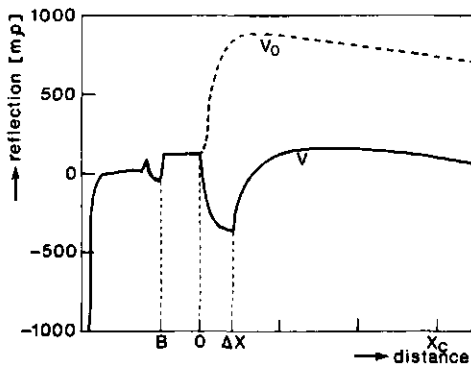


Fig. 3.2.1 Reflection of an electromagnetic pulse in parallel transmission lines in soil,  $V$ , and in air,  $V_0$ ;  $B$  is the position of the balun,  $0$  is the place where the probes enter the soil,  $\Delta x$  is the measured probe length and  $x_c$  is a convenient distance.

**Sample experiment:** For practical purposes we measured the reference signal in air instead of vacuum. On the cable tester distance is shown on the x-axis, so  $t_{c0}$  has to be converted into  $x_{c0}$ , using the following relation:  $x_{c0} = 10 \times L/\epsilon$ . Assuming a probe length of 18 cm and  $\epsilon = 1$  (in a vacuum)  $x_{c0}$  is equal to 1.8 m. In moist soil  $\epsilon = 15$  can be found and  $x_c = 10 \times L/\epsilon$ . Thus,  $x_c$  should equal 7 m to be directly comparable with the reference measurement.

The weaker signal reflection in soil is now compared to that in vacuum or air. Using eq's (3.2.6) and (3.2.7) the attenuation can be written as:

$$\alpha = (1/2L) \ln(V_0(x_{c0})/V(x_c)) \quad (3.2.8)$$

It should be noted that (3.2.8) is independent of multiple reflections. An attendant advantage of this method is that  $V_0(x_{c0})$  is a constant for a given measuring configuration and has to be determined only once. This leaves only one parameter to be measured in order to obtain the attenuation namely,  $V(x_c)$ . Combining equations (3.2.4) and (3.2.8), the bulk conductivity can then be calculated from  $\alpha$  and  $\epsilon$ :

$$\sigma = \frac{\gamma \epsilon}{L \times \eta_0} \times \ln \left[ \frac{V_0(x_{c0})}{V(x_c)} \right] \quad (3.2.9)$$

### 3.2.3 Materials and methods

Calibration measurements in water and in saturated soil were performed at different calcium chloride ( $\text{CaCl}_2$ ) concentrations. Separate columns were used for each solute concentration. The following materials were used:

1. 8 columns of water with solute concentrations varying from 0 to 2 g/l  $\text{CaCl}_2$ .
2. 6 columns of fine sand (sand fraction >92.4%, from the 'C' horizon of Caledon sandy loam, classified as a Brunisolic Gray Brown Luvisol [Agricultural Canada, 1987; Elrick and Bowman, 1964]) at 30 % vol. moisture content with  $\text{CaCl}_2$  concentrations varying from 0 to 6 g/l.  
Note: at 6 g/l the TDR technique proved to be at the limits of its range, consequently these data have not been reported).
3. 5 columns of Guelph loam (classified as a Gleyed orthic Melanic Brunisol [Agricultural Canada, 1987; Reynolds, 1986]) at 40 % vol. moisture content with  $\text{CaCl}_2$  concentrations varying from 0.4 to 4.4 g/l.

The measurements took place in cylinders, 76 mm in diameter and 190 mm high. The structureless sand was air dried and packed in the cylinders to a mean bulk density of 1.86 Mg/m<sup>3</sup>. The Guelph loam was highly structured. To obtain a more homogeneous material it was gently crumbled and passed through a 5 mm sieve. This material was then air dried and packed in the cylinders to a mean bulk density of 1.60 Mg/m<sup>3</sup>.

The parallel TDR probes (2.4 mm in diameter, 180 mm long and spaced 20 mm apart) were installed vertically into the dry soil columns (see Fig. 3.2.2). Next, the columns were placed into containers with well defined  $\text{CaCl}_2$  solutions. A porous screen at the bottom of each column allowed the solution to enter the soil. The water table was kept constant at 95 mm, so that a midpoint saturation was obtained. Thus, the bottoms of the columns were at a positive water potential of 0.95 kPa while the top was at a negative pressure of -0.95 kPa (= -95 mm water column). The latter value is well below the air entry values for both soils according to their soil water characteristic curves (see [Elrick and Bowman, 1964] and [Reynolds, 1986]). Thus, the columns may be considered saturated with a mean water potential of zero.

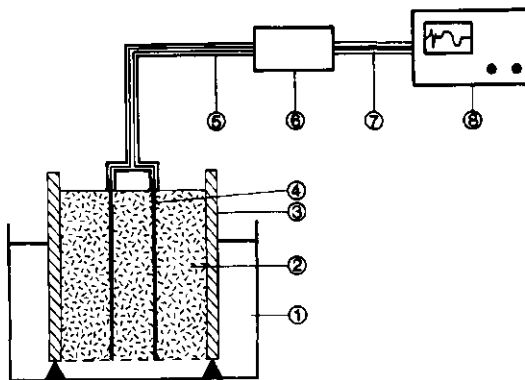


Fig. 3.2.2 Experimental set up with: 1.  $\text{CaCl}_2$  solution, 2. soil, 3. cylinder, 4. TDR probes, 5. shielded parallel TV wire, 6. balun (impedance matching transformer), 7. coaxial cable and 8. cable tester.

### 3.2.4 Results and discussion

Calibrations were made in water and in two saturated, disturbed soils. Data were expressed as a product of solute concentration and water content to give the solute concentration on a bulk basis. The results of the measurements are shown in Fig. 3.2.3. This figure also shows the linear regression models. Ideal behaviour should result in a linear relationship: the electrical conductivity is then directly proportional to the amount of ions per volume bulk. For the soil free system this ideal behaviour holds.

Table 3.2.1 shows that in water the coefficient of determination was very high ( $r^2 = 0.993$ ) and the slope is close to literature values at  $21^\circ\text{C}$  [Weast, 1975]. However, the model had a small but significant intercept (probability for zero-hypothesis is 14%). If the regression is forced through the origin, the correlation decreases slightly:  $r^2 = 0.989$  and the slope increases slightly:  $164 \text{ mS m}^2/\text{kg}$ . This is again close to literature values as can be seen in Table 3.2.1. Taken together, these findings appear to validate the new measuring method.

Our results are comparable with those of Dalton [1987], Heimovaara et al. [1988] and Topp et al. [1988]. Dalton [1987] found a reasonable 1:1 relationship between bulk soil electrical conductivity determined using the TDR with parallel probes and that measured with a standard low frequency conductivity bridge. Heimovaara et al. [1988] have also tried to cope with the impedance mismatch problem in determining the electrical conductivity. They calculated the impedance of the soil by comparing an 'open end circuit' with a 'short circuit'. The 'open end circuit' is the measurement as described above (without the parallel probes connected) while in the 'short circuit' the probes are shorted at the end with a very good conductor. A disadvantage of this procedure is that two wave forms have to be recorded for each measurement.

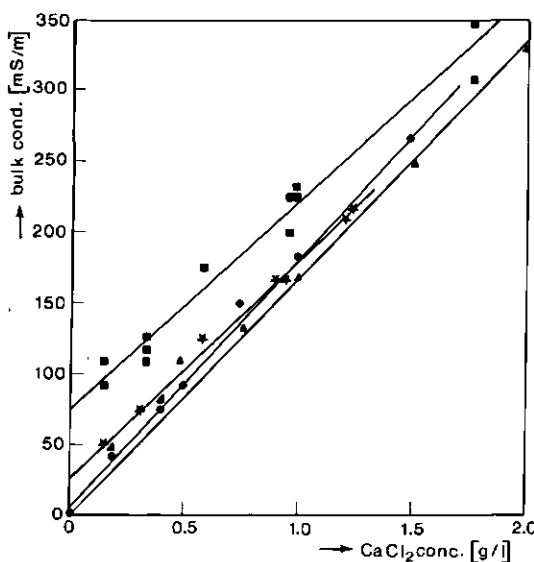


Fig. 3.2.3 Measured bulk electrical conductivity with the new TDR-method as a function of the product of water content and solute concentration in water ( $\Delta$ ) sand ( $*$ ) and loam ( $\blacksquare$ ). The EC-meter measured conductivity is given as a reference ( $\bullet$ ).

Table 3.2.1 Linear regression models between solute concentration ( $\text{CaCl}_2$ ) and bulk electrical conductivity measured with TDR, with [lit] the values given in [Weast, 1975]

material	$\theta_w$ vol%	intercept mS/m	slope mS $\times$ m <sup>2</sup> /kg	$r^2$	n
water	100	12	159	0.993	8
water (no int.)	100	-	164	0.989	8
water (EC meter)	100	5(NS)†	179	0.998	8
sand	30	26	153	0.993	12
loam	40	78	145	0.968	14
$\text{CaCl}_2$ 20°C [lit]	-	0	157	-	-
$\text{CaCl}_2$ 21°C [lit]	-	0	161	-	-
$\text{CaCl}_2$ 22°C [lit]	-	0	165	-	-

† NS = not significant at 90% probability level

Topp et al. [1988] also measured bulk electrical conductivity with the TDR in Rubicon silty loam and Bainesville clayey loam using the TDR in coaxial configuration. The problem of multiple reflection was avoided by analysing the signal after one round trip. The TDR data were then compared with electrical conductivities measured with a resistance bridge. The slope for their measurements combined was 1.31 with an  $r^2$  of 0.968, which means that that most of the TDR determined  $\sigma$  values are more than twice as high as those measured with a resistance bridge. This large difference has been attributed to losses caused by their definition of imaginary part of the dielectric constant of soil  $\epsilon_y$ .

Another way the measurements were analysed in [Topp et al., 1988] is the thin sample approach (as suggested by Giese and Tieman [1975]). The results obtained were much closer to the resistance bridge measurements (the slope for both soils combined was 1.15 with an  $r^2$  of 0.998). Furthermore, the intercept was not significantly different from zero, which suggests that  $\epsilon_y$  had a negligible influence on  $\sigma$ . The same authors also compared the TDR determined electrical conductivity of water with added salts (KCl) to that measured with a conductivity meter. Once again the Giese and Tieman [1975] approach gave better results than the signal analysis after one round trip. These findings appear to support the validity of our assumption 2 (i.e.:  $w\epsilon_y\ll\sigma$ ).

The combined effect of our assumptions 1 and 2 (the attenuation due to the measuring system itself is a constant at a certain point in the time domain and the negligible contribution of  $\epsilon_y$ , respectively) may vary with choice of the measurement location  $x_c$ . This might be more noticeable in soils at water contents below saturation. The effect of varying  $x_c$  on the calculated values of  $\sigma$  should be investigated.

The intercepts for the soils in Table 3.2.1 may have a physical meaning related to the surface charge of clay minerals. Soils differ slightly in the number of exchange sites per unit area of particle surface (surface charge density), but differ greatly in their specific surface areas [Baver et al., 1972]. Specific surface area is strongly related to particle size distribution or clay content. Assuming a uniform surface charge density then, the intercepts in Table 3.2.1 can be related to the clay contents of the two soils. The clay content of the Guelph loam is much higher than that for the sand: 20% and 1% respectively [Elrick and Bowman, 1964 and Reynolds, 1986]. Together with the values for water (specific surface area equals 0 and clay content equals 0) a high correlation between intercepts and clay contents can be found:  $r^2 = 0.94$ . However the significance of the correlation is doubtful because only three different materials have been examined.

### 3.2.5 Conclusions

In determining the bulk electrical conductivity with TDR the amplitude of the reflection must be measured as accurately as possible. Impedance mismatches of the measuring system may cause errors in determining this amplitude. These impedance mismatches can be corrected by comparing the reflection of an electromagnetic pulse in soil with a reference reflection in vacuum or air.

The method was calibrated in water with different  $\text{CaCl}_2$  concentrations, and an excellent correlation was found:  $r^2 = 0.993$ . In two different, saturated soils the effective electrical conductivity also correlated significantly with the amount of ions ( $r^2$  equal to 0.993 and 0.968 for Caledon sand and Guelph loam, respectively). In addition, significant intercepts were found, suggesting that the soils themselves also contributed to the electrical conductivity.

A more precise way of visualizing the intercepts might be in terms of cation exchange capacity (CEC). This measurement allows for variable surface charge densities. Thus, a parameter of interest in future bulk electrical conductivity studies using TDR might be the volumetric cation exchange capacity (i.e. CEC $\times$  bulk density).

### 3.3 Application of dispersion theory to time-domain reflectometry in soils

#### 3.3.0 Abstract

With time domain reflectometry (TDR) two dispersive parameters can be measured: the dielectric constant,  $\epsilon$ , and the electrical conductivity,  $\sigma$ . Both parameters are nonlinear functions of the volume fractions in soil. Because the volume fraction of water ( $\theta_w$ ) can change widely in the same soil, empirical equations have been derived to describe these relations. In this paper a theoretical model is proposed, based upon the theory of dispersive behaviour [Maxwell, 1873]. This is compared with the empirical equations. The agreement between the empirical and theoretical approaches was highly significant: the  $\epsilon(\theta_w)$  relation of Topp et al. [1980] had a coefficient of determination  $r^2 = 0.996$  and the  $\epsilon(\theta_u)$  relation of Smith and Tice [1988], for the unfrozen water content,  $\theta_u$ , at temperatures below 0°C, had an  $r^2 = 0.997$ . To obtain  $\sigma(\theta_w)$  relations, calibration measurements were performed on two soils: Caledon sand and Guelph silt loam. For both soils an  $r^2 = 0.983$  was obtained between the theoretical model and the measured values. The correct relations are especially important at low water contents, where the interaction between water molecules and soil particles is strong.

#### 3.3.1 Introduction

With time domain reflectometry (TDR) the dielectric constant,  $\epsilon$ , and electrical conductivity,  $\sigma$ , of the soil-water-air system can be measured. Both parameters are dependent on the volume fractions of the components. Because the volume fraction of water,  $\theta_w$ , can change both spatially and temporally within this system, it is important to know the  $\epsilon(\theta_w)$  and  $\sigma(\theta_w)$  relations. Topp et al. [1980] were the first to present an empirical relation between the volumetric water content and the dielectric constant obtained with TDR. They used a third order polynomial to describe the relation. This equation is still used today, because it is the same for most unfrozen soils. Recently, Smith and Tice [1988] have developed another third order polynomial to describe the relation between unfrozen water content,  $\theta_u$ , and dielectric constant in soils below 0°C. In the case of  $\sigma(\theta_w)$ , the relation is also non-linear. This non-linearity has been explained in terms of an interaction between water molecules and solutes with

the soil surface at low water contents [Rhoades et al., 1976 and Rhoades et al., 1989].

Older theories about the non-linear behaviour of  $\epsilon$  and  $\sigma$  in porous media can be found. Maxwell [1873] described the electrical conductivity of spherical grains inside a continuous medium. This can be seen as a simplified model for soils. By the first half of the twentieth century many measurements of electrical conductivity had been performed in 'granular' materials and emulsions [e.g. Polder and Van Santen, 1946 and De Vries, 1952 and references therein].

De Vries [1952] described the analogy between different dispersive properties, such as the dielectric constant and electrical conductivity, as a function of the volume fractions of the components. In this paper the influence of  $\theta_w$  on  $\epsilon$  and  $\sigma$ , as measured with TDR, is studied. The recent empirical  $\epsilon(\theta_w)$  equations are compared with the old dispersion theories of Maxwell and De Vries. The model of Oliphant [1985] for dielectric constants in frozen soils is also compared with our theoretical model. For the electrical conductivity, a general  $\sigma(\theta_w)$  relation based on dispersion theory is developed. Finally this equation is compared with the work of Rhoades et al. [1989].

### 3.3.2 Dielectric constant as a function of water content

#### 3.3.2.1 Soil as a two phase dielectric medium

Consider soil to be a two phase medium with a continuous water phase and a discontinuous phase D. In saturated, unfrozen soil D consists only of soil particles. In unsaturated, unfrozen soil D consists of soil particles and air. In the case of dielectric constants  $\epsilon$  it is appropriate to consider soil (s) and air (a) to be one medium with respect to water (w) because:  $\epsilon_w = 81$  (at 20°C),  $\epsilon_s = 4$  and  $\epsilon_a = 1$  [Weast, 1975]. Thus:

$$\epsilon_w/\epsilon_a \gg \epsilon_s/\epsilon_a \text{ and } \epsilon_w/\epsilon_s \gg \epsilon_a/\epsilon_s \quad (3.3.1)$$

That is, changes in dielectric behaviour of the combined air-soil phase are negligible with respect to changes in the water phase. As a first approximation, soil and air can be considered one medium.

Under frozen conditions, the continuous phase consists of unfrozen (liquid) water. Furthermore, air is normally absent in the presence of pore ice [Miller, 1973]. Since  $\epsilon_i = 6$  [Weast, 1975] it is appropriate to consider soil and ice as a single medium. Thus:

$$\epsilon_w/\epsilon_i \gg \epsilon_s/\epsilon_i \text{ and } \epsilon_w/\epsilon_s \gg \epsilon_i/\epsilon_s \quad (3.3.2)$$

That is, as a first approximation, changes in the dielectric behaviour of the combined ice-soil phase are negligible compared to changes in the unfrozen water phase.

### 3.3.2.2 Unfrozen soils

We assume that the soil-water-air system can be described as an isotropic medium with dielectric constant  $\epsilon$  in which different types of grains coexist. Grains with the same shape, same size and consisting of the same material are considered to be one class, with one dielectric constant. Similar sized grains consisting of the same material but different in shape, will have different (effective) dielectric constants, because the electro-magnetic field behaves differently at their respective interfaces. This behaviour can be expressed in terms of a shape factor,  $K$ . The theory of Maxwell [1873] as quoted in De Vries [1952] gives the following general definition for the shape factor  $K$  in medium D:

$$K_D = EFD/EFC \quad [\text{De Vries, 1952, eq 9a}] \quad (3.3.3)$$

with  $EFD$  the electrical field in the discontinuous phase D and  $EFC$  the electrical field in the continuous phase C. From this definition it follows that:

$$K_C = 1 \quad (3.3.4)$$

For ellipsoid bodies the shape factor is:

$$K_D = \frac{1}{3} \sum_{i=a,b,c} \frac{1}{1 + (\epsilon_D/\epsilon_C - 1)g_i} \quad (3.3.5)$$

with  $a, b, c$  the three coordinate axes of the body and  $g_i$  the axis factor. For spheres  $g_a = g_b = g_c = 1/3$ . Thus, the shape factor for spheres  $K_{sphere}$  equals:

$$K_{sphere} = \frac{1}{3} \times \frac{(1+1+1)}{1 + (\epsilon_D/\epsilon_C - 1) \times 1/3}$$

$$K_{sphere} = 3\epsilon_C/(2\epsilon_C + \epsilon_D) \quad (3.3.6)$$

Because of the assumptions this model can only be used at high volumetric water contents ( $\theta_w > 0.5$ ). However, the major non-linearities occur at low water contents [Rhoades, 1989]. In this case, the water can be found in thin films around the soil particles. These thin films can be modeled by thin plates (if the curvature of the plates is ignored). We shall therefore derive the  $\epsilon(\theta_w)$  relation for parallel plates (which results in a layered system). For this system the axis factors are:  $g_a = g_b = 0$  and  $g_c = 1$ . Thus, the shape factor for parallel planes  $K_{pp}$  equals:

$$K_{pp} = \frac{1}{3} \times \frac{2}{1 + 0} + \frac{1}{1 + (\epsilon_D/\epsilon_C - 1) \times 1}$$

or

$$K_{pp} = (\epsilon_C/\epsilon_D + 2)/3 \quad \text{or} \quad 1/3(\epsilon_C/\epsilon_D + 2) \quad (3.3.7)$$

The most simple model for porous media is now a layered system of water (with volume fraction  $\theta_w$ ) and of soil-air (with volume fraction  $\theta_{sa}$ ). The dielectric constant  $\epsilon$  of the porous medium according to Maxwell [1873] is simply the weighed mean of the components:

$$\sum_i \epsilon_i \theta_i K_i / \sum_i \theta_i K_i \quad (3.3.8)$$

where  $i$  is water or soil-air.

In soil, water is the continuous medium even at low water contents ( $\theta_w \ll 1$ ). The discontinuous medium for unsaturated, unfrozen soil is soil and air with a combined dielectric constant of  $\epsilon_{sa}$  and volume fraction,  $\theta_{sa} = 1 - \theta_w$ . The shape fac-

tor for water equals one by definition (3.3.4), whereas the shape factor for the soil-air system in parallel planes can be obtained from (3.3.7):

$$K_{sa} = (\epsilon_w/\epsilon_{sa} + 2)/3 \quad \text{of} \quad 1/3(\epsilon_w/\epsilon_{sa} + 2) \quad (3.3.9)$$

Applying eq (3.3.8) for this two phase, layered system we obtain:

$$\epsilon_{pp} = \frac{\epsilon_{sa} \theta_{sa} K_{sa} + \epsilon_w \theta_w K_w}{\theta_{sa} K_{sa} + \theta_w K_w} \quad (3.3.10)$$

Thus, the dielectric constant  $\epsilon_{pp}$  can be obtained by using eq (3.3.9) in eq (3.3.10):

$$\epsilon_{pp} = \frac{\epsilon_{sa} (1 - \theta_w) (\epsilon_w/\epsilon_{sa} + 2)/3 + \epsilon_w \theta_w}{(1 - \theta_w) (\epsilon_w/\epsilon_{sa} + 2)/3 + \theta_w}$$

or

$$\epsilon_{pp} = \frac{\epsilon_{sa} (\epsilon_w + 2 \epsilon_{sa} - 2 \theta_w (\epsilon_w - \epsilon_{sa}))}{\epsilon_w + 2 \epsilon_{sa} - \theta_w (\epsilon_w - \epsilon_{sa})} \quad (3.3.11)$$

Topp et al. [1980, 1982] developed an empirical relationship between water content and measured dielectric constant, which is widely used for unfrozen soils:

$$\epsilon = 3.03 + 9.3 \times \theta_w + 146 \times \theta_w^2 - 76.7 \times \theta_w^3 \quad (3.3.12)$$

If we compare this empirical relation with eq (3.3.11), the layered system, (and assuming  $\epsilon_w = 81$  and  $\epsilon_{sa} = 3$ ) we see some similarity. At low water contents ( $\theta_w < 0.05$ ) the two functions differ less than 1% (see Fig. 3.3.1).

In soils at very low water contents the water can be found in thin films around the soil particles. Thus, a model for the configuration of water in (parallel) plates is most applicable under these conditions.

At very high water contents ( $\theta_w > 0.85$ ) the relationship between  $\epsilon$  and  $\theta_w$  can be modeled with a linear function (Fig. 3.3.1). In this situation the medium behaves like an ideal mixture of water and soil (without interaction). Thus for  $\theta_w > 0.85$ :

$$\epsilon_{lin} = \epsilon_{sa} + \theta_w (\epsilon_w - \epsilon_{sa}) \quad (3.3.13)$$

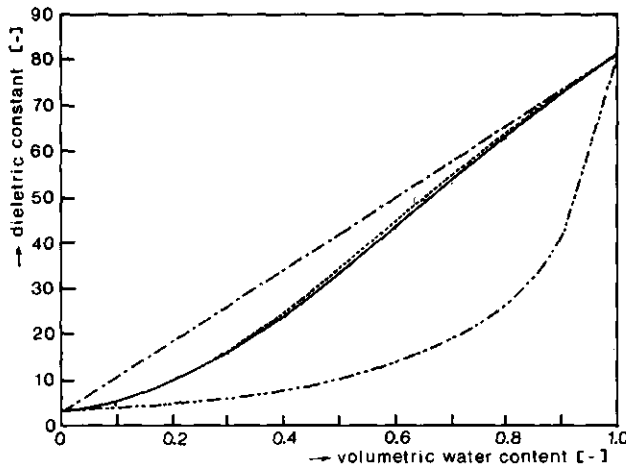


Fig. 3.3.1 The dielectric constant as a function of volumetric water content:  
 — empirical relation (eq 3.3.12), - - - linear behaviour (eq 3.3.13), - - - layered system (eq 3.3.11) and ..... new dispersive model (eq 3.3.20).

With the behaviour of the soil-air-water mixture at its extremes, it is now possible to derive a third order relation for the dielectric constant. The general form of this relationship is given by:

$$\epsilon_{\text{disp}} = A + B \times \theta_w + C \times \theta_w^2 + D \times \theta_w^3 \quad (3.3.14)$$

with A, B, C and D regression coefficients.

At  $\theta_w = 0$  we linearize the model for parallel plates, i.e.  $\epsilon_{\text{disp}}(0) = \epsilon_{\text{pp}}(0)$  and  $d\epsilon_{\text{disp}}(0)/d\theta_w = d\epsilon_{\text{pp}}(0)/d\theta_w$ . Comparing (3.3.11) with (3.3.14) we find that (see appendix 3.3.7):

$$A = \epsilon_{\text{sa}} \quad (3.3.15)$$

and

$$B = 3\epsilon_{\text{sa}}(\epsilon_w - \epsilon_{\text{sa}})/(\epsilon_w + 2\epsilon_{\text{sa}}) \quad (3.3.16)$$

Similarly, at  $\theta_w = 1$  the linear (ideal mixture) model is applied, i.e.  $\epsilon_{\text{disp}}(1) = \epsilon_{\text{lin}}(1)$  and  $d\epsilon_{\text{disp}}(1)/d\theta_w = d\epsilon_{\text{lin}}(1)/d\theta_w$ . Comparing (3.3.13) with (3.3.14) we find that:

$$A + B + C + D = \epsilon_w \quad (3.3.17)$$

and

$$B + 2C + 3D = \epsilon_w - \epsilon_{\text{sa}} \quad (3.3.18)$$

Solving the system of four equations (3.3.15 to 3.3.18) for the four coefficients (see appendix 3.3.7) and applying them in the power series (3.3.14) results in the following expression:

$$\epsilon(\theta_w) = \epsilon_{\text{sa}} + \frac{\epsilon_w - \epsilon_{\text{sa}}}{\epsilon_w + 2\epsilon_{\text{sa}}} [3\epsilon_{\text{sa}}\theta_w + (\epsilon_w - \epsilon_{\text{sa}})(2 - \theta_w)\theta_w^2] \quad (3.3.19)$$

This equation can be seen as a power series with a theoretical background. When we take  $\epsilon_w = 81$  at  $20^\circ\text{C}$  [Weast, 1975] and  $\epsilon_{\text{sa}} = 3$  (which is the effective value for a dry soil with air inside the pores) the following numerical expression is obtained:

$$\epsilon_{\text{disp}} = 3 + 8.1\theta_w + 140\theta_w^2 - 70\theta_w^3 \quad (3.3.20)$$

In Fig. 3.3.1 it can be seen that the new dispersive model (3.3.20) agrees very well with the empirical relation of Topp et al. [1980] (3.3.12). The standard error between the two lines is 0.5 in  $\epsilon$  or 1% in volumetric water content. This supports the application of dispersion theory to the dielectric constant in unfrozen unsaturated soils.

### 3.3.2.3 Frozen soils

We will now investigate whether the dispersion theory for the dielectric constant is also applicable in (partially) frozen soils. Two elements of the system remain the same: liquid water and soil. The third element (air) is now replaced with ice [Miller, 1973]. Patterson and Smith [1984] and Smith and Tice [1988] developed an empirical relation between unfrozen water content,  $\theta_u$ , and measured dielectric constant  $\epsilon$ , which is different from the equation of Topp et

al [1980]. The existence of this relationship is possible because of the very different dielectrical behaviour of (unfrozen) water and ice. Liquid water has a very high dielectric constant ( $\epsilon_w = 88$  at  $0^\circ\text{C}$  [Weast, 1975]) because the dipoles can orientate themselves according to the electro-magnetic field. In ice, the  $\text{H}_2\text{O}$  molecules have less freedom to move than in liquid water, so the dipoles are to a large degree impeded in their ability to orientate in the electro-magnetic field. This causes an enormous decrease in the dielectric constant:  $\epsilon_{\text{ice}} = 6$  [Weast, 1975].

In frozen soil the dielectric constant of the solid phase  $\epsilon_{\text{si}}$  consists of two parts: soil and ice (which is different from the unsaturated unfrozen condition as described in the previous section). Hence its value will be in between  $\epsilon_s$  (=4) and  $\epsilon_{\text{ice}}$  (=6). A convenient value for  $\epsilon_{\text{si}}$  is 5. As a first approximation for the dielectric constant of unfrozen water we take  $\epsilon_u = 88$ , the value for free water at  $0^\circ\text{C}$ . Using these values in equation (3.3.19) results into the following  $\epsilon(\theta_u)$  relation:

$$\epsilon_{\text{disp}} = 5 + 12.7 \times \theta_u + 140.6 \times \theta_u^2 - 70.3 \times \theta_u^3 \quad (3.3.21)$$

Smith and Tice [1988] developed their empirical relation between  $\epsilon$  and  $\theta_u$  by measuring the unfrozen water content with nuclear magnetic resonance. They performed measurements on 16 soils, varying from sands to heavy clays. After establishing the relation they checked it with another 8 soils. Their relation can be written as:

$$\theta_u = -0.1458 + 0.0387 \times \epsilon - 8.5 \times 10^{-4} \epsilon^2 + 9.9 \times 10^{-6} \epsilon^3 \quad (3.3.22)$$

Equation (3.3.22) has to be inverted in order to compare with our theoretical equation (3.3.21). We obtained a least squares approximation of the inversion by performing multiple regression analyses:

$$\epsilon = A + B \times \theta_u + C \times \theta_u^2 + D \times \theta_u^3 \quad (3.3.23)$$

with A, B, C and D regression coefficients and  $\theta_u$  calculated with use of (3.3.22).

This procedure leads to the following inversion of eq (3.3.22):

$$\epsilon = 4.57 + 17.1 \times \theta_u + 94 \times \theta_u^2 - 63 \times \theta_u^3 \quad (3.3.24)$$

The inversion is quite accurate:  $r^2 = 0.9996$  and the standard error in  $\epsilon$  equals 0.3.

If (3.3.21) is compared with (3.3.24) we see a large difference: the third and fourth coefficient in (3.3.21) are higher than those in (3.3.24). This can also be seen in Fig. 3.3.2. The difference is largest at high values of  $\theta_u$ . This suggests that the assumption of  $\epsilon_w = 88$  is wrong. The dielectric constant of unfrozen water in frozen soil may be lower than the dielectric constant of supercooled free water at the same temperature. In frozen soil  $\epsilon_w$  is probably influenced by the vicinity of pore ice. This causes a partial orientation of the water dipoles through the Workman-Reynolds effect [Parameswaran and Mackay, 1983]. The next step is to adjust  $\epsilon_w$ , so that with (3.3.19) a good approximation is obtained of the measuring points of Smith and Tice [1988]. The best fit is found at  $\epsilon_w = 65$ , (with  $r^2 = 0.984$ ) which yields the following expression:

$$\epsilon_{\text{disp}} = 5 + 12 \times \theta_u + 96 \times \theta_u^2 - 48 \times \theta_u^3 \quad (3.3.25)$$

With a standard error in  $\epsilon$  of 2, which is the same as in the Smith and Tice relation.

Oliphant [1985] also developed an  $\epsilon(\theta_u)$  relation with a theoretical background. In that paper the mixing rule of Polder and Van Santen [1946] was used. A disadvantage of this mixing rule is that it is an implicit equation. Thus, the values can only be calculated by numerical regression methods. Oliphant also found a close agreement with the experimental equation (3.3.22). Furthermore he concluded that the dielectric constant of soil water was influenced by the vicinity of ice. His best fit resulted in a value of  $\epsilon_u = 67.8$ , which is very close to our estimate of  $\epsilon_u = 65$ .

In the interval  $\theta_w = 0$  to 0.5 equation (3.3.25) agrees very well with the empirical relation (3.3.22) as can be seen in Fig. 3.3.2. Regression analyses confirm the visual impression:  $r^2 = 0.997$ , with a standard error in  $\epsilon$  of 0.4,

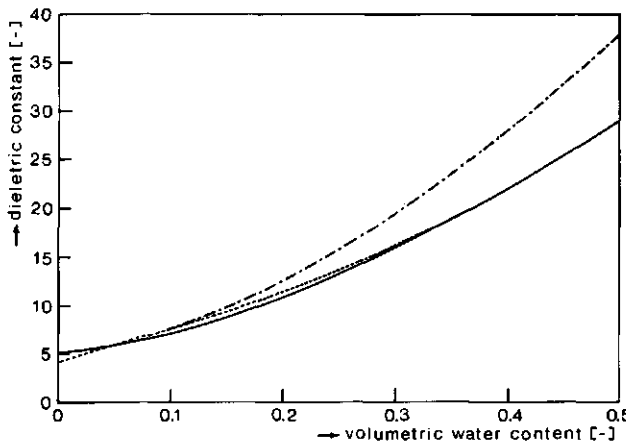


Fig. 3.3.2 The dielectric constant as a function of unfrozen water content in frozen soils. — empirical relation (eq 3.3.24), - - - theoretical relation with  $\epsilon_w = 88$  (eq 3.3.21) and ..... with  $\epsilon_w = 65$  (eq 3.3.25).

which is a lot smaller than the standard error of the curve fit. Thus, it can be concluded that dispersion theory also applies for the  $\epsilon(\theta_w)$  relation in frozen soils.

### 3.3.3 Bulk electrical conductivity as a function of water content

De Vries [1952] showed that theoretical equations (3.3.8) and (3.3.11) can be applied for all kinds of dispersive behaviour. They are also applicable for the magnetic permeability  $\mu$ , the electrical conductivity  $\sigma$  and the thermal conductivity  $\lambda$ . From this analogy it follows that:

1. the behaviour of  $\sigma$  at low water contents can be modeled with a layered system
2. water and soil behave like an ideal mixture at high water contents
3. a third order polynomial can be used to interpolate the intermediate values.

These three assumptions taken together allow us to transform the power series (3.3.19) for the electrical conductivity  $\sigma(\theta_w)$ . By analogy, the bulk electrical conductivity can now be written as:

$$\sigma(\theta_w) = \sigma_s + \frac{\sigma_w - \sigma_s}{\sigma_w + 2\sigma_s} [3\sigma_s \theta_w + (\sigma_w - \sigma_s)(2 - \theta_w) \theta_w^2] \quad (3.3.26)$$

Thus,  $\sigma(\theta_w)$  is not only a function of water content  $\theta_w$ , but also of soil surface conductivity  $\sigma_s$  and soil solution (water with dissolved salts) conductivity  $\sigma_w$ . In order to investigate this relation we performed some simple experiments which are described in the following sections.

### 3.3.4 Materials and methods

The bulk electric conductivity  $\sigma$  was measured using the TDR according to the method of [Van Loon et al., 1990b]:

$$\sigma = \frac{\gamma \epsilon}{(L \times \eta_0)} \ln \left[ \frac{V_0(10 \times L)}{V(x_c)} \right] \quad (3.3.27)$$

with  $L$  the length of the measuring probe,  $\eta_0 = 120 \times \pi \Omega$ ,  $V_0$  the reference reflection in dry air at distance  $10 \times L$ ,  $V$  the reflection in soil at distance  $x_c = 10 \times L \times \gamma \epsilon$ .

Measurements were performed in columns of wetting soil at different calcium chloride ( $\text{CaCl}_2$ ) concentrations. Two soil types were used and separate columns were prepared for each solute concentration:

1. 8 columns of fine sand (sand fraction >92.4%, from the 'C' horizon of Caledon sandy loam, classified as a Brunisolic Gray Brown Luvisol [Agriculture Canada, 1987; Reynolds, 1986]) up to 30% vol. moisture content with  $\text{CaCl}_2$  concentrations varying from 0 to 10 g/l (note: at 6 g/l the TDR technique proved to be at the limit of its range. Consequently, these data and data taken at 10 g/l column have not been reported).
2. 6 columns of Guelph loam (classified as a Gleyed orthic Melanic Brunisol [Agriculture Canada, 1987, Elrick and Bowman, 1964]) up to 40% vol. moisture content with  $\text{CaCl}_2$  concentrations varying from 0.4 to 10.4 g/l (note: the data taken from the 10 g/l column have not been reported).

Parallel TDR probes (2.4 mm in diameter, 180 mm long and spaced 20 mm apart) were installed vertically into the dry soil and the columns were placed into containers. The experimental design is described in detail in section 3.2.3.

Starting with a dry soil small amounts of well defined  $\text{CaCl}_2$  solutions were added stepwise. A porous screen at the bottom of each column allowed the solution to enter the soil. After a new amount of water had been added, the soil was allowed to equilibrate for several hours before a TDR measurement was performed. The experiments were terminated when a midpoint level of saturation was achieved. The tops of the columns were at a negative water pressure of -0.95 kPa while the bottoms were at a positive pressure of 0.95 kPa. Thus, the columns were considered saturated with a mean water pressure of zero.

### 3.3.5 Results and discussion

#### 3.3.5.1 Validation of the model for bulk electrical conductivity

Results for the Caledon sand are shown in Fig. 3.3.3 (number of measuring points  $n=48$ ). The non-linear effect of the water content is apparent. In Guelph loam the non-linear relationship is even more clear, as can be seen in Fig. 3.3.4 ( $n=46$ ). At low water contents ( $\theta_w < 0.10$ ) hardly any difference in electrical conductivity can be measured between the different  $\text{CaCl}_2$  solutions in both soils. In the literature a linear representation is often used for the whole range of  $\theta_w$ . Looking at Figs. 3.3.3 and 3.3.4 we see, that this must be an oversimplification, only acceptable as a first approximation. According to this approach, the bulk electrical conductivity would be directly proportional to the amount of ions per volume of soil. The electrical conductivity then equals the product of volumetric water content  $\theta_w$ , the specific electrical conductivity of  $\text{CaCl}_2$  ( $E=161 \text{ mS m}^2/\text{kg}$  at  $21^\circ\text{C}$  [Weast, 1975]) and the solute concentration  $SC$  in  $\text{kg/m}^3$ . An intercept can be added to the model in order to allow a conductivity due to surface charge of the soil particles. This simple model is given by:

$$\sigma = \text{intercept} + A \times \theta_w \times SC \times E \quad (3.3.28)$$

with  $\sigma$  the measured bulk electrical conductivity and  $A$  the regression coefficient.

In terms of regression analyses the linear model (3.3.28) gave a relatively good fit:  $r^2 = 0.79$  and 0.88 for the loam and the sand, respectively (see Table 3.3.1). The slopes are rather close to the expected value 'one', but the intercepts are negative. This cannot be true, because negative conductivities are physically impossible.

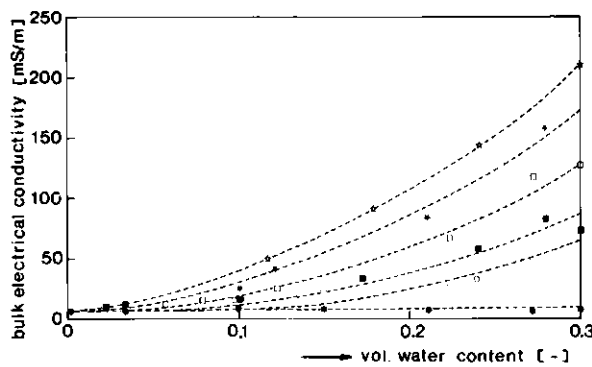


Fig. 3.3.3 The measured electrical conductivity in Caledon sand as a function of water content for different solute concentrations:  $\bullet = 0 \text{ g/l}$ ,  $\circ = 0.4 \text{ g/l}$ ,  $\blacksquare = 1 \text{ g/l}$ ,  $\square = 2 \text{ g/l}$ ,  $\ast = 3 \text{ g/l}$  and  $\times = 4 \text{ g/l}$ .

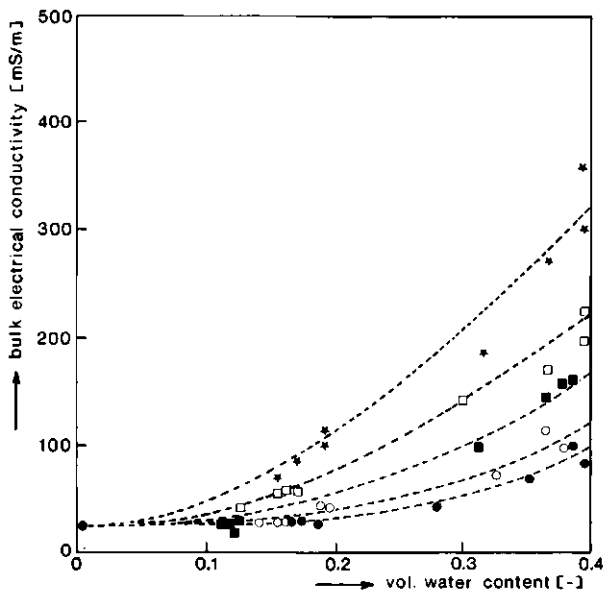


Fig. 3.3.4 The measured electrical conductivity in Guelph loam as function of water content for different solute concentrations:  $\bullet = 0.4 \text{ g/l}$ ,  $\circ = 0.8 \text{ g/l}$ ,  $\blacksquare = 1.4 \text{ g/l}$ ,  $\square = 2.4 \text{ g/l}$  and  $\ast = 4.4 \text{ g/l}$ .

Table 3.3.1 Multiple regression analyses of bulk electrical conductivity in Caledon sand and Guelph loam for the model:  
 $\sigma = \text{int} + A \times \theta_w \times \text{SC} \times E + B \times \theta_w^2 \times \text{SC} \times E + C \times \theta_w^3 \times \text{SC} \times E$

medium	int	A	B	C	$r^2$	SE†
sand	-5	0.89	-	-	0.883	20
loam	-7	0.98	-	-	0.791	37
sand	0	0.04	3.24	-	0.959	12
loam	10	-0.48	3.79	-	0.942	20
sand	0	0.27	1.01	4.93	0.960	12
loam	9	-0.10	0.93	4.90	0.943	20

† SE = standard error

Because the linear model is too simple, Rhoades et al. [1989] have included a second order term:

$$\sigma = \text{intercept} + A \times \theta_w \times \text{SC} \times E + B \times \theta_w^2 \times \text{SC} \times E \quad (3.3.29)$$

with A and B the regression coefficients.

The results of this model are statistically better than the linear model (see Table 3.3.1). The coefficients of determination are 0.94 and 0.96 respectively for the loam and sand. Another improvement is that the intercepts are no longer negative; now they can be related to the soil surface conductivity  $\sigma_s$ . A disadvantage of this model, however, is that the regression coefficients do not have a physical meaning: Table 3.3.1 shows that the A parameter is no longer close to one and that the second order term has become larger than the linear term ( $B \times \theta_w^2 \gg A \times \theta_w$  for  $\theta_w > 0.1$ ).

Adding a third order term (i.e.  $C \times \theta_w^3 \times \text{SC} \times E$ ), as is suggested by our theoretical model (3.3.26), does not significantly improve the regression (Table 3.3.1). Furthermore, the number of regression parameters is getting rather high (four). To approach the measuring points directly with the theoretical model is quite complicated. This model is a non-linear function of  $\theta_w$ ,  $\sigma_s$  and  $\sigma_w$ . Thus, we need values for both  $\sigma_s$  and  $\sigma_w$ . A good approximation for  $\sigma_w = \text{SC} \times E$ . In order to simplify the theoretical model in  $\sigma_s$  and  $\sigma_w$ , we assume that  $\sigma_s \ll \sigma_w$ .

Then (3.3.26) can be written as:

$$\sigma = \sigma_s(1 + 3\theta_w) + \sigma_w(2 - \theta_w)\theta_w^2 \quad (3.3.30)$$

We can now perform regression analyses on two terms:

$$\sigma = A(1 + 3\theta_w) + B(2 - \theta_w)\theta_w^2 \times SC \times E \quad (3.3.31)$$

with A and B the regression coefficients.

The regression analysis for this model is very accurate (see Table 3.3.2): the  $r^2$  is larger than 0.98 for both soils. This represents a significant improvement over the other models. Moreover, there are only two degrees of freedom. This model does not allow an intercept, because this is hidden in the term  $(1+3\theta_w)A$ .

Table 3.3.2 Multiple regression analyses of bulk electrical conductivity in Caledon sand and Guelph loam for the model:  
 $\sigma = A(1 + 3\theta_w) + B(2 - \theta_w)\theta_w^2 \times SC \times E$

medium	A	B	$r^2 \dagger$	SE
sand	12	1.91	0.983	12
loam	26	1.46	0.984	18

$\dagger$  redefined  $r^2$  because there is no intercept in the model

According to (3.3.31) A should approximate  $\theta_s$  and B should be equal to one, because  $\sigma_w = SC \times E$ . The regression gives A parameters of 12 and 26 mS/m for the sand and loam respectively, which might be reasonable values for the soil surface conductivity  $\sigma_s$ . The Guelph loam has a larger silt and clay fraction than the Caledon sand [Elrick and Bowman, 1964; Reynolds, 1986]. Thus, a larger specific surface is expected and hence a larger surface conductivity [Van Loon et al., 1990b].

The regression coefficient B clearly differs from one: 1.91 and 1.46 for sand and loam, respectively. However, if it is assumed that for saturated soil, water

and soil particles behave like an ideal mixture (which is suggested in [Van Loon et al., 1990b]), then the following approximation of (3.3.30) must be true:

$$\sigma_{\text{sat}} = (1 + 3 \times \theta_{\text{sat}}) \sigma_s + \theta_{\text{sat}} \text{SC} \times E \quad (3.3.32)$$

Comparing (3.3.32) with (3.3.31) at saturation suggests the following relationship:

$$B = 1 / [(2 - \theta_{\text{sat}}) \theta_{\text{sat}}] \quad (3.3.33)$$

The B parameter can now be estimated using the measured volumetric water contents: in sand  $\theta_{\text{sat}} = 0.30$ , which results in  $B = 1.91$  and in loam  $\theta_{\text{sat}} = 0.40$ , which results in  $B = 1.56$ . These values agree well with the values, obtained by regression analyses.

The above results are only applicable to unfrozen conditions. However, because of the generality of the dispersion theory, and the good correspondence found between the theory and experimental data for  $\epsilon$  in both frozen and unfrozen soils, it is anticipated that they should be equally applicable for modeling  $\sigma(\theta_u)$  relations under frozen conditions. Few data are presently available for testing this assumption. Consequently, the application of dispersion theory for deriving  $\sigma(\theta_u)$  relations in frozen soil will require further research. This is particularly important in the light of current interest in saline and subsea permafrost [Perfect et al., 1991].

### 3.3.5.2 Comparison with other models

The relation between bulk electrical conductivity and soil water content has also been described by Rhoades et al. [1989]. They divided the soil water into two parts: 'immobile' water that is present close to the soil surface and 'mobile' water that is situated in the larger pores. To obtain the bulk electrical conductivity  $\sigma$  they combine the electrical conductivities of the surface of the solid particles  $\sigma_s'$  and of the soil water  $\sigma_w$  in a series parallel model. The electrical conductivity by direct particle-to-particle contact is neglected and it is assumed that  $\sigma_s' \ll \sigma_w$ . This leads to the following relation [Rhoades et al., 1989]:

$$\sigma = [(\theta_s + \theta_{iw})^2 \theta_s'] / \theta_s + (\theta_w - \theta_{iw}) \sigma_w \quad (3.3.34)$$

where  $\theta_s$  is the volumetric fraction of the solid (soil) phase,  $\theta_{iw}$  is the volumetric fraction of the immobile water and  $\theta_w$  is the total volumetric water fraction. At zero moisture content  $\sigma = \theta_s \sigma_s'$ , which is comparable with  $\sigma_s$  in our model.

According to Rhoades et al. [1989] all the water molecules are supposed to be immobile at low water contents. Thus,  $\theta_w = \theta_{iw}$  for  $\theta_w < 0.1$ . If terms with  $\theta_w^2$  are neglected, eq (3.3.34) can be rewritten for  $\theta_w < 0.1$  as follows:

$$\sigma = (1 + 2 \theta_w / \theta_s) \sigma_s' \theta_s \quad (3.3.35)$$

This model is close to the parallel plate model of Maxwell (read in eq (3.3.11)  $\sigma$  instead of  $\epsilon$ ). If in Maxwell's model it is supposed that  $\sigma_s \ll \sigma_w$ , then for low water contents (3.3.11) can be written as:

$$\sigma = (1 + 3 \theta_w) \theta_s \quad (3.3.36)$$

As stated above  $\sigma_s = \sigma_s' \theta_s$ . Both models lead to similar conclusions at low water contents. Firstly, the electrical conductivity of the soil water has little influence (which seems to be a contradiction with  $\sigma_s \ll \sigma_w$ ). Secondly, the product of the soil surface conductivity with water content is very important. The factor in front of this product is also similar: if the solid fraction equals for instance  $\theta_s = 0.6$  then  $2/\theta_s = 3.3$  (second term of right hand side of (3.3.35)), which is close to 3 (second term of right hand side of (3.3.36)). However, at higher water contents the two models look very different, because the higher order terms in  $\theta_w$  are not present in the model of Rhoades et al. [1989].

If our data are used only at saturated conditions, a linear relation is obtained between  $\sigma$  and  $\sigma_w$  [Van Loon et al., 1990b]. For Guelph loam:

$$\sigma = 78 + 0.90 \times \theta_{sat} \sigma_w \quad (3.3.37)$$

and for Caledon sand:

$$\sigma = 26 + 0.95 \times \theta_{\text{sat}} \sigma_w \quad (3.3.38)$$

The intercepts are much higher than the  $\sigma_s$  values estimated using (3.3.31). This is because the relation between the intercepts in (3.3.37) and (3.3.38) and  $\sigma_s$  has to be:

$$\text{intercept} = (1+3 \times \theta_{\text{sat}}) \sigma_s \quad (3.3.39)$$

From eq (3.3.39),  $\sigma_s$  for loam and sand is 35 and 14 mS/m, respectively while from eq (3.3.31) these values are 26 and 12 mS/m. Both estimates are in good agreement considering mean square errors of 7 and 3 mS/m, respectively.

### 3.3.6 Conclusions

In time-domain reflectometry, empirical equations have been applied to describe the non-linear relations between various dispersive parameters (e.g.  $\epsilon$  and  $\sigma$ ) and the water content. In this paper a theoretical background has been provided for these equations which appears to describe them with great accuracy.

At low water contents ( $\theta_w < 0.05$ ) the soil water can be found in thin films of water around the soil particles. For the dielectric constant, this geometry can be modeled with Maxwell's equations for the dispersive behaviour of two materials arranged in parallel plates [Maxwell, 1873]. At water contents close to one, water and soil behave like an ideal mixture. These two conclusions can be translated into a third order power series in  $\theta_w$  (eq 3.3.19).

The dielectric constant of unfrozen water in partially frozen soil appears to be lower than that for supercooled water at the same temperature. Oliphant [1985] came to the same conclusion by using another  $\epsilon(\theta_u)$  relation. The decrease in  $\epsilon_w$  is probably caused by partial orientation of water molecules in the immediate vicinity of pore ice (the Workman-Reynolds effect [Parameswaran and Mackay, 1983]).

The electrical conductivity at low water contents can also be modeled with water and soil in parallel plate configuration. At saturation, water and soil again behave like an ideal mixture. These two extremes can be interpolated with a third order polynomial using only two degrees of freedom. The two corresponding regression parameters allow physical interpretation:  $\sigma_s$  and  $1/[(2-\theta_{sat})\theta_{sat}]$ . The polynomial has a better correlation coefficient with experimental data compared to other models. In summary, the advantages of the present model are:

1. it has a theoretical background,
2. there are less parameters to be determined (only two),
3. the formulation is explicit, so the values can be calculated easily,
4. the agreement with experimental data is very good.

### 3.3.7 Appendix

*Derivation of eq's (3.3.15) and (3.3.16).*

To obtain (3.3.15) one simply uses (3.3.11) at  $\theta_w=0$ :

$$\epsilon_{pp}(0) = \frac{\epsilon_{sa} (\epsilon_w + 2 \epsilon_{sa} + 0)}{\epsilon_w + 2 \epsilon_{sa} - 0} = \epsilon_{sa} \quad (A3.3.1)$$

For (eq 3.3.16)  $d\epsilon_{pp}/d\theta_w$  has to be taken at  $\theta_w = 0$ :

$$\frac{d\epsilon_{pp}}{d\theta_w} = \frac{3 \epsilon_{sa} (\epsilon_w + 2 \epsilon_{sa}) (\epsilon_w - \epsilon_{sa})}{[\epsilon_w + 2 \epsilon_{sa} - \theta_w (\epsilon_w - \epsilon_{sa})]^2} \quad (A3.3.2)$$

at  $\theta_w = 0$ :

$$\frac{d\epsilon_{pp}}{d\theta_w} = \frac{3 \epsilon_{sa} (\epsilon_w - \epsilon_{sa})}{(\epsilon_w + 2 \epsilon_{sa})} \quad (A3.3.3)$$

*Derivation of (eq 3.3.19)*

Rewrite (3.3.17) as:

$$C + D = \epsilon_w - A - B \quad (A3.3.4)$$

Using (3.3.15) and (3.3.16) in (A3.3.4):

$$C + D = \frac{(\epsilon_w - \epsilon_{sa})(\epsilon_w - \epsilon_{sa})}{(\epsilon_w + 2\epsilon_{sa})} \quad (A3.3.5)$$

Then rewrite (3.3.18) as:

$$D = \epsilon_w - \epsilon_{sa} - B - 2(C+D) \quad (A3.3.6)$$

Using (3.3.16) and (A3.3.5) in (A3.3.6):

$$D = \frac{(\epsilon_w - \epsilon_{sa})(\epsilon_w + 2\epsilon_{sa})}{(\epsilon_w + 2\epsilon_{sa})} - \frac{3\epsilon_{sa}(\epsilon_w + \epsilon_{sa})}{(\epsilon_w + 2\epsilon_{sa})} - \frac{2(\epsilon_w - \epsilon_{sa})(\epsilon_w - \epsilon_{sa})}{(\epsilon_w + 2\epsilon_{sa})}$$

or

$$D = \frac{-(\epsilon_w - \epsilon_{sa})(\epsilon_w - \epsilon_{sa})}{(\epsilon_w + 2\epsilon_{sa})} \quad (A3.3.7)$$

now C can be obtained by combining (A3.3.7) and (A3.3.5):

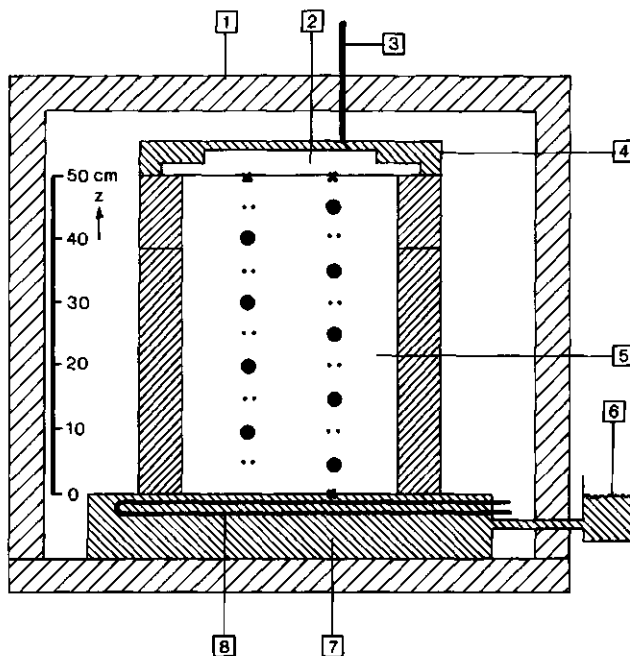
$$C = \frac{2(\epsilon_w - \epsilon_{sa})(\epsilon_w - \epsilon_{sa})}{(\epsilon_w + 2\epsilon_{sa})} \quad (A3.3.8)$$

### 3.4 Description of the experiments to measure heat and mass transfer in freezing porous media

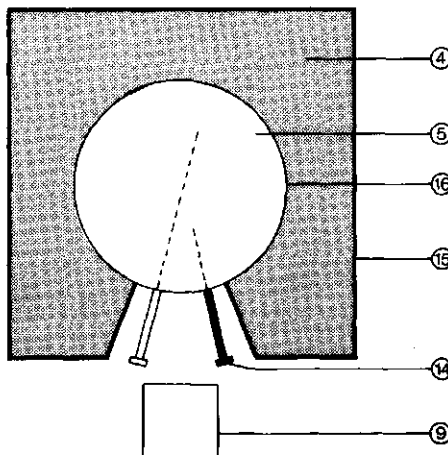
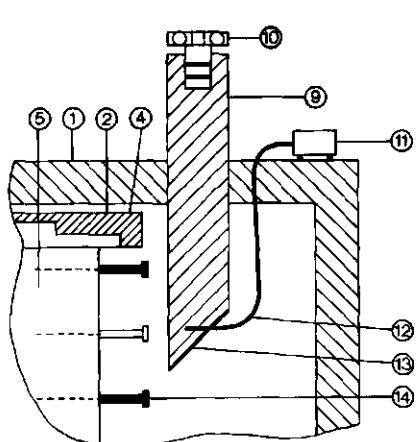
#### 3.4.1 Experimental set-up

Imitation in the laboratory of what is happening in nature is the main goal of laboratory experiments. This means, that edge effects (caused by finite horizontal dimensions of the test material) are to be avoided as much as possible and that freezing conditions are to be comparable with natural freezing conditions. So the tested soil sample has to be rather large, the temperature gradient rather small and the overburden pressure small too. On the other hand, the models have to be as simple as possible, so we use one dimensional models both for the theory and the experiments. This agrees well with reality, because in natural soils the transport phenomena caused by freezing occur mainly in the vertical direction.

The tested columns have a height of 450 to 500 mm and a diameter of 300 mm. They are placed inside a climate case which is kept at  $+0.5^{\circ}\text{C}$ . The top of the column is covered with a flat heat exchanger, whose temperature can be controlled (see Fig. 3.4.1). The pressure of the heat exchanger can be compared with the weight of a 70 mm asphalt or soil layer (with an overburden load of 1.3 kPa). The bottom of the sample is placed on a saturated sand. The water level in the sand is externally controlled with a water reservoir, so a constant water table together with free water supply can be maintained. The bottom of the column is kept at  $+4^{\circ}\text{C}$ . Both the upper flat heat exchanger and the bottom with the saturated sand are carefully thermally insulated. The vertical, cylindrical boundary is also covered with insulating material except for a slit which represents 10% of the vertical surface. In this slit the measuring probes are installed (see Fig. 3.4.1). They cannot be covered with insulating material because they need the freedom to move with respect to the insulation, together with the heaving soil. The slit in the insulation between column and climate case gives also the possibility to observe the heaving process in detail. Fig. 3.4.1 shows how with the help of a periscope part of the bare soil surface can be observed. By moving the periscope up and down the whole slit can be sampled. The light is conducted from an outside light source to the slit by glass fiber wires. With this method only light and no heat is transmitted to the slit. On the periscope a photocamera has



a. freeze test cel with soil column



b. vertical cross section with periscope    c. horizontal cross section with slit

Fig. 3.4.1 Freeze test cel with soil column, periscope and slit in insulation, in which: 1. insulated climate case, 2. flat heat exchanger at  $T < 0^\circ\text{C}$ , 3. rod for observation of total heave, 4. heat insulation of soil sample, 5. soil sample, 6. water table, 7. saturated sand, 8. heat exchanger at  $T = +4^\circ\text{C}$ , 9. periscope, 10. photo camera, 11. light source, 12. glasfibre wire, 13. mirror and 14. measuring probes, x thermocouple probes, .. parallel TDR probes and ● thermal conductivity probes.

been attached to make pictures of the freezing soil. Because also rulers have been placed inside the slit, the location and amount of differential heave can be determined exactly.

There are three different measuring probes: thermocouple probes for the measurement of the temperature in the centre of the column, parallel TDR probes to measure volumetric water content and bulk electrical conductivity (see section 2.2) and thermal conductivity probes.

For the thermal conductivity the nonsteady state probe method is applied to measure in situ the effective thermal conductivity of a soil- water- ice- air mixture [Van Haneghem, 1981; Bruijn et al., 1983 and section 3.1]. The short measuring time of three minutes and the low temperature rise of 0.15 K allow to follow transient processes in frozen soils. In this probe an extra temperature sensor is built in: an electronic device called AD-590 [Analog Devices, 1988], which generates an electrical current proportional to the absolute temperature. With the extra temperature sensor the temperature of the soil at a certain height can be measured and from this the temperature gradient can be calculated.

Because of the slit in the insulation, the temperature and thus the heave on that location will deviate from the average heave. Therefore the average total heave needs to be measured separately. This measurement can be performed with a thin rod, which is placed (through small holes in the environmental chamber and insulation) on top of the upper heat exchanger, so it will move upwards with the soil. The heave can be determined by measuring the relative displacement of the rod.

The measurements were performed with six different porous materials, defined in more detail in the next section: one waste material, two highly inorganic sands and three undisturbed soil columns. The two inorganic sands are supposed to be not frost susceptible, which will be proved by independent measurements in section 4.3. The non-frost susceptibility allows us to modify the experiments somewhat: the two inorganic sands are frozen in a closed system (without external water supply or heave) so all probes can be fixed.

This also allows us to put the heat insulation all around the column (see also section 4.1) so that the heat insulation improves considerably and a better agreement with the simplified heat balance equation can be obtained.

For most materials the following properties can be measured in situ:

1. temperature
2. thermal conductivity
3. water content
4. bulk electrical conductivity
5. position or differential heave.

### 3.4.2 Used materials

First, the in section 3.4.1 mentioned porous materials are defined more precisely. In the undisturbed soil columns two or three horizontally oriented zones can be distinguished. These zones (called horizons) can be different in colour, structure, mineral composition and other physical properties. Within a horizon these properties show less variation than within the column. Therefore the horizons are classified according to the the ISRIC [1988] standard:

B45 Concrete forms an important part of demolition waste. When it is crushed it looks at first sight like a gravelly sand, with, in our case, aggregates up to 31.5 mm. As testing material we took the fraction smaller than 2 mm of a high quality concrete: B45 (which has a compression strength of 36 MPa).

RSA In order to be able to compare the concrete with sands, a river sand (from the river Rhine) has been tested, which has about the same particle size distribution as the crushed concrete. This river sand consists mainly (>99.9%) of quartz.

SSA Silver sand is the most homogeneous porous material used, because it consists of only one sieve fraction 150-210  $\mu\text{m}$ . This is again a pure quartz sand.

LSA To make the link to real soils, an undisturbed column of loamy sand ('Eng Sand' or Mollie Gley Sol [ISRIC 1988]) from a lot at the Mansholtlaan in Wageningen (NL) has been tested. This soil consists of three horizons: the root zone (Ap12) or LSA-1, the anthropogenic zone (Apg2b) or LSA-2 and the gley zone (ACgb) or LSA-3. Each layer consists roughly of 80% sand, 10% silt and 10% clay.

SLO As an example of a loam, an undisturbed column of sandy loam ('Achterhoeks Loam' or Eutric Gley Sol [ISRIC, 1988]) from a lot at the Weidehoek in

Bredenbroek (NL) has been tested. This soil consists of three horizons: antropogenic zone (Ap) or SLO-1, loamy zone (C1g) or SLO-2 and rusted sand zone (C2r) or SLO-3. The loamy zone had a very high silt content of about 40%, while the two other zones consist roughly for 20% of silt. Each zone contains for about 5% clay particles.

CLA As an example of a clay, an undisturbed column of river foreland clay (Calceric Fluvi Sol [ISRIC, 1988]) from the foreland of the river Rhine near Randwijk (NL) has been tested. This soil consists of two horizons: the clayey zone (BW1) or CLA-1 and the sandy zone (BW2) or CLA-2.

The water retention curves of the six materials are reproduced in Fig. 3.4.2. In order to save the surveyability of this figure only the most characteristic horizon of each undisturbed soil column is presented.

From Fig. 3.4.2 it can be seen that the crushed concrete has a low saturated water content ( $\theta_w = 0.28$  at  $pF = 0$ ). Silver sand and river sand have the typical chairlike curves of sands. The three horizons of the undisturbed soil columns have a more smooth relation between water content and suction. These soils retain a lot more water at high negative pressures, compared with the other materials. This is due to the larger fraction of small soil particles (see Table 3.4.1).

The particle size distributions can be found in Fig. 3.4.3. Some characteristic mass fractions are given in Table 3.4.1: fines (=fine particle) fraction  $\Phi_{125}$ , which is the fraction that passes the 125  $\mu\text{m}$  sieve; the fraction which passes the 50  $\mu\text{m}$  sieve  $\Phi_{50}$ , which is the sum of the clay and the silt fraction; and  $\Phi_2$ , which is the clay fraction. Also some other soil physical and electro-chemical parameters are inserted in Table 3.4.1.

The hydraulic conductivity  $k$  does not show important variation in the materials examined in Table 3.4.1 ( $k$  can vary easily 3 to 5 orders of magnitude between different soils). This is probably due to the existence of macropores in the undisturbed soil columns.

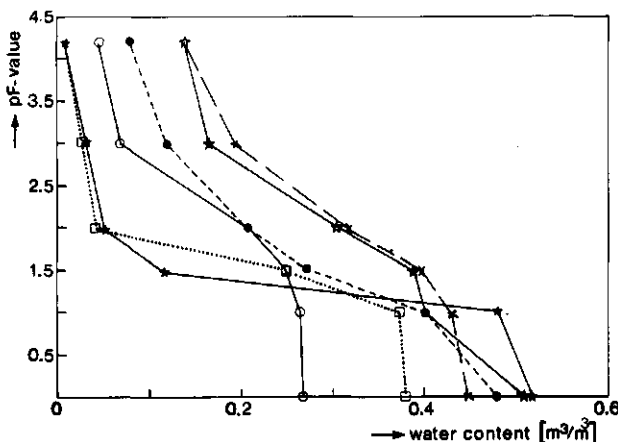


Fig. 3.4.2 Water retention curves of a selection of the materials used: B45 (○), SSA (\*), RSA (□), LSA-2 (●), SLO-2 (×) and CLA-1 (◊).

Table 3.4.1 Properties of the examined materials with  $\Phi_{125}$  the fraction that passes the  $125 \mu\text{m}$  sieve,  $\Phi_{50}$  the fraction that passes the  $50 \mu\text{m}$  sieve (silt + clay fraction),  $\Phi_2$  the clay fraction,  $k$  the unfrozen saturated hydraulic conductivity,  $S$  the specific surface area (determined according to the BET method [Gregg and Sing, 1982]), CEC the cation exchange capacity and  $\zeta$  the mobility or zeta potential.

medium	$\Phi_{125}$ [g/g]	$\Phi_{50}$ [g/g]	$\Phi_2$ [g/g]	$k \times 10^5$ [m/s]	$S$ [m <sup>2</sup> /g]	CEC [μg/kg]	$\zeta \times 10^8$ [m <sup>2</sup> /Vs]
B45	0.138	0.05	0.0	1.1	10.8	323	-1.5°
SSA	0.008	0.0	0.0	50	0.2†	4.5	-2.8°
RSA	0.120	0.01	0.0	20	0.5†	24.5	-2.8°
LSA-1	0.407	0.225	0.05	33	1.0†	40	-2.5
LSA-2	0.379	0.225	0.04	33	1.0†	38	-2.5
LSA-3	0.466	0.240	0.05	3.4	1.0†	39	-2.5
SLO-1	0.474	0.270	0.046	4	2.9	68	-2.4
SLO-2	0.452	0.434	0.064	4	9.5	67	-2.6
SLO-3	0.498	0.243	0.040	4	2.8	68	-2.4
CLA-1	0.885	0.83	0.26	3	7.1	93	-1.3
CLA-2	0.540	0.35	0.11	3	4.2	76	-1.3

†  $S$  is too small to be measured accurately with BET

° too few small particles available to make a suspension which is representative for the material examined.

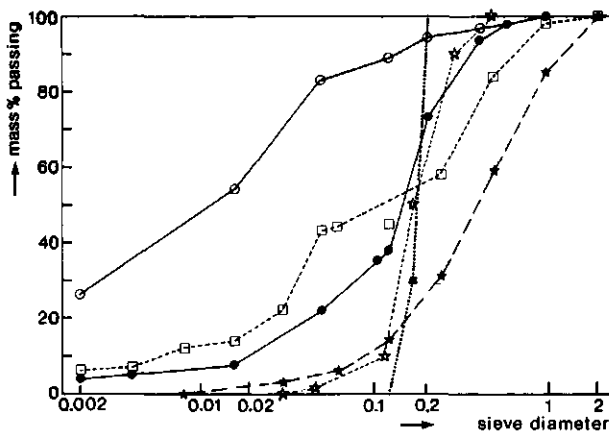


Fig. 3.4.3 Particle size distribution curves of a selection of the materials used: B45 (\*), SSA (x), RSA (▲), LSA-2 (●), SLO-2 (□), and CLA-1 (○).

### 3.4.3 Relations between soil physical and electro-chemical properties

In Chapter 1 it has been indicated that the soil physical and electro-chemical properties influence the heat and mass transfer in frozen soil. Therefore these properties are to be analysed in more detail, before we deal with the experiments of heat and mass transfer themselves (Chapter 4). The relevant analyses are presented in this section.

The specific surface area  $S$  is mainly determined by the clay fraction [Koorevaar et al., 1983].  $S$  is inversely proportional to the average diameter  $d$  of the fraction concerned: the amount of particles is proportional to  $d^{-3}$  and the surface area per particle proportional to  $d^2$ . The correlation of  $S$  and  $\Phi_2$ , as given in Table 3.4.1, is poor:  $r^2 = 0.09$  (see also Fig. 3.4.4). This is mainly caused by the high  $S$ -value for the crushed concrete. Crushed concrete remains highly aggregated. So the particles are extremely irregularly shaped and a large part of the surface area is caused by internal pores. Apart from this, crushed concrete has a different mineral composition compared with the other materials: it consists partly of cement. Another material which has a different mineral com-

composition is the loamy horizon of Achterhoeks sandy loam (SLO-2): it contains a lot of iron oxyde. When the regression between S and  $\Phi_2$  is performed without these two materials (i.e. B45 and SLO-2), the correlation improves (see Fig. 3.4.4):

$$S = A + B \times \Phi_2 \quad (3.4.1)$$

with regression coefficient A not significantly different from zero, regression coefficient B  $26 \pm 4 \text{ m}^2/\text{g}$ , the standard error SE  $0.9 \text{ m}^2/\text{g}$  and the coefficient of determination  $r^2 0.87$ .

The cation exchange capacity CEC is largely determined by specific surface area and mineral composition [Baver et al., 1972]. This can be confirmed with our measurements. The coefficient of determination between CEC and S equals 0.60. When the two materials with different mineral composition are taken out, the regression between CEC and S improves:

$$CEC = A + B \times S \quad (3.4.2)$$

with  $A = 23 \mu\text{mol/g}$ ,  $B = 12 \pm 2 \mu\text{mol/m}^2$ , standard error SE =  $12 \mu\text{mol/g}$  and  $r^2 = 0.84$ .

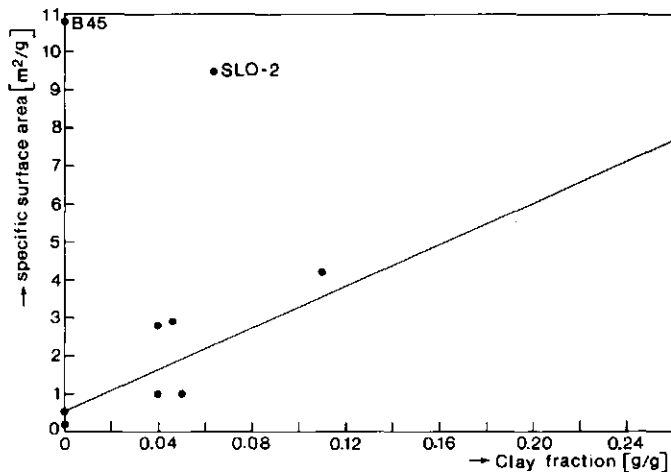


Fig. 3.4.4 Specific surface area as a function of clay fraction, with eq (3.4.1) as regression line.

The zeta potential or mobility  $\zeta$  is a measure for the electrical surface charge per unit of surface area. It should be constant for all materials with the same mineral composition. It is therefore expected that  $\zeta$  is more or less constant for all materials except for B45 and SLO-2. However, the measurements for B45, SSA and RSA are not representative, because only an extremely small fraction (less than 0.1%) had a particle diameter small enough to remain in suspension during the  $\zeta$  measurements. For the reliable  $\zeta$ -values it can be stated that they are rather constant. Even SLO-2 does not have a different value.

The influence of the soil physical and electrochemical properties on frost heave will be discussed in section 4.3.

## 4 RESULTS AND DISCUSSION

### 4.0 Introduction to the chapter

In this chapter two independent papers can be found. The first section (4.1) contains the oldest paper and describes heat transfer in closed system freezing. This paper has been revised due to a growing understanding of the complicated influences of the freezing process on thermal conductivity. Next, our major experiments (with external water supply) about heat and moisture transfer are described in sections 4.2 and 4.3, respectively.

These two sections are written exclusively for the thesis. Then the second paper is presented in section 4.4, where the solute redistribution (or transport) is described. The chapter finishes with the description of the influence of added solutes on the moisture transport in section 4.5.

The two papers included in this chapter are:

- 4.1 Loon W.K.P. van, Haneghem I.A. van and Boshoven H.P.A., 1988. Thermal and hydraulic conductivity of unsaturated frozen sands, Proc. Fifth Int. Sym. Ground Freezing, Vol. 1, Balkema, Rotterdam NL pp 81-90.
- 4.4 Loon W.K.P. van, Perfect E., Groenevelt P.H. and Kay B.D., 1990a. Application of time domain reflectometry to measure solute redistribution during soil freezing. Proc. Int. Frozen Soil Symp., CRREL report 90-1, Hannover NH, USA, pp 186-194.

## 4.1 Thermal conductivity of unsaturated frozen sands

### 4.1.0 *Abstract*

The heat flow in unsaturated silver sand and river sand is determined by measuring thermal conductivities and temperatures at several depths in laboratory experiments. The thermal conductivity of the unfrozen sand is a function of the volume fraction of water. In the frozen sand however the thermal conductivity cannot only be explained in terms of volume fractions of the components water, ice and sand. From the measured thermal conductivity and an assumed constant heat flow, a systematic measuring error in the thermal conductivity of the frozen soil can be determined. The maximum value in river sand is 2 W/mK and in silver sand 5 W/mK. This error is larger as the temperature approaches 0°C, indicating an influence of the frost front.

### 4.1.1 *Introduction*

Frost phenomena in soils are important in technical and agricultural engineering. Frost can damage pipelines, roads and buildings, but it can also improve the structure of the soil. Other fields of interest are artificial freezing (for instance of foods or human organs) and freeze-drying processes.

During the past few decades several theories have been developed to describe frost penetration as well as frost heave. It became clear that a coupling of heat and mass transfer takes place [e.g. Dirksen and Miller, 1966; Kay and Groenevelt, 1974]. The coupling is very important to explain the secondary heave mechanism. A suction pressure was introduced to explain the water movement towards the freezing front and thermodynamic theories for equilibrium pressures were derived [Groenevelt and Kay, 1980]. Of course there was always a strong interaction between the development of these theories and laboratory experiments. In these experiments heave was measured, temperature was determined on several depths and often also the water content was followed.

However, up to now some important physical parameters were never determined *in situ* during a frost penetration test. For a good knowledge of the heat transport

also the thermal conductivity has to be known as a function of time and place. Especially in unsaturated soil samples this physical property is hard to estimate. And for a better knowledge of the water transport through the frozen fringe the hydraulic conductivity has to be known in this area.

Our laboratory is specialized in thermal conductivity measurements with the nonsteady state probe method [Van Haneghem, 1981 and Van Loon et al., 1989b]. Recent developments made it possible to perform these measurements in a short measuring time (about 3 minutes). This allows us to follow quasi steady state processes. Besides, the averaging volume in which the effective thermal conductivity is determined has become smaller (a cylindrical volume with a diameter of about 3 cm). So, now a position dependent thermal conductivity can be measured. Theoretically it is also possible to obtain simultaneously a value for the volumetric heat capacity by this method [Van Loon, 1989b].

In this section the heat transport through two different sand samples is evaluated. Heat transport is coupled with other physical phenomena: e.g. water transport. The results will be compared with experiments performed by others.

#### *4.1.2 Experimental set-up*

In real soils most of the transport phenomena caused by freezing occur in the vertical direction. Temperature is mainly a function of the distance to the earth surface and the water content is highly influenced by the distance to the water table. Usually the different soil layers are also horizontally orientated. This allows us to use one-dimensional models both for the theory and experiments. So the properties of the sand- water- ice- air mixture are supposed to vary only in time and in the vertical direction. To attain this in the laboratory, an insulated and closed measuring box was designed. This box has to contain the medium and has to provide the possibility to perform different kinds of measurements (see Fig. 4.1.1).

The temperature range in which the experiments were performed is between -10°C and +10°C. For minimizing heat losses in horizontal direction, the ambient temperature has to be in the middle of this range. We put therefore the insulated

box into a climate case. For the ambient temperature  $+0.5^{\circ}\text{C}$  was taken: freezing of the walls of the climate case had to be avoided. The overall vertical temperature difference was controlled by two flat heat exchangers. The heat exchangers were connected with thermostatic baths, so the temperature inside the heat exchangers remains constant until the temperature of the thermostatic bath is changed.

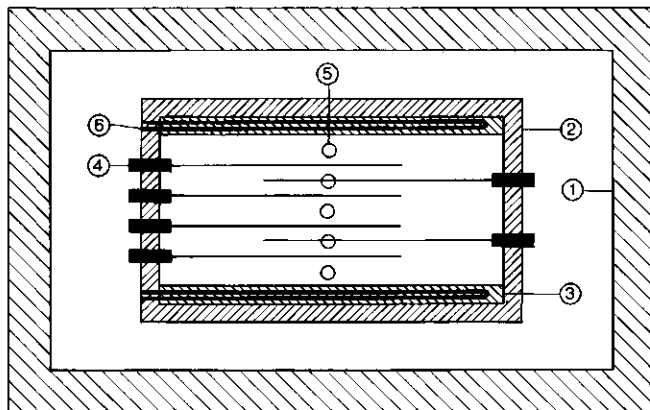


Fig. 4.1.1 Schematic cross-section of the measuring box, with 1. insulated climate case, 2. insulated measuring box, 3. lower flat heat exchanger, 4. thermal conductivity probes, 5. thermocouples, 6. upper flat heat exchanger.

Inside the measuring box with sand we placed thermocouples on several depths. Also six thermal conductivity probes were horizontally embedded in the sand. With these instruments it is possible to measure *in situ* the effective thermal conductivity of a sand- water- ice- air mixture. The most important parts of the needle-shaped probe are a double folded constantan heating wire and a constantan-manganine thermocouple, both with a diameter of 0.1 mm and carefully fitted into a stainless steel envelope (see Fig. 4.1.2). The hot junction of the thermocouple is placed very close to the heating wire; the cold junction is placed at the end of the probe and is considered to stay at its original temperature. To fix the position of the wires in the cylindrical envelope and to prevent electrical contact, the remaining space is filled with a silicon rubber compound. The length of the probe is about 200 mm and its diameter is 2 mm.

In the nonsteady-state probe method the temperature response of the probe on a suddenly starting constant energy dissipation inside the probe is measured. At time  $t=0$  a constant electrical heating current is switched on and the temperature response is recorded once per second. The thermal conductivity is inversely proportional to the measured temperature response.

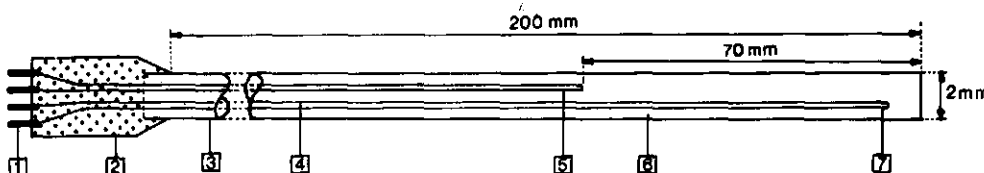


Fig. 4.1.2 Cross-section of the needle-shaped thermal conductivity probe, with 1. contacting wires, 2. polyvinyl chlorid protector, 3. metallic tube, 4. hot junction of thermocouple, 5. heating wire, 6. insulating material, 7. cold junction of thermocouple.

Apart from these, other experiments were performed to characterise the sands more accurately. The following properties of the sand package were determined: hydraulic conductivity of the saturated sand, water retention curve (pF-curve), porosity, particle size distribution (sieve curve) and thermal conductivity as a function of the water content (for room temperature).

#### 4.1.3 Theoretical approach

The medium, in which the experiments were performed, consists of a solid matrix with pores. Inside the pores air, (liquid) water, vapor and, at temperatures below 0°C, also ice is present. In the latter temperature range liquid water and ice exist in a thermodynamical equilibrium. At temperatures below the freezing point the liquid water consists of a film close to the surface of the soil mineral particles. In the temperature range below 10°C in which the experiments were performed, heat transport by radiation can be ignored. The low temperatures cause also low vapor pressures, so heat transport in the vapor phase is also ignored. For our experiments a one dimensional model was constructed: only changes along the vertical (or z-) axis are considered. This enables us to write the continuity equation for mass (i.e. water) in one dimension:

$$\rho_w \partial \theta_w / \partial t + \rho_i \partial \theta_i / \partial t = - \partial (\rho_w v_w) / \partial z \quad (4.1.1)$$

with  $\rho_w$  the density of water,  $\rho_i$  the density of ice,  $\theta_w$  the volume fraction water,  $\theta_i$  the volume fraction ice,  $t$  the time and  $v_w$  the apparent or superficial water velocity. The left hand side terms of (4.1.1) account for accumulation of (liquid) water and ice, respectively, while the right hand side represents the net result of the transport term for the liquid phase. The continuity equation for heat yields in this case:

$$C \partial T / \partial t + L \rho_w \partial \theta_w / \partial t = \partial / \partial z [\lambda (\partial T / \partial z) - v_w C_w T - v_w L \rho_w] \quad (4.1.2)$$

with  $C$  the volumetric heat capacity,  $T$  the temperature,  $L$  the heat of fusion,  $z$  the (vertical) position and  $\lambda$  the thermal conductivity.

Here the left hand side accounts for an increase in temperature of the medium and for the latent heat to melt ice. (The eventual change in  $C$  can be neglected with respect to the large contribution of  $L$ .) The right hand side consists of the conduction term and the convection terms of sensible heat and latent heat respectively (in the liquid water phase).

Most measurements were performed under quasi steady state conditions, so the first term of equation (4.1.2) equals 0. The convection of sensible heat is ignored with respect to the conduction. The convection of latent heat might play a role near the freezing front. However, when no heave occurs (no water transport takes place), also this term can be neglected. Then (4.1.2) can be simplified into:

$$L \rho_w \partial \theta_w / \partial t = \partial / \partial z [\lambda (\partial T / \partial z)] \quad (4.1.3)$$

It is possible to integrate this equation over  $z$ . As a result heat flow  $Q$  is obtained (see also [Holden et al., 1985]):

$$Q_L = Q_f - Q_u \quad (4.1.4)$$

in which  $Q_L$  is the heat flow caused by the production of latent heat due to the moving freezing front (with position  $X$ ),  $Q_u$  is the heat flow by conduction in the unfrozen zone and  $Q_f$  is the heat flow by conduction in the frozen zone.

The mathematical description of the heat flows yields:

$$Q_L = -\rho_w L \theta_w dX/dt \quad (4.1.5)$$

$$Q_f = -\lambda_f \partial T_f / \partial z \quad (4.1.6)$$

$$Q_u = -\lambda_u \partial T_u / \partial z \quad (4.1.7)$$

In determining the heat flow, the thermal conductivity  $\lambda$  is a very important parameter. To measure  $\lambda$  with the probe method, heat has to be dissipated. During a measurement in the temperature range below 0°C, always a fraction of the ice will melt to establish a new thermodynamical equilibrium. As a result of this melting effect both the measured thermal conductivity and the measured heat capacity differ from their steady state values.

#### 4.1.4 Properties of the used sands

First we give a short characterisation of the two sands which are used (see Table 4.1.1). The greyish 'silver' sand consists of only one sieve fraction (150-210  $\mu\text{m}$ ). The river sand is from the river Rhine and is well graded: bigger as well as smaller particles are present.

Table 4.1.1 Physical properties of the used sands, with  $d_{10}$  the equivalent sieve diameter through which 10 mass percent does not pass,  $k$  the hydraulic conductivity,  $\emptyset$  the pore volume,  $\theta$  the volume fraction and  $S$  the specific surface area

property	unit	silver sand	river sand
$d_{10}$	$\mu\text{m}$	204	300
$d_{50}$	$\mu\text{m}$	180	170
$d_{90}$	$\mu\text{m}$	156	117
$d_{99}$	$\mu\text{m}$	150	45
$k_{\text{saturated}}$	$10^{-4} \text{m/s}$	2	2
$\emptyset$	$\text{m}^3/\text{m}^3$	0.517	0.379
$\theta_{\text{quartz}}/\theta_s$	$\text{m}^3/\text{m}^3$	1.000	0.999
$\theta_{\text{organic}}/\theta_s$	$\text{m}^3/\text{m}^3$	0.0	0.0
$\theta_w$	$\text{m}^3/\text{m}^3$	0.076	0.123
$S$	$\text{m}^2/\text{g}$	0.1-0.5	0.3-1.0

This can be seen from the different diameters: e.g. 10 mass % of the particles has a bigger diameter than d10. Especially the presence of smaller particles (shown by the d90 and d99 diameters) influences the other physical properties of the river sand if it is compared with the silver sand. The capillary rise is bigger and the porosity  $\emptyset$  is smaller. The water retention curves have been shown in section 3.4 (Fig. 3.4.2).

Because the capillary rise of the sands is low, we added only a little amount of water (0.076 and 0.123 respectively, averaged over the total measuring box). To obtain a relationship between water content and thermal conductivity some experiments under steady state conditions ( $\partial T / \partial t < 0.03 \text{ K/day}$ ) were performed (at room temperature). First the thermal conductivity was measured at several depths. Immediately afterwards the water content was determined by taking sand samples at the same vertical position as the conductivity probes. The sand was weighed, dried in a stove and weighed again.

From these simple measurements the water content could be calculated and compared with the measured thermal conductivities (see Fig. 4.1.3). Because this kind of water content determination is destructive, these measurements were done after the freezing tests.

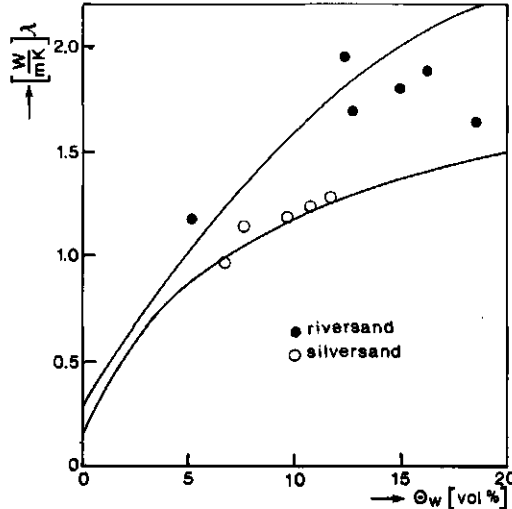


Fig. 4.1.3 Thermal conductivity  $\lambda$  as function of volumetric water content  $\theta_w$  in silver sand (outlined signs) and river sand (closed signs) under steady state conditions. The drawn lines are the best fits of the semi empirical Johanson and Frivik relation [1980] (see equation 4.1.8).

The measured relation between water content  $\theta_w$  and thermal conductivity  $\lambda$  confirms the semi empirical equation of Johanson and Frivik [1980] or Frivik [1980]:

$$\lambda = \lambda_s + \alpha(\lambda_{ws} - \lambda_s)^{10} \log(\theta_w/\phi + 1) \quad (4.1.8)$$

in which  $\lambda_s$  the thermal conductivity of the dry soil,  $\lambda_{ws}$  the thermal conductivity of the water saturated soil,  $\phi$  the porosity and  $\alpha$  a soil dependent factor, calculated from the best fit of the relation (4.1.8).

For silver sand the following values are obtained:  $\lambda_s = 0.13 \text{ W/mK}$ ,  $\lambda_{ws} = 1.96 \text{ W/mK}$  and  $\alpha = 0.53$ . For river sand these parameters are:  $\lambda_s = 0.26 \text{ W/mK}$ ,  $\lambda_{ws} = 2.87 \text{ W/mK}$  and  $\alpha = 0.83$ . This semi-empirical relation is for silver sand more accurate than for river sand (see Fig. 4.1.3). The average difference between measured and estimated  $\lambda$  is respectively 0.05 and 0.19 W/mK, which gives relative errors of 5% and 12%.

#### 4.1.5 Measured heat flows

The different non-isothermal experiments performed in the measuring box (see Fig. 4.1.1) are overviewed in Table 4.1.2. To test the experimental set-up a temperature difference was established for non-freezing conditions. Under quasi steady state conditions the temperature gradient was determined by linear interpolation from the thermocouples:  $\text{grad}(T) = \Delta T / \Delta z$ . For position  $z$  of the thermal conductivity probe we find the measured heat flow  $Q'(z) = -(\lambda(z) \times \text{grad}(T))'$ .

For the five probes heat flows of respectively 7.3, 7.9, 6.9, 7.1 and 7.2 W/m<sup>2</sup> were determined. When a constant vertical heat flow through sand is assumed, this method results into an accuracy of the measured heat flow of  $7.3 \pm 0.6 \text{ W/m}^2$ . This means that the measuring method for the heat flow by conduction is accurate to within 8%.

After the determination of the accuracy of the method (test 0), the freezing tests started. For different boundary temperatures the heat flow and the position of the freezing front were measured. Apart from the heat transport by conduction, the heat absorbed or dissipated by the moving freezing front  $Q_L$  (eq 4.1.5) had to be measured.

Table 4.1.2 Overview of tests in silver sand (test nr: 0-3) and river sand (test nr: 11-14)

test nr	initial temp. [°C] bottom on z=0	initial temp. [°C] top z=202 mm	final temp. [°C] bottom on z=0	final temp. [°C] top z=202 mm	freezing front position [mm]
0	5.2	3.8	5.2	3.8	-
1	1.3	3.8	- 9.0	3.2	77
2	-9.0	3.2	- 7.2	3.3	88
3	-7.2	3.3	- 5.0	3.2	106
11	10.0	10.1	- 4.9	3.0	114
12	-4.9	3.0	- 9.7	2.9	66
13	-9.7	2.9	-12.1	2.9	40
14	-6.4	1.6	- 5.6	2.2	79

The position of the freezing front itself is determined by linear interpolation of the measured temperatures. Its derivative to the time is calculated using the average displacement of the front during 12 hours. The only unknown quantity left is the water content of the volume element which is freezing. This quantity is estimated with the use of the measured thermal conductivity and (eq 4.1.8). We admit that this can give errors in  $\theta_w$  up to 30% (see Fig. 4.1.3: measured  $\theta_w$ - $\lambda$ -relations), but Table 4.1.3 shows that  $Q_L$  itself is small compared with  $Q'$ , so the error in  $Q' - Q_L$  remains relatively small.

Table 4.1.3 Heat flow  $Q'(z)$  [ $\text{W/m}^2$ ] on on several heights in the first freezing test in silver sand (horizontal heat flows were smaller than  $0.5 \text{ W/m}^2$ )

t[h]	$Q'(132) - Q_L$	$Q'(107) - Q_L$	$Q'(80) - Q_L$	$Q'(57)$	$Q'(32)$	$Q_L$
42	50	50	66	53	53	2
42	51	52	65	52	52	1.5
66	51	52	67	49	51	0.5
90	50	50	64	48	51	0.2

In Table 4.1.3 80% of the measurements of the heat flow has about the same value, even when frost penetration causes the largest value for  $Q_L$ :

$$Q = Q' - Q_L = 51 \pm 3 \text{ W/m}^2.$$

However, the values on  $z=80$  mm are significantly too big. This has to be caused by the measurement of the thermal conductivity  $\lambda$  on that depth. The position of the probe is just behind the freezing front (in the frozen area). In this area the liquid water content is highly temperature dependent. During the measurement of  $\lambda$  a small amount of heat is dissipated and some ice will melt, which causes an increase  $\Delta\lambda$  in thermal conductivity.

$$\Delta\lambda = \lambda' - \lambda \quad (4.1.9)$$

If we now assume that also on  $z=80$  mm the heat flow  $Q = 51 \text{ W/m}^2$ , we can calculate the real thermal conductivity:

$$\lambda(80) = -(Q + Q_L)/\text{grad}(T_{80}) \quad (4.1.10)$$

The results of the calculation are shown in Table 4.1.4.

Table 4.1.4 Thermal conductivities on depth  $z=80$  mm during the first freezing test in silver sand

$t[\text{h}]$	$\lambda'[\text{W/mK}]$	$\lambda[\text{W/mK}]$	$\Delta\lambda[\text{W/mK}]$	$T[^\circ\text{C}]$
42	1.89	1.47	0.42	-0.10
48	1.90	1.47	0.43	-0.07
66	2.00	1.53	0.47	-0.10
90	2.03	1.62	0.41	0.00

This kind of calculation has been done for each of the measured thermal conductivities in the frozen zone. Differences between the measured and the supposed thermal conductivity can go up to  $5 \text{ W/mK}$ . Because the temperature is a very important parameter in the water-ice equilibrium, the calculated  $\Delta\lambda$ -values are presented as a function of the temperature. The different depths are indicated by using different signs (see Fig. 4.1.4)

From Fig. 4.1.4 some remarkable conclusions can be drawn:

- $\Delta\lambda$ -values measured in river sand (filled signs) are bigger than those measured in silver sand (outlined signs).
- most points in Fig. 4.1.4 are found in two bands: one band for silver sand and one for river sand.
- the depth of the measuring probe is not significant for the measured  $\lambda$ .
- some values of  $\Delta\lambda > 0$  are also found in the area  $T > 0^\circ\text{C}$  (only for silver sand). They are always measured very close to the freezing front. Knowing that the measured thermal conductivity is always a result of an averaged value over a finite region (a cylindrical volume with a diameter of about 3 cm), the top of this region can be frozen and then influences the measurement strongly. Of course the cylindrical symmetry around the measuring probe, which is necessary for the calculations of  $\lambda$ , is not present here, so these results are not reliable.

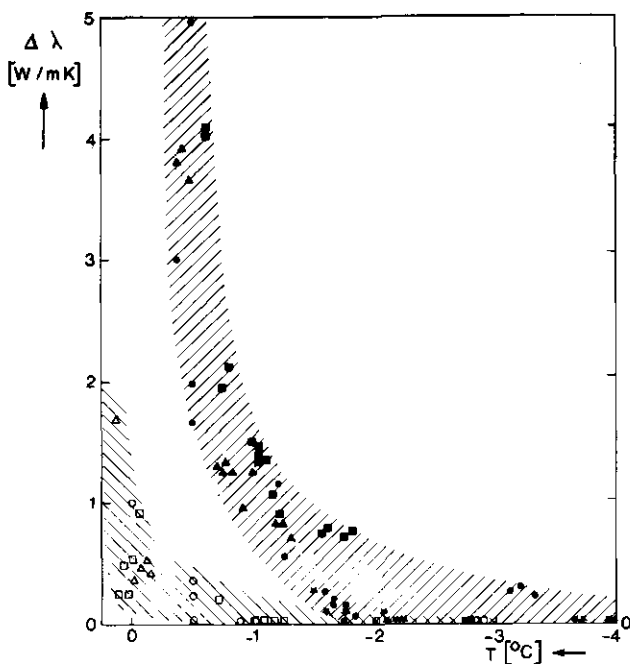


Fig. 4.1.4 Calculated extra thermal conductivity  $\Delta\lambda$  as a function of the temperature  $T$ . Closed signs are for river sand, outlined for silver sand, on several heights: (★) 156 mm, (○) 132 mm, (□) 107 mm and (Δ) 80 mm.

#### 4.1.6 Measured thermal conductivities

In the frozen zone an estimation for the real conductivity can be given (see eq 4.1.10). But for lower temperatures, the measured thermal conductivity is very close to the real thermal conductivity.

From Fig. 4.1.4 we can see that in silver sand  $\Delta\lambda < 0.03 \text{ W/mK}$  for  $T < -1^\circ\text{C}$ . So, in this temperature range a relationship between the ice content  $\theta_i$  and thermal conductivity  $\lambda$  can be expected [see also Johanson and Frivik, 1980].

This datum has been checked with some cylinders filled with silver sand with a given water content. We performed three succeeding freezing-thawing cycles. In a cycle the temperature varies from  $+10^\circ\text{C}$  to  $-10^\circ\text{C}$  and back in 24 steps.

The temperature is adjusted with a thermostatic bath, in which the cylinder with the humid sand and thermal conductivity probe is placed. Again a very small amount of water was added to the sand, because a homogeneous medium was needed. The results are presented in Fig. 4.1.5.

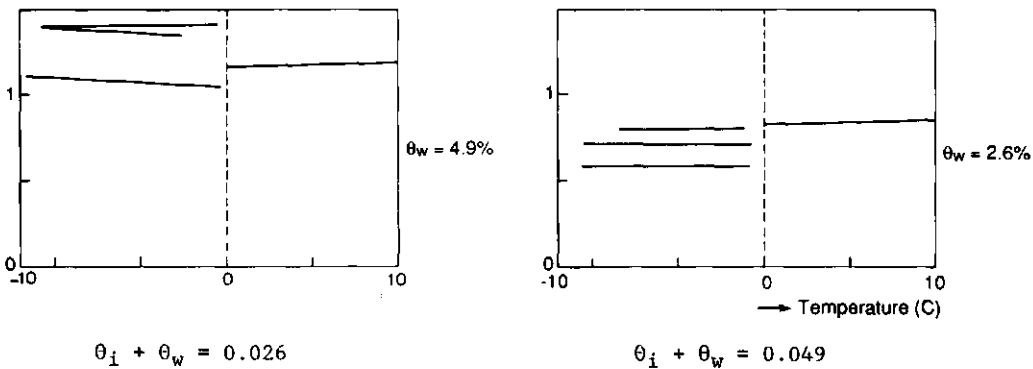


Fig. 4.1.5 Measured thermal conductivities of humid silver sand as a function of temperature  $T$  during three freezing cycles.

The first thing that is striking, is that the measured thermal conductivities for  $T > 0^\circ\text{C}$  are well reproducible (for all cycles they can be found on one line). This means that during a cycle the average water content (on a macroscopical scale) around the probe does not change. So, during the freezing part of the cycle only reversible water transport or no water transport at all took place. The reversible water transport can only take place if it is on a microscopical scale.

On contrary the measured thermal conductivities for  $T < 0^\circ\text{C}$  are 'cycle-dependent' (within one cycle the values are rather constant). This can not be caused by the melting of a small fraction of the ice during the thermal conductivity measurement, because the considered temperatures are too low (see also Fig. 4.1.4).

Also the total water content  $(\rho_i/\rho_w)\theta_i + \theta_w$  averaged over a bigger volume has to be a constant, because of the results above the freezing point. An explanation might be that the microscopical equilibrium between ice, water and sand is for each freezing cycle different. This could be caused by a different mutual configuration of the different particles. Thermal conductivities in granular materials are not only dependent on the volume fractions of the different components, but also on the way the solid particles contact each other [Van Haneghem, 1981].

#### 4.1.7 Discussion

When heat flow in porous media is evaluated, often the thermal conductivity is estimated. Data obtained from the composition of the multi-phase medium is used to calculate this physical property. Our experiments confirmed the empirical relation (4.1.8) of Johanson and Frivik [1980] for  $T > 0^\circ\text{C}$ . For frozen soils however this simple kind of relationship can not be applied: also here the mutual configuration of the components might be important (see Fig. 4.1.5).

So the direct measurement of the thermal conductivity has become necessary. Here also some difficulties arise: the averaging area of the nonsteady state probe method is a cylinder with a diameter of about 3 cm. So, when the sand is not homogeneous (e.g. near the freezing front) it is not clear in which way the averaging exactly takes place. The averaging volume, which has to be as small as possible, is proportional to the temperature response of the probe. We adjusted it on only 0.15 K.

The heat capacity can be determined simultaneously with the nonsteady state probe method [Van Loon et al., 1989b]. However, with the very small temperature rise it is not possible to obtain accurate data for the heat capacity, because the determination of this quantity is only possible using higher order terms of the theoretical model for the nonsteady state probe method.

With the measured thermal conductivity and the assumption of a constant heat flow through the sand samples, a systematic measuring error in thermal conductivity  $\lambda$  of frozen sand has been determined. A more detailed explanation of the observed systematic deviation of thermal conductivity in frozen soils will be given in the next sections.

## 4.2 Heat transfer

Heat transfer in frozen soils is a complex phenomenon, in which many parameters play a role. Some effects might compensate each other, while other effects just might reinforce each other. Therefore, the different parameters are first considered separately.

In this section the influence of the freezing process on heat capacity, thermal conductivity and temperature field is dealt with, successively. Next, heat flows are calculated from these parameters and related to one another. Finally, the course of the different heat flows with time is investigated.

### 4.2.1 Heat capacity

In this section the influence of the freezing process on the heat capacity is investigated. As long as no phase change occurs, the volumetric heat capacity  $C$  of a soil can be calculated from the heat capacities and volume fractions of its constituents: solid mineral particles ( $s$ ), liquid water ( $w$ ), ice ( $i$ ) and air ( $a$ ), i.e.:

$$C = \theta_s C_s + \theta_w C_w + \theta_i C_i + \theta_a C_a \quad (4.2.1)$$

However, at temperatures between  $-2^\circ\text{C}$  and  $0^\circ\text{C}$ , the measured heat capacity is strongly influenced by the latent heat of melting. This effect can be incorporated by introducing the apparent heat capacity  $C'$  (see 2.3.16). From eq (2.3.16) it can be seen that the term which expresses the latent heat effect  $\Delta C$  ( $\Delta C = C' - C$ ) can be written as:

$$\Delta C = \rho_w L (\partial \theta_w / \partial T) \quad (4.2.2)$$

To obtain values for the normal and apparent heat capacity of the soils used at temperatures below  $0^\circ\text{C}$  some calculations are performed. In our case the three undisturbed soil samples (LSA, SLO and CLA; the materials have been introduced in section 3.4) and the crushed concrete were saturated or at least brought close to saturation. Thus, in the sample calculation of the (normal) heat capacity the air fraction can be taken as zero (and  $\theta_i = 1 - \theta_w - \theta_s$ ).

Because most soils have about the same heat capacity for their solid mineral particles ( $C_s = 2.0 \text{ MJ/m}^3\text{K}$  [e.g. Koorevaar et al., 1983]), the variation in heat capacity is mainly caused by variation of the volume fractions. When the values of the heat capacity of the two remaining constituents are considered, it can be seen that  $C_i \approx C_s$  ( $C_i = 1.9 \text{ MJ/m}^3\text{K}$ ) and that  $C_w$  is about twice as large ( $C_w = 4.2 \text{ MJ/m}^3\text{K}$ ). Thus, the ice phase and the solid mineral phase can be considered as one phase with a heat capacity of  $\frac{1}{2}(C_i + C_s)$ . This leaves only one independent parameter in the calculation of the heat capacity: the unfrozen water content. Thus, when no in situ measurements of  $C$  are possible, an acceptable approximation of  $C$  can be given with the measurement of only one parameter ( $\theta_w$ ):

$$C = \theta_w C_w + (1 - \theta_w)(C_i + C_s)/2 \quad (4.2.3)$$

Table 4.2.1 shows that for a large range in solid mineral fraction  $\theta_s$  the heat capacity is hardly influenced by this parameter. The same table indicates also the important contribution of the unfrozen water content  $\theta_w$ .

Table 4.2.1 Calculated volumetric heat capacities  $C$  of soil-water-ice mixtures, with  $C_s = 2.0 \text{ MJ/m}^3\text{K}$ ,  $C_w = 4.2 \text{ MJ/m}^3\text{K}$  and  $C_i = 1.9 \text{ MJ/m}^3\text{K}$

$\theta_s [\text{m}^3/\text{m}^3]$	C [ $\text{MJ/m}^3\text{K}$ ]				
	$\theta_w=0.0$	$\theta_w=0.1$	$\theta_w=0.2$	$\theta_w=0.3$	$\theta_w=0.4$
0.4	1.94	2.17	2.40	2.63	2.86
0.5	1.95	2.18	2.41	2.64	2.87
0.6	1.96	2.19	2.42	2.65	2.88

For the calculation of  $\Delta C$  following (4.2.2) the  $\theta_w(T)$ -relation needs to be known. In this research measurements of unfrozen water content (using TDR, see section 2.2.2) have been taken in three undisturbed soil columns: Engs loamy sand (LSA), Achterhoeks sandy loam (SLO) and river foreland clay (CLA). The measurements were performed under non-isothermal conditions. Because the measuring volume of TDR has finite dimensions [Baker, 1989], the unfrozen water content is an average value over the measuring volume. Due to the existing temperature gradient, it is therefore also averaged over the temperatures present in the measuring volume. The results of the measurements are presented in Figs. 4.2.1, 4.2.2 and 4.2.3 for LSA, SLO and CLA, respectively.

The measured unfrozen water curves in Figs. 4.2.1, 4.2.2 and 4.2.3 (in which the soil was close to saturation before freezing) show the typical shape that many soil scientists already have published: e.g. Koopmans and Miller [1966], Horiguchi [1985] and Black and Tice [1989]. Close to 0°C a sharp decrease of unfrozen water content occurs at decreasing temperatures, while at lower temperatures the unfrozen water content remains nearly constant. The amount of water that remains unfrozen is characteristic for the soil type: the finer the soil, the more water remains unfrozen.

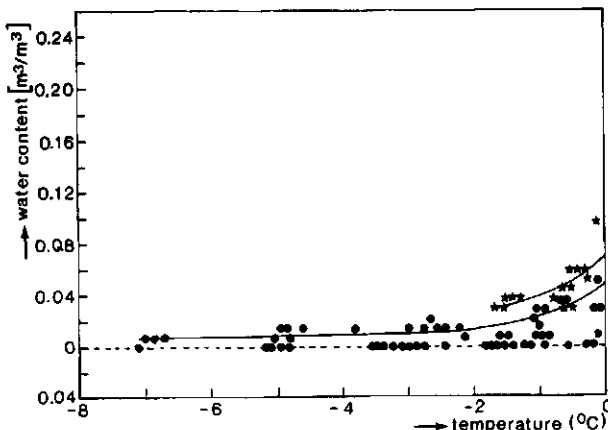


Fig. 4.2.1 Unfrozen water content of Engs loamy sand (LSA) as a function of temperature, for two different horizons: LSA-2 (\*) (z=175 to 275 mm). LSA-1 (●) (z=275-425 mm) and — graphical best fits.

For all soils the freezing front proceeded into two different horizons. A horizon is a geological determined soil layer; between horizons a sudden change in soil properties can be expected. For the Engs loamy sand and the Achterhoeks sandy loam this resulted in two different  $\theta_w(T)$ -relations (see Fig. 4.2.1 and 4.2.2, respectively), while for clay the horizons could not be distinguished this way (Fig. 4.2.3).

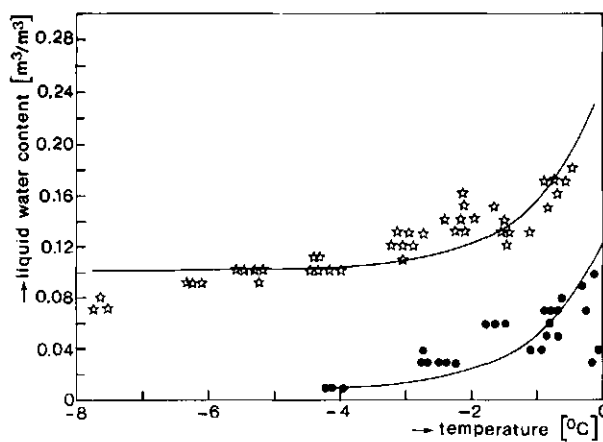


Fig. 4.2.2 Unfrozen water content of Achterhoeks sandy loam (SLO) as a function of temperature for two different horizons, with SLO-2 (●) ( $z=175-325$  mm), SLO-1 (★) ( $z=325-425$  mm) and — the graphical best fits.

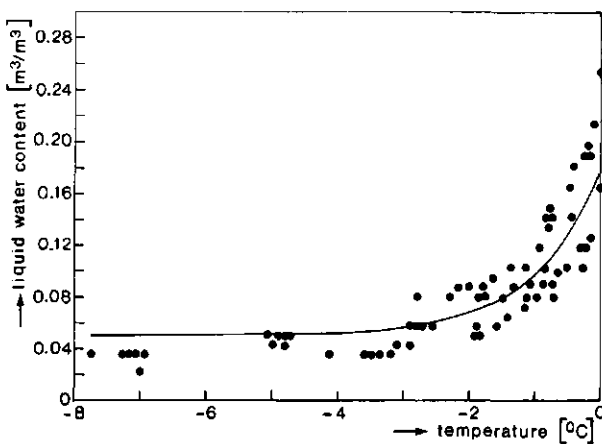


Fig. 4.2.3 Unfrozen water content of river foreland clay (CLA) as a function of temperature, with measuring points (●) ( $z=175-425$  mm) and — the graphical best fit.

To obtain a value for the extra term in heat capacity  $\Delta C$  first the best fit for the  $\theta_w(T)$ -relation was determined graphically<sup>1</sup>. This procedure was followed for each soil or horizon, which was subjected to freezing. Next the derivatives  $\partial\theta_w/\partial T$  were determined from these fits at two temperatures to indicate the temperature dependence. And finally the values of the derivatives were used in eq (4.2.2) to obtain  $\Delta C$ . The results of this procedure are presented in Table 4.2.2.

Table 4.2.2 The derivative of unfrozen water content with respect to temperature  $\partial\theta_w/\partial T$ , determined with the graphical method, at  $T=0^\circ\text{C}$  and  $T=-1^\circ\text{C}$ , with corresponding increase in heat capacity  $\Delta C$  (following eq 4.2.2).

soil	position [mm]	$T=0^\circ\text{C}$ $\partial\theta_w/\partial T$ [ $^\circ\text{C}^{-1}$ ]	$T=-1^\circ\text{C}$ $\partial\theta_w/\partial T$ [ $^\circ\text{C}^{-1}$ ]	$T=0^\circ\text{C}$ $\Delta C$ [ $\text{MJ}/\text{m}^3\text{K}$ ]	$T=-1^\circ\text{C}$ $\Delta C$ [ $\text{MJ}/\text{m}^3\text{K}$ ]
LSA-2	175-275	0.08	0.03	27	10
LSA-1	275-425	0.04	0.02	13	5
SLO-2	175-325	0.12	0.05	40	14
SLO-1	325-425	0.15	0.06	50	18
CLA	175-425	0.13	0.05	43	16

In Table 4.2.2 it can be seen that the extra term  $\Delta C$  is an order of magnitude higher than the heat capacity itself: i.e.  $\Delta C = 13$  to  $50 \text{ MJ}/\text{m}^3\text{K}$  for  $T = 0^\circ\text{C}$ . This is not surprising because of the relatively large value of  $L$ . Even at  $T + -1^\circ\text{C}$  the extra term is higher than  $C$  itself:  $\Delta C = 5$  to  $18 \text{ MJ}/\text{m}^3\text{K}$ . The results are close to the direct measured apparent heat capacities presented by Williams [1973]. In his paper values are presented for the apparent heat capacity  $C'$  of different clays at  $T = -0.6^\circ\text{C}$  that vary in between 5 and  $66 \text{ MJ}/\text{m}^3\text{K}$ .

<sup>1</sup>) To obtain the best fit no regression analysis has been used, because only high order polynomials (more than third order) describe the measured trend adequately. Our data set is not accurate enough to allow that many degrees of freedom.

#### 4.2.2 Thermal conductivity

In this section the influence of the freezing process on the measured thermal conductivity is investigated. Our thermal conductivity measurements were performed using the non steady state probe method (see section 3.1). In this method the temperature response of the measuring probe on a stepwise change in dissipated heat is analysed. The method has been modified in order to minimize the heat dissipation and measuring time (see section 3.1).

The measured thermal conductivity is an effective value of the total heat transport through the different soil constituents. It is the result of series conduction (heat is conducted from one constituent to another) as well as parallel conduction (heat is conducted parallel through different constituents). This results into a complex series parallel model for the thermal conductivity [De Vries, 1952 and De Vries, 1963]. Because the theoretical models are complicated, we have to rely on the experimental data up to now. Farouki [1986] gives a good overview of this experimental research. However, some complications in the measurement of thermal conductivity are not included in this review.

In the forthcoming subsections some major influences on measured thermal conductivity values in frozen soils will be discussed with reference to our experimental results:

1. the temperature dependence of the mass ratio between the pore ice content and the unfrozen water content,
2. the extra contribution of the apparent thermal conductivity:  
$$\lambda' = \lambda + \Delta\lambda$$
 [Kay et al., 1981],
3. the segregated ice content and
4. the presence of the freezing front close to the measuring probe.

These four influences have very different physical backgrounds, which will come up in the final discussion in Chapter 5. The process of ice segregation will be treated in section 4.3.

#### 4.2.2.1 Influence of the temperature dependence of the poor ice versus unfrozen water content

The mass fractions of the different soil constituents do not remain constant during the freezing process. The pore ice content increases and the unfrozen water content of a frozen porous medium decreases with decreasing temperature. Since the thermal conductivity of ice is about four times larger than that of liquid water, any variation in temperature will result in a change of the thermal conductivity of the frozen soil [Farouki, 1986]. The influence of total water content on the thermal conductivity has been shown by Yershov et al. [1988] and Fukuda and Jingsheng [1989].

The influence of temperature on the measured thermal conductivity for two different total water contents (liquid water plus ice content) in Engs loamy sand (LSA) can be seen in Fig. 4.2.4. This material was not completely water saturated before freezing (due to its water retention characteristics): the higher in the column, the less water was present. It is assumed that at  $T < -1^\circ\text{C}$  no water redistribution took place and that for  $0 > T > -1^\circ\text{C}$  (where the redistribution in the frozen fringe does take place) the redistribution process needs to continue for at least 24 hours before it becomes significant. With these two assumptions the initial water content of  $0.27 \text{ m}^3/\text{m}^3$  did not change for the highest measuring probe (at  $z > 375 \text{ mm}$ ). At this position the average measured  $\lambda$  equals  $1.8 \pm 0.2 \text{ W/mK}$ , while the temperature dependency is not significantly different from zero. At the other measuring positions in the frozen zone ice lenses were formed, so the total water content is equal or higher than the original pore volume of  $0.40 \text{ m}^3/\text{m}^3$ . The average  $\lambda$  at these positions ( $225 \text{ mm} < z < 375 \text{ mm}$ ) equaled  $2.5 \pm 0.6 \text{ W/mK}$ , again with no significant temperature dependency.

In section 4.1 it has been argued already that the thermal conductivity of a soil is not a simple function of the thermal conductivities and volume fractions of its constituents, but also a function of their mutual configuration. Thus, when a non homogeneous soil is analysed, the inhomogeneities will cause considerable scattering of the measuring data. This is one of the reasons why in Fig. 4.2.4 for Engs loamy sand the relation between thermal conductivity and

temperature is not significant. (The occurrence of high  $\lambda$ -values at  $T>-1^{\circ}\text{C}$  will be explained in subsections 4.2.2.3 and 4.2.2.4).

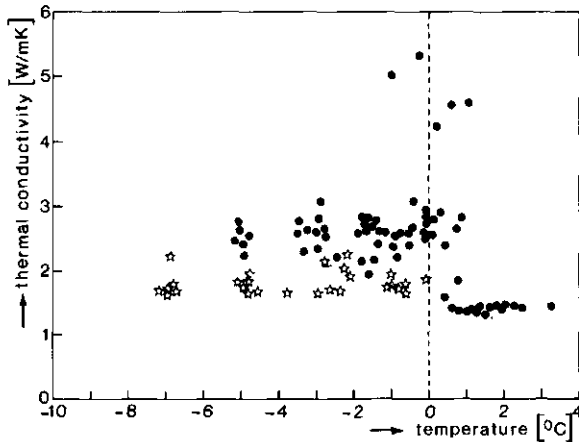


Fig. 4.2.4 Thermal conductivity as a function of temperature for freezing Engs loamy sand (LSA), for two different water contents: (●) saturated at  $225 \text{ mm} < z < 375 \text{ mm}$  and (✗) unsaturated at  $z > 375 \text{ mm}$ .

A more homogeneous test material is the crushed concrete (B45). In this material the  $\lambda(T)$ -relation can be determined more accurately: in Fig. 4.2.5 most measuring points for  $T<-1^{\circ}\text{C}$  can be found on a straight line. This line can be represented with the following relation:

$$\lambda = A + B \times T \quad (4.2.4)$$

To obtain values for slope, B, and intercept, A, linear regression analysis was performed between  $\lambda$  and T for  $T<-1.0^{\circ}\text{C}$ . Using this method the following regression parameters were found:  $A = 2.6 \text{ W/mK}$ ,  $B = -0.022 \pm 0.005 \text{ W/mK}^2$ ,  $SE = 0.1 \text{ W/mK}$  and  $r^2 = 0.12$  (significant at 95% probability level). The negative B coefficient confirms the effect mentioned in section 4.2.2, that lower temperatures result in higher thermal conductivities. This can be understood by assuming that in this region a lower temperature results in a higher ice content while  $\lambda_i > \lambda_w$ .

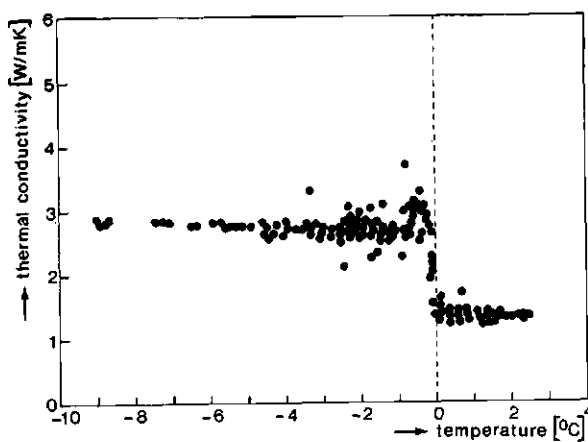


Fig. 4.2.5 Thermal conductivity as a function of temperature in freezing crushed concrete (B45).

For the  $\lambda(T)$  relation of Achterhoeks sandy loam the scatter is higher than for the crushed concrete, but the measuring points are still situated in the neighbourhood of a straight line (Fig. 4.2.6). Regression analysis quantifies this result:  $A=2.3 \text{ W/mK}$ ,  $B=-0.09 \pm 0.02 \text{ W/mK}^2$ ,  $r^2=0.28$  and  $SE=0.3 \text{ W/mK}$ .

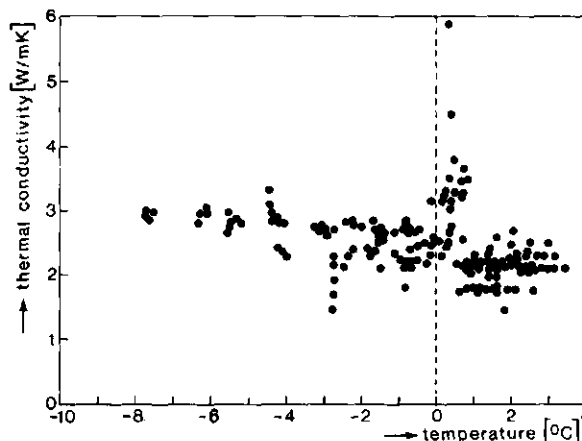


Fig. 4.2.6 Thermal conductivity as a function of temperature in freezing Achterhoeks sandy loam (SL0).

The fourth material examined is river foreland clay (see Fig. 4.2.7). Again the measuring points for  $-8^{\circ}\text{C} < T < -1^{\circ}\text{C}$  can be found close to a straight line. In contrast to the other materials, the slope of this line is slightly positive. This has been confirmed with the regression analysis:  $B=0.04 \pm 0.01 \text{ W/mK}^2$  (the other regression coefficients for this soil are  $A=2.6 \text{ W/mK}$ ,  $SE=0.2 \text{ W/mK}$  and  $r^2=0.13$ ). An explanation of the positive  $\lambda(T)$ -relation will be given in the next section.

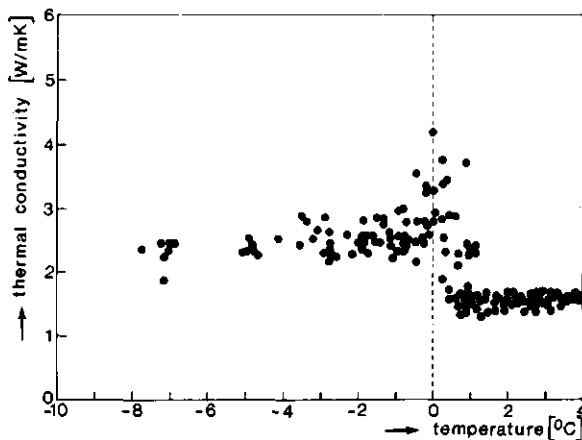


Fig. 4.2.7 Thermal conductivity as a function of temperature in freezing river foreland clay (CL).

#### 4.2.2.2 Contribution of the apparent thermal conductivity

The significance of water flow, due to a temperature gradient during the measurement of thermal conductivity was assessed by Kay et al. [1981]. These authors incorporated the transport of heat due to water migration into an extra term  $\Delta\lambda$ , making the apparent thermal conductivity  $\lambda' = \lambda' + \Delta\lambda$ . They suggested that in frost susceptible soils at temperatures close to  $0^{\circ}\text{C}$  the transport of latent heat contributed by water flow will be much greater than the real heat conduction. This causes a steep rise of apparent thermal conductivity close to  $0^{\circ}\text{C}$ . Van Haneghem and Leij [1985] have demonstrated this phenomenon experimentally in glass beads packings.

According to Kay et al. [1981] the difference between thermal conductivity and apparent thermal conductivity  $\Delta\lambda$  ( $\Delta\lambda = \lambda' - \lambda$ ) is related to the hydraulic conductivity  $k$  of the frozen soil (see also eq 2.3.17; the hydraulic conductivity has been introduced in section 2.1.6).

Because the unfrozen water content increases with increasing temperature, the hydraulic conductivity, and thus  $\Delta\lambda$  should increase too. This causes an effect on the  $\lambda(T)$ -relation opposite to the one discussed above (the effect of ice being replaced by water). Thus the slope  $B$  in the  $\lambda(T)$ -relation depends on which effect is the most important in the temperature range considered (for increasing  $T$ ): the replacement of ice by water resulting in a decreasing  $\lambda$ , or the increase in hydraulic conductivity resulting in an increasing  $\lambda$ .

In Table 4.2.3 it can be seen that there is a qualitative agreement of  $B$  coefficients from (4.2.4) with the fraction of fines  $\Phi_{125}$ : the most coarse material (B45) has a negative  $B$ -value, while the most fine material (CLA) has a positive  $B$ -value ( $r^2=0.52$ ) (for SSA and RSA the temperature range was too restricted to determine a significant value for  $B$ ). It can be concluded that the finer the material, the stronger the effect of the hydraulic conductivity at subzero temperatures.

Table 4.2.3 Slopes  $B$  of  $\lambda(T)$  relation (4.2.4) compared with fines fraction  $\Phi_{125}$

material	B W/mK <sup>2</sup>	$\Phi_{125}$ m <sup>3</sup> /m <sup>3</sup>
LSA-1	NS	0.407
LSA-2	NS	0.379
SLO	-0.09	0.46
CLA	+0.04	0.885
B45	-0.022	0.138

#### 4.2.2.3 Segregated ice content

The soil matrix is changing due to the formation of ice lenses: the (thermal) contact between mineral soil particles decreases when heave takes place. Secondary heave causes supersaturation: the total water content (liquid water plus ice content) is higher than the original pore volume. In supersaturated soils the soil mineral fraction has been decreased with an increased total water content.

Because ice has a lower thermal conductivity than soil particles, the effective thermal conductivity of the soil is decreased [Farouki, 1986]. To quantify the effect of the segregated ice two assumptions are made:

1. Ice lenses are distributed homogeneously throughout the frozen zone; the segregated ice content equals the total heave divided by the height of the frozen zone.
2. If the ice lenses actually influence the thermal conductivity, this influence appears only after the growth of such lenses. The most likely way to determine this influence is comparing the unfrozen soil with the frozen soil (containing the segregated ice).

To evaluate the influence of segregated ice on the thermal conductivity, all other effects need to be eliminated as well as possible. For instance at temperatures in the interval  $-1^{\circ}\text{C} < T < +1^{\circ}\text{C}$  some very high thermal conductivities are measured. Therefore, measurements within this temperature interval have not been used for the evaluation in this section. To obtain  $\lambda$ -values for the unfrozen, saturated condition, the average thermal conductivity is taken at  $\theta_w > 0.40$  and  $T > 1^{\circ}\text{C}$ . For the frozen zone the A-value of eq (4.2.4) is taken (see Table 4.2.4).

The difference between the thermal conductivity in the frozen and the unfrozen soil depends on the material considered: in B45 the difference is large, while in SLO the difference is small. From Table 4.2.4 it can be seen, that a negative trend exists between  $\lambda_f - \lambda_u$  and the segregated ice content. Thus, supersaturation with ice has a significant influence on the thermal conductivity of the frozen zone. This is in good agreement with the prediction in the first paragraph of this subsection.

Table 4.2.4 Influence of total heave on measured thermal conductivities of oversaturated porous media

material	$\lambda_f$ [W/mK]	$\lambda_u$ [W/mK]	$\lambda_f - \lambda_u$ [W/mK]	total heave [mm]	frozen zone [mm]	segregated ice content [-]
LSA	2.5	1.8	0.7	67	350	0.19
SLO	2.3	2.0	0.3	80	339	0.24
CLA	2.6	1.8	0.8	35	246	0.17
B45	2.6	1.5	1.1	34	395	0.09

#### 4.2.2.4 Presence of the freezing front close to the measuring probe

To describe the temperature response of our thermal conductivity probe analytically, homogeneous and isotropic conditions over the measuring volume have to be assumed. These conditions are not satisfied when the freezing front is situated within the measuring volume: the thermal properties of a frozen porous medium differ from the corresponding unfrozen porous medium. Furthermore the melting of ice causes a large latent heat effect. Apart from that, the frozen fringe, where a large pressure gradient exists, might also disturb the measurement (the thickness of the frozen fringe (5 to 15 mm) is in the same order of magnitude as the measuring volume (30 mm)). In this subsection the influence of the presence of the freezing front close to the measuring probe is investigated.

As can be seen in Figs. 4.2.4 to 4.2.7 and in Fig. 4.1.4 in the temperature interval  $-1^{\circ}\text{C} < T < +1^{\circ}\text{C}$  the measured  $\lambda_m$  can be as much as three times larger than  $\lambda$  measured at  $-4^{\circ}\text{C}$ . The occurrence of high  $\lambda_m$ -values above  $0^{\circ}\text{C}$  is caused by the finite measuring volume (a cylinder with a diameter of about 30 mm) and the non steady state measuring method. In this measuring volume the average temperature can be above freezing, while a small part is frozen. The presence of the freezing front in the measuring volume causes a higher thermal conductivity as follows. During the measurement heat is dissipated by the thermal conductivity probe. When the freezing front is close to this probe, part of dissipated energy will be used to melt ice at the freezing front. Thus, less energy is available for the temperature rise of the probe with surrounding medium, which apparently leads to an increased value for  $\lambda_m$ .

The difference  $\Delta\lambda_m$  between measured and expected thermal conductivity also shows a soil dependency. When we look at Fig. 4.2.4 to 4.2.7 and Fig. 4.1.4, it seems that  $\Delta\lambda_m$  is larger for the more coarse soils. This is in disagreement with the soil dependency of the apparent thermal conductivity of subsection 4.2.2.2, because from this conclusion a larger value is expected for the more fine textured soils. Thus, this  $\Delta\lambda_m$  has to arise from an origin different from the apparent conductivity effect. To be able to explore  $\Delta\lambda_m$  in some detail, we quantify this parameter as follows: a significant value for the parameter is found if  $\Delta\lambda_m > \text{SE}(\lambda)$ , where  $\text{SE}(\lambda)$  is the standard error of measuring points with respect to the linear  $\lambda(T)$ - relation (eq 4.2.4).

Table 4.2.5 Measured thermal conductivity  $\lambda_m$  compared with  $\lambda$  in six porous materials related with total water content ( $\theta_w + \theta_i$ ) and fines fraction  $\Phi 125$

material	$\Phi 125$	$\theta_w + \theta_i$	$\lambda$	$\lambda_m$	$\Delta\lambda_m$
SSA	0.008	0.08	1.0	$1.5 \pm 0.5$	0.5
RSA	0.12	0.12	1.8	$4.3 \pm 1.5$	2.5
LSA-1	0.407	0.27	1.8	$2.2 \pm 0.1$	0.4
LSA-2	0.379	$\geq 0.4$	2.5	$4.6 \pm 0.9$	2.1
SLO	0.46	$\geq 0.4$	2.3	$3.8 \pm 0.7$	1.5
CLA	0.885	$\geq 0.4$	2.6	$3.5 \pm 0.4$	0.9
B45	0.138	$\geq 0.4$	2.6	$3.1 \pm 0.3$	0.5

These significant measuring points of  $\Delta\lambda_m$  are averaged by material (see Table 4.2.5). By comparing LSA-1 with LSA-2, we see that a higher total water content results in a higher  $\Delta\lambda_m$ . The  $\Delta\lambda_m$ -value is also dependent on the material. When the three undisturbed, (super-) saturated soils are taken together (with total water content  $> 0.4$ ) we see, that the higher the fines fraction  $\Phi 125$ , the lower  $\Delta\lambda_m$ . The same is true when RSA is compared with LSA-1: both materials have the same thermal conductivity when they are frozen, but the more coarse RSA has a larger  $\Delta\lambda_m$ . This confirms that the presence of the freezing front causes an increase in measured thermal conductivity. In coarse textured soils the change in liquid water content at  $0^\circ\text{C}$  is more pronounced than in fine textured soils. It is therefore to be expected that the largest errors in the calculations for the thermal conductivity are made in the coarse textured soils.

Theoretical research is needed to determine more precisely the effects of non homogeneous measuring conditions. To determine the thermal conductivity with use of the non steady state probe method in the presence of a macroscopic temperature gradient, a model needs to be developed, which includes a stepwise change in thermal properties. From there, another model can be developed that includes a phase change boundary in the measuring volume. Because analytical solutions for this kind of problems do not exist, numerical methods are to be applied.

#### 4.2.3 Latent heat of *in situ* freezing

The heat flow  $Q_L$  that accompanies the *in situ* freezing of pore water is investigated by comparing two independent measurements close to the 0°C isotherm: temperature and water content. From both measurements an estimation of this latent heat production can be found:

1. Temperature measurements: the penetration rate of the 0°C isotherm ( $X$ ) is followed and it is assumed that the pores are saturated with water, and that all of this water freezes *in situ*. This  $Q_L$ -value can be calculated using (2.3.21).
2. Water content measurements: the rate of change in unfrozen water content is followed, assuming that all water freezes<sup>1</sup> in between 0°C and -2°C. The  $Q_L$ -value can now be calculated using the following equation:

$$Q_L(\theta_w) = \rho_w L \Delta z (\partial \theta_w / \partial t) \quad (4.2.7)$$

When equilibrium between the two phases of water is assumed, the two values of  $Q_L$  need to be identical. This identity is represented with the drawn lines in Figs. 4.2.8 to 4.2.10. It can be seen that most measuring points are scattered below this line. Thus, the equilibrium between the two water phases is not present, which is not so surprising under transient conditions. It can also be concluded that the penetration of the 0°C isotherm does not result into the straightforward freezing of pore ice. Due to the inhomogeneity of the materials used, some scattering in the results is to be expected. To quantify the deviation of the equilibrium relation, it is assumed that another linear relation exists between the two differently calculated values of the heat flows associated with the *in situ* freezing of pore water:

$$Q_L(\theta_w) = B \times Q_L(T) \quad (4.2.6)$$

with  $B$  the slope (in case of equilibrium  $B=1$ ). The results of this analysis can be seen in Table 4.2.6.

Both series of calculated  $Q_L$ -values have been pictured in Figs. 4.2.8 to 4.2.10.

<sup>1</sup>) The average temperature of the sampling volume of the TDR method can be above 0°C, while nevertheless a part of this volume starts to freeze. The measured  $\theta_w$  is assumed to be the average value of the liquid water content in the measuring section, which has a height  $\Delta z=0.05$  m. In this measuring section the average temperature can be above 0°C, while a part is already frozen. Thus, water content measurements in the temperature interval -2°C < T < +1°C are considered.

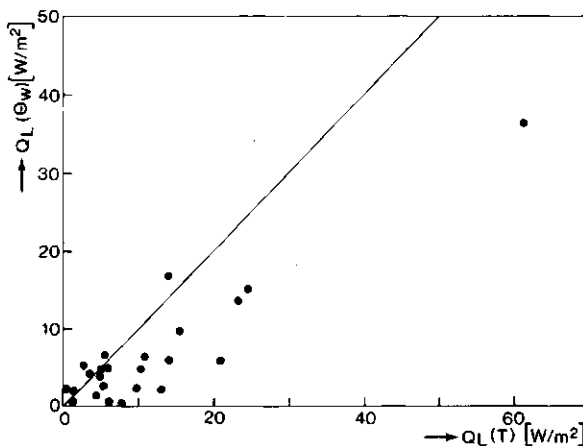


Fig. 4.2.8 Heat flows caused by the in situ freezing of pore water in Engs loamy sand (LSA): with vertical the heat flow, as calculated from changing water content, and horizontal the heat flow, estimated from the penetration of the 0°C isotherm. The theoretical equilibrium relation between them is represented by the drawn line.

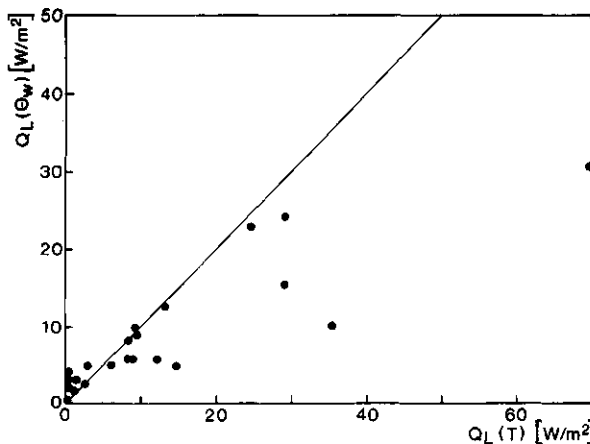


Fig. 4.2.9 Heat flows caused by the in situ freezing of pore water in Achterhoeks sandy loam (SLO): with vertical the heat flow, as calculated from changing water content, and horizontal the heat flow, estimated from the penetration of the 0°C isotherm. The theoretical equilibrium relation between them is represented by the drawn line.

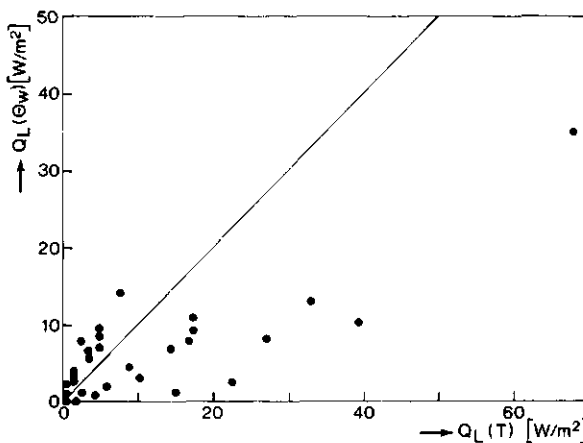


Fig. 4.2.10 Heat flows caused by the in situ freezing of pore water in river foreland clay (CLA): with vertical the heat flow, as calculated from changing water content, and horizontal the heat flow, estimated from the penetration of the 0°C isotherm. The theoretical equilibrium relation between them is represented by the drawn line.

Table 4.2.6 Relation between heat flows caused by the in situ freezing of pore water, with regression model  $Q_L(\theta_w) = B \times Q_L(T)$  (eq 4.2.6).

material	B [-]	$r^2$	SE [W/m <sup>2</sup> ]
LSA	0.55±0.05	0.80	3
SLO	0.44±0.04	0.79	3
CLA	0.15±0.06	0.18	3

As expected, the B-coefficients are much lower than 1: 0.15 to 0.55 (B has been calculated using regression analyses). A possible reason is that not all pore water is frozen at -2°C. Looking at Figs. 4.2.1 to 4.2.3, we see that the maximum unfrozen water content at -2°C is about 0.12 m<sup>3</sup>/m<sup>3</sup> (SLO-2), thus a maximum of 0.12/0.40 = 0.30 of the water remains unfrozen. This would result into a B-coefficient of about 1.0 - 0.3 = 0.7. All B-coefficients from Table 4.2.6 are significantly lower than that value. Thus, the remaining unfrozen water content can not be the only reason for the low B-coefficients in Table 4.2.6.

Another reason might be that the pore water freezes later in time than one would expect. The highest values for  $Q_L$  are all calculated shortly after a stepwise temperature change took place in the upper heat exchanger. As a result, the 0°C isotherm penetrates faster than the corresponding rate of change in unfrozen water content (see also next section).

Some days later the opposite is true: the unfrozen water content is still decreasing, while the 0°C isotherm does not move. The accompanying  $Q_L$ -values are about zero now. This results in a  $B$ -value which is less than 1 (see Table 4.2.6). Because  $B$  is lowest in clay, the retardation has to be most pronounced in clay.

#### 4.2.4 Heat balances

In the present research the heat flows were not measured directly. However, they can be calculated from measured parameters (on the same position) such as water content, temperature and distances between measuring probes. Calculations can then be performed using eq (2.1.8) for the conductive heat flow, eq (2.3.19) for the dissipation of latent heat related to heave and eq (2.3.21) for the in situ freezing of pore water. In this section the heat balance equation is used to test the experimental set up and to evaluate the heat balance equation itself.

A possible representation of the heat balance is given in eq (2.3.22): the heat flow by conduction in the frozen zone ( $Q_f$ ) is the sum of conductive heat flow in the unfrozen zone ( $Q_u$ ), the heat flow related with the formation of ice lenses ( $Q_h$ ) and the heat flow related with the in situ freezing of pore water ( $Q_L$ ). In this equation it is assumed that  $C(\partial T / \partial t) \ll \rho L (\partial \theta_w / \partial t)$  (or  $C \ll \Delta C$ ). In section 4.2.1. it has been demonstrated that this assumption is justified for temperatures just below 0°C. For  $Q_u$  the conductive heat flow at  $z=100$  mm has been used, because the soil remained unfrozen on this position during the entire experiment. For  $Q_f$  the conductive heat flow at  $z=400$  mm has been used.

The position of the latter measuring probe shifts during the experiment in positive vertical direction due to the growth of ice lenses underneath. From the first measuring time (at  $t=1$  day) this probe has been located inside the frozen zone. When the different heat flows are compared with each other one has to be aware of the large differences in value: average values for  $Q_f$ ,  $Q_u$ ,  $Q_L(T)$ ,

$Q_L(\theta_w)$  and  $Q_h$  are 75, 30, 10, 5 and 2  $\text{W/m}^2$ , respectively. An average value for the heat loss is then  $(75-30-10-2)= 33 \text{ W/m}^2$ , which is about 40% of the conductive heat flow in the frozen zone. It is clear that the smaller heat flows have a less significant contribution to the heat balance equation than the two heat flows by conduction. To investigate this significance regression analysis is performed using the following regression model:

$$Q_f = A + B \times Q_u + D \times Q_L + E \times Q_h \quad (4.2.7)$$

with A, B, D and E the regression coefficients. Starting from our model we could expect that  $A=0$  and  $B=D=E=1$ .

Because there are two different ways in which  $Q_L$  can be calculated (see section 4.2.3), the regression has to be performed for both cases. The calculated values can be seen in Table 4.2.7.

Table 4.2.7 Regression analysis for heat balance equation (4.2.7),  
 $Q_f = A + B \times Q_u + D \times Q_L + E \times Q_h$  with model I  $Q_L = Q_L(T)$  and model II  
 $Q_L = Q_L(\theta_w)$

material	model	A [ $\text{W/m}^2$ ]	B [-]	D [-]	E [-]	$r^2$ [-]	SE [ $\text{W/m}^2$ ]
LSA	I	-31	$2.7 \pm 0.3$	$0.4 \pm 0.2$	NS	0.75	11
SLO	I	NS	$2.6 \pm 0.4$	$0.7 \pm 0.1$	$1.7 \pm 0.5$	0.87	7
CLA	I	48	$2.5 \pm 0.5$	$0.6 \pm 0.2$	NS	0.63	13
B45	I	9	$0.9 \pm 0.2$	$0.7 \pm 0.14$	$5.7 \pm 1.4$	0.86	8
LSA	II	-29	$2.6 \pm 0.3$	$0.6 \pm 0.3$	NS	0.74	11
SLO	II	NS	$2.9 \pm 0.5$	$1.3 \pm 0.2$	$1.0 \pm 0.7$	0.84	8
CLA	II	47	$2.4 \pm 0.4$	$1.5 \pm 0.4$	NS	0.64	13

† For B45 it is impossible to evaluate model II, due to the absence of unfrozen water content measurements.

This table shows that  $Q_u$  gives the major contribution to the heat balance equation: all other effects are minor. The B-values (which belong to  $Q_h$ ) are hardly affected by the choice of model I or II. For the three natural soils the B-value is significantly higher than expected: about 2.6 instead of one. This reflects the heat loss that takes place perpendicularly to the column axis between two measuring positions for the conductive heat flow. This heat loss

flows from the warmer ambient air to the column. Looking at Table 4.2.7 we have to conclude that in our actual presentation the heat loss can be found in an enlarged B-value, together with an adapted A-value.

The heat loss is probably caused by the sublimation of vapor from the air in the slit in the insulation (Fig. 3.4.1) to the bare soil surface. White frost was visible on the bare soil surface of the three undisturbed soil samples, while the crushed concrete remained unaffected. This agrees well with the A- and B-values for B45, which are simultaneously much more close to the expected values of zero and one, respectively.

The second contribution to the heat balance equation is the heat associated with the in situ freezing of pore water,  $Q_L$ . Especially when the freezing front is penetrating fast, high  $Q_L(T)$ -values are obtained. The associated regression parameter D is rather constant for all materials: D is about 0.6. This is lower than the expected value of one. It might indicate that not all water inside the pores freezes, which agrees well with the conclusion of section 4.2.3. Yet another link with section 4.2.3 can be made: The quotient of  $D_I$  and  $D_{II}$  has to be similar with the slope of (eq 4.2.6) B(4.2.6):

$$\frac{D_I}{D_{II}} = \frac{\partial Q_f / \partial Q_L(T)}{\partial Q_f / \partial Q_L(\theta_w)} = \frac{\partial Q_L(\theta_w)}{\partial Q_L(T)} = B(4.2.6) \quad (4.2.8)$$

The quotients are 0.7, 0.5 and 0.4 for LSA, SLO and CLA, respectively, while the B(4.2.6)-values are 0.6, 0.4 and 0.2, respectively. Thus, our experiments confirm the similarity as expressed in (4.2.8). This can be considered as an extra indication that the D values are significant.

The third contribution to the heat balance results from the heat flow associated with secondary heave,  $Q_h$ . Because the  $Q_h$ -values are small with respect to the other heat flow values, this contribution is often not significant.

However, for the material with the highest  $Q_h$ -values (SLO) and for the most homogeneous material B45 significant contributions to the heat balance are found. For these materials also the best regression models are found. For Achterhoeks sandy loam (SLO) regression parameter E tends to be somewhat larger than one. For crushed concrete (B45), E is clearly larger than one. This might indicate that (especially for B45) in the formation of ice lenses more energy is involved than just the latent heat. For instance some energy might be demanded

to break the structure of the porous medium, in order to create space for the ice lenses.

#### 4.2.5 Temperature fields

In frozen soils transport of heat and moisture is mainly caused by a temperature gradient (see section 2.3). Therefore the temperature  $T$  needs to be analysed carefully as a function of position  $z$  and time  $t$  to evaluate the dynamics of the different processes. In this section the frost penetration problem is solved analytically for idealised conditions and then compared qualitatively with the measured temperature course in Engs loamy sand.

When a sudden step change in temperature is applied to the surface of a soil sample, a change in heat flow is initiated. When the surface temperature is put below freezing, the freezing front progresses into the soil.

The most simple analytical description of this kind of temperature response with phase change is the Neumann solution [Carslaw and Jaeger, 1950]. For this solution the following assumptions are made:

1. the soil is sharply separated by freezing front  $X$  into the frozen zone and the unfrozen zone (i.e. no frozen fringe exists),
2. no heave or water redistribution takes place,
3. no volumetric expansion of water takes place when it freezes,
4. the temperature at the upper surface remains unchanged,
5. all water freezes at  $0^\circ\text{C}$ ,
6. the soil column is infinitely long, homogeneous and isotropic,
7. the solution can be adapted to the stepwise changes in temperature of the upper soil surface (see Fig. 4.2.11) using the superposition principle (Duhamel).

Because in our experiments for instance heave does take place and the column has a finite length, the Neuman solution can only be seen as a first approximation for the soil relatively close to the upper soil surface. And because the temperature at the upper surface varies stepwise, the superposition principle of Duhamel has to be applied. Since we are only interested in the kind of time

dependency, the Duhamel approach is accurate enough. Now the following three relations are obtained (4.2.9 - 4.2.11):

the temperature  $T_f$  in the frozen part

$$T_f = T_t + A' \operatorname{erf} \frac{h-z}{2\sqrt{a_f t}} \quad (4.2.9)$$

the temperature  $T_u$  in the unfrozen part:

$$T_u = T_o + B' \operatorname{erfc} \frac{h-z}{2\sqrt{a_u t}} \quad (4.2.10)$$

and the position of frost front  $X$ :

$$X = h - D' \sqrt{t} \quad (4.2.11)$$

with  $T_0$  the initial temperature,  $T_t$  the new temperature at the upper soil surface,  $h-z$  the distance from the upper soil surface,  $\operatorname{erf}$  the error function,  $a$  the thermal diffusivity,  $\operatorname{erfc}$  the conjugated error function,  $A'$ ,  $B'$  and  $D'$  constants depending on the thermal soil properties [Carslaw and Jaeger, 1950].

For small arguments in the error function, it can be assumed that  $\operatorname{erf}(y)=y$  and  $\operatorname{erfc}(y)=1-y$ . For our experiments the absolute maximum of this argument is usually smaller than 0.6 (with  $h-z=0.25$  m,  $a=0.5 \times 10^{-6}$  m<sup>2</sup>/s and  $t=86400$  s, it results in  $y=(h-z)/(2\sqrt{at})=0.6$ ). In this case the relative error in the assumption is less than 5%. Thus, for most cases we can rewrite (4.2.9) as:

$$T_f = T_t + A' (h-z)/\{2\sqrt{a_f t}\} \quad (4.2.12)$$

A similar relation holds for the temperature in the unfrozen zone. The conductive heat flow can be obtained by substituting (4.2.9) in its definition:

$$Q_f = -\lambda_f (\partial T / \partial z)_f = [\lambda_f A' / (2\sqrt{\pi a_f t})] \exp(-y^2) \quad (4.2.13)$$

When it is assumed that  $y \leq 0.6$ , the factor  $\exp(-y^2)$  has less influence and the heat conduction is mainly proportional with  $1/\sqrt{t}$ .

In our experiments the initial condition was a uniform overall temperature of  $+4^\circ\text{C}$ . At time  $t=0$ , the temperature of the upper heat exchanger (see Fig. 3.4.1) was set at  $-4^\circ\text{C}$ , while the lower heat exchanger remained at its original temperature of  $+4^\circ\text{C}$ . After 14 days the temperature of the upper heat exchanger (at  $z=450$  mm) was changed to  $-6^\circ\text{C}$ , after 28 days to  $-9^\circ\text{C}$  and after 42 days to  $-12^\circ\text{C}$ . During the entire experiment the temperature of the lower heat exchanger was maintained at  $+4^\circ\text{C}$ . The thawing of the soil after the freezing experiments was not controlled and therefore will not be analysed. The observed temperature response of a soil can be seen in Fig. 4.2.11.

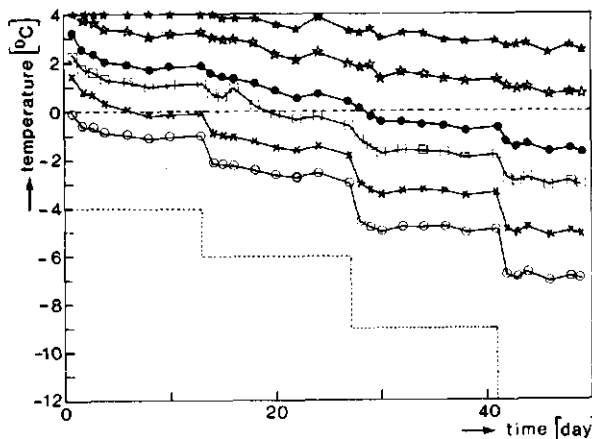


Fig. 4.2.11 Temperature as a function of time in Engs loamy sand (LSA) with original measuring positions ( $\ast$ )  $z=50$  mm, ( $\triangle$ )  $z=150$  mm, ( $\bullet$ )  $z=250$  mm, ( $\square$ )  $z=300$  mm, ( $\times$ )  $z=350$  mm and ( $\circ$ )  $z=400$  mm. Straight lines indicate the temperature course of the upper soil surface at  $z=450$  mm.

In Fig. 4.2.11 it can be seen that the rate of change in temperature in the soil is strongest just after a change in temperature in the upper heat exchanger. The temperature profile tends to become stationary after some days. Thus, the assumption that temperature should be related to  $1/\sqrt{t}$ , together with the Duhamel principle, does not seem incorrect according to Fig. 4.2.11.

#### 4.2.6 Dynamics of heat flows in frozen porous materials

In general, when heat flows are evaluated in frozen soils, the heat removal in the frozen fringe is compared with the rate of frost heaving. Penner [1972], Horiguchi [1979], Loch [1979] and McCabe and Kettle [1985] all found similar relations: as the heat removal increased, the rate of frost heave increased, reached a maximum and then decreased. Recently, Konrad [1987] observed the same phenomenon, but he also observed an influence of time in his experiments, although he did not draw any conclusion from it. He presented the typical results of a freezing test under constant boundary temperatures [Konrad 1987, Fig. 1a]. Unsteady heat flow exists as long as the frost front continues to penetrate the sample. In this period only small ice lenses are formed, and a large part of the total heave consists of the volume expansion of the in situ freezing of pore water. A period in which the 0°C isotherm is stationary follows, during which a major ice lens grows until the test is stopped. Apart from an optimal rate of heat removal (at which maximum heave occurs) a critical rate of heat removal is also defined: at higher values of the heat removal no heave is observed. At high rates of heat removal only further penetration of the 0°C isotherm occurs.

In the present section it is investigated whether the above described dependency between heave rate and heat removal can be contained in terms of time dependency of the different parameters. In Fig. 4.2.11 it can be seen that the measured temperature is related to the time relative at which the temperature in the upper heat exchanger has been changed. This relative time will be used in search of the type of time dependency of the different heat flows. The conductive heat flow, the heat flow associated with the in situ freezing of pore ice and the heat flow associated with the formation of ice lenses will successively be analysed as a function of time. Finally, the different time dependencies are compared with each other.

In section 4.2.5 it has been made clear that in first approximation the heat flow by conduction is proportional to  $1/\sqrt{t}$ . The conductive heat flow on position  $j$  is calculated from the measured values on positions  $j-1$ ,  $j$  and  $j+1$  as follows:

$$Q_j = -\lambda(T_{j+1} - T_{j-1})/(z_{j+1} - z_{j-1})$$

To show the time dependency, we performed regression analysis on the following model:

$$Q = A + B/\sqrt{t} \quad (4.2.14)$$

with A and B the regression coefficients.

The regression coefficients are collected in Table 4.2.8. In this table and in Fig. 4.2.12 it can be seen that, as a first approximation, the time dependency for the conductive heat flow reflects the  $1/\sqrt{t}$  model. At different settings of temperature in the upper heat exchanger the measuring points can be found on or around straight lines with a standard error of in general not more than  $7 \text{ W/m}^2$ . At each temperature setting a steady state heat flow exists. The steady state is reached for very large values of  $t$ , or as  $1/\sqrt{t}$  approaches 0.

Thus the A-coefficient of the regression model (4.2.14) might be a fair approximation for that steady state heat flow. For a given material this steady state heat flow only depends on the overall temperature gradient. This has been confirmed with our experiments: e.g. for B45 the thus obtained steady state heat flow as a function of the overall temperature (see Table 4.2.8) fits very well on a straight line ( $r^2=0.99$ ).

The B/A-value in (4.2.14) is a kind of time constant: the larger B/A the more time is needed, before the steady state heat flow is reached. This time constant is largest at the start of the experiment, where the change in temperature of the upper heat exchanger is largest: from  $+4^\circ\text{C}$  to  $-4^\circ\text{C}$ . The high time constant for the first experiment results in the intersection of the two lower lines in Fig. 4.2.12.

This simple time dependency does not hold for all heat flows, as can be seen in Fig. 4.2.13. The heat flow related with the penetration rate of the  $0^\circ\text{C}$  isotherm still gives a rather good correlation with the model (see also as I in Table 4.2.9). Following eq (4.2.11) the penetration rate  $dX/dt$  can be written as:

$$dX/dt = D'/(2\sqrt{t}) \quad (4.2.15)$$

Thus for the accompanying heat flow  $Q_L(dX/dt)$  the same kind of time dependency is expected as for the heat flow by conduction.

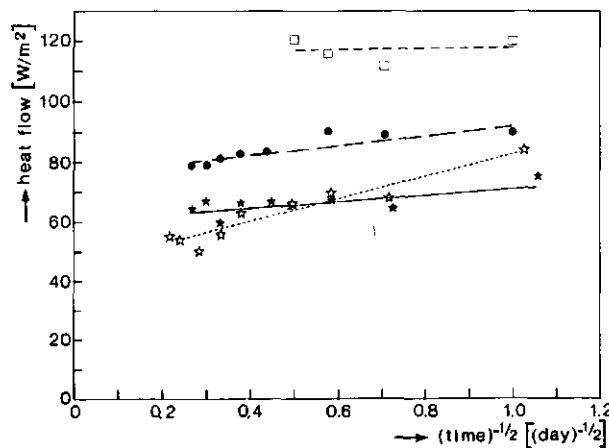


Fig. 4.2.12 Conductive heat flow in frozen Achterhoeks sandy loam (SLO) as a function of  $1/\sqrt{t}$ , for different temperatures  $T$  in upper heat exchanger with ( $\star$ )  $T = -4^\circ\text{C}$ , ( $\bullet$ )  $T = -6^\circ\text{C}$ , ( $\circ$ )  $T = -9^\circ\text{C}$  and ( $\square$ )  $T = -12^\circ\text{C}$  together with their regression lines.

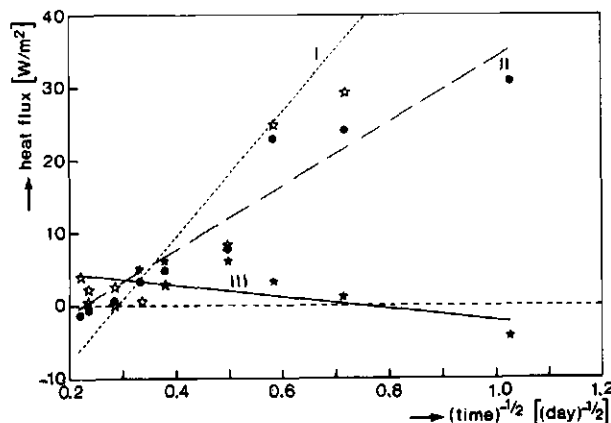
Note: the time runs from right to left along the horizontal axis.

Table 4.2.8 Regression analyses for conductive heat flow in frozen soil for the model:  $Q = A + B/\sqrt{t}$

material	$T(450)$ [ $^\circ\text{C}$ ]	$A$ [ $\text{W}/\text{m}^2$ ]	$B$ [ $\text{W}/\text{s}/\text{m}^2$ ]	$r^2$ [-]	$SE$ [ $\text{W}/\text{m}^2$ ]
LSA	-4	30	$27 \pm 5$	0.83	4
LSA	-6	61	NS	0.09	5
LSA	-9	82	NS	0.09	5
LSA	-12	88	NS	0.00	18
SLO	-4	45	$38 \pm 2$	0.91	3
SLO	-6	60	$11 \pm 5$	0.53	3
SLO	-9	76	$16 \pm 4$	0.77	3
SLO	-12	116	NS	0.01	5
CLA	-4	59	$56 \pm 13$	0.70	12
CLA	-6	68	$40 \pm 4$	0.93	3
CLA	-9	101	$12 \pm 6$	0.48	4
CLA	-12	119	$20 \pm 11$	0.39	7
B45	-2	16	$43 \pm 9$	0.78	6
B45	-4	28	$14 \pm 6$	0.52	4
B45	-6	43	$11 \pm 4$	0.61	2
B45	-8	52	$17 \pm 12$	0.23	8
B45	-12	87	$3 \pm 3$	0.20	2

**Table 4.2.9** Regression analyses for heat flow as a function of time:  
 $Q = A + B/\sqrt{t}$ , with I. heat flow caused by moving  $0^\circ\text{C}$ -isotherm, II. heat flow caused by change in unfrozen water content and III. heat flow caused by formation of ice lenses

material	model	A [W/m <sup>2</sup> ]	B [Ws/m <sup>2</sup> ]	r <sup>2</sup> [-]	SE [W/m <sup>2</sup> ]
LSA	I	-10	36±6	0.57	8
SLO	I	-16	49±7	0.64	10
CLA	I	-14	45±6	0.63	9
B45	I	NS	19±6	0.20	8
LSA	II	-6	22±4	0.58	5
SLO	II	NS	22±4	0.50	6
CLA	II	NS	17±3	0.44	5
LSA	III	3	4±1	0.21	2
SLO	III	4	5±3	0.13	3
CLA	III	NS	16±5	0.27	7
B45	III	3	NS	0.01	2



**Fig. 4.2.13** Heat flows in Achterhoeks sandy loam (SLO) for  $T(450) = -4^\circ\text{C}$  as a function of  $1/\sqrt{t}$ : (I)  $Q_L(T)$  due to moving  $0^\circ\text{C}$  isotherm, (II)  $Q_L(\theta_w)$  due to change in unfrozen water content and (III)  $Q_h$  due to secondary heave.

Note: the time runs from right to left along the horizontal axis.

The heat flow related with a change in unfrozen water content (II) and the heat flow related with total heave (III) show less significant relations with time

(see Fig. 4.2.13) than the heat flow related with the penetration of the 0°C isotherm (I). Also the coefficients of determination are less (see Table 4.2.9). As has been shown before in Table 4.2.6, the heat flow related with the change in unfrozen water content shows some retardation with respect to the heat flow related with the penetrating 0°C isotherm. This retardation appeared to be stronger for finer soils. In Table 4.2.9 we see, that the B-coefficient as well as the coefficient of determination for model II have their minima for clay. This indicates that for the finest soil (CLA), the deviation from the  $1/\sqrt{t}$ -model is the largest, which might indicate that indeed the retardation is largest for this material.

The heat flow related to the heave rate  $Q_h$  shows an even worse relationship with time (see also Fig. 4.2.13): the coefficients of determination are small. When Fig. 4.2.13 is analysed in detail, a maximum in  $Q_h$  seems to occur at  $1/\sqrt{t} \approx 0.4$  ( $t=6$  days). This maximum occurs later than the maxima in the other heat flows (at  $t=1$  day). This indicates even more retardation in the formation of ice lenses with respect to in situ freezing of pore water. This agrees with the tentative conclusion of section 4.2.4, where it has been stated that it might take some extra energy to create ice lenses.

### 4.3 Moisture transfer

Moisture transfer has its clear evidence in secondary heave<sup>1</sup>, which is caused by the formation of ice lenses. As has been shown in section 2.3.1, the heave rate is proportional to the temperature gradient over the frozen fringe under equilibrium conditions. The coupling constant is called the segregation potential (SP). In this paragraph the SP of the different materials is calculated by analysing the heave measurements (section 4.3.1). Next, the influence of the soil physical and electrochemical properties is investigated (section 4.3.2).

#### 4.3.1 Segregation potential

When a fine grained soil is subjected to freezing, frost heave occurs as a result of two simultaneous processes: pore water in the soil freezes in situ (relative volume expansion =  $(\rho_w - \rho_i)/\rho_i$ ) and water from the unfrozen soil is sucked to the freezing front, where it freezes at temperatures below 0°C, leading to the development of ice lenses. In this section the latter effect (secondary heave,  $h_{sec}$ ) is analysed. However, with our experimental setup the total heave is measured (see section 3.4). The total heave is the sum of two phenomena: the secondary heave and the volume expansion of the in situ freezing of pore water. The most direct way to correct for the volume expansion is using the rate of change in unfrozen water content,  $d\theta_w/dt$ , which has been measured with TDR:

$$\frac{dh_{sec}}{dt} = \frac{dh}{dt} - \frac{(\rho_w - \rho_i)}{\rho_i} \times \frac{d\theta_w}{dt} \times \Delta z \quad (4.3.1)$$

with  $\Delta z$  the initial distance between two pairs of TDR probes.

Konrad and Morgenstern [1980] developed the segregation potential theory for the water flux density  $v$ , which is equal to the water intake rate from the reservoir divided by the cross sectional area of the soil column. Since we did not measure the water intake rate, we have to calculate  $v$  from the secondary heave rate:

$$v = (\rho_i/\rho_w)(dh_{sec}/dt) \quad (4.3.2)$$

<sup>1</sup>) Primary heave is the formation of pure ice at the top of the soil at zero overburden pressure.

Another important parameter in this theory is the temperature gradient over the frozen fringe. Sometimes the overall temperature gradient has been used to calculate SP (e.g. in field experiments). We compared the overall temperature gradient of our experiments with the gradient measured over the frozen fringe (see Fig. 4.3.1). It can be concluded that, although both temperature gradients follow the same trend ( $r^2=0.40$ ), they are far from equal to one another. Thus large inaccuracies in SP might occur, when the overall temperature gradient is considered, instead of the temperature gradient over the frozen fringe.

To derive the segregation potential the Clapeyron equation has been used (see section 2.3.1), in which thermodynamic equilibrium between water and ice is assumed. We now assume that this equilibrium is sufficiently present, when the rate of change in temperature near the freezing front is less than 0.1 K/day (due to the penetration of the 0°C isotherm associated with a heat flux density of about 10 W/m<sup>2</sup>).

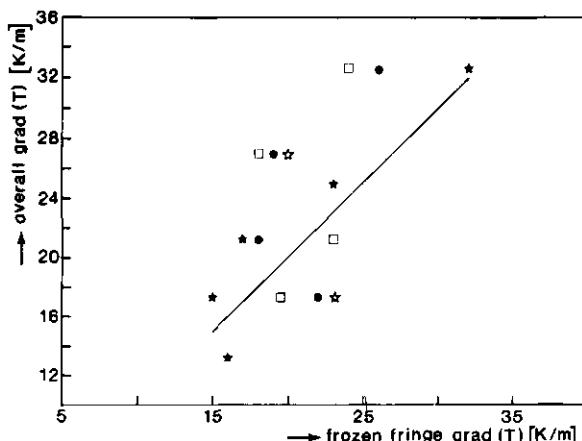


Fig. 4.3.1 Overall temperature gradient as a function of the temperature gradient over the frozen fringe, with (●) Engs loamy sand, (□) Achter hoeks sandy loam, (★) river foreland clay, (★) crushed concrete and — line  $f(x)=x$ .

Note: since the temperature gradients are negative, their absolute values are presented.

This quasi steady state was usually reached within three days after the change in the upper heat exchanger had occurred. We averaged both the temperature gradient and the heave rate over each quasi steady state, to decrease the relative measuring error and to cope with the variability of the materials used. The result can be seen in Fig. 4.3.2, where the secondary heave rate is presented as a function of the temperature gradient of the frozen fringe.

In Fig. 4.3.2 it can be seen that the observations for each material allow a representation as a straight line. These lines can be mathematically represented by the following equation:

$$dh_{sec}/dt = A - B \times (\partial T / \partial z)_{ff} \quad (4.3.3)$$

with A the intercept and B the slope. From section 2.3 (eq 2.3.13) it follows that the theoretical value for A=0, while B=SP×ρ<sub>w</sub>/ρ<sub>i</sub>, with SP the segregation potential. In Fig. 4.3.2 it can be seen that the line for crushed concrete, B45, and also the line for river foreland clay, CLA, intersect the horizontal axis. This is in disagreement with the theoretical value A=0.

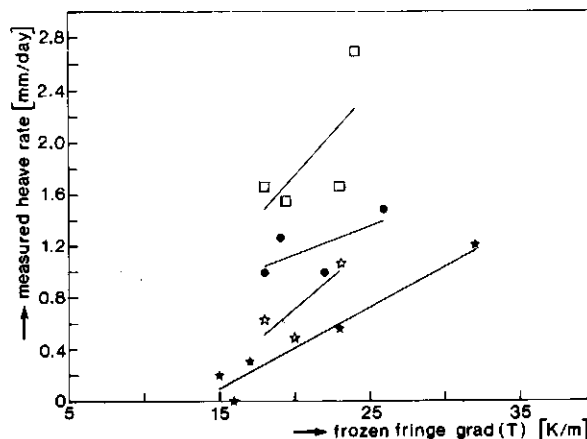


Fig. 4.3.2 Secondary heave rate as a function of the absolute value of the temperature gradient of the frozen fringe for four porous materials: (●) Engs loamy sand, (□) Achterhoeks sandy loam, (✕) river foreland clay and (\*) crushed concrete, with — lines according to eq (4.3.3).

To obtain values for the intercept and slope of (4.3.3) we performed regression analysis. Although the amount of measuring points is too small to assume a normal distribution of distances from the measuring points to the regression line, we used this distribution as a first approximation to perform the regression analyses. The lines in Fig. 4.3.2 were found according to this method. The results of the analyses can be seen in Table 4.3.1.

Table 4.3.1 Regression analysis for the segregation potential concept eq (4.3.3)

material†	n	A [10 <sup>-8</sup> m/s]	B [10 <sup>-10</sup> m <sup>2</sup> /Ks]	r <sup>2</sup> [-]	SE [10 <sup>-8</sup> m/s]	A/B [K/m]
LSA	4	0.2	0.05±0.04	0.46	0.2	5
SLO	4	-0.9	0.13±0.10	0.47	0.5	-7
CLA	3	-1.2	0.10±0.07	0.65	0.3	-13
B45	5	-0.8	0.06±0.01	0.94	0.1	-13
RSA <sup>1</sup>	3	0	0	-	-	-
SSA <sup>1</sup>	3	0	0	-	-	-

† see section 3.4 for explanation of material abbreviations

As can be seen in Table 4.3.1 the regression analysis does not result in significantly different B-values. Thus the segregation potential SP of the different materials can be considered as more or less the same. The differences in B-values in Table 4.3.1 only suggest a trend that SLO is the most frost susceptible material and LSA the least frost susceptible material among those which show heave.

<sup>1</sup>) In order to compare the frost experiments in river sand RSA and silver sand SSA, as described in section 4.1 (closed system freezing) with the above described frost heave tests, some additional experiments were performed. In the Northern Road Testing Laboratory in Groningen (NL) some open system frost heave tests were performed, according to the TRRL prescriptions [Roe and Webster, 1984]. In this test three small columns of each material (150 mm high and 90 mm diameter) were frozen by contacting the upper soil surface with cold air (T=-15°C), while the bottom remained unfrozen and was in hydraulic contact with water of +4°C. In spite of the high measured temperature gradients (30 to 50 K/m) no frost heave took place. In other words the heave rate as a function of temperature gradient can be considered zero (see Table 4.3.1).

A phenomenon which has not been described by Konrad and Morgenstern [1980, 1981, 1982 and 1983], is the intersection of the horizontal axis for B45 and CLA (Fig. 4.3.2). With use of regression analysis these intercepts and the corresponding A/B-values<sup>1</sup> (see Table 4.3.1), have been calculated.

The absolute A/B-values for B45 and CLA are larger than those for LSA and SLO. In fact the latter two intercepts of the horizontal axis (or A/B-values) do not have a significant meaning, since the extrapolation is far beyond the measuring points. This intercept agrees with a minimum absolute value of the temperature gradient (or water pressure gradient) at which heave starts. This pressure gradient is probably required to break the structure of the soil or concrete in order to create a plane of weakness in which an ice lens can be formed and to lift the overburden associated with the overlying frozen soil. Nixon [1988], building on the work of Miller [1978], concluded that an excess pressure is required to initiate a new lens.

#### *4.3.2 Influence of soil physical and electrochemical properties*

In section 1.3 a microscopic model of the frozen fringe has been proposed to explain in which way soil physical and electrochemical properties might influence moisture transport in columns of freezing porous material. In section 2.1 the definition and determination of each property has been presented.<sup>1</sup> In the present paragraph the actual moisture transport measurements are related to the measured properties of the different porous materials. Firstly, the relation between the soil properties and the segregation potential is analysed and secondly, a relation between the minimum pressure gradient, at which heave occurs (see previous section), and the soil properties is sought.

In section 1.3 it has been suggested that SP has a positive relation with the following properties: mass fraction of small particles  $\Phi_x$  (with a diameter less than x), specific surface area S, cation exchange capacity CEC and surface

<sup>1)</sup> Both the temperature gradient in the frozen fringe and the A/B-value are negative. Therefore the absolute values of these properties are considered (see also Fig. 4.3.2).

charge density of the mineral particles  $\zeta$  (zeta potential). For  $\Phi$  three different measures can be used: fines fraction  $\Phi_{125}$ , silt fraction  $\Phi_{50}$  and clay fraction  $\Phi_2$ . So we arrive at six material properties. In general SP is material dependent, but theoretically SP might also be material independent. Thus, altogether seven properties P can be related with SP (for a soil independent SP,  $P=1$ ). Following (2.3.13), in which the relation between water flux density and temperature gradient is expressed, the following regression model for P can be written:

$$dh_{sec}/dt = A - B(\partial T/\partial z)_{ff} \times P \quad (4.3.4)$$

with A and B the regression coefficients.

In Table 4.3.2 it can be seen that a material independent SP ( $P=1$ ) results in a poor regression model ( $r^2=0.11$ ). Apart from this the negative B coefficient is in contradiction with the SP theory. Thus, SP has to be material dependent. However, most properties P did not result in a good regression model either. Only the fines fraction and the silt fraction gave reasonable models (with  $r^2$  equaled 0.39 and 0.32, respectively).

This is in agreement with other frost heave research, in which is stated that fine textured soils are more frost susceptible than coarse textured soils [e.g. Jones and Lomas, 1983; Nixon, 1988 and Jessberger and Jagow, 1989]. (The influence of the clay content will be discussed later.)

Table 4.3.2 Regression analyses for secondary heave rate, eq (4.3.4)

P	unit(P)	A [10 <sup>-8</sup> m/s]	B×unit(P) [10 <sup>-11</sup> m <sup>2</sup> /Ks]	r <sup>2</sup> [-]	SE [10 <sup>-8</sup> m/s]
1	-	1.5	-30 ± 20	0.11*	0.8
$\Phi_{125}$	100 g/g	NS	1.0 ± 0.2	0.39**	0.6
$\Phi_{50}$	100 g/g	NS	0.8 ± 0.3	0.32**	0.7
$\Phi_2$	100 g/g	NS	1.6 ± 1.0	0.10*	0.8
S	m <sup>2</sup> /g	NS	3 ± 2	0.11*	0.8
CEC	mg/kg	0.8	NS	0.01	0.8
$\zeta$	10 <sup>-8</sup> m <sup>2</sup> /Vs	1.2	7 ± 5	0.09*	0.8

\*, \*\* significant at  $P_0 < 0.15$  and  $P_0 < 0.05$ , respectively, with  $P_0$  the probability for the zero hypothesis.

In most research the frost susceptibility is only evaluated for soil material. In our research also other porous media are evaluated (i.e. SSA and B45). Therefore the extension of the existing models can be necessary. Indeed, the simple model for frost heave (Table 4.3.2) results in larger distances between measuring points and model relation (or larger SE-values), than the distances for the individual materials (or SE-values in Table 4.3.1). To overcome this problem, it is assumed that the segregation potential depends on more than one property. This is allowed since we have sufficient measuring points: 22 measuring points when all 6 materials are taken together. The most simple relation is then a linear combination of properties. With this linear combination (4.3.4) can be extended as follows:

$$dh_{sec}/dt = A - B(\partial T/\partial z)_{ff}(B_1 + B_2P_2 + \dots + B_nP_n) \quad (4.3.5)$$

with  $A$ ,  $B_1$  to  $B_n$  the regression coefficients and  $P_1$  to  $P_n$  the different properties. A complication in (4.3.5) is the interdependency of properties. As has been proved in section 3.4 the specific surface area depends on the clay fraction and the CEC depends on the specific surface area, when the materials of the same mineral composition are considered. However, when all materials (including B45 and SLO-2) are considered,  $\Phi_2$  and CEC are independent, while S and CEC show a weak interrelation. Also the zeta potential is a real independent parameter. Only the clay, silt and fines fraction are strongly interrelated ( $r^2(\text{clay-fines}) = 0.78$ ,  $r^2(\text{clay-silt}) = 0.92$  and  $r^2(\text{silt-fines}) = 0.85$ ). However, the stepwise regression procedure selects parameters based upon their independent contribution to the model. Thus, interdependency is taken into account. To compensate for the interrelation effect, an increased significance level of 95% is now assumed. (Thus, the zero hypothesis for a significant parameter needs to be rejected with a certainty of 95%. This means that the relative error of the regression coefficient ( $\Delta B_j/B_j$ ) has a maximum of 0.5).

With the 95% significance level the multiple regression can now be performed. Here the stepwise procedure is followed:  $P_1$  is the parameter with the highest model  $r^2$  ( $P_1 = \Phi_{125}$ , see Table 4.3.2). Then  $\Phi_{125}$  is combined with each other parameter and from the combination, which results into the highest model  $r^2$ ,  $P_2$  is chosen. Next, a third parameter is added to the model and so on. The extension

of the model stops, when no significant improvement of the prediction of the heave rate can be found.

In our case, clay fraction  $\Phi_2$  is determined as second regression parameter (see Table 4.3.3). In contradiction with the fines fraction, its influence is negative: a higher clay fraction impedes the heave rate. The same has been observed by Rieke et al. [1983] and Knutsson et al. [1985]. They all observe that the SP increases with an increasing amount of fine particles until an optimum has been reached.

Table 4.3.3 Stepwise regression of soil properties on the secondary heave (eq 4.3.5). With  $P_1=\Phi_{125}$  [g/g],  $P_2=\Phi_2$  [g/g] and  $P_3=S$  [ $m^2/g$ ]

A [ $10^{-8}m/s$ ]	$B_1 \times \text{unit}(P_1)$ [ $10^{-11}m^2/Ks$ ]	$B_2 \times \text{unit}(P_2)$ [ $10^{-11}m^2/Ks$ ]	$B_3 \times \text{unit}(P_3)$ [ $10^{-11}m^2/Ks$ ]	$r^2$ [-]	SE [ $10^{-8}m/s$ ]
NS	1.0±0.2	0	0	0.39	0.6
NS	2.2±0.5	-4±2	0	0.57	0.5
-0.5	2.2±0.4	-5±1	3±1	0.67	0.5

For very high values of  $\Phi_{125}$  (which must result in high clay contents) SP decreases considerably. Knutsson et al. [1985] state that: "In clay rich soils the permeability of the frozen fringe is not the only crucial zone, here the permeability of the unfrozen soil is a controlling factor as well". It is assumed that a high clay content causes a low permeability of the unfrozen soil and that this low permeability impedes the formation of ice lenses. Another reason for the negative influence of clay content might be the shrinkage of the matrix during frost penetration. Clay does not have a rigid matrix and when pure clay material is frozen, some shrinkage might take place. Thus, the negative relation of clay content with water flux density, as we found, is to be expected.

The third property, influencing the segregation potential (see Table 4.3.3), is the specific surface area S. Here a positive relation is found from the regression analyses, which is in agreement with the microscopic theory. Other scientists also found a positive relation between water flux density and specific surface area: e.g. Ratkje et al. [1982] and Rieke et al. [1983]. In our case the

influence of S is most pronounced for B45 and SLO-2, where the highest S-values have been measured, together with relatively high heave rate values. Because these two materials have a different mineral composition compared with the other materials, S might reflect another property, e.g. a chemical property, which has not been measured. The other properties did not influence the segregation potential significantly. So we arrive at a three parameter model. This model explains 67% of the variation in heave rate.

Miller [1972] and Nixon [1988] concluded that an excess pressure is needed to initiate a new ice lens (see also section 2.3). In section 4.3.1 it has been concluded that a negative A-coefficient in (4.3.4) agrees with this pressure. Also for the last (and best) model of Table 4.3.3 a negative A coefficient has been found (significant at the 85% probability level), indicating again the necessity of the excess pressure. The next step is to relate one of the material properties (represented with  $P_4$ , since we have already a three parameter model) with the intercept A. The most simple relation is a linear combination of a material independent part,  $A_0$ , and a material dependent part,  $A_1 \times P_4$ . This combination results in the following regression model:

$$\frac{dh_{sec}}{dt} = A_0 + A_1 \times P_4 - (\partial T / \partial z)_{ff} (B_1 \times \Phi_{125} + B_2 \times \Phi_2 + B_3 \times S) \quad (4.3.6)$$

with  $A_0$ ,  $A_1$ ,  $B_1$ ,  $B_2$  and  $B_3$  the regression coefficients.

In Table 4.3.4 it can be seen that the material independent intercept was not significant. As far as we know, no theoretical evidence for such a material independent intercept exists. The cation exchange capacity, CEC, is best suitable as material property  $P_4$ , resulting in a large improvement of the model: the coefficient of determination for the water flux density increased from 0.67 (last model in Table 4.3.3) to 0.78 (model in Table 4.3.4). In Fig. 4.3.3 the measured water flux density is presented as a function of the model. It can be seen that most measuring points are not far from the ideal line, which is also reflected in the low standard error of  $0.4 \times 10^{-8} \text{ m/s}$ .

The physical interpretation of the negative relation of CEC with the heave rate is, that more charged soil particles result into a stronger electrical field.

Table 4.3.4 Regression model for the secondary heave rate (4.3.6) with material dependent intercept

property	coefficient	value	unit
1	$A_0$	NS	$[10^{-8} \text{m/s}]$
CEC	$A_1$	$-4 \pm 1$	$[10^{-8} \text{m/s}] / [\text{mg/kg}]$
$\Phi_{125}$	$B_1$	$1.9 \pm 0.4$	$[10^{-11} \text{m}^2/\text{Ks}] / [\text{kg/kg}]$
$\Phi_2$	$B_2$	$-5 \pm 1$	$[10^{-11} \text{m}^2/\text{Ks}] / [\text{kg/kg}]$
S	$B_3$	7 $\pm 2$	$[10^{-11} \text{m}^2/\text{Ks}] / [\text{g/m}^2]$

This stronger field attracts more ions in the soil water. And the ions attract on turn other charged soil particles. Thus a higher CEC results in higher cohesion forces between the soil particles. This leads into the conclusion that with a higher CEC more energy, or a higher excess pressure, is needed to initiate an ice lens. Also Van Loon and Zeilmaker [1989] suggested that the cohesion forces in the aggregates (cohesion is often measured in civil engineering) might be a good measure to relate with the excess pressure.

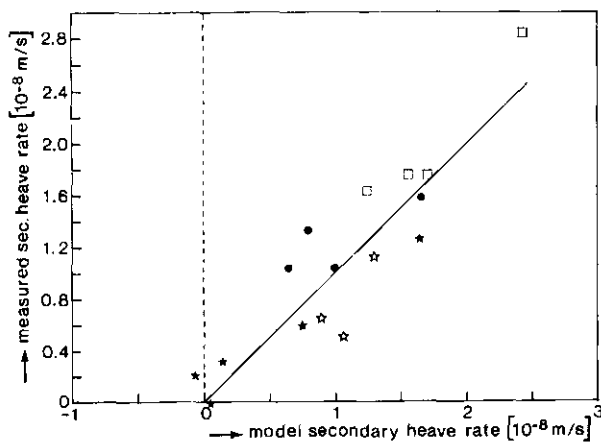


Fig. 4.3.3 Measured secondary heave rate as a function of model secondary heave rate (4.3.6). With (★) B45, (○) CLA, (□) SLO, (●) LSA and — the function  $f(x)=x$ .

#### 4.4 Application of time-domain reflectometry to measure solute concentration during soil freezing

##### 4.4.0 Abstract

The redistribution of water and solutes during soil freezing was investigated in the laboratory. Uniaxial freezing tests were performed on twelve columns of Guelph loam. The columns differed in average bulk density and concentration of solutes added. Volumetric (unfrozen) water content and bulk electrical conductivity,  $\sigma$ , were measured *in situ* using time domain reflectometry (TDR). Temperature profiles were also monitored. A regression model was developed to explain  $\sigma$  in terms of solute concentration, unfrozen water content and temperature; the coefficient of determination ( $r^2$ ) was 0.985. The relationship between  $\sigma$  and unfrozen water content was non-linear. The temperature effect could be related to the viscosity of liquid water. After correcting for unfrozen water content and temperature, residual peaks in were assumed to indicate an increase in solute concentration. The peaks advanced downwards with a velocity of 6 mm/day ahead of the 0°C isotherm, suggesting redistribution of solutes as a result of freezing.

##### 4.4.1 Introduction

The influence of solutes on ground freezing is threefold. Firstly, the presence of solutes determines, in part, the freezing point depression (and thus the unfrozen water content) [Banin and Anderson, 1974, and Young et al., 1979]. Secondly, solutes oppose heave, since the osmotic pressure reduces the maximum heaving pressure [Cary, 1987; and Chamberlain, 1983]. Thirdly, solutes are themselves redistributed during the freezing process. This is due to the exclusion of solutes by ice formation [Kadlec et al., 1988; Kay and Groeneveld, 1983; Mahar et al., 1983]. Solutes are also transported into the frozen fringe when water is drawn upwards to form ice lenses [Gray and Granger, 1986]. The net result is a concentration of solutes in the vicinity of the freezing front.

The redistribution of solutes during soil freezing is of interest to agronomists and environmental engineers seeking to minimize contamination of ground water

supplies during winter. The phenomenon is also important for construction projects in areas of saline and subsea permafrost. It forms a part of the entity of coupled heat and mass transfer processes which can be presented as a matrix [Perfect et al., 1991].

Different techniques have been used to monitor solute redistribution as a result of freezing. Starting with a known solute profile, the most direct way is destructive sampling at the end of the freezing experiment [e.g. Cary and Mayland, 1972]. A major disadvantage with this method, is that it is only possible to sample once per volume element, so changes over time are impossible to determine. Gray and Granger [1986] solved this problem in the field by sampling different volumes at different times and assuming that all samples had the same history. In the laboratory, Cary et al. [1979] extracted small amounts of pore water over time from different locations within a freezing column. The amount of dissolved salts was determined by measuring the electrical conductivity of these samples. Mahar et al. [1983] also used extracted soil water to monitor the changes in salinity due to freezing.

In order to obtain a better knowledge of the mass transfer processes, non-destructive in situ measurements are desirable. An applicable method is the measurement of the bulk electrical conductivity,  $\sigma$ . Baker and Osterkamp [1988] and Hayhoe and Balchin [1988] have used the in situ  $\sigma$  as a measure of the solute concentration during soil freezing. However, the relationship between  $\sigma$  and solute concentration is quite complex. The influence of liquid (unfrozen) water content is non-linear and the surface conductivity of the soil particles must be taken into account [Van Loon et al., 1991].

Recently, time domain reflectometry (TDR) has been used to measure  $\sigma$  as well as the water content of unfrozen soils [Dalton et al., 1984]. It may also be possible to measure the  $\sigma$  under frozen conditions using TDR [Van Loon et al., 1991]. Measurement of the unfrozen (liquid) water content of frozen soils is well established [Patterson and Smith, 1985]. Thus, TDR is a promising method for the simultaneous measurement of unfrozen water content and solute concentration (as indicated with  $\sigma$ ) in frozen soils.

In this research, unfrozen water content profiles and bulk electrical conductivity were measured during freezing using the TDR technique. The major objective was to identify which parameters (solute concentration, temperature, and unfrozen water content) the measured  $\sigma$  is most sensitive to under frozen conditions. The possibility of using TDR to monitor solute redistribution during transient freezing will be investigated.

#### 4.4.2 Materials and methods

Uniaxial freezing tests were performed using twelve 270 mm diameter columns with a height of 180 mm. The material used was aggregated Guelph silt loam, classified as a Gleyed orthic Melanic Brunisol. This material is described in Van Loon et al., [1990b]. To obtain a more homogeneous medium the field soil was air dried and sieved. The columns were packed to specific bulk densities, depending on the degree of aggregation (Table 4.4.1). The influence of aggregate size and bulk density on the freezing process will be reported in a future publication. Parallel TDR probes and thermocouples were installed horizontally into the dry soil at different heights (Fig. 4.4.1). These were allowed to move (in response to frost heave) by cutting a narrow slit in the columns at a height  $> 70$  mm. All heights were measured relative to the base of the columns and are reported as positive upwards.

Table 4.4.1 Details of column packing and solutions of  $\text{CaCl}_2$  added

column no.	Sieve size [mm]	Bulk density [Mg/m <sup>3</sup> ]	Solution concentration [g/l]
1,2,3	10	1.15	1
4,5	5	1.31	1
6	crushed	1.39	1
7,8,9	5	1.31	2
10,11,12	5	1.31	4

All of the columns were placed into containers with well defined  $\text{CaCl}_2$  solutions (Table 4.4.1). Holes (with porous screens) at the bottom of each column allowed the solution to enter the soil by capillarity. The fluid level was kept constant

by adding solution of the same concentration to the reservoirs. The columns with solute reservoirs were then set up in an environmental chamber, which could be maintained below freezing. The reservoirs were kept unfrozen by a heat exchanger, which was connected to a thermostatic bath (Fig. 4.4.1). Both columns and reservoirs were carefully insulated with styrofoam, so the  $0^{\circ}\text{C}$  isotherm could only penetrate from the (upper) soil surface. Temperatures in the reservoirs and in the air (near the soil surface) were also measured by thermocouples. All temperatures were recorded automatically every six hours using a data logger. The TDR readings were taken once a day by hand.

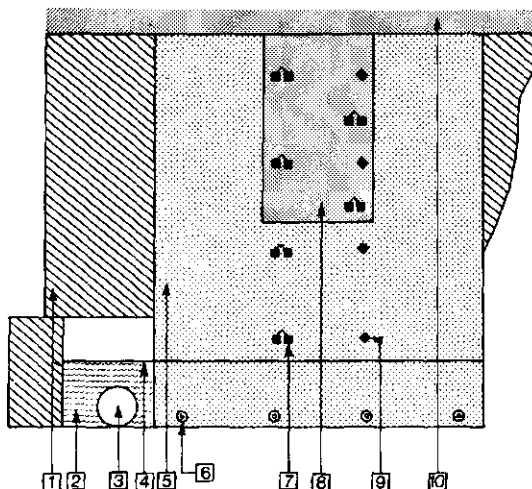


Fig. 4.4.1 Cross section of column used for uniaxial freezing test.

1. insulation
2.  $\text{CaCl}_2$  solution reservoir
3. tubular copper heat exchanger ( $T=4^{\circ}\text{C}$ )
4. constant water table
5. soil column
6. water inlet with porous screen
7. parallel TDR probes
8. slit with bare soil
9. thermocouple
10. soil surface contacting air ( $T<0^{\circ}\text{C}$ )

The TDR method is based upon the reflection of an electromagnetic pulse within transmission lines, which are installed in the medium. By this means the (effective) dielectric constant of the medium can be determined. This value depends on the volume fraction of the components in the medium. Topp et al. [1980] obtained an empirical relation to convert the effective dielectric constant  $\epsilon$  into the volumetric water content  $\theta_w$ :

$$\theta_w = -0.053 + 0.0292\epsilon - 5.5 \times 10^{-4}\epsilon^2 + 4.3 \times 10^{-6}\epsilon^3 \quad (4.4.1)$$

Similarly, Smith and Tice [1988] developed an empirical relation between  $\epsilon$  and the unfrozen water content  $\theta_u$  at subzero temperatures:

$$\theta_u = -0.146 + 0.0387\epsilon - 8.5 \times 10^{-4}\epsilon^2 + 9.9 \times 10^{-6}\epsilon^3 \quad (4.4.2)$$

The bulk electrical conductivity of the medium can be obtained from the amplitude of the reflected pulse. However, this reflection is influenced by the measuring system, as well as by the medium itself.

Van Loon et al. [1990b] have developed a method to correct for influences of the measuring system. In this method a reflection measurement in soil,  $V$ , is compared with a reference measurement in dry air,  $V_0$ . The bulk electrical conductivity  $\sigma$  is then given by the following equation:

$$\sigma = \{\epsilon / (\eta_0 \times L)\} \times \ln(V_0/V) \quad (4.4.3)$$

with  $\eta_0 = 120 \times \pi \Omega$  and  $L$  the length of the probes.

#### 4.4.3 Results and discussion

The measured  $\sigma$  in column number 12 was examined, as an example, to show the relationship between  $\sigma$  and temperature and unfrozen water content (see Fig. 4.4.2).

Regression analyses were performed on the 915 datapoints obtained from the twelve columns (exceptions are always indicated). As a first approximation, the measured  $\sigma$  was assumed to be a function of the solute concentration on a bulk basis. In this model, however, no interaction with the soil particles is included, so it can only be applied close to saturation. For  $\theta_w \geq 40\%$  we tested the following model:

$$\sigma = A + B \times SC \times \theta_w \quad (4.4.4)$$

where  $A$  and  $B$  are regression coefficients and  $SC$  the solute concentration of the pore water. This simple model was highly significant:  $r^2=0.88$ . From the regression it follows that  $A=61$  mS/m and  $B=80$  mS m<sup>2</sup>/kg.

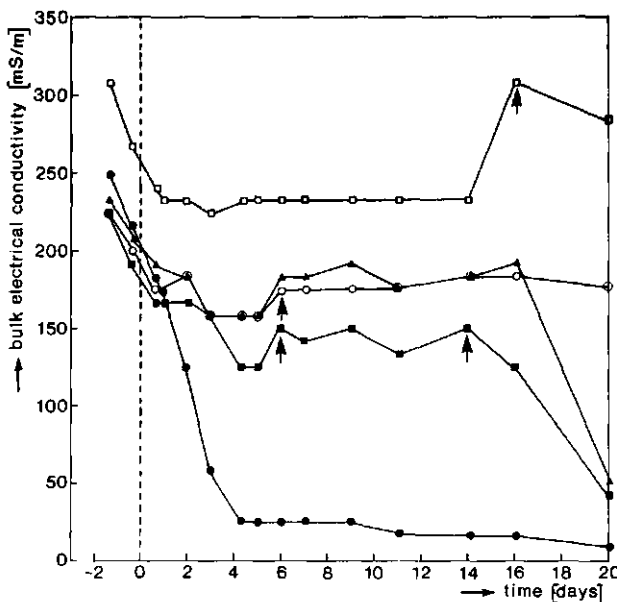


Fig. 4.4.2 Measured bulk electrical conductivity as a function of time in column 12 (with a solute concentration of 4 g/l). Initial positions of TDR measuring probes: ( $\bullet$ )  $z=160$  mm, ( $\blacksquare$ )  $z=140$  mm, ( $\blacktriangle$ )  $z=120$  mm, ( $\circ$ )  $z=100$  mm and ( $\square$ )  $z=40$  mm. Arrows indicate significant increases in measured  $\sigma$ .

#### 4.4.3.1 Influence of temperature

Changes in bulk electrical conductivity,  $\sigma$ , over time for different TDR probes in column number 12 are shown in Fig. 4.4.2. Before time  $t=0$  the climate room was cooled from  $12^\circ\text{C}$  to  $4^\circ\text{C}$ . At  $t=0$  the temperature was dropped to  $-5^\circ\text{C}$ . The first thing that happened, during the first three measuring days, was a decrease in bulk electrical conductivity for all five measuring probes (Fig. 4.4.2). At the same time the temperature in the soil decreased from  $12^\circ\text{C}$  to  $1.5^\circ\text{C}$  (averaged over column). The water content profile, which was also measured with TDR, did not change by more than 2% by volume during this period ( $t=-1.2$  to  $0.6$  day). Thus, the measured  $\sigma$  is temperature dependent. The next step is to include the

temperature effect into our model for  $\sigma$ , where the regression is again limited to water contents close to saturation (i.e.  $\theta_w \geq 40\%$ ):

$$\sigma = A + B \times SC \times \theta_w + D \times T \quad (4.4.5)$$

The  $r^2$ -value for this model was 0.92 and the regression coefficients were:  $A=60$  mS/m,  $B=79$  mS  $m^2/kg$  and  $D=3.4$  mS/ $^{\circ}C/m$ . The inclusion of temperature was statistically highly significant. The physical meaning of a positive D coefficient is increased mobility of ions with higher temperatures. This effect is probably related with the viscosity of water. The electrical conductivity of a solution is inversely proportional to the viscosity of water, and the viscosity of water is directly temperature dependent [Weast, 1978]. Thus, if we express the measured  $\sigma$  relative to a standard  $\sigma$  at room temperature (i.e.  $20^{\circ}C$ ), the following expression is obtained:

$$\sigma(T) = \sigma(20) \times \text{viscosity}(20) / \text{viscosity}(T) = \sigma(20) \times \text{Vis}(T) \quad (4.4.6)$$

In the temperature range  $-8^{\circ}C < T < +30^{\circ}C$ , the ratio of viscosities  $V(T)$  can be modeled with a second order power expansion on T:

$$\text{Vis}(T) = 0.5584 + 0.0193 \times T + 0.00014 \times T^2 \quad (4.4.7)$$

with T in  $^{\circ}C$ . The agreement between (4.4.7) and Weast [1978] is excellent:  $r^2 > 0.99995$  with a standard error of 0.001.

The effect of viscosity can now be incorporated into a new regression model for bulk electrical conductivity:

$$\sigma = A + B \times SC \times \theta_w \times \text{Vis}(T) \quad (4.4.8)$$

The regression coefficients for this model were now  $A=61$  mS/m and  $B=130$  mS  $m^2/kg$  and the coefficient of determination was the same as that for the model that was extended with the temperature influence (i.e.  $r^2=0.92$ ). However, (4.4.8) has two important advantages over (4.4.5): firstly, it uses fewer degrees of freedom, and secondly, it has a better physical background.

#### 4.4.3.2 Influence of liquid water content

Another feature of Fig. 4.4.2 is the continued reduction in bulk electrical conductivity  $\sigma$  at  $z=160$  mm for  $t>0.6$  day. Between  $t=1$  and  $t=4.2$  day the measured  $\sigma$  fell from 171 to 26 mS/m. During this time interval the temperature remained constant (within the measuring accuracy), while the liquid water content decreased from 0.41 to 0.12 m<sup>3</sup>/m<sup>3</sup>. This was probably due to ice nucleation and freezing of the pore water. It is unlikely, however, that the decrease in liquid water content (by a factor of 3.4) would cause a such large reduction in bulk solute concentration (a factor 6.6). In fact, the opposite must be true if solutes were expelled from the freezing zone by a solute concentration gradient (concentration on unfrozen water basis). Therefore the reduction of solute concentration (if present at all) has to be less than the reduction of the liquid water content.

At low water contents  $\sigma$  is a non-linear function of the water content [e.g. Hayhoe and Balchin, 1988]. Van Loon et al. [1991] developed the following theoretical relation between bulk electrical conductivity, solute concentration and liquid water content at room temperature:

$$\sigma(20) = (1+3\theta_w)\sigma_s + \frac{\theta_w^2(2-\theta_w)\sigma_w}{\theta_{sat}(2-\theta_{sat})} \quad (4.4.9)$$

where  $\theta_{sat}$  the water content at saturation,  $\sigma_s$  is the electrical conductivity of the soil particles and  $\sigma_w$  the electrical conductivity of the pore solution. The relation between the latter property and the solute concentration is simply:  $\sigma_w = Q \times SC$ , with  $Q$  the specific conductivity at 20°C in S·m<sup>2</sup>/kg.

Equations (4.4.6), (4.4.7) and (4.4.9) can now be combined to obtain a quasi-theoretical model for the bulk electrical conductivity at different temperatures, water contents and solute concentrations:

$$\sigma(T, \theta_w, SC) = ((1+3\theta_w)\sigma_s + \frac{\theta_w^2(2-\theta_w)Q \times SC}{\theta_{sat}(2-\theta_{sat})}) \text{ Vis}(T) \quad (4.4.10)$$

To generate an equivalent regression model the following assumptions were made:

1.  $\sigma_s$  is unknown and has to be found by regression (i.e.  $A=\sigma_s$ ),
2. the specific electrical conductivity for  $\text{CaCl}_2$  is  $Q=161 \text{ mS m}^2/\text{kg}$  [Weast, 1978].
3.  $\theta_{\text{sat}}$  is unknown, so a second regression parameter is needed (i.e.  $B = 1/((2-\theta_{\text{sat}})\theta_{\text{sat}})$ ).
4. (4.4.7) can be used for the viscosity effect.
5. no intercept is needed in the regression, since it is included in the A coefficient.

The resultant regression model for  $\sigma$  can then be written as:

$$\sigma(T, \theta_w, SC) = (1+3\times\theta_w)V(T)\times A + \theta_w^2(2-\theta_w)Q\times SC\times \text{Vis}(T)\times B \quad (4.4.11)$$

The results of the regression analysis are summarized in Table 4.4.2. It can be seen that the combined model for  $\sigma(T, \theta_w, SC)$  was highly significant.

Table 4.4.2 Regression coefficients for the model:

$$\sigma(T, \theta_w, SC) = (1+3\times\theta_w)V(T)\times A + \theta_w^2(2-\theta_w)Q\times SC\times \text{Vis}(T)\times B$$

data range	number [-]	A [mS/m]	B [-]	$r^2$ [-]	SE† [mS/m]
ALL	915	37	1.24	0.985	13
$T < 0^\circ\text{C}$	403	24	1.60	0.974	10
$T \geq 0^\circ\text{C}$	614	42	1.17	0.990	13

† SE = standard error

It is to be expected that the coefficients will be different for the frozen and unfrozen cases: in the frozen case  $\theta_w = \theta_u$ , the unfrozen water content, and in the unfrozen case  $\theta_w$  equals the total water content. However, the influence of ice versus air on the measured  $\sigma$  is surprisingly small. If all data points are taken together, the model explains 98.5% of the variation in  $\sigma$ . If only the data points for frozen conditions are considered, the  $r^2$  decreases slightly. Conversely, if the data points for unfrozen conditions are taken the  $r^2$  increases slightly (Table 4.4.2).

The soil particle electrical conductivities  $\sigma_s$  given in Table 4.4.2 agree well (within the accuracy of the regression model) with the value for the same material at 20°C ( $\sigma_s=26$  mS/m) estimated by Van Loon et al. [1990b]. The agreement is closest for the frozen material ( $\sigma_s=24$  mS/m). In all probability  $\sigma_s$  will have been determined less accurately in the unfrozen case, because the water contents are always rather high:  $\theta_w = 0.40 \pm 0.10$ . This causes the second term (with the B-coefficient) to be much larger than the first term, so this first term is determined less accurately.

Since A was overestimated in the unfrozen case, B was probably underestimated. The B-coefficient of the entire data set looks more reasonable. A value of 1.24 for B would result into a saturated water content of 0.56, which is comparable with the lowest bulk density value given in Table 4.4.1. The higher B-coefficient for the frozen soil might indicate an increase of the solute concentration (SC) due to ice formation: solutes are excluded from the ice and confined to the unfrozen water films under frozen conditions.

Hayhoe and Balchin [1988] gathered a similar data set using an AC conductivity signal conditioner module to measure the electrical conductance. This parameter can be transformed into  $\sigma$  as follows:  $\sigma = \text{conductance}/d$ , with  $d$  the spacing between the probes (i.e.  $d=50$  mm). From Figs. 1, 2 and 3 in Hayhoe and Balchin [1988] we obtained datasets of 33 points for sand, 26 points for loam and 19 points for clay. When these data sets are analysed with our  $\sigma$  model (4.4.10), we again found high correlations:  $r^2=0.96$ , 0.97 and 0.95 for sand, loam and clay respectively. However, the model produced negative estimates of  $\sigma_s$  in each case, which is physical impossible. Inaccuracies in determining  $\sigma_s$  may be related to the restricted range of water contents available for analysis.

#### 4.4.3.3 Redistribution of solutes

Apart from the initial decrease in bulk electrical conductivity, Fig. 4.4.2 also shows some significant (i.e.  $\Delta\sigma > 13$  mS/m) transitory increases in measured  $\sigma$ . Temperature and unfrozen water content always decreased over time, so these peaks cannot be explained with the above model. Excluding measurement errors, an increase in  $\sigma$  can only be caused by solute redistribution effects. Altogether 29

increases (some determined with more than one probe) were identified from the 12 columns over the 13 measuring dates. From these, two variables were evaluated: the amplitude of the increase ( $\Delta\sigma$ ) and the mean height at which the increase occurred (z). Parameters that might be important in the redistribution process include position of the 0°C isotherm (X), initial solute concentration (SC) and time (t). Using these parameters the following regression model was developed for the increase in bulk electrical conductivity ( $\Delta\sigma$ ):

$$\Delta\sigma = A + B \times X + D \times SC + E \times t \quad (4.4.12)$$

The regression coefficients were  $B = 0.2 \mu\text{S}/\text{m}^2$  and  $D = 4 \text{ mS m}^2/\text{kg}$ ; A and E were not significantly different from zero. The coefficient of determination was low ( $r^2=0.18$ ) but statistically significant at  $p<0.15$ . Because of the poor correlation, further conclusions are hard to make.

A similar model was developed for the location (z) of the measured increases in  $\sigma$ :

$$z = A + B \times X + D \times C + E \times t \quad (4.4.13)$$

where the regression coefficients are  $A = 9 \text{ cm}$ ,  $B = 0.5$  and  $E = -6 \text{ mm/day}$ , with D was not significantly different from zero. This model appears to describe the measurements better:  $r^2=0.77$ . We can use (4.4.13) to calculate the redistribution of solutes during soil freezing; predicted values for time  $t=0$ ,  $X=18 \text{ cm}$  and  $t=16 \text{ days}$ ,  $X=8 \text{ cm}$  are  $z=18$  and  $z=3 \text{ cm}$ , respectively. Thus, the enriched solute peak appears to have moved faster than and ahead of the 0°C isotherm.

The velocity of the solute peak (-6 mm/day) is in good agreement with analyses performed by Kay and Groenevelt [1983]. These authors measured the redistribution of nitrate in the same Guelph loam under field conditions; the nitrate peak moved down 15 cm during the first 26 days of freezing. Their hypothesis that solute redistribution occurs on a local scale is also applicable to our research. The increases we measured were very small compared to the total bulk electrical conductivity (see Fig. 4.4.2). Thus, only a small fraction of the solutes could have been transported over macroscopic distances.

#### 4.4.4 *Conclusions*

Time-domain reflectometry can be used to measure the unfrozen water content and bulk electrical conductivity simultaneously under frozen conditions. The *in situ* bulk electrical conductivity,  $\sigma$ , depends on the solute concentration, unfrozen water content and temperature. The temperature effect can be related to the mobility of ions, through the viscosity of water. The influence of unfrozen water content on  $\sigma$  is non-linear.

Redistribution of solutes during soil freezing can also be monitored using the  $\sigma$  measurement with TDR. After temperature and water content corrections are applied, it is possible to identify increases in  $\sigma$  associated with solute enrichment. These solute peaks appear to move faster than and ahead of the 0°C isotherm.

#### 4.5 Influence of added solutes on moisture transfer

When solutes are present in the soil water, an osmotic potential exists, which is proportional to the solute concentration (Van 't Hoff's law, eq 2.3.27). The osmotic potential causes a decrease in the water potential (eq 2.3.7). Then also the water potential gradient decreases, which results in less water transport. This agrees with Cary [1987] and Chamberlain [1983], who demonstrated that solutes reduce the maximum heaving pressure, resulting in less heave.

To investigate the influence of solutes on the heaving process, uniaxial heaving tests were performed on twelve columns of repacked Guelph silt loam. To obtain a more homogeneous medium, the soil was air dried and sieved, before the columns were packed. All of the columns were placed into containers with well known  $\text{CaCl}_2$  (calcium chloride) solutions. The solute concentration was 1 g/l for six columns, 2 g/l for three other columns and 4 g/l for the last three columns (see also section 4.4.2).

The water in the reservoirs was kept at a constant level by adding water with the same solute concentration. All twelve columns with solute reservoirs were then set up in one environmental chamber, which could be maintained below freezing. So the columns could be cooled with air below 0°C. The solute reservoirs and the bottoms of the columns were kept unfrozen by a heat exchanger, which was connected with a thermostatic bath. Both columns and reservoirs were carefully insulated with styrofoam, so the 0°C isotherm could only penetrate from the (upper) soil surface (see Fig. 4.4.1).

The temperature was measured with thermocouples, which were installed at different heights in all columns. The temperature gradient over the frozen fringe was calculated following the procedure from section 4.3.1. Considerable differences in temperature gradient were found: columns situated in the corners of the environmental chamber had higher temperature gradients, than ones in the centre of the chamber, due to differences in air circulation [Perfect et al., 1990b].

The height of the upper soil surface was measured at five different places, from the edge to the centre of the column. These heights were averaged, from which the average heave was calculated.

Quasi steady state was assumed two days after the start of the freezing experiment, because  $\partial T / \partial t \leq 0.1$  K/day. The segregation potential requires quasi steady state, so the average heave rate is calculated for  $t \geq 2$  days. Also the temperature gradient is averaged over this period. Using the segregation potential theory (see section 2.3) it is assumed that the heave rate is a linear function of the temperature gradient over the frozen fringe. So first regression was performed according to eq (4.3.3) between those two parameters. In spite of a poor coefficient of determination ( $r^2 = 0.41$ ), a positive relation between the heave rate and the temperature gradient was found.

Because it is expected that the added solutes with concentration  $SC$  impede the heave rate we extend the segregation potential relation (4.3.3) as follows:

$$dh_{sec}/dt = A - B \times \text{grad}(T)_{ff} (1 + D \times SC) \quad (4.5.1)$$

with  $A$ ,  $B$  and  $D$  the regression coefficients.

With this model (eq 4.5.1) the measuring points can be described better: now  $r^2 = 0.66$ . Intercept  $A$  was not significantly different from 0. The regression coefficient  $B$  can be seen as the segregation potential (actually  $B = SP \times \rho_w / \rho_i$ ) at zero solute concentration:  $B = 2.8 \times 10^{-11} \text{ m}^2/\text{Ks}$ . The influence of the solution is represented with:  $D = -0.15 \text{ m}^3/\text{kg}$  ( $1 \text{ m}^3/\text{kg} = 1 \text{ l/g}$ ).  $D$  is negative because higher solute concentrations impede the heave rate.

In Fig. 4.5.1 the model heave rate, as represented with eq (4.5.1), is presented as a function of the measured heave rate. In this figure it can be seen that the higher solute concentrations results in general in lower heave rates than the lowest solute concentration.

From the measurements it follows that the heave rates of repacked Guelph loam with added solute concentrations can be explained with the segregation potential concept. The negative influence of added solute concentrations agrees well with the results of other studies [Cary, 1987 and Chamberlain, 1983]. Thus even in these special circumstances the SP concept results in reliable relations.

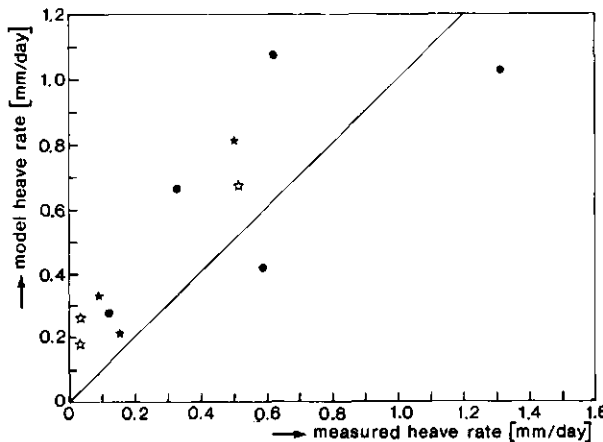


Fig. 4.5.1 Model heave rate as a function of average heave rate under quasi steady state conditions for 12 columns Guelph silt loam. With  $\text{CaCl}_2$  concentration of (●) 1 g/l, (\*) 2 g/l and (△) 4 g/l.

## 5 CONCLUSIONS AND FINAL DISCUSSION

In this section the most important conclusions of the present research have been collected, and compared with existing literature. The conclusions refer to our measuring methods as well as to the models developed to describe the transport processes in freezing porous media. The chapter ends up with some practical recommendations.

### 5.1 General discussion

An important measuring method to obtain the liquid water content in porous media is the determination of the *dielectric constant* with use of time-domain reflectometry. This method has been outlined in section 2.2. The dielectric constant  $\epsilon$  is a complex property and thus consists of a real and an imaginary part. From eq (2.2.6) it follows that the imaginary part  $\epsilon''=G/\omega C_0$ , with  $\omega$  the angular frequency of the electromagnetic wave and  $G$  and  $C_0$  the conductance and capacitance of the transmission line, respectively. In the twin article of Yanuka et al. [1988] and Topp et al. [1988] it has been argued that the measured  $\epsilon''$  is larger than predicted with the above equation, due to extra energy losses (see section 3.2). To count for the extra energy loss Topp et al. [1988] introduced the  $\epsilon_y$  parameter:  $\epsilon''=\epsilon_y+G/\omega C_0$ . This parameter has been used by these scientists to understand systematic measuring errors in his signal analysis with TDR after one 'round trip'. However, other research [Dalton, 1987 and Heimovaara, 1988] using very different methods did not need an extra parameter  $\epsilon_y$  to describe the measurements. Even in the article concerned itself, where the Giese and Tieman approach is used this extra parameter is not needed. Therefore it is our conclusion that the extra energy losses, which are corrected with the  $\epsilon_y$ -parameter, have to be ascribed to a wrong measuring procedure. The introduction of a special  $\epsilon_y$  parameter is therefore unnecessary.

The application of the *dispersion theory* for the relation between dielectric constant and unfrozen water content in frozen porous media has been described in section 3.3. The dielectric constant of unfrozen water in partially frozen soil appears to be lower than that for free supercooled water at the same tempera-

ture: 65 instead of 88. This can be understood by assuming a partial orientation of water molecules in the immediate vicinity of pore ice (in that case the dipoles are impeded to follow the changing electromagnetic field caused by the TDR method). The partial orientation has been suggested by Parameswaran and Mackay [1983]. They state that an electrical double layer consisting of a few layers of oriented water dipoles is formed at the interface between liquid water and ice. The double layer behaves like a semipermeable membrane, allowing one kind of charge to pass through more easily than the other. This causes selective incorporation of excess charge of one sign in the frozen part and an equal opposite charge in the unfrozen part. This is called the Workman-Reynolds effect and the hence developed potential is called the freezing electric potential. Values of 100 to 1350 mV have been measured under field conditions [Parameswaran and Mackay, 1983 and references therein]. Thus the freezing of water in soils also causes electrical effects.

In soils with a large cation exchange capacity the water dipoles also interact quite strongly with the surface charge of the clay plates. Because in such soils the average distance between water molecules and surface of soil mineral particles even at saturation is relatively small, this should also lower the dielectric constant of the soil water. The reduced  $\epsilon_w$ -value results in a deviation of the  $\epsilon(\theta_w)$ -relation as follows: a lower dielectric constant is measured at a certain water content when a heavy clay is compared with a sandy or silty soil. This agrees with the observations of Topp et al. [1980]. Again the hypothesis of partial orientation of water dipoles agrees with the observed phenomena.

In section 4.4 some effects of the freezing process on the *solute transfer* has been demonstrated experimentally. Time-domain reflectometry can be used to measure the unfrozen water content and bulk electrical conductivity simultaneously under frozen conditions. The *in situ* bulk electrical conductivity,  $\sigma$ , depends on the solute concentration, unfrozen water content and temperature. The temperature effect can be related to the mobility of ions through the viscosity of water. The influence of unfrozen water content on  $\sigma$  is non-linear. This influence can be represented with the third order polynomial, which has been derived with use of the dispersion theory (section 3.3). When measurements

are corrected for the temperature and water content influences, they only depend on the solute concentration. Following this approach the solute concentration can be monitored with use of TDR in frozen soils. In the measurements performed in freezing Guelph loam it is possible to identify increases in  $\sigma$  associated with increases in solute concentration. The increases in  $\sigma$  were identified as enriched solute peaks, which moved downwards ahead of the 0°C isotherm.

When heat flow in porous media is evaluated, often the *thermal conductivity* is estimated. In frozen unsaturated soils this quantity can not be applied unambiguously: also the mutual configuration of the components might be important (see Fig. 4.1.5). At the same water content for one packing of silver sand different values for the thermal conductivity have been measured during different freezing cycles. The only possible difference in the soil-air-water-ice mixture between the different freezing cycles is the configuration of the different components. Especially the geometrical shape in which the liquid and solid water constituents are present might be different. This influences the path through which heat is conducted through the mixture. Thus the thermal conductivity in unsaturated sand depends on the way the different components are configurated.

In saturated soils the influence of the freezing process on thermal conductivity  $\lambda$  is also very complex. Apart from the effects mentioned above for the unsaturated soil, we have to deal with the following.

Firstly, the unfrozen water content decreases with decreasing (subzero) temperature  $T$ . Because the thermal conductivity of ice is larger than that of liquid water this results in an underlying negative  $\lambda(T)$ -relation.

Secondly, an increase in unfrozen water content causes an increase in hydraulic conductivity. Thus, the apparent thermal conductivity [Kay et al., 1981] will exhibit a positive relation with temperature. This effect can be quite strong close to 0°C, since the hydraulic conductivity increases exponentially with unfrozen water content. The above two relations tend to compensate one another. However, when a particular material is analyzed, always one of the two effects appears to be dominant. In our experiments the first effect was stronger for crushed concrete and sandy loam, while the second effect was most pronounced in light clay.

The slope of the measured  $\lambda(T)$ -relation showed a positive correlation with the mass fraction of particles smaller than  $125 \mu\text{m}$ , indicating the finer the material, the larger the hydraulic conductivity effect.

*Thirdly*, a large increase in thermal conductivity was observed close to the zero degree isotherm. This represents a systematic measuring error due to the presence of frozen and unfrozen soil within the probe sampling volume. This condition violates the assumption of an isotropic and homogeneous medium. Heat that is dissipated by the probe during the measurement will cause some ice to melt at the freezing front. This means there is less energy available for the temperature rise of the probe and surrounding medium. Thus, the presence of the freezing front will cause an apparent increase in the measured value of  $\lambda$ . The discontinuity in liquid water content at the freezing front will be greatest in coarse materials. Therefore, it is to be expected that the increase in thermal conductivity due to the systematic measuring error will be greatest in these materials. This increase in  $\lambda$  cannot be explained by an increase in hydraulic conductivity, since that effect is most pronounced in fine soils.

*Finally*, the presence of ice increases the thermal conductivity of the soil compared to the unfrozen state. When a saturated soil freezes and the ice pressure is too small to generate ice lenses, some water will leave the frozen zone, because the specific volume of ice is larger than that of liquid water. This water expulsion often takes place when the freezing front is rapidly penetrating the soil [Konrad, 1987]. In this case the soil matrix remains unchanged and thus the thermal contact between the soil particles remains constant. However, when ice lenses are present, the magnitude of this increase is offset by the amount of ice segregation.

The first reason for this offset is that now the thermal contact between the soil mineral particles has been decreased. The second reason is that ice lensing decreases the volume fraction of soil mineral particles. Because the thermal conductivity of mineral material is higher than that of ice, ice segregation will lower the thermal conductivity of the frozen soil compared to the case where ice exists only in the pores. In our experiments a linear relationship was found between the segregated ice content and the difference in the thermal conductivity between the frozen zone and the unfrozen soil.

The *latent heat*, that is released when the pore water freezes *in situ*, can be calculated in two different ways. One way uses the penetration rate of the frost front (calculated from the temperature distribution), while the other way uses the rate of change of (directly measured with TDR) liquid water content. When these two series of calculations are compared, it can be seen that the frost front penetrates faster than the corresponding rate of change in unfrozen (liquid) water content.

Later in the experiments the unfrozen water content still decreases, while the temperature remains constant. From this, a time delay in the forming of pore ice can be concluded. The observed delay is strongest for river foreland clay. This time delay might be the time required for ice nucleation to occur. The ice front might take some time to penetrate through the soil pores. In river foreland clay, which has the largest clay fraction, and therefore the largest amount of very small pores, the expected time delay is largest. This is in agreement with our observations (section 4.2.3). A possible description of the delay on a microscopic scale might be given with use of the above mentioned orientation of the water dipoles. Because in clay all water dipoles are already more or less oriented to the electric field of the soil mineral surface, more energy and time is needed to reorientate the water molecules in order to fit in the ice crystals.

Using a simplified Neuman solution, it can be demonstrated analytically that, as a first approximation, the temperature at a certain fixed position in a freezing soil relates to  $t^{-\frac{1}{2}}$ . Also the conductive heat flow and the heat flow, related to the penetration of the frost front, show this kind of time dependency. This has been confirmed experimentally (see Table 4.2.8 and 4.2.9). However, the heat flow related with a change in unfrozen water content and the heat flow related with heave do not show such a clear time dependency. The agreement with the  $t^{-\frac{1}{2}}$ -relation of the former heat flow is worst for river foreland clay. This supports the earlier conclusion, that the ice front penetrates slower into smaller pores.

As long as the frost front continues to penetrate the sample, only small ice lenses are formed, and a large part of the total heave consists of the volume expansion of the *in situ* freezing of pore water. A period in which the 0°C

isotherm is stationary follows, during which a major ice lens grows. The growing rate of this major ice lens decreases during the test. From our observations it follows that the growth of ice lenses can not be described with a  $t^{-\frac{1}{2}}$ -relation. This is not surprising, because one of the assumptions of the simplified Neuman solution is the absence of heave. The maximum heave rate (as a function of time) can also be explained as a time delay: this maximum in heave rate occurs later than the maximum in the conductive heat flow.

The retardation of the freezing of water can also be treated as a hysteresis effect: the freezing takes place at a temperature that differs from the equilibrium temperature. Since hysteresis is a non linear process, it might be interesting to analyse the freezing of water in porous media from this point of view. However, the description and application of these non linear processes is a very special scientific area that was not considered in this thesis.

In section 4.3 the *moisture transport* has been analysed according to the segregation potential (SP) concept: i.e. the heave rate is a function of the temperature gradient in the frozen fringe. This concept can explain the measured heave rates quite well, when the six materials are analysed separately. However, for river foreland clay and crushed concrete a minimum temperature gradient has been observed, where the heaving process starts. This is in disagreement with the original model of Konrad and Morgenstern [1980], who found that the heave rate is directly proportional to the temperature gradient over the frozen fringe. With use of the theory in section 2.3 (eq 2.3.12) it can be shown that this temperature gradient represents a pressure gradient. This pressure gradient is probably required to create a plane, in which the ice lens can be formed. Furthermore it has been described in section 2.3 that the ice pressure is larger than the overburden pressure, when a new ice lens starts to grow. Also Nixon [1988], starting from the work of Miller [1978], concludes that an excess pressure is needed to initiate a new ice lens. When all materials are taken together, it seems that the minimum pressure depends on the Cation Exchange Capacity (CEC). This can be understood by assuming that a higher CEC results into a stronger electrical force field between the soil particles. Thus, at higher CEC-values more energy, or a higher excess pressure, is needed to initiate a new ice lens.

From the evaluation of the heat balance equation (2.3.22), it can be concluded that for crushed concrete and probably also for Achterhoeks sandy loam more energy is involved in the formation of ice lenses, than just the latent heat. For instance some energy might be demanded to break the soil structure in order to create space for ice lenses. (The effect is strongest for crushed concrete, which has the largest CEC-value). Also Perfect et al. [1991] suggest that stresses in the soil matrix must be included in the equation for energy dissipation. The direct driving force for soil movement (heave) would be a gradient in total pressure, with the transport coefficient being equivalent to a Newtonian friction relation. Ladanyi and Shen [1989] mention in their review article the evaluation of internal stresses as a criterion for the start of frost heaving.

To obtain an explanation of the water transport in the frozen fringe we first studied the process on a microscopic scale. From this we learned that the moisture transport must be related with unfrozen water content and/or the specific surface or surface charge density. Thus, the material dependency of the segregation potential has been studied. Multiple dependency of SP on material properties results into a much better model for the measured heave rate. The following three material properties influence the segregation potential for our selection of materials.

*Firstly*, fines fraction  $\Phi_{125}$ , has a positive relation with the heave rate. The positive relation can be understood by knowing that the outside specific surface area of a packing of soil particles is inversely proportional to the particle size. The larger the outside specific surface, the more water remains unfrozen in the frozen fringe and the easier the water transport in this area. The positive relation is in agreement with many other results in the field of frost heave research [e.g. Jones and Lomas, 1983; Nixon, 1988; and Jessberger and Jagow, 1989].

*Secondly*, clay fraction  $\Phi_2$  influences the heave rate negatively. In materials with a high clay content it is not the permeability of the frozen fringe, which controls the moisture flow: the low permeability of the unfrozen soil is a controlling factor as well [Knutsson et al., 1985]. Thus, the influence of the clay content to the heave rate is partly direct to the frozen fringe (and to SP) and partly to the unfrozen layers.

And *thirdly* specific surface area  $S$  influences the heave rate positively. This is in agreement with the research of Ratkje et al. [1982]. They calculated hydraulic conductivitie  $k$  of frozen soils with help of the thermodynamics of the irreversible processes for a clay and a silt. They related this property to the specific surface area  $S$ : higher values of  $k$  are correlating with higher values of  $S$ .

In the last two decades of frost research in porous media two *major concepts* have been developed to understand the observed phenomena: the rigid ice concept of Miller [1978] and the segregation concept of Konrad and Morgenstern [1980]. The latter concept formed the basis of the theory of the present thesis and has been discussed quite extensively. So we have to explain why this concept has been chosen and not the rigid ice concept. First of all we must stress that Miller developed earlier two important concepts which are the basis of any modern frost heave research: the frozen fringe and the secondary heave. These two concepts are needed to understand that ice lenses grow at temperatures below  $0^{\circ}\text{C}$ .

However, from here the two earlier mentioned concepts start to deviate. Miller [1978] assumes that pore ice is rigid (i.e. acts as one body) but not immobile. Movement of the ice phase with respect to the soil matrix occurs as a result of locally melting of ice, movement of liquid water, and subsequent refreezing (regelation). Thus, the ice body (pore ice plus ice lens) moves uniformly. Next a certain stress partition between the different constituents is assumed in order to calculate the stresses. And from there the location of a new ice lens can be predicted. However, we find the existance of the rigid ice body less attractive than the direct flow of liquid water towards the ice lens as is suggested with the segregation potential (SP) concept. The regelation proces complicates the way the water transport takes place and a model has to be as simple as possible. However, the SP concept is less clear about the stresses existing during frost heave. Because of this omission we have extended the SP concept with the minimum pressure at which heave starts and assume that this pressure is needed to create room for the new ice lens (as is suggested by Miller [1978]).

In general, the major objection against the SP concept is its dicontinuous character: when only one dimension is considered the heave rate is increasing

and decreasing with every newly formed ice lens. However, when three dimensions are considered it is very likely that several ice lenses are growing at different heights, different temperatures and different rates at the same time. The three dimensional character will average the different heave rates and the measured heave rate will be this averaged, smoothed value. This agrees with the rather constant observed heave rates, which are mentioned by all scientists.

## 5.2 Recommandations in connection with frost in porous media

The research presented in this thesis was performed from a theoretical point of view. So direct applications were hardly analysed. However, some of our conclusions can be related with the applications of frost in porous media as mentioned in chapter 1.

In the field of agriculture an important phenomenon caused by frost penetration is the improvement of the *soil structure*. According to Perfect et al. [1990a] the soil structural stability depends strongly on the water content. For Guelph Loam (for definition see section 4.4) in the moisture content range of 0.08 to 0.27 kg/kg this can be seen as a reversible process: when the soil becomes wetter, the aggregate stability decreases, and when the soil dries it regaines its stability again. This conclusion was drawn on the basis of field experiments in South Ontario (Canada). When the water content influence on the soil structure stability is removed and the data are analysed over time, it can be seen that the structure improves during the winter. The following process is suggested [Perfect et al., 1990b]: small ice lenses are formed during winter frost periods. Soil water is drawn towards these lenses from soil in between. When also water from the diffuse double layers is migrating, the distance between the primary soil particles might decrease and cementing agents (e.g. organic material) might increase in concentration.

These two possible processes result in an easier cementing of primary soil particles into aggregates. To enhance frost penetration farmers often plow their fields in the fall. This treatment is only favorable for frost susceptible soils, where the soil water will be concentrated in (micro) ice lenses. The present research shows that the soil must have a large fine fraction and/or specific surface area. A high clay content decreases frost heave (section 4.3) by impeding water uptake from the ground water table.

This phenomenon is not disadvantageous for the increased soil structural stability. In contrary, the soil aggregates are dried out more easily. So probably soils with a high clay content gain a maximum increase in structural stability during winter time when they are plowed in the fall.

In constructing tunnels and mine shafts the walls are sometimes strengthened by *artificial ground freezing* to prevent collapses. In section 4.2 it has been concluded that during the freezing process (transient conditions) the water in the soil pores freezes later than expected. This delay occurs especially in loam and clay. Therefore when a new frozen wall is made in this kind of material, it is safer to start the freezing at a lower temperature. After a week the temperature can be reduced to its originally calculated value. However, the frozen reinforcements are usually made in gravelly or sandy soil [Harris, 1988 and Klein, 1988] and in these soils the delay in the freezing process is hardly present.

In paralysing *soil pollution* by artificial ground freezing the same physical processes occur as described in the previous paragraph. So one has to freeze the soil at lower temperatures during the first days than in the steady state condition. When the soil is slowly frozen downwards, solute redistribution may take place (see section 4.4). If a pollutant is solved in the soil water, this pollutant can also be transported by the freezing process. If this process has to be prevented, rapid freezing must take place. However, the redistribution process might also be developed as a new technique to clean contaminated soils. In that case the freezing front must advance as slow as possible.

The last application mentioned in chapter 1 is the *prevention of frost damage* to road constructions. This damage occurs when secondary heave takes place in the road foundation. So the use of materials which are not frost susceptible is preferred: i.e. coarse materials, materials with a low specific surface area or, in contrast, materials with an extreme high clay content. The heave rate also depends on the temperature gradient. The heave can remain even zero if at the existing temperature gradient the pressure gradient is insufficient to built up the minimum pressure required to create room for the new ice lens and to lift the overburden. Thus a more frost susceptible material can still be used on a location where the expected temperature gradient is small; i.e. deeper in the road construction.

## 6 SUMMARY

Seasonal ground freezing may cause damage to roads, buildings and other constructions. Frost also influences the soil properties that are relevant to agriculture. To study ground freezing in some detail it is necessary to investigate the transport phenomena that occur during soil freezing together with the accompanying physical processes. From this context we formulated the physical aim of the present thesis (see chapter 1): to investigate processes and parameters associated with heat and mass transfer in frozen porous media both on a theoretical and empirical basis. We start then the actual research with a sample frost heave experiment which shows that a microscopic model is needed to understand what is macroscopically happening.

In chapter 2 all existing relevant models, equations and definitions are reviewed. It starts with the definition of the soil electrochemical and physical properties needed such as: particle size distribution, specific surface area, cation exchange capacity, zeta potential, water retention, hydraulic conductivity and thermal conductivity.

Next the physical principles of time-domain reflectometry are explained. This method is used to measure water content and bulk electrical conductivity simultaneously. The chapter finishes with the derivation of the heat and mass transfer equations.

In frozen porous media the most important flux is the water flux which causes frost heave (caused by the growth of ice lenses). Three major theories have contributed to understand the frost heave. Firstly Miller [1972] demonstrated that ice lenses grow at temperatures below 0°C and in that connection he developed the concept of the frozen fringe. Secondly, Kay and Groenevelt [1974] provided with use of thermodynamics a theoretical background for suction of liquid water towards the ice lens. And thirdly, Konrad and Morgenstern [1980] used this theory in their segregation potential concept to link the heave rate to a macroscopic temperature gradient. Since the heat flux also depends on the temperature gradient, both heat and moisture transfer in frozen porous media are mainly governed by the macroscopic temperature gradient.

In chapter 3 it is described how some existing measuring methods needed to be improved, in order to obtain the measurements required.

Firstly, an improved model has been developed for the measurement of *thermal conductivity* with use of the non steady state probe method (see section 3.1). The modified Jaeger model [Van Haneghem, 1981] provided the physical basis to describe the temperature response of a needle shaped probe in a medium. With the method in principle three thermal parameters can be obtained simultaneously: thermal conductivity, heat capacity and contact resistance. If a second order time correction is added, also the steeper part of the temperature response is described accurately. When this part is included less measuring time is required, and a smaller heat dissipation rate is needed during the measurement leading to a substantially improved accuracy.

However, in frozen soils (in non equilibrium conditions) the measuring conditions do not allow simultaneous determinations of the three thermal parameters (see also section 4.1).

The second improved measuring method is the measurement of *bulk electrical conductivity* with use of time-domain reflectometry (TDR, see section 3.2).

In determining the bulk electrical conductivity with TDR the amplitude of the reflection must be measured. Impedance mismatches of the measuring system may cause errors in determining this amplitude. These impedance mismatches can be corrected by comparing the reflection of an electromagnetic pulse in soil with a reference reflection in vacuum or air. The method was calibrated in water with different  $\text{CaCl}_2$  concentrations. In two different, saturated soils the effective electrical conductivity also showed a clear relation with the amount of ions.

The third improvement is the use of the *dispersion theory* in the description of relations between water content and bulk electrical conductivity or dielectric constant (see section 3.3).

At low water contents soil water is to be found in thin films of water around the soil particles. For the dielectric constant, this geometry can be modeled with Maxwell's equations for the dispersive behaviour of two materials arranged in parallel plates [Maxwell, 1873].

At water contents close to one, water and soil behave like an ideal mixture. The behaviour at these two extremes can be adequately summarized into a third order power series in water content (eq 3.3.19). The dielectric constant of unfrozen water in partially frozen soil appears to be lower than that for supercooled

water at the same temperature. Using a different method Oliphant [1985] came to the same conclusion.

The decrease in the dielectric constant of water is probably caused by partial orientation of water molecules in the immediate vicinity of pore ice (the Workman-Reynolds effect [Parameswaran and Mackay, 1983]). The electrical conductivity at low water contents can also be modeled with water and soil in parallel plate configuration. At saturation, water and soil again behave like an ideal mixture. These two extremes can be interpolated with a third order polynomial using only two degrees of freedom. The two corresponding regression parameters allow physical interpretation.

The *experimental set-up* to monitor the heat and mass transfer through a freezing porous medium has been described in section 3.4. Also the measured values of the properties of porous media used are discussed here. In soils some properties strongly depend on each other: e.g. clay content and specific surface area or cation exchange capacity. Because in our selection of materials also other minerals than the usual soil minerals are present, the media properties are mostly independent of each other (only clay, silt and fines fraction are strongly interrelated).

In section 4.1 *thermal conductivity and heat transfer measurements* are presented in two freezing unsaturated sands. Not only temperature and volume fractions of the different components influenced the thermal conductivity, but also the mutual configuration of these components.

In section 4.2 the thermal parameters and heat flows of saturated frozen porous media are evaluated.

*Thermal conductivity measurements* were made using the nonsteady state probe method in six different frozen porous media subjected to macroscopic temperature gradient. The results indicate four separate effects on the thermal conductivity temperature relation,  $\lambda_f(T)$ .

Firstly, unfrozen water content decreases with decreasing subzero temperature, resulting in a negative  $\lambda_f(T)$ -relation.

Secondly, convective transport of heat due to liquid water flow will cause an apparent positive  $\lambda_f(T)$ -relation.

Thirdly, a large increase in thermal conductivity occurs close to the freezing front, due to non-homogeneous sampling conditions. Finally, ice segregation reduces  $\lambda_f$  compared to the case where ice exists only in pores.

The *heat capacity* is strongly influenced by the latent heat of melting. This effect can be incorporated with use of the extra term into the apparent heat capacity (eq 2.3.16). With use of empirically determined unfrozen water-temperature-relations, the extra term can be calculated (eq 4.2.5), resulting in values, which are an order of magnitude higher than the heat capacity itself. This is in agreement with directly measured heat capacities in literature [e.g. Williams, 1973].

The *latent heat*, that is released when the pore water freezes *in situ*, has been calculated directly from the change in unfrozen water content (measured with TDR). It has also been calculated from the penetration rate of the frost front. From these calculations it follows that the frost front penetrates faster than the corresponding rate of change in unfrozen (liquid) water content. A time delay in the forming of pore ice can be concluded. This delay is strongest for river foreland clay. Also in the formation of ice lenses a time delay has been observed.

In section 4.3 the *moisture transport* in the form of frost heave has been presented. The segregation potential (SP) concept has been used to describe the observed heave rates: the temperature gradient over the frozen fringe is associated with a pressure gradient which causes the moisture transport to the warmest ice lens. For four of the analysed materials this concept could be followed straightforward. The segregation potential appears to have a positive relation with fines fraction and specific surface area, while a negative relation with clay content has been observed. However, for crushed concrete and river foreland clay a minimum temperature gradient has been observed at which heave starts. This minimum temperature gradient has a positive relation with the cation exchange capacity.

In section 4.4 some effects of the freezing process on the *solute transfer* has been demonstrated experimentally. Time-domain reflectometry can be used to

measure the unfrozen water content and bulk electrical conductivity simultaneously under frozen conditions.

The *in situ* bulk electrical conductivity,  $\sigma$ , depends on the solute concentration, unfrozen water content and temperature. The temperature effects the viscosity of water, which in its turn can be related to the mobility of ions. The influence of unfrozen water content on  $\sigma$  is non-linear. Redistribution of solutes during soil freezing can also be monitored using the  $\sigma$  measurement with TDR: it is possible to identify increases in  $\sigma$  associated with solute enrichment. These solute peaks appear to move faster than and ahead of the 0°C isotherm.

The *influence of solutes to the frost heave* has been demonstrated experimentally in section 4.5. When the (added) solute concentration is incorporated into the segregation potential theory, a good model for the heave rate can be built. The negative influence of added solutes agrees with the results of other scientists [Cary, 1987 and Chamberlain, 1983].

In chapter 5 the major conclusions of this thesis are discussed from a more general point of view. In particular the rigid ice concept of Miller [1978] and the segregation potential concept of Konrad and Morgenstern [1980] are discussed in mutual relation. From our results an effort was made to come to a synthesis of both concepts. The chapter finishes with some applications in connection with the improvement of soil structure, frost heave and artificial ground freezing.

## 7 SAMENVATTING

### Massa- en warmtetransport in bevroren poreuze media

Vorst kan 's winters schade veroorzaken aan wegen, gebouwen en andere constructies. Vorst beïnvloedt ook eigenschappen van grond, die belangrijk zijn voor de landbouw. Om iets meer over vorstverschijnselen in de grond te kunnen zeggen, is het noodzakelijk de daarbij behorende transportverschijnselen en andere fysische processen te bestuderen. Grond wordt in dit proefschrift gezien als een voorbeeld van een poreus medium.

Vanuit deze context zijn we in Hoofdstuk 1 tot de volgende fysische doelstelling van het proefschrift gekomen: het empirisch en theoretisch bepalen van de processen en grootheden, die een rol spelen bij het massa- en warmtetransport in bevroren poreuze media.

Het onderzoek begint met een voorbeeld-experiment voor vorstheffing, waarin wordt aangetoond dat een model op microscopische schaal noodzakelijk is, om te begrijpen wat er macroscopisch gebeurt.

In hoofdstuk 2 wordt een overzicht gegeven van alle huidige modellen, vergelijkingen en definities, die nodig zijn voor dit onderzoek.

Het begint met de definitie van enkele bodemfysische en elektrochemische grootheden als: korrelgrootteverdeling, specifiek oppervlak, kationenuitwisselingscapaciteit, zeta potentiaal, vochtkarakteristiek, waterdoorlatendheid en warmtegeleiding.

Vervolgens worden de fysische principes van tijddomeinreflectometrie uiteengezet. Deze methode wordt gebruikt om het volumetrisch watergehalte en de elektrische geleidendheid in de grond te meten.

Het hoofdstuk eindigt met de afleiding van de vergelijkingen voor massa- en warmtetransport. De belangrijkste flux in bevroren poreuze media is de water flux die vorstheffing veroorzaakt (door het groeien van ijslenzen). Drie belangrijke theorieën hebben bijgedragen aan de begripsvorming van die heffing. Ten eerste heeft Miller [1972] aangetoond dat ijslenzen groeien bij temperaturen onder 0°C. Hiervoor heeft hij het 'frozen fringe' (letterlijk betekent dit "bevroren franje"; in ons verband is het duidelijker om te spreken van "bevroren overgangszone") concept ontwikkeld. Ten tweede hebben Kay en Groeneveld [1974]

met behulp van de thermodynamica een theoretische onderbouwing gegeven voor het transport van vloeibaar water naar de ijslens toe. En ten derde hebben Konrad en Morgenstern [1980] deze onderbouwing gebruikt voor het concept van de scheidingspotentiaal. Dit concept koppelt de heffingssnelheid aan een macroscopische temperatuurgradiënt. Omdat de warmteflux ook voornamelijk van de temperatuurgradiënt afhangt, is deze laatste grootheid bepalend voor zowel het massa- als het warmtetransport in bevroren poreuze media.

Om de benodigde metingen naar behoren te kunnen verrichten, dienden eerst enkele meetmethoden te worden verbeterd. De wijze waarop wordt omschreven in Hoofdstuk 3. Ten eerste is een verbeterd model ontwikkeld om de *warmtegeleidingscoëfficiënt* te bepalen m.b.v. de niet-stationaire naaldmethode (paragraaf 3.1). Het model is gebaseerd op het gemodificeerde Jaegermodel [Van Haneghem, 1981]. Hierin wordt de temperatuur 'responsie' (reactie) van een meetnaald in het te onderzoeken medium op een fysisch-mathematische manier beschreven.

Met de methode kunnen in principe drie thermische grootheden simultaan verkregen worden: de warmtegeleidingscoëfficiënt, de warmtecapaciteit en de contactweerstand. Als hieraan een tweede-orde tijdcorrectie wordt toegevoegd, wordt het meer steile deel van de 'responsie' ook nauwkeurig beschreven. Met dit nieuwe model kan de meting met een geringere vermogensafgifte dan voorheen worden gerealiseerd, kan met een kortere meettijd worden volstaan en wordt de nauwkeurigheid vergroot.

De meetomstandigheden in bevriezende grond (waar de toestand ver van het thermodynamische evenwicht af is) staan echter de simultane bepaling van de drie grootheden in de weg (zie ook paragraaf 4.1).

De tweede verbeterde meetmethode is de bepaling van de *elektrische geleidendheid* m.b.v. tijddomeinreflectometrie (TDR, zie paragraaf 3.2). Bij deze bepaling moet de amplitude van het gereflecteerde signaal worden gemeten. Impedantie-overgangen in het meetsysteem veroorzaken afwijkingen in de amplitude. Voor de impedantie-overgangen kan worden gecorrigeerd als het gereflecteerde signaal in grond wordt vergeleken met een referentiesignaal in lucht of vacuüm. De nieuwe methode werd geïjkt in water met verschillende  $\text{CaCl}_2$ -oplossingen.

Ook in twee verschillende, met (zout) water verzadigde, grondsoorten was er een duidelijke relatie tussen de gemeten elektrische geleidendheid en de zoutconcentratie.

De derde verbetering is het gebruik van de *dispersietheorie*. Hiermee kan de relatie tussen watergehalte enerzijds en elektrische geleidbaarheid of diëlektrische constante anderzijds beschreven worden (paragraaf 3.3). Bij lage watergehaltes bevindt het water in de grond zich als een dunne schil rondom de bodemdeeltjes. Voor de diëlektrische constante kan deze geometrie beschreven worden met de relaties van Maxwell [1873] voor het geval van dispersie in twee materialen, gerangschikt in parallelle platen. Bij volumetrische watergehaltes van bijna één (bijna 100% water) gedragen grond en water zich als een ideaal mengsel. Het gedrag tussen deze twee extremen kan adequaat worden samengevat tot een derde-orde relatie in het watergehalte (vergelijking 3.3.19).

De diëlektrische constante van onbevroren water in gedeeltelijk bevroren grond blijkt lager te zijn dan de waarde van onderkoeld water van dezelfde temperatuur. Oliphant [1985] kwam met gebruik van een andere methode tot dezelfde conclusie. De verminderde waarde van de diëlektrische constante van water wordt waarschijnlijk veroorzaakt door de gedeeltelijke ordening van de waterdipolen, als gevolg van de onmiddellijke nabijheid van poriën (het Workman-Reynolds-effect [Parameswaran en Mackay, 1983]).

De elektrische geleidbaarheid bij lage watergehalten kan ook met het parallelle platenmodel voor water en grond weergegeven worden. En bij verzadiging gedragen water en grond zich weer als een ideaal mengsel. Deze twee extremen kunnen geïnterpoleerd worden met een derde-orde polynoom met maar twee vrijheidsgraden. De beide regressieparameters kunnen fysisch geïnterpreteerd worden.

De *laboratoriummeetopstelling* om het massa- en warmtetransport in het bevriezen-de poreuze medium te bestuderen wordt beschreven in paragraaf 3.4. Ook de gemeten eigenschappen van de onderzochte poreuze media worden hier behandeld. Sommige eigenschappen zijn sterk onderling afhankelijk als alleen naar grond wordt gekeken: b.v. kleigehalte en specifiek oppervlak of kationenuitwisselingscapaciteit en kleigehalte.

Maar omdat in onze selectie van materialen ook andere bestanddelen aanwezig zijn, zijn de eigenschappen meestal onafhankelijk van elkaar (alleen de klei-, leem- en fijnzandfractie zijn sterk aan elkaar gekoppeld).

De *warmtegeleidings- en warmtefluxmetingen* in twee bevroren onverzadigde zandsoorten worden beschreven in paragraaf 4.1. De warmtegeleidingscoëfficiënten

waren niet alleen afhankelijk van de temperatuur en van de volumefracties van de verschillende componenten, maar ook van de onderlinge rangschikking van deze componenten. In paragraaf 4.2 worden de thermische parameters en warmtefluxen in verzadigde, bevroren poreuze media behandeld.

In zes verschillende bevroren poreuze media werden *warmtegeleidingsmetingen* verricht met de niet-stationaire naaldmethode. Over de media werd een temperatuurgradiënt aangelegd. Uit de meetresultaten blijken er vier verschillende effecten op de relatie tussen warmtegeleidingscoëfficiënt en temperatuur,  $\lambda_f(T)$ , te bestaan.

Ten eerst neemt het onbevroren watergehalte toe bij toenemende temperatuur, wat een negatieve  $\lambda_f(T)$ -relatie tot gevolg heeft.

Ten tweede veroorzaakt het convectieve warmtetransport, gekoppeld aan het transport van vloeibaar water, een positieve schijnbare  $\lambda_f(T)$ -relatie.

Ten derde veroorzaken de inhomogene meetomstandigheden in de buurt van het vorstfront een forse toename van de gemeten  $\lambda_f$ -waarde. En tenslotte veroorzaken ijslenzen een vermindering van de  $\lambda_f$ -waarde ten opzichte van het geval waar slechts ijs in de poriën aanwezig is.

De *warmtecapaciteit* wordt sterk beïnvloed door de latente warmte behorende bij de ijs-water overgang. Dit effect kan met behulp van een extra term in de schijnbare warmtecapaciteit opgenomen worden (vgl. 2.3.16). Vervolgens kan met de experimenteel verkregen relaties tussen temperatuur en onbevroren watergehalte de extra term berekend worden. Dit resulteert in waarden die een orde van grootte hoger kunnen zijn dan de warmtecapaciteit zelf. Dit komt goed overeen met direct gemeten schijnbare warmtecapaciteiten uit de literatuur [b.v. Williams, 1973].

De *latente warmte*, die vrijkomt als het poriënwater in situ bevriest, is rechtstreeks berekend uit de verandering in onbevroren watergehalte (gemeten met TDR). Daarnaast is de latente warmte ook berekend uit de indring-snelheid van het vorstfront. Uit deze berekeningen volgt dat het vorstfront sneller indringt dan de bijbehorende verandering van onbevroren watergehalte doet vermoeden. Kennelijk treedt er een vertraging op in de vorming van het poriën-ijs. Deze vertraging is het sterkst voor Uiterwaardenklei. Ook in de vorming van ijslenzen is een tijdvertraging waargenomen.

Het *watertransport*, zoals dat optreedt in de vorm van vorstheffing, is in paragraaf 4.3 beschreven. De waargenomen heffingssnelheden zijn verklaard m.b.v. het scheidingspotentiaal-concept (SP). Dit houdt in dat de temperatuurgradiënt over de 'frozen fringe' wordt geassocieerd met de aandrijvende drukgradiënt, die het vloeibare water naar de 'warmste' ijslens doet stromen.

Voor vier van de bestudeerde materialen kon dit concept zonder meer worden toegepast. De scheidingspotentiaal blijkt een positieve samenhang te vertonen met de fractie fijn materiaal en met het specifiek oppervlak, terwijl een negatieve samenhang werd waargenomen met de kleifractie. Voor twee andere materialen moest het SP concept uitgebreid worden met een minimum in temperatuurgradiënt, waarbij de heffing begint. Deze minimum temperatuurgradiënt hangt samen met de kationen uitwisselingscapaciteit.

In paragraaf 4.4 worden enkele effecten van de vorst op het *zouttransport* experimenteel aangetoond. Tijddomeinreflectometrie kan toegepast worden in bevroren poreuze media voor zowel het onbevroren watergehalte als de elektrische geleidendheid. De *in situ* gemeten elektrische geleidendheid,  $\sigma$ , hangt af van de zoutconcentratie, het onbevroren-watergehalte en de temperatuur.

De temperatuur beïnvloedt de viscositeit van water, die op zijn beurt de beweeglijkheid van de daarin opgeloste ionen bepaalt. De invloed van het onbevroren watergehalte op  $\sigma$  is niet-lineair. Met TDR is het mogelijk om pieken in  $\sigma$  te detecteren, die duiden op een verhoogde lokale zoutconcentratie. Dit kan alleen veroorzaakt zijn door een zeker zouttransport. De pieken in  $\sigma$  blijken zich voor de 0°C-isotherm uit naar beneden te bewegen.

De *invloed van zouten op de vorstheffing* is experimenteel aangetoond in paragraaf 4.5. De scheidingspotentiaal kan worden gemodificeerd voor de zoutconcentratie en zo kan een model voor de heffingssnelheid worden verkregen.

De negatieve relatie tussen zoutconcentratie en heffingssnelheid komt overeen met de bevindingen van andere onderzoekers [Cary, 1987 en Chamberlain, 1983].

In hoofdstuk 5 worden de voornaamste *conclusies* van dit proefschrift uitgebreid belicht. Vooral het 'rigid ice' (star ijs) concept van Miller [1978] is vergeleken met het scheidingspotentiaalconcept van Konrad en Morgenstern [1980]. Met behulp van onze eigen resultaten is getracht tot een synthese tussen beide modellen te komen.

Het hoofdstuk eindigt met de mogelijke toepassingen van de verkregen resultaten op enkele praktijkomstandigheden, zoals het verbeteren van de bodemstructuur t.g.v. vorst, het kunstmatig bevriezen van poreuze media, en het voorkómen van vorstheffing door een geschikte keuze van materialen.

## 8 REFERENCES

Agricultural Canada Expert Committee on Soil Survey, 1987. The Canadian system of soil classification, 2nd ed., Agr. Can. Publ. 1646, Ottawa, Canada, 164 pp.

Akagawa S., 1988. Experimental study of frozen fringe characteristics, Cold Regions Sci. Techn. 15, pp 209-223

Analog Devices, 1988. Linear Products Databook, Analog Devices Inc., Norwood MA, USA, p 10-7.

Anderson D.M. and Morgenstern N.R., 1973. Physics, chemistry and mechanics of frozen ground. In Permafrost: the north American contribution to the second Int. Conf., Nat. Ac of Sci, Washington D.C., USA, pp. 257-288.

Baker G.C. and Osterkamp T.E., 1988. Salt redistribution during freezing of saline sand columns, Proc. Fifth Int. Symp. on Ground Freezing, Vol. 1, Balkema, Rotterdam NL, pp 29-33.

Baker J.M. and Lascano R.J., 1989. The spatial sensitivity of time-domain reflectometry, Soil Sci. 147, pp 378-383.

Banin A. and Anderson D.M., 1974. Effects of salt concentration changes during freezing on the unfrozen water content of porous materials, Water Resour. Res. 10, pp 124-128.

Bauer L.D., Gardner W.H. and Gardner W.R., 1972. Soil Physics, Wiley, New York NY, USA, 489 pp.

Beck W.J. and Muttzal K.M.K., 1975. Transport Phenomena, Wiley, New York, NY USA, p 106.

Black P.B. and Tice A.R., 1989. Comparison of soil freezing curve and soil water curve data for Windsor sandy loam, Water Resources Res. 25, pp 2205-2210.

Blackwell J.H., 1954. A transient-flow method for the determination of thermal constants of insulating materials in bulk, part 1: theory. J. Appl. Phys. 25, pp 137-144.

Bruijn P.J., Haneghem I.A. van and Schenk J., 1983. An improved nonsteady state probe method for measurements in granular materials, part 1: theory. High Temp.High Press. 15, pp 359-366.

Carslaw H.S. and Jaeger J.C., 1950. Conduction of heat in solids, Clarendon Press, Oxford UK, 386 pp.

Cary J.W. and Mayland H.F., 1972. Salt and water movement in unsaturated frozen soil, Soil Sci. Soc. Am. J. 36, pp 549-555.

Cary J.W., Papendick R.I. and Campbell G.S., 1979. Water and salt movement in unsaturated frozen soil: principles and field observations, *Soil Sci. Soc. Am. J.* 43, pp 3-8.

Cary J.W., 1987. New method for calculating frost heave including solute effects, *Water Resour. Res.* 23, pp 1602-1624.

Chamberlain E.J., 1983. Frost heave of saline soils, *Proc. Fourth Int. Conf. on Permafrost*, Nat. Acad. Press, Washington DC, USA, pp 121-126.

Dahlquist G. and A. Björck, 1986. *Numerical Methods*, Prentice Hall, England Cliffs, NJ USA.

Dalton F.N., Herkelrath W.N., Rawlins D.S. and Rhoades J.D., 1984. Time-domain reflectometry: simultaneous measurement of soil water content and electrical conductivity with a single probe, *Science* 224, pp 988-990.

Dalton F.N. and van Genuchten M.Th., 1986. The time-domain reflectometry for measuring soil water content and salinity, *Geoderma* 38, pp 237-250.

Dalton F.N., 1987. Measurement of soil water content and electrical conductivity using time-domain reflectometry, *Proc. Int. Conf. on measurement of soil and plant status*, Utah State Univ., Vol 1, pp 95-98.

Dasberg S. and Dalton F.N., 1985. Time-domain reflectometry field measurements of soil water content and electrical conductivity, *Soil Sci. Soc. Am. J.* 49, pp 293-297.

Dirksen C. and Miller R.D., 1966. Closed-system freezing of unsaturated soil, *Soil Sci. Soc. of Am. Proc.*, vol. 30, no 2, pp 168-173.

Duquennoi C., Fremond M. and Levy M., 1989. Modelling of thermal soil behaviour, *Proc. Frost in Geotech. Eng.* 2, VTT Symp. 95, Espoo Finland, pp 895-915.

Elrick D.E. and Bowman D.H., 1964. Note on an improved apparatus for soil moisture flow measurements, *Soil Sci. Soc. Am. Proc.*, 28, pp 450-453.

Farouki O.T., 1986. Thermal properties of soils, Series on rock and soil mechanics vol 11, *Trans Tech. Publ.*, Clausthal Zellerfield, FRG.

Fukuda M., 1976. Measurements of thermal conductivity of frozen soils by the thermal probe method. *Low Temp. Sci. Ser. A*, 34, pp 249-252.

Fukuda M. and Jingsheng Z., 1989. Hydraulic conductivity measurements of partially frozen soil by needle probe methods, *Proc. Frost in Geotech. Eng.* 1, VTT symp. 94, Espoo Finland, pp 251-266.

Frivik P.E., 1980. Ground Freezing: Thermal properties, modelling of processes and thermal design, *Proc. Second Int. Sym. Ground Freezing*, Norwegian Inst. of Techn., Trondheim, Norway, pp 354-373.

Giese K. and Tieman R., 1975. Determination of the complex permittivity from thin-sample time-domain reflectometry, improved analysis of the step response waveform, *Adv. in Molecular Relaxation Processes* 7, pp 45-49.

Gray D.M. and Granger R.J., 1986. In situ measurements of moisture and salt movement in freezing soils, *Can. J. Earth Sci.* 23, pp 696-704.

Greacan E.L., 1981. Soil water assessment by the neutron method, *C.S.I.R.O.*, Adelaide, Australia, 140 p.

Gregg S.J. and Sing K.S.W., 1982. *Adsorption, Surface Area and Porosity*, Academic press, London UK.

Groeneveld P.H. and Kay B.D., 1980. Pressure distribution and effective stress in frozen soils, *Proc Second Int. Symp. Ground Freezing*, Norwegian Inst. of Techn., Trondheim, pp 597-610.

Haneghem I.A. van, 1981. Een niet stationaire naaldmethode (warmtegeling, warmtecapaciteit en contactweerstand). PhD-thesis (Dutch), Agr. Un. Wageningen, the Netherlands.

Haneghem I.A. van and Leij F.L., 1985. Thermal properties of moist porous media below 0°C, *Hi. Temp. Hi. Press.*, vol. 17, pp 611-621.

Harris J.S., 1988. State of art: Tunneling using artificial frozen ground, *Proc. Fifth Int. Symp. on Ground Freezing*, Vol. 1, Balkema Rotterdam NL, pp 245-253.

Heimovaara T., Dalton F.N. and Poss J.A., 1988. Time-domain reflectometry, a method for measuring volumetric water content and bulk electrical conductivity of soils. US salinity lab. research report 88, Riverside CA, USA.

Hayhoe H.N. and Balchin D., 1988. Time-domain reflectometry and electrical conductance measurements during seasonal frost, *Cold Regions Sci. and Techn.* 15, pp 195-200.

Holden J.T., Piper D. and Jones R.H., 1985. Some developments of a rigid-ice model of frost heave, *Proc. Fourth Int. Sym. Ground Freezing*, Balkema, Rotterdam NL, pp 93-99.

Horiguchi K., 1979. Effect of the rate of heat removal on the rate of frost heaving, *Engineering Geology* 13, pp 63-71.

Horiguchi K., and Miller R.D., 1980. Experimental studies with frozen soils in an "Ice Sandwich" Permeameter. *Cold Regions Sci. and Techn.* 3, pp 177-184.

Horiguchi K., 1985. Determination of unfrozen water content by DSC, *Proc. Fourth Int. Sym. on Ground Freezing*, Balkema, Rotterdam, NL, pp 33-38.

Horiguchi K., 1986. An Osmotic model for soil freezing, *Cold Regions Science and Technology* 14, pp 13-22.

Hunter R.J., 1981. *Zeta potential in colloid science: principles and applications*, Academic Press, London UK.

ISRIC, 1988. Revised legend of the FAO-UNESCO soil map of the world, ISRIC, Wageningen NL.

Jaeger J.C., 1956. Conduction of heat in an infinite region bounded internally by a circular cylinder of a perfect conductor. *Austr. J. Phys.* 9, pp 167-179.

Jessberger H.L., Jagow R. and Jordan P., 1988. Thermal design of a frozen soil structure for stabilization of the soil on top of two parallel metro tunnels, *Proc. Fifth Int. Symp. Ground Freezing*, Vol. 1, Balkema, Rotterdam NL, pp 349-356.

Jessberger H.L. and Jagow R., 1989. Determination of frost susceptibility of soils, *Proc. Frost in Geotechnical Engineering, VTT Symp.* 94, Espoo Finland, pp 449-569.

Johanson O. and Frivik P.E., 1980. Thermal properties of soils and rock materials, *Proc. Second Int. Sym. Ground Freezing*, Norwegian Inst. of Techn., Trondheim, Norway, pp 427-453.

Jones R.H. and Lomas K.J., 1983. The frost susceptibility of granular materials, *Proc. Fourth Int. Conf. on Permafrost*, Nat. Acad. Press, Washington DC, USA, pp 554-559.

Kadlec R.H., Xiang-Ming Li and G.B. Cotten, 1988. Modeling solute segregation during freezing of peatland waters, *Water Resour. Res.* 24, pp 219-244.

Kay B.D. and Groenevelt P.H., 1974. On the interaction of water and heat transport in frozen and unfrozen soils, *Soil Sci. Soc. Am. Proc.* 38, pp 395-404.

Kay B.D., Fukuda M., Izuta H. and Sheppard M.I., 1981. The importance of water migration in the measurement of the thermal conductivity of unsaturated soils, *Cold Regions Sci. and Technology* 5, pp 95-106.

Kay B.D. and Groenevelt P.H., 1983. The redistribution of solutes in freezing soil: exclusion of solutes, *Proc. Fourth Int. Conf. Proc. on Permafrost*, Nat. Acad. Press, Washington DC, USA, pp 584-588.

Kay B.D. and Perfect E., 1988. State of the art: Heat and mass transfer in freezing soils, *Proc. Fifth Int. Symp. on Ground Freezing*, Vol. 1, Balkema, Rotterdam NL, pp 3-21.

Klein J., 1988. State of art: Engineering design of shafts, Proc. Fifth Int. Symp. on Ground Freezing, Vol. 1, Balkema, Rotterdam NL, pp 235-243.

Klute A. (ed.), 1986. Methods of soil analysis Part 1 Physical and mineralogical methods, Am. Soc. Agron/Soil Sci. Soc. Am., Madison WI, USA, 1188 pp.

Knutsson S., Domaschuk L., and Chandler N., 1985. Analyses of large scale laboratory and in situ frost heave tests, Proc. Fourth Int. Symp. on Ground Freezing, Balkema, Rotterdam NL, pp 65-70.

Konrad J.M. and Morgenstern N.R., 1980. A mechanistic theory of ice lens formation in fine-grained soils, Can. Geotech. J., 17, pp 473-486.

Konrad J.M. and Morgenstern N.R., 1981. The segregation potential of a freezing soil. Can. Geotech. J. 18, pp 482-491.

Konrad J.M. and Morgenstern N.R., 1982. Prediction of frost heave in the laboratory during transient freezing, Can. Geotech. J. 19, pp 250-259.

Konrad J.M. and Morgenstern N.R., 1983. Frost susceptibility of soils in terms of their segregation potential, Proc. Fourth Int. Conf. on Permafrost, Nat. Acad. Press, Washington DC, USA, pp 660-665.

Konrad J.M., 1987. The influence of heat extraction rate in soils, Cold Regions Sci. Techn. 14, pp 129-137.

Koopmans R.W.R. and Miller R.D., 1966. Soil freezing and soil water characteristic curves, Soil Sci. Soc. Am. Proc. 30, pp 680-685.

Koorevaar P., Menelik G and Dirksen C., 1983. Elements of soil physics, Elsevier Amsterdam NL, 228 pp.

Kronik Y.A., 1982. Thermomechanical enthalpy model for ground freezing design, Proc. Third Int. Symp. on Ground Freezing, USA CRREL report 82-16, Hanover NH, USA, pp 167-175.

Lewis R.W and Sze W.K., 1988. A finite element simulation of frost heave in soils, Proc. Fifth Int. Symp. on Ground Freezing, Balkema, Rotterdam NL, pp 73-80.

Ladanyi B., and Shen M., 1989. Mechanics of freezing and thawing in soils, Proc. Frost in Geotechnical Engineering, VTT symposium 94, Espoo Finland, pp 73-103.

Loch J.P.G., 1979. Influence of heat extraction rate on ice segregation of soils, Frost i Jord 30, pp 19-30.

Loon W.K.P. van, 1987. De verwerking van metingen gedaan met de niet stationaire naaldmethode. Internal report (in Dutch) Dept. Phys. and Meteo., Agricultural University Wageningen, NL.

Loon W.K.P. van, Haneghem I.A. van and Boshoven H.P.A., 1988. Thermal and hydraulic conductivity of unsaturated frozen sands, Proc. Fifth Int. Sym. on Ground Freezing, Vol. 1, Balkema, Rotterdam NL, pp 81-90.

Loon W.K.P. van and Zeilmaker J., 1989a. The influence of soil physical and chemical parameters on the frost behaviour of granular materials, Proc. Frost in Geotechnical Engineering, VTT symposium 94, Espoo Finland, pp 341-352.

Loon W.K.P. van, Haneghem I.A. van and Schenk J., 1989b. A new model for the nonsteady state probe method to measure thermal properties of porous materials, Int. J. Heat Mass Transfer 32, pp 1473-1481.

Loon W.K.P van, Perfect E., Groeneveld P.H. and Kay B.D., 1990a. Application of time-domain reflectometry to measure solute redistribution during soil freezing, Proc. Int. Frozen Soil Symp., CRREL report 90-1, Hannover NH, USA, pp 186-194.

Loon W.K.P van, Perfect E., Groeneveld P.H. and Kay B.D., 1990b. A new method to measure bulk electrical conductivity in soils with time-domain reflectometry, Can. J. Soil Sci. 70, pp 403-410.

Loon W.K.P van, Perfect E., Groeneveld P.H. and Kay B.D., 1991. Application of dispersion theory to time-domain reflectometry, Transport in Porous Media (in press).

Mahar L.J., Wilson R.M. and Vinson T.S., 1983. Physical and numerical modeling of uniaxial freezing in saline gravel, Proc. Fourth Int. Conf. on Permafrost, Nat. Acad. Press, Washington DC, USA, pp 773-778.

Maxwell C., 1873. Treatise on electricity and magnetism I, Oxford, UK.

McCabe E.Y. and Kettle R.J., 1985. Thermal aspects of frost action, Proc. Fourth Int. Symp. on Ground Freezing, Vol. 1, Balkema, Rotterdam NL, pp 47-54.

Miller R.D., 1972. Freezing and heaving of saturated and unsaturated soils, Highway Research Record 393, pp 1-11.

Miller R.D., 1973. Soil freezing in relation to pore water pressure and temperature, Proc Second Int. Conf. on Permafrost, Nat. Ac. Press, Washington DC, USA, pp 344-352.

Miller R.D., 1978. Frost heaving in non colloidal soils, Proc. Third Int. Conf. on Permafrost, National Research Council of Canada, Ottawa Ont., Canada, pp 707-713.

Nixon J.F., 1988. Ground freezing and frost heave - a review, Northern Engineer 19, pp 8-18.

Oliphant J.L., 1985. A model for dielectric constants of frozen soils. *Freezing and thawing of soil-water systems*, Am. Soc. Civil Eng. New York, NY USA, pp 46-57.

Parameswaran V.R. and Mackay J.R., 1983. Field measurements of electrical freezing potentials in permafrost areas. Proc. Fourth Int. Conf. on Permafrost, Nat. Acad. Press, Washington DC, USA, pp 962-967.

Patterson D.E. en Smith M.W., 1984. Unfrozen water content in saline soils results using Time Domain Reflectometry, *Can. Geotech. J.*, 95-101.

Penner E., 1972. Influence of freezing rate on frost heaving, *Highway Res. Rec.* 393, pp 56-64.

Perfect E., Kay B.D., Loon W.K.P. van, Sheard R.W. and Posajok T., 1990a. Factors influencing soil structural stability within a growing season, *Soil Sci. Soc. Am. J.* 54, pp 173-179.

Perfect E., Loon W.K.P. van, Groenevelt P.H. and Kay B.D., 1990b. Influences of ice segregation and solutes on soil structural stability, *Can. J. Soil Sci.* 70, pp 571-581.

Perfect E., Groenevelt P.H. and Kay B.D., 1991. Transport phenomena in frozen porous media, in: *Transport Processes in Porous Media*, NATO/ASI, Pullman WA, USA, (in press).

Pikul J.L. Jr., Boersma L. and Rickman R.W., 1989. Temperature and water profiles during diurnal soil freezing and thawing: Field measurements and simulation, *Soil Sci. Soc. Am. J.* 53, pp 3-10.

Polder D. and Santen J.H. van, 1946. The effective permeability of mixtures of solids, *Physica* vol 12, 5, pp 257-271.

Powell R.W., Ho C.Y. and Ciley P.E., 1966. Thermal conductivity of selected materials, *National standard reference data series*, Nat. Bureau of Stand. 8, Washington DC, USA.

Ramo S. and Whinnery J.R., 1959. *Fields and waves in modern radio*, Wiley, New York, NY, USA.

Ratkje S.K., Yamamoto H., Takashi T., Ohrai T. and Okamoto J., 1982. The hydraulic conductivity of soils during frost heave, Proc Third Int. Symp. on Ground Freezing, USA CRREL report 82-16, Hanover NH, USA, pp 131-135.

Reynolds W.D., 1986. The Guelph permeameter method for in situ measurement of field saturated hydraulic conductivity and matrix flux potential, Ph.D. thesis, Dept. of Land Res. Sci., University of Guelph, Canada.

Rhoades J.D., Raats P.A.C. and Prather R.J., 1976. Effects of liquid-phase electrical conductivity, water content and surface conductivity on bulk soil electrical conductivity. *Soil Sci. Soc. Am. J.* 40, pp 651-655.

Rhoades J.D., 1982. Cation exchange capacity, in: *Methods of soil analyses 2: chemical and microbiological properties* (ed. A.L. Page), ASA/SSSA, Madison Wisc., USA, pp 167-175.

Rhoades J.D., Manteghi N.A., Shouse P.J. and Alves W.J., 1989. Soil electrical conductivity and soil salinity: new formulations and calibrations, *Soil Sci. Soc. Am. J.* 53, pp 433-439.

Rieke R.D., Vinson T.S. and Mageau D.W., 1983. The role of specific surface area and related properties in frost heave susceptibility of soils, *Proc. Fourth Int. Conf. on Permafrost*, Nat. Acad. Press, Washington DC, USA, pp 1066-1071.

Roe P.G. and Webster D.C., 1984. Specifications for the TRRL frost heave test, TRRL supplementary report 829, Crowthorne, Berkshire U.K.

Shen M. and Ladanyi B., 1989. Numerical solutions for freezing and thawing of soils using boundary conforming curvilinear coordinate systems, *Proc. Frost in Geotech. Eng.* 1, VTT Symp. 94, Espoo Finland, pp 391-400.

Sheng D., Knutsson S. and Axelsson K., 1989. Verification and application of a numerical model for frost penetration, *Proc. Frost in Geotech. Eng.* 1, VTT Symp. 94, Espoo Finland, pp 401-414.

Smith M.W. and Tice A.R., 1988. Measurement of the unfrozen water content of soils: a comparison of NMR and TDR methods, *Proc. Fifth Int. Conf. on Permafrost*, Trondheim, Norway, Tapir Publ., pp 473-477.

Sullivan J.M.Jr. and Stefanov L.A., 1990. Comparison on numerical simulations with experimental data for a prototype artificial ground freezing, *Proc. Int. Frozen Soil Symp.*, CRREL report 90-1, Hannover NH, USA, pp 37-43.

Tektronix, 1987, 1502B. Metallic time-domain reflectometer: operator manual, Beaverton, OR, USA.

Topp G.C., Davis J.L., and Annan A.P., 1980. Electromagnetic determination of soil water content: Measurements in coaxial transmission lines, *Water Resource Res.* 16, pp 574-582.

Topp G.C., Davis J.L. and Annan A.P., 1982. Electromagnetic determination of soil water content using TDR: II evaluation of installation and configuration of parallel transmission lines, *Soil Sci. Soc. Am. J.* 46, pp 678-684.

Topp G.C., Yanuka M., Zebchuk W.D. and Zegelin S., 1988. The determination of electrical conductivity using TDR: soil and water experiments in coaxial lines, *Water Resource Res.* 24, pp 945-952.

Vries D.A. de, 1952. *Het warmtegeleidingsvermogen van grond* (in Dutch, Ph.D. thesis), *Mededelingen van de Landbouwhogeschool Wageningen, the Netherlands*, Vol. 52.

Vries D.A. de and A.J. Peck, 1958. On the cylindrical probe method of measuring thermal conductivity with special reference to soils, part 1: extension of theory and discussion of probe characteristics, *Austr. J. Phys.* 11, 255-271.

Vries D.A. de, 1963. Thermal properties of soils, in: *Physics of plant environment* (ed. W.R. van Wijk), North Holland publ. co., Amsterdam, NL.

Weast R.C., *Handbook of Chemistry and Physics*, 1975. CRC Press, Cleveland, Ohio, USA.

Werkgroep E4, 1986. *'t Kan vriezen of dooien* (in Dutch), *Mededeling 55, Stichting Studiecentrum Wegenbouw, Arnhem NL*.

Williams P.J., 1973. Determination of heat capacities of freezing soils, *Proc. Symp. on frost action on roads*, Vol. 1, pp 153-163.

Yanuka M., Topp G.C., Zegelin S. and Zebchuk W.D., 1988. Multiple reflection and attenuation of time domain reflectometry pulses: theoretical considerations for applications to soil and water, *Water Resources Res.* 24, pp 939-944.

Yershov E.D., Komarov I.A. and Smirnova N.N., 1988. Thermal characteristics of fine grained soils, *Proc. Fifth Int. Symp. on Ground Freezing Proc.*, Vol. 1, Balkema. Rotterdam NL, pp 135-140.

Young R.N., Cheung C.H. and Sheeran D.E., 1979. Prediction of salt influence on unfrozen water content in frozen soils, *Eng. Geol.* 13, pp 137-155.

## 9 LIST OF SYMBOLS

The symbols might be used differently in some sections. When such deviations from the here described standard notation occur it is always repeated a few times in that section.

symbol	description	unit	introduced in section
A	constant for unit consistency, regression coefficient	$m^4 J^{-1}$	2.3.1
a	thermal diffusivity of the medium	$m^2 s^{-1}$	3.1.4
B	regression coefficient	-	3.3.2
B45	crushed concrete	-	3.4.2
C	volumetric heat capacity electric capacitance	$J m^{-3} K^{-1}$	2.1.7
CEC	cation exchange capacity	$mmol\ kg^{-1}$	2.1.3
CLA	river foreland clay	-	3.4.2
D	regression coefficient	-	3.3.2
d	grain diameter	$m$	2.1.1
E	regression coefficient	-	3.3.2
g	gravitational acceleration	$m\ s^{-2}$	2.1.1
h	heave	$m$	2.3.1
$h_m$	pressure head of water	$m$	2.1.5
I	electrical current	A	2.2.1
i	imaginary unit $i=\sqrt{-1}$	-	2.2.1
k	hydraulic conductivity	$m\ s^{-1}$	2.1.6
L	heat of fusion of water	$J\ kg^{-1}$	2.3.1
LSA	Engs loamy sand	-	3.4.2
NS	not significant	-	4.2.2
p	pressure	$N\ m^{-2}$	2.1.5
Q	heat flow, heat flux density	$W\ m^{-2}$	2.1.7
$r^2$	coefficient of determination	-	3.2.4
RSA	river sand	-	3.4.2
S	specific surface area	$m^2 g^{-1}$	2.1.2
SC	solute concentration	$kg\ m^{-3}$	2.3.3

SE	standard error	-	3.3.5
SLO	Achterhoeks sandy loam	-	3.4.2
SP	segregation potential	$m^2 K^{-1} s^{-1}$	2.3.1
SSA	silver sand	-	3.4.2
T	temperature	$^{\circ}C$ or K	2.3
t	time	s	2.2.1
V	electric potential	V	2.2.1
V'	reflection coefficient	$V V^{-1}$	2.2.2
v	(apparent) velocity, flux density	$m s^{-1}$	2.1.6
X	position of the freezing front	m	2.3
Z	electric impedance	$\Omega$	2.2.2
z	vertical coordinate	m	2.1.6

greek symbol	description	unit	section
$\alpha$	attenuation coefficient	$m^{-1}$	2.2.3
$\Gamma$	contact resistance per unit length	$K m W^{-1}$	2.1.7
$\epsilon$	relative dielectric constant	-	2.2.1
$\zeta$	zeta potential	$m^2 V^{-1} s^{-1}$	2.1.4
$\eta$	dynamic viscosity	$kg m^{-1} s^{-1}$	2.1.1
$\theta$	volume fraction	$m^3 m^{-3}$	2.1.6
$\lambda$	thermal conductivity	$W m^{-1} K^{-1}$	2.1.7
$\mu$	relative magnetic permeability	-	2.2.3
$\pi$	osmotic pressure head	m	2.3.1
	trancedental number 3.1415...	-	2.2.3
$\rho$	specific mass	$kg m^{-3}$	2.1.1
$\sigma$	bulk electrical conductivity	$S m^{-1}$	2.2.3
$\tau$	dimensionless time	$s s^{-1}$	3.1.5
$\Phi$	mass fraction	$kg kg^{-1}$	2.1.1
$\Phi_{125}$	mass fraction consisting of particles smaller than 125 $\mu m$	$kg kg^{-1}$	3.4.2
$\chi$	surface tension	$N m^{-2}$	2.1.5
$\omega$	angular frequency	$s^{-1}$	2.2.1

**subscripts**

0 zero degree Celcius, vacuum, reference value  
a air  
f frozen  
ff frozen fringe  
i ice  
L phase change water-ice, fusion  
m measured value  
s soil, solid in combination with C,  $\epsilon$ ,  $\theta$  and  $\lambda$   
s segregation in combination with p and T  
u unfrozen, unfrozen water  
w (liquid) water

**other notations**

— (underlined) vector  
' apparent value  
 $|x|$  absolute value of x  
 $\Delta$  difference operator  
 $\partial$  partial derivative operator

## 10 CURRICULUM VITAE

Wilko (Wilhelmus Kors Petrus) van Loon werd op 23 augustus 1960 geboren in Bergen op Zoom.

Na de lagere scholen in Bergen op Zoom, Roosendaal en Terneuzen bezocht hij de Rijksscholengemeenschap "Petrus Hondius" te Terneuzen, waar hij het examen ongedeeld VWO behaalde in 1978.

Aansluitend begon hij zijn natuurkunde studie aan de Technische Hogeschool te Eindhoven (nu Technische Universiteit Eindhoven). Naast zijn studie was hij ook enkele jaren werkzaam als studentassistent in de Fysikawinkel, de Wetenschaps-winkel van de afdeling der Technische Natuurkunde.

Tijdens de kandidaats- en doctoraalfase lag de nadruk op numerieke methoden en massa- en warmtetransport in poreuze media. Het afstudeerwerk stond onder leiding van prof.ir. C.W.J. van Koppen en prof.dr.ir. G. Vossers en werd in 1986 afgerond.

Hierop volgde in het kader van een promotie-onderzoek de aanstelling als wetenschappelijk assistent binnen de sectie Natuurkunde van de toenmalige vakgroep Natuur- en Werkunde (nu deel uitmakend van de vakgroep Agrotechniek en -fysica). Een deel van het onderzoek werd verricht bij de "Department of Land Resource Science" van de University of Guelph, Canada.

Sinds 1990 is hij werkzaam als Universitair Docent bij de vakgroep Agrotechniek en -fysica op het gebied van de fysische transportverschijnselen.